UNIVERSITY OF OKLAHOMA

GRADUATE COLLEGE

ENHANCING HYDROGEN ENERGY STORAGE AND TRANSPORTATION SYSTEMS: PREDICTIVE MODELING OF SEALING MATERIALS THROUGH EX-SITU EXPERIMENTAL ANALYSIS

A DISSERTATION

SUBMITTED TO THE GRADUATE FACULTY

in partial fulfillment of the requirements for the

Degree of

DOCTOR OF PHILOSOPHY

By

Ahmed Nazmus Sakib

Norman, Oklahoma

2024

ENHANCING HYDROGEN ENERGY STORAGE AND TRANSPORTATION SYSTEMS: PREDICTIVE MODELING OF SEALING MATERIALS THROUGH EX-SITU EXPERIMENTAL ANALYSIS

A DISSERTATION APPROVED FOR THE

SCHOOL OF AEROSPACE AND MECHANICAL ENGINEERING

BY THE COMMITTEE CONSISTING OF

Dr. Zahed Siddique, Chair

Dr. Pejman Kazempoor

Dr. Yingtao Liu

Dr. Talayeh Razzaghi

Dedicated to:

To the Almighty Allah, With an Apology

My Father, Faruque Ahmed

My Mother, Hasina Akther Chowdhury

My Brother, Ahmed Sadman Sakif

My paternal Late Grandfather, Aziz Uddin Ahmed, and

My maternal Late Grandfather Dr. Abdul Zalil Chowdhury

ACKNOWLEDGMENT

First and foremost, I am grateful to Allah Almighty for the blessings and knowledge bestowed upon me. My Lord has continuously strengthened me to carry on in my journey and helped me to achieve more through determination, courage, and integrity.

I sincerely appreciate and express my gratitude to my academic advisor and committee chair, Dr. Zahed Siddique, for his continuous support, motivation, and remarkable guidance throughout my Ph.D. program. He always believed in my potential and helped me to bring the best out of me in my academic and research life. He has been more than an advisor to me. I am indebted to his patience and vision that have inspired me to push the boundaries of my research and getting various accomplishments from Gallogly College of Engineering and learn the time management. I am so glad that all my dissertation committee members, Dr. Pejman Kazempoor, Dr. Yingtao Liu and Dr. Talayeh Razzaghi believe in my ability to do independent research work. I appreciate their commitment, time, and constructive comments throughout my PhD program that improved the quality of my work. I am thankful to Dr. Preston Larson for assisting in the SEM image processing. My special thanks to Dr. Raghu Madhavan, industry collaborator from Schlumberger for his great mentorship and guidance. My appreciation also goes to all other collaborators from Schlumberger. This dissertation would not have been possible without their intellectual contribution. I want to acknowledge and thank the School of Aerospace and Mechanical Engineering staff for their continuous support. I would like to thank my colleagues whom I worked with in different aspects; Alfredo Becerril Corral, Philip M Resnick, and Md. Monjur Hossain Bhuiyan. I am acknowledging Alfredo Becerril Corral in this dissertation for supporting the aging chamber and Philip M Resnick for supporting the leak test chamber design and installation for my experiment.

I am to remember Dr. Abu Yousuf; my undergraduate research advisor who initiated the motivation of research and Dr. John O'Haver; my master's degree advisor who encouraged me pursuing the PhD degree onwards. Last but not least, I would like to convey my gratitude to all of my teachers starting from primary school to graduate school for their contribution to making me the todays me. I would like to thank my friends and colleagues from Bata, Chevron, Bashundhara Oil & Gas and Avery Dennison whom I have interacted with at different phases of life. I feel indebted to their love and support that always helped me to move forward.

I do not have enough words to express my deep gratitude toward my father Advocate Faruque Ahmed who continued his profession at the age of 70 just to let me keep focused on my PhD degree. I am here today for your priceless dedication, my dear father. My utter respect to my mother, Hasina Akther Chowdhury, who is my lifetime teacher and my only brother Engr. Ahmed Sadman Sakif who took the enormous responsibility of our family in my absence during my graduate journey. I would like to acknowledge my uncles Martuza Ahmed, Dr. Mushtaq Ahmed, Dr. Monsur Ahmed Chowdhury, who are my childhood idols from the inside of the family, to touch the pinnacle of the academic journey. I sincerely remember my paternal grandfather late Azizuddin Ahmed and maternal grandfather late Dr. Abdul Zalil Chowdhury who may be the happiest people to see me here today.

Finally, I dedicate this dissertation to my father, Advocate Faruque Ahmed, who taught me to learn and grow in every aspect of life with love, kindness, morality and quality. This successful accomplishment would not have been conceivable without his everlasting support. I am grateful to you for anything and everything, my father. Thank you!

TABLE OF CONTENTS

LIST OF TABLES

LIST OF FIGURES

ABSTRACT

As the global energy trend shifts towards cleaner alternatives, hydrogen arises as a prospective candidate due to its high energy density and zero carbon emissions. However, significant challenges persist, particularly in the durability and reliability of materials used for hydrogen storage and sealing. This study explores the challenges and opportunities associated with hydrogen production, incorporating CO2 capture technology and the interaction of materials to understand the correlation between materials and hydrogen exposure. This dissertation presents a literature review and experimental analysis focused on hydrogen-induced aging in polymeric sealing materials, specifically nitrile butadiene rubber (NBR), ethylene propylene diene monomer (EPDM), and silicon. The research reviewed hydrogen-induced aging mechanisms, including thermal, chemical, mechanical, and thermo-mechanical aging, which leads to the loss of integrity of sealing materials. A series of controlled experiments were conducted to simulate real-world conditions, with the aim of assessing the effects of high-pressure hydrogen exposure on the physical, mechanical and electrical properties of NBR, EPDM and silicon.

Findings from the experimental results indicate a complex interaction among swelling, hardness reduction, and tensile strength degradation in sealing materials under hydrogen exposure. Tensile strength degradation was strongly associated with crack formation. At the same time, Silicon exhibited the lowest swelling due to its Si-O-Si backbone but showed significant reductions in tensile strength and hardness and high crack and cavity counts. EPDM displayed moderate swelling and hardness loss, coupled with strong leak resistance and minimal morphological degradation, due to its saturated backbone and low hydrogen solubility. Despite the higher hydrogen solubility and free volume, NBR retained hardness better than Silicon but exhibited

moderate morphological degradation that weakened the leak resistance over time. NBR's absolute resistivity was found to remain much lower than that of Silicon and EPDM with hydrogen exposure. Both EPDM and NBR maintained comparable sealing performance up to 1500 psi, however, EPDM's resilience against further degradation under prolonged pressures suggests it as the optimal elastomeric material for consistent sealing under high-pressure hydrogen system.

Several machine learning approaches were applied to predict key sealing properties of materials exposed to hydrogen. This study employed multiple models like Multivariate Linear Regression (MLR), Generalized Additive Model (GAM), and Random Forest to capture linear and non-linear dependencies between pressure and sealing properties. It was observed that MLR performed better handling linear relationships, especially for tensile strength and hardness, while GAM performed better in capturing non-linear resistivity behavior. A CNN model is trained on SEM images to capture morphological changes, showing the lowest MAE for Silicon. The final recommendation is a combined MLR-CNN model, which balances numerical and morphological predictions for optimal material property assessment under hydrogen exposure, suggesting EPDM for high-pressure applications.

This research is expected to contribute to the life cycle estimation and customization of elastomeric materials for hydrogen infrastructure. That will assist in accurately improving the scheduling of e the predictive maintenance of the seals used in the hydrogen industry. Thus, this research will help the industry to meet ISO 15869 and the ASME B31.12 through the developed predictive models for seal failure and performance in hydrogen pipelines. It provides a foundation for future research in sealing technology, aimed at enhancing the long-term safety and performance of hydrogen storage and transportation systems.

CHAPTER 1: POLYMERIC SEALING PERFORMANCE ANALYSIS AT GASEOUS HYDROGEN ENVIRONMENT

1.1. INTRODUCTION

The global focus on mitigating environmental impact and reducing greenhouse gas emissions has significantly increased in recent years. Hydrogen emerges as a prospective route to a clean energy carrier. The transition from traditional oil and gas operations to hydrogen as a clean energy alternative is influenced by a set of technical, environmental, and economic considerations. Hydrogen's versatility in serving as an energy source, storage medium, and feedstock for various industries makes it a viable solution for achieving decarbonization. In the hydrogen industry, the assessment of sealing performance is critical due to the unique challenges posed by the properties of gaseous hydrogen. Hydrogen, while being a clean energy source, has inherent risks associated with its ability to dissolve through polymers, potentially leading to leakage and material failure. Hydrogen leaks can result in gas cloud formation, and if ignited, hydrogen cloud explosions may occur. Material failure due to hydrogen-induced cracking, hydride embrittlement, and other detrimental effects poses significant safety concerns. Additionally, long-term exposure to a hydrogen environment accelerates the degradation and damage rate of materials, emphasizing the importance of understanding aging processes in hydrogen environment. As the hydrogen industry aims to replace conventional energy sources, ensuring the service life and safety performance of materials, including seals, is crucial. A systematic approach is needed to assess sealing materials and designs under various conditions to address the challenges, minimize risks, and contribute to the successful and safe implementation of hydrogen as a sustainable energy source.

1.2. MOTIVATION

The motivation for research on the assessment of sealing systems in the emerging hydrogen industry is emphasized by the need to address environmental safety and operational challenges associated with storage and transport. In the oil and gas industry, the significance of preventing fugitive emissions is a challenge due to the industry's substantial contribution to greenhouse gas emissions and the adverse environmental impacts associated with leakage. This research has been motivated in the context of preventing fugitive emissions in the oil and gas industry. Therefore, the motivation of this dissertation is:

enhanced understanding of the integrity of the sealing system in hydrogen industry in order to contribute next generation sealing design for systems in the hydrogen industry in order to contribute to the generation sealing design for hydrogen environments. While hydrogen presents a promising alternative to conventional fuels, its potential for leakage and material failure, particularly due to its ability to dissolve into metals and seals, raises safety concerns. Studies investigating hydrogen-induced cracking and hydride embrittlement show the complexities associated with hydrogen exposure to storage and sealing materials. The motivation is further supported by the industry's objective of sustainable energy solutions and the potential benefits of hydrogen energy in several applications. Despite the advantages of hydrogen, understanding and mitigating the risks associated with its production, storage, transportation, and application is essential. The research aims to provide insights into the design and performance of sealing systems in hydrogen applications, suggesting solutions to enhance safety, prevent leaks, and contribute to the successful integration of hydrogen into the global energy chapter. Data, such as the specific energy density of hydrogen and emission percentages from different components in industries,

claims the quantitative importance of the sealing assessments in driving effective and sustainable practices in hydrogen industry.

1.3. BACKGROUND

The oil and gas industry plays a vital role in meeting global energy demands, yet it is accompanied by challenges, fugitive emissions is one such challenge, which represent a significant environmental concern. Fugitive emissions refer to the unintentional release of gases or vapors from various components within the oil and gas infrastructure into the atmosphere. These emissions often contain volatile organic compounds (VOCs), including methane, a potent greenhouse gas contributing substantially to climate change. Studies indicate that nearly 2-3% of produced natural gas is lost to fugitive emissions, with methane emissions being a major focus due to its high global warming potential. Hydrogen is being considered as a potential candidate to replace or integrate with fossil fuel to promote environmental sustainability. But hydrogen, being a prospective candidate in the transition to clean energy, also presents unique challenges to permeate through sealing materials, raising concerns about leakage and safety in the energy industry. Unlike traditional hydrocarbons, hydrogen molecules are small and possess high diffusivity, making containment more challenging. The consequences of hydrogen leakage are multifaceted, encompassing safety hazards, material degradation, and environmental impact. Hydrogen-induced material degradation is a critical aspect of the challenge. Hydrogen embrittlement is a phenomenon where exposure to hydrogen gas can lead to a reduction in material ductility and increased susceptibility to fracture. This is particularly raising concern in industries where structural integrity is important, such as the aerospace and energy sectors. Polymers and composites experience hydrogen-induced degradation, necessitating the need for thorough

assessments of sealing materials. The consequences of hydrogen leakage extend beyond material degradation, imposing safety risks due to the potential formation of flammable hydrogen-air mixtures.

Hydrogen is highly flammable, and if leaked in sufficient quantities and ignited, it can lead to fires or explosions. Mitigating these risks requires a comprehensive understanding of the behavior of different sealing materials under varying hydrogen concentrations and operational conditions. Sealing materials, ranging from elastomers to metals, are exposed to different conditions in hydrogen environments. Hydrogen can permeate through materials, leading to issues like blistering in elastomeric materials, a phenomenon observed in rubbery O-rings due to the rapid decompression of highly pressurized hydrogen gas. This emphasizes the need for seals capable of sustaining the challenges hydrogen poses. The performance of seals is essential in preventing hydrogen leakage and ensuring the integrity of equipment, pipelines, and storage systems. As the hydrogen industry attempts to replace conventional energy sources, understanding the behavior of sealing materials is essential for ensuring the safety and reliability of infrastructure. Research in this domain aims to contribute insights into the hydrogen-induced effects on seals, providing a baseline for developing materials capable of withstanding the challenges associated with hydrogen environments.

1.4. OBJECTIVES

Objective-1: Assessing Hydrogen Energy Resilience in Global Energy Transitions: Technological, Economic and Strategic Perspectives:

The first objective is to review the resilience of hydrogen energy in the context of global energy transitions. This objective aims to analyze the technological, economic, and strategic factors that influence hydrogen's role as a sustainable energy carrier, focusing on its application in reducing greenhouse gas emissions, supporting clean energy initiatives, and facilitating advancements in transportation and power generation. This objective is to explore the potential of hydrogen energy to contribute to global net-zero targets through investments, policy measures, and infrastructure developments and assess the need for international cooperation to drive innovation and adoption in the hydrogen economy.

Objective-2: Addressing Challenges in Hydrogen Energy: Production, Storage and Material Compatibility:

The second objective will review and identify the primary challenges in implementing hydrogen energy technologies, focusing on important areas such as production methods, storage solutions, and material compatibility. This is to provide a baseline for understanding the technical barriers associated with hydrogen production processes, including efficiency, cost, and carbon emissions. Additionally, it explores the limitations of current hydrogen storage techniques, particularly emphasizing the effects of hydrogen embrittlement on materials and the possible routes to enhance material durability. The objective is to extract the challenges and possible mitigation routes for hydrogen production, storage, and transportation to support more resilient and economically viable hydrogen energy systems in the future.

Objective-3: Investigating Hydrogen-Induced Aging in Storage and Sealing Materials: Mechanisms, Challenges, and Mitigation Strategies:

This study is further continued to review the mechanisms, challenges, and mitigation strategies associated with hydrogen-induced aging in storage and sealing materials. This aims to provide a comprehensive analysis of how hydrogen environments impact the structural integrity of storage and transport materials, focusing on various aging processes, including thermal, chemical, mechanical, mechanical-chemical, and thermo-mechanical aging. The goal is to identify key factors influencing material degradation, durability analysis and review the existing methods to enhance the performance of materials exposed to hydrogen. That will assist in contributing to the development of more suitable and sustainable hydrogen storage and sealing systems.

Objective-4: Experimental Investigation of Hydrogen Exposure on Polymer-Based Sealing Materials: Effects on Mechanical, Electrical, and Physical Properties:

The coupled objective of this dissertation is narrowed down to perform a comprehensive experimental investigation into the effects of hydrogen exposure on the electrical, mechanical and physical properties of polymer-based sealing materials, specifically focusing on NBR, EPDM, and silicon. The study aims to understand hydrogen-induced aging by analyzing changes in tensile strength, swelling behavior, hardness, resistivity and microstructural morphology of these elastomers under controlled conditions. It intends to develop predictive models for quantifying seal performance deterioration due to hydrogen permeation across a range of pressures. By establishing the relationship between hydrogen permeation and the deterioration of mechanical properties at the molecular level, this investigation seeks to identify the critical factors influencing the long-term performance and stability of sealing materials.

1.5. ORGANIZATION OF THE DISSERTATION

Chapter 2, titled "Resilience of Hydrogen Energy," explores how hydrogen is a sustainable alternative to fossil fuels, focusing on its high energy density and zero CO2 emissions. It discusses the current global reliance on petroleum fuel and the urgent need to reduce greenhouse gas emissions during rising energy demands. The chapter reviews hydrogen's production versatility and environmental benefits compared to conventional fuels. It also examines the energy transition, elaborating on the increased investments in clean energy and regional variations in energy strategies, with a focus on Europe and the US. The resilience and growing confidence in hydrogen as a key player in the clean energy transition are emphasized, focusing on the critical role of policy measures, financial support, and public engagement in accelerating the hydrogen sector's development. Thus Chapter 2 is designed to address the first research objective of this dissertation to assess the prospect of hydrogen energy in the perspective of global energy market.

The key challenges in implementing hydrogen energy are discussed in Chapter 3. It starts by identifying core research areas using density visualization methods to highlight significant keywords in hydrogen research. Density visualization method is an algorithm used to highlight the areas with high concentrations of research topics based on keywords and assist to identify the dominant areas needed to be under consideration by showing clusters of related terms in a visual network. The chapter emphasizes key issues in hydrogen production, storage, transport and sealing processes to understand the challenges in broader aspects to implement hydrogen energy. The chapter details the challenge and opportunities for hydrogen production from natural gas, electrolysis, coal, biomass and methane splitting. It discusses the materials and composites used in hydrogen infrastructure, addressing issues like hydrogen embrittlement and the performance of

polymers and metals under hydrogen exposure. Finally, it briefly discusses the challenges of the sealing systems under hydrogen environment for detailing the constraints of hydrogen storage and transportation. Once the prospect of hydrogen energy is outlined in Chapter 2, the associate challenges of hydrogen production, storage and transportation are extracted in Chapter 3. This is how Chapter 3 is designed to address the second research objective of the dissertation.

While Chapter 3 identifies the diverse challenges in different domains consisting of hydrogen production, storage, transportation and commercialization, Chapter 4 narrowed down to analyze one particular domain which is hydrogen storage and transportation. Therefore, Chapter 4 elaborates on the challenges of hydrogen-induced aging for storage and sealing materials. It discusses the complications of hydrogen as an energy source from a material perspective, such as hydrogen-induced cracking, hydride embrittlement, and blistering. The chapter reviews historical incidents related to hydrogen-induced material degradation. It reviews the impact of operating conditions, such as pressure, temperature, stress, and the presence of residual water on material aging. Various aging mechanisms, including thermal, chemical, mechanical, mechanical-chemical, and thermo-mechanical aging, are analyzed in detail. Laboratory tests and findings are reviewed to illustrate how these aging processes affect different materials. The chapter concludes by stating the importance of selecting appropriate materials to mitigate hydrogen-induced aging and ensure the longevity and reliability of hydrogen storage and sealing systems. This is how Chapter 4 theoretically investigate the hydrogen induced aging in storage and sealing materials and analyze the available remedies in order to address the third objective outlined in this dissertation.

Chapter 5 and Chapter 6 further narrowed down in proceedings of the theoretical discussion of hydrogen storage and sealing material and approached to investigate the hydrogen sealing materials through an experimental analysis and machine learning model to contribute to the hydrogen storage system and thus meeting the fourth objective of this dissertation. Chapter 5 details the materials and methods used to investigate hydrogen-induced aging in sealing materials. The objective is to understand how hydrogen exposure affects various elastomers, which have not been thoroughly studied in this context before. The study focuses on the interaction of gaseous hydrogen pressure and exposure time on the sealing resistance of selective sample materials. This chapter aims to identify polymer compounds that offer better resilience to hydrogen permeation. The selected materials, including NBR, Silicon, and EPDM, are subjected to specific annealing processes to relieve residual thermal stress before high-pressure hydrogen exposure followed by a number of mechanical characterizations. The chapter describes the chemical composition, mechanical properties, thermal properties, and chemical resistance of these materials, explaining their suitability for hydrogen applications. It outlines the experimental approach for analyzing the impact of hydrogen gas on polymer materials used in sealing applications. It details the characterization tests, including tensile strength, swelling, hardness, resistivity, and morphology analysis, to understand how hydrogen exposure affects these materials. The chapter describes the experimental method of hydrogen-assisted aging of sealing samples and post-aging characterization techniques and develops a predictive machine learning model to predict the properties of sealing materials under different operating conditions. This comprehensive approach aims to evaluate the suitability and reliability of different polymers in hydrogen-rich environments, guiding material selection and design for optimized performance.

Chapter 6 presents the results and discusses the experimental analysis of the impact of hydrogen-induced aging on various polymer materials used in sealing applications. It analyzes the findings from tensile strength tests, resistivity measurements, swelling behavior, hardness tests, and leak rate assessments for NBR, EPDM, and Silicon. Chapter 6 also elaborates on morphological analysis using SEM to observe microstructural changes in the materials. Additionally, it discusses the result and application of predictive machine learning models to forecast the performance of these materials under different conditions and determine the most important critical properties of sealing material dictating the performance. The results highlight the varying degrees of strength and degradation among the polymers, providing insights for selecting appropriate sealing materials for hydrogen-rich environments. Chapter 7 concludes the dissertation by discussing how the objectives outlined in chapter 1 are met in different sections. The chapter also discusses the limitations along with future recommendations that can be considered to promote the integrity of sealing system for hydrogen application. A visual representation of the organization of this dissertation is outlined in Figure 1.1.

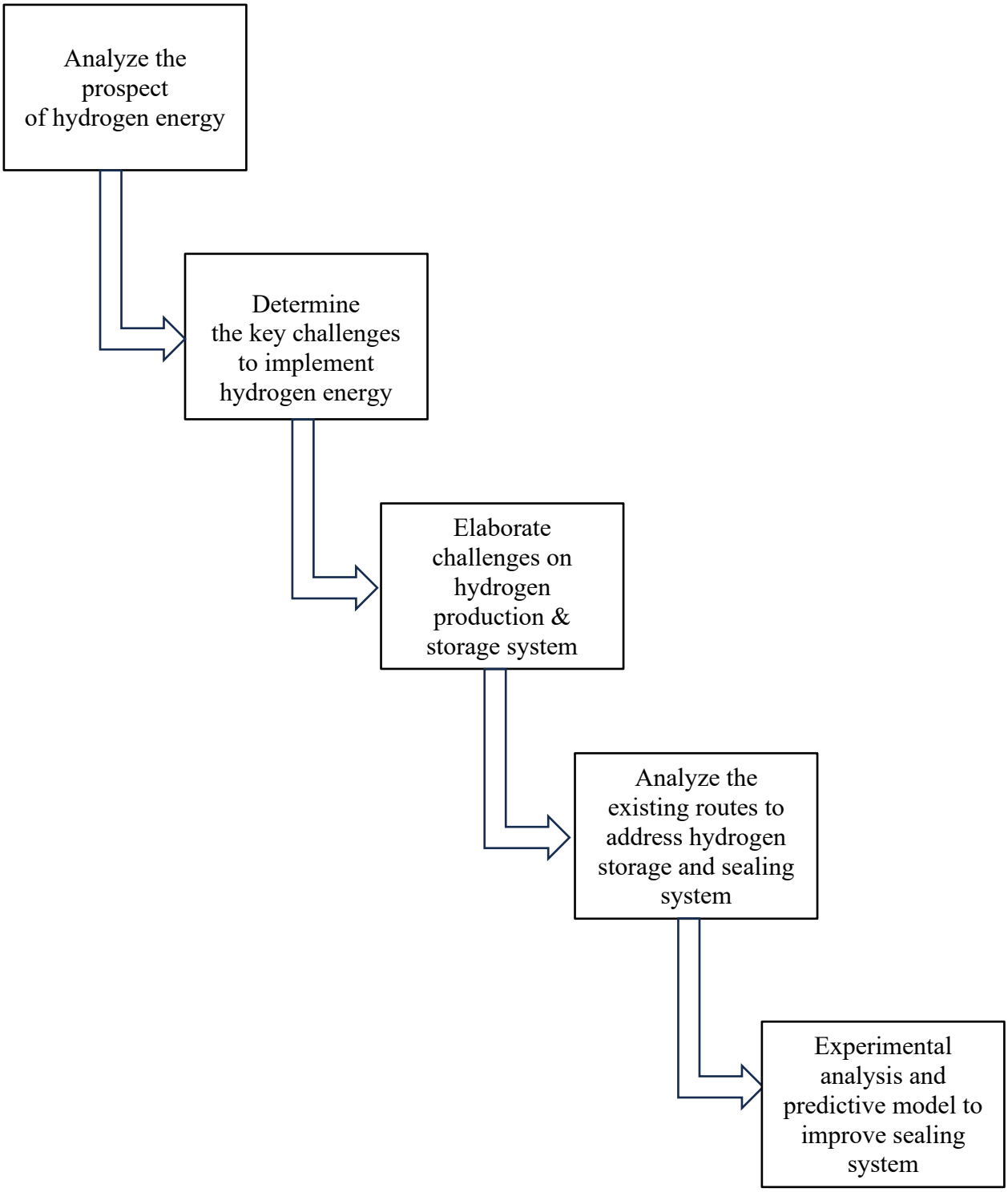

Figure 1. 1: Organization of the Dissertation

CHAPTER 2: RESILIENCE OF HYDROGEN ENERGY

Chapter 2 of the dissertation focuses on the strength and prospect of hydrogen energy within the global transition to sustainable energy systems. This chapter reviews the advantages of hydrogen, such as its high specific energy density and zero CO2 emissions when used in fuel cells, making it a cleaner alternative to traditional fossil fuels. It analyzes the significant investments and policy measures required to foster the hydrogen economy, emphasizing the importance of international cooperation and regulatory frameworks. It also discusses the current and projected roles of hydrogen across various sectors, including transportation, power generation, and industrial processes. The chapter focuses on the need for substantial financial support and technological advancements to fully realize hydrogen's potential in reducing greenhouse gas emissions and achieving net-zero goals. Additionally, it discusses the regional variations in hydrogen strategies and the critical role of public engagement and industry collaboration in driving the adoption of hydrogen as a key component for a sustainable and resilient energy future.

2.1. Why Hydrogen

In the present day, energy and transport systems are significantly driven by petroleum fuels, which are not sustainable. According to the International Energy Agency (IEA); the global demand for energy is expected to rise in the upcoming decades by more than 50% until 2030 [1]. In order to prevent anthropogenic interference with the climate system, the increasing greenhouse gas (GHG) emissions need to be reduced. From a diverse mix of energy sources, industrially, hydrogen can be produced in large quantities, which could be able to play a key role in the energy sector [2].Using hydrogen to produce energy is advantageous to fossil fuels because the primary

byproducts of the process are energy, heat, and water. Different environmental issues still need to be minimized if hydrogen is to replace or integrate with current energy stream [3]. Another advantage of hydrogen is its high specific energy density; it can provide around three times as much energy per unit of mass as conventional fuels like diesel or gasoline, i.e., approximately 120 MJ/kg [4]. Therefore, hydrogen fuel cell vehicles, as opposed to traditional transportation systems, may be a sustainable choice because they can reduce greenhouse gas emissions, eliminate fuel feedstock discrepancy, and improve onboard fuel efficiency [5]. While hydrogen is used in fuel cells, it transforms its chemical energy into electrical energy and produces water as a byproduct, which is considered zero emission. According to the Paris Agreement goal of keeping the temperature globally below 20º C, world leaders, countries, and companies are moving forward to achieve net zero emission by 2050 and to rise of clean hydrogen revolution [15, 16]. According to a Goldman Sachs report [16], clean hydrogen can potentially aid in decarbonizing 45% of global anthropogenic emissions, . Hydrogen can be utilized as an energy carrier in transportation, power generation, and chemical industries with zero carbon emissions. The global market for hydrogen gas is around USD 154.74 billion by 2022 and keep increasing [17,18]. A comparison of the important properties of different fuels with hydrogen is summarized in Table 2.1 [6-14].

Table 2. 1: Feasibility comparison of Hydrogen with existing fuels [6-14]

Property	Hydrogen	Natural Gas	Petrol
Energy content per unit mass	High (120-142 MJ/kg)	Moderate (55.5 MJ/kg)	Low (45.8 MJ/kg)
Emission upon Burning	Water vapor (H_2O) - Zero CO_2 emissions	CO_2, water vapor - Lower CO_2 than petrol	CO_2, water vapor, NOx, SOx, particulates
Storage	Requires high pressure or cryogenic temperatures	Stored under pressure, less demanding than hydrogen	Easily liquified, stored at room temperature
Production Source	Electrolysis of water, steam reforming of methane, gasification of coal	Extracted from underground reservoirs, fracking	Refining of crude oil
Safety	Lower ignition energy, non-toxic, disperses quickly	Flammable, risk of leaks and explosions	Highly flammable, toxic fumes
Sustainability	Renewable when produced from water using renewable energy	Non-renewable, though cleaner than petrol	Non-renewable, contributes to pollution
Transportation Feasibility	High potential for fuel cells in vehicles	Used in compressed form for vehicles	used in internal combustion engines

2.2. Energy Transition

In 2021, the global refining industry experienced its first drop in refining capacity in thirty years. This happened because more refineries were closed than new ones opened, especially in China and the Middle East, where there was only slight growth. Within the persistent uncertainty regarding the long-term route of oil demand, the industry's recent robust financial performance and high utilization rates may not necessarily translate into increased investment levels. As a result, there is increasing pressure on oil and gas companies to realign their investments with the evolving energy transition requirements [19]. According to the International Energy Agency (IEA), meeting the

escalating global demand for energy services in a sustainable manner necessitates a substantial increase in investments in efficiency, electrification, and low-carbon energy sources [21]. Figure 2.1 illustrates a significant shift in investment trends for energy [20].

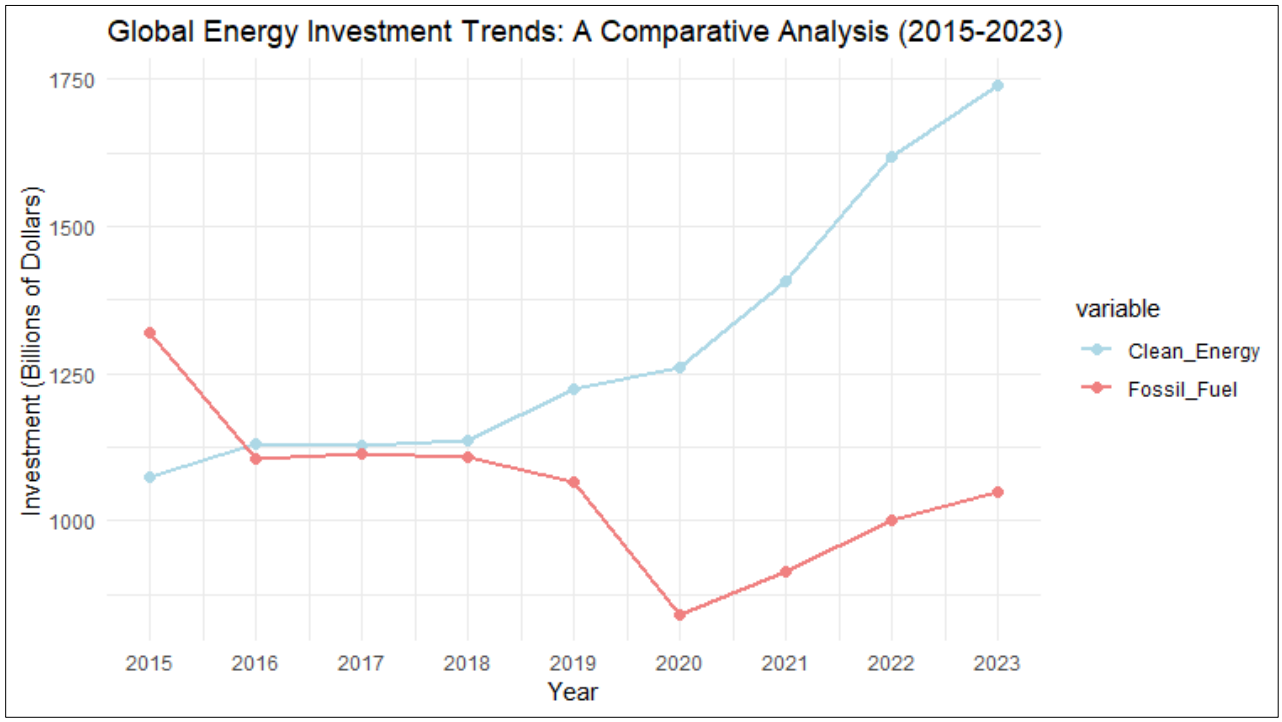

Figure 2. 1: Investment by Oil and Gas companies on clean energy [20]

A significant observation is that, prior to 2018, global fossil fuel investment was nearly on average with clean energy investment. However, post-2018, we witness the emergence of a consistent decline in fossil fuel investments, concluding at an unprecedented all-time low during the COVID-19 pandemic. In contrast, clean energy investments have shown a steady increase since 2018, with a notable flow in investment showing the transition from the global investment perspective. Governments and industries need to implement a comprehensive set of policy measures to accelerate the adoption of hydrogen as a clean energy source. This approach would align with both economic recovery efforts and long-term sustainability objectives. The European model

demonstrates an approach by integrating financial support for critical sectors, including energy and transportation, with a commitment to significant reductions in carbon emissions over the next decade [22]. This model is further enriched by adopting a strategy for the hydrogen value chain, consisting of compensatory measures for short-term revenue shortfalls estimated between EUR 450-500 million and promoting the development of early commercial markets for green hydrogen through a combination of incentives, regulatory frameworks, and public funding [23, 24]. A critical aspect of this discussion involves the identification of targeted policy interventions, such as tax incentives and subsidies for green hydrogen production, alongside significant investments in research and development [25]. These measures are intended to drive innovation, lower production costs, and support economic recovery by creating jobs in the green energy sector [26]. Moreover, these measures are linked to long-term sustainability, reflecting hydrogen's role in achieving net-zero emissions, its acceptance across transportation, industrial processes, and power generation, and the necessity for regulatory frameworks that ensure the environmental integrity of hydrogen production.

The significance of promoting international cooperation and partnerships is essential for harmonizing standards, sharing technological advancements, and scaling the hydrogen economy globally. Additionally, public engagement initiatives are important for enhancing acceptance and understanding of hydrogen energy, ensuring broad support for infrastructure development and technology adoption. Collectively, these strategies outline a comprehensive approach essential for promoting hydrogen energy as a key component of sustainable post-pandemic recovery and long-term environmental stewardship [27, 28]. In the post-COVID-19 era, the hydrogen sector in the United States has witnessed significant growth and transformation, with a particular focus on clean

hydrogen as a key driver of decarbonization efforts. The U.S. Gulf Coast (USGC) region, known for its convenient ports and highways, has emerged as a strategic location for substantial CO_2 reduction through clean hydrogen adoption in various sectors. With a growing emphasis on reducing carbon emissions and achieving net-zero pledges, the demand for clean hydrogen has increased across industries such as ground transportation, power and utilities, and more. The Inflation Reduction Act (IRA) has played a vital role in making clean hydrogen more affordable, offering incentives through tax credits and supporting the development of clean hydrogen projects. This legislative support, along with the collaborative efforts of public and private sector players, has positioned the USGC region to potentially become a hydrogen hub, driving the transition to a more sustainable and decarbonized future [29].

2.3. Resilience of Hydrogen Energy

Throughout the global economic slowdown triggered by the pandemic, hydrogen has demonstrated remarkable prospect. Between January 2019 and mid-2021, companies involved in hydrogen production, distribution, and utilization raised a sum of approximately USD 11 billion in equity, representing a substantial increase compared to recent years. This resilience and growth of the hydrogen sector, even as the world faces COVID-19, suggests a significant shift in public and investor sentiment towards cleaner energy alternatives. The pandemic situation assisted in understanding the importance of sustainability and the strength of hydrogen energy [30]. The sector's ability to attract investments even during challenging times proves the growing confidence in hydrogen as a key player in the clean energy transition. Nonetheless, while hydrogen has received substantial funding, it is still not yet able to achieve its full potential for reducing CO2 emissions. According to the Net Zero Emissions Scenario, hydrogen has the potential to play an

important role in reducing emissions by a staggering 60 gigatons, offering a powerful solution to address climate change. To achieve this goal, additional investments and innovative financing mechanisms are needed to accelerate hydrogen technology advancements and its widespread adoption. Although hydrogen has progressed significantly, there's still more it could achieve with the right financial backing to make a bigger impact on cutting emissions and promoting environmental sustainability [31]. The strength and adaptability of the hydrogen sector have come to the focus as stakeholders across the U.S. have recognized the vital role clean hydrogen can play in addressing climate change and advancing sustainability goals, which can be clearly observed from Figure 2.2 [31].

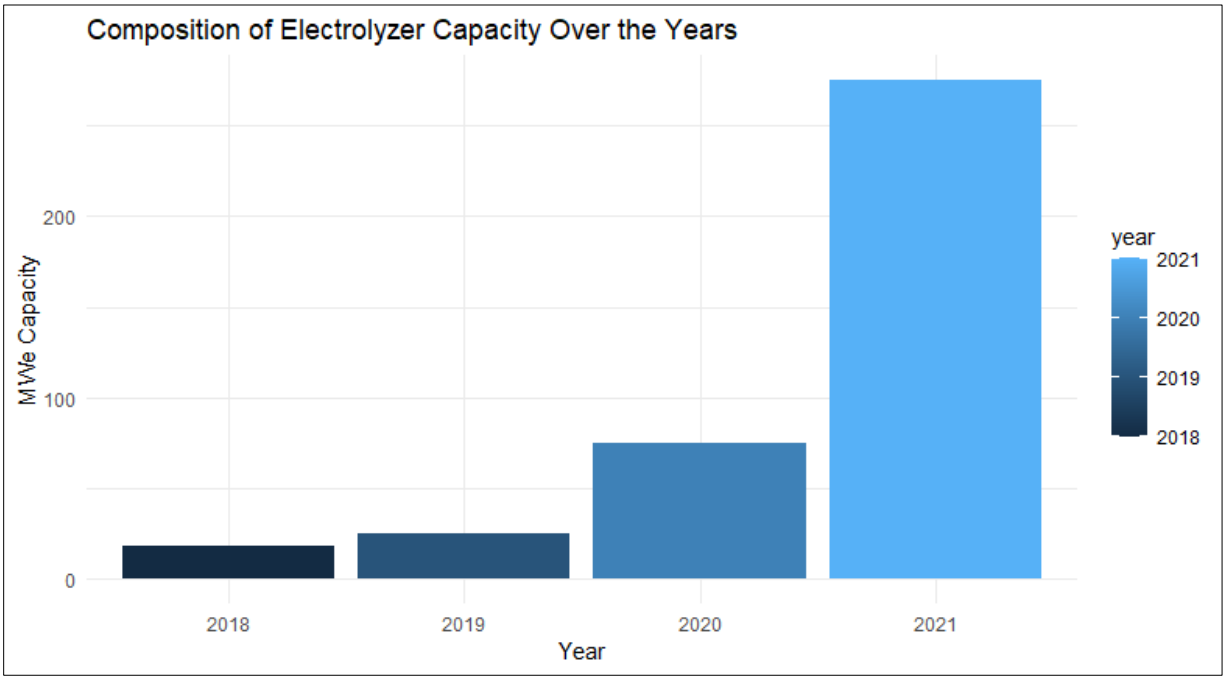

Figure 2. 2: Capacity of electrolyzers for hydrogen production by commissioning year [31]

There was a substantial growth in electrolyzer capacity from 2020 to 2021. With an increasing number of companies committing to net-zero emissions, the demand for clean hydrogen in various applications, from ground transportation to power generation, has surged. All of which require

increased electrolyzer capacity. The flexibility and versatility of hydrogen, along with the economic incentives provided by the IRA, have made it a game-changer in the journey to achieving net-zero emissions in the U.S. The collaborative approach among industry players and government initiatives, such as the Regional Clean Hydrogen Hubs program, is driving the growth of the hydrogen sector and positioning the US as a leader in the global hydrogen economy [32].

2.4. Investment in Hydrogen Energy

As of mid-2021, hydrogen stood out as a particularly promising fuel source, with a more positive outlook than pre-pandemic times, despite facing challenges during the outbreak. The key driving force behind this positive trend was the extensive economic recovery initiatives introduced worldwide. While the utilization and production of low-carbon hydrogen remain somewhat limited at present, the expectations for its future growth have never been higher. In 2020, investments in the low-carbon hydrogen sector reached unprecedented levels, consisting of four key categories: project planning, project completion, equipment production, and equity acquisitions. The activation of new electrolyzer facilities in 2020 alone suggests that capital expenditures in the low-carbon hydrogen sector are prepared for significant expansion. During 2020, global expectations centered around the completion of 65 megawatts of water electrolyzer plants for energy applications. Although this figure fell short of the initial 140 megawatts projected by developers at the start of the year, it still marked a more than twofold increase compared to 2019 levels. These electrolyzer projects were designed for a range of hydrogen applications, including industrial use and vehicle fueling. In Europe, industries such as steel and refining have garnered considerable attention as potential early adopters of in-house, low-carbon hydrogen production. Nevertheless, it's worth noting that most of the larger-scale electrolyzer projects are initially planned to utilize

grid electricity rather than focusing exclusively on low-carbon hydrogen production. Furthermore, along with the installation of electrolyzer facilities, there have been record highs in stock investments in electrolyzer technology companies and substantial investment activities in electrolyzer manufacturing. The surge in investments and the acceleration of hydrogen projects, highlighted by our study, offer substantial practical implications for the energy industry.

They indicate a clear direction for future energy infrastructures and investment strategies, urging companies to adapt to a rapidly evolving market where sustainability and green technologies become key competitive differentiators [33]. Efforts to drive change and foster innovation depend on providing the necessary nurturing environment. Governments worldwide have recognized the importance of hydrogen energy and have extended support through investments, incentives, and initiatives. China, after initially treading cautiously, has emerged as a significant player in the deployment of electrolysis technology. Projections indicate that China is on track to achieve an impressive installed electrolysis capacity of 1.2 GW by the close of 2023, representing a substantial 50% of the global capacity. Notably, a groundbreaking electrolysis project, having a record-breaking capacity of 260 MW, has initiated operations this year, highlighting China's remarkable progress in this field [34]. Simultaneously, The Biden-Harris Administration, as part of the Investing in America agenda, has allocated $7 billion to establish seven Regional Clean Hydrogen Hubs (H2Hubs) across the United States. These H2 Hubs are pivotal for accelerating the deployment of low-cost, clean hydrogen to achieve climate and energy security goals. Supported by the Bipartisan Infrastructure Law, these hubs will collectively produce three million metric tons of hydrogen annually, reducing emissions from hard-to-decarbonize sectors and creating tens of thousands of jobs. The investment aims to strengthen the clean manufacturing sector and reduce harmful emissions. Each H2 Hub mrequst develop a Community Benefits Plan

to ensure the clean energy transition benefits impacted communities. Additionally, DOE is soliciting a U.S. entity to execute a demand-side initiative to support the clean hydrogen economy's long-term success [35]. The federal government's significant investment of $7 billion will be supplemented by over $40 billion from H2 Hub selectees, along with tax incentives and continued research and development endeavors. This will encourage private sector investment in clean hydrogen. This initiative highlights the commitment to build an equitable and inclusive clean energy future while promoting the growth of emerging clean energy industries. The H2 Hub represents a critical step toward achieving long-term decarbonization objectives and addressing the climate crisis. As the success of hydrogen energy development relies on widespread acceptance, assessing public sentiment is crucial. Understanding the viewpoint of the public, who are the ultimate consumers, allows the private sector to adapt their offerings in alignment with public sentiment and preferences, thereby facilitating the broader adoption of hydrogen energy solutions. Figure 2.3 [31] illustrates the different investment stages of hydrogen-based energy companies from 2019 to 2021.

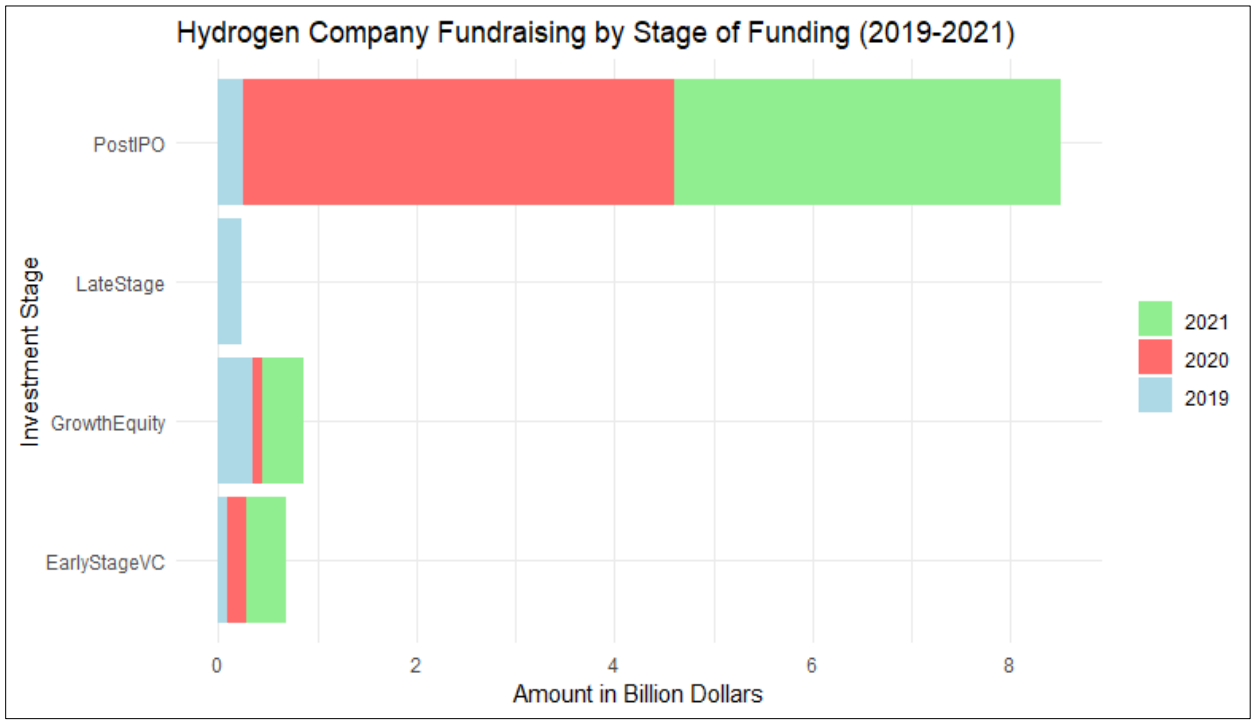

Figure 2. 3: Investment stages of hydrogen-based energy companies [31]

Companies listed on stock exchanges played an important role in securing the bulk of the additional capital for the hydrogen sector in both 2020 and 2021. To fuel the expansion of their manufacturing facilities, organizing projected demands for electrolyzers and fuel cells, these companies opted to issue new shares to attract investment. Investors in hydrogen-related enterprises remained strong throughout the initial half of 2021. This was partly driven by the expectation that these efforts would gain government backing through recovery programs [34].

2.5. Global Budgeting for Hydrogen Energy

Government initiatives are considered as a driving force behind the rise in hydrogen investment. These initiatives include funding within COVID-19 recovery plans and the establishment of long-term directives within national hydrogen programs. This public investment is expected to catalyze

a substantial increase in private sector spending, thus expediting the adoption of hydrogen technology. As a case in point, Germany unveiled a EUR 9 billion package as part of its national hydrogen strategy, with the German government projecting an additional EUR 33 billion in private sector investments as a result. On a global scale, the business sector has displayed a remarkable eagerness for investment in hydrogen-related projects. The Hydrogen Council reports that private sector commitments have already exceeded USD 300 billion through 2030, despite only USD 80 billion in funding having been formally pledged [34]. In its June 2023 update, the IEA Government Energy Spending Tracker reports that governments worldwide have allocated an impressive USD 1.34 trillion since 2020 to support clean energy investments. This substantial government spending has played an important role in driving the rapid growth of clean energy investments, overtaking the growth in fossil fuels by nearly 25% from 2021 to 2023. The latest expenditures primarily focus on enhancing mass transit options, low-carbon electricity generation projects, and promoting low-carbon vehicle sales. Notably, direct incentives for manufacturers aimed at boosting domestic production of clean energy technologies now total around USD 90 billion. Additionally, governments have allocated USD 900 billion for short-term consumer affordability measures since the start of the global energy crisis, complementing pre-existing support programs and subsidies. However, there is room for improvement in targeting these measures, with only 25% directed towards low-income households and the most affected industries. The European Union has taken the lead in providing consumer affordability support, accounting for two-thirds of such spending globally, largely in response to steep increases in electricity and gas prices in 2022. It is worth noting that consumer support spending has also risen in emerging and developing economies, as governments compensate energy companies to stabilize prices during the crisis. Nevertheless, the imbalance between supporting consumers and investing in clean energy could challenge some

countries' efforts to balance short-term relief with long-term energy security and affordability goals. This challenge is particularly pronounced in emerging markets and developing economies due to pre-existing financial strains. Consequently, a majority of spending on both affordability and clean energy investments remains concentrated in advanced economies, which represent 93% of total government clean energy investment support and 85% of consumer affordability support followed to date [36]. As revealed in our analysis, the governmental focus on hydrogen energy emphasizes its societal implications. By driving the transition to clean energy, these policies aim to reduce environmental impact, enhance energy security, and offer economic opportunities through job creation in green industries. For society, this transition promises a cleaner environment and a shift towards a more sustainable and resilient economy.

2.6. Deployment of Fuel Cell Vehicles and Hydrogen Refueling Station Infrastructure

Figure 2.4 illustrates the progression in the utilization of Fuel Cell Vehicles (FCVs) from 2017 to 2021 [37]. While data collection for all vehicles started in 2018, the initial passenger car statistics date back to 2017. It can be noted that the Toyota Mirai was introduced in Japan at the close of 2014, and Hyundai initiated leasing the ix35 Fuel Cell, the world's first mass-produced fuel cell vehicle, in the United States in 2014. In the scope of passenger automobiles, the most significant rise of 69% occurred from 2018 to 2019, closely following a 56% rise in the annual deployment rate from 2017 to 2018.

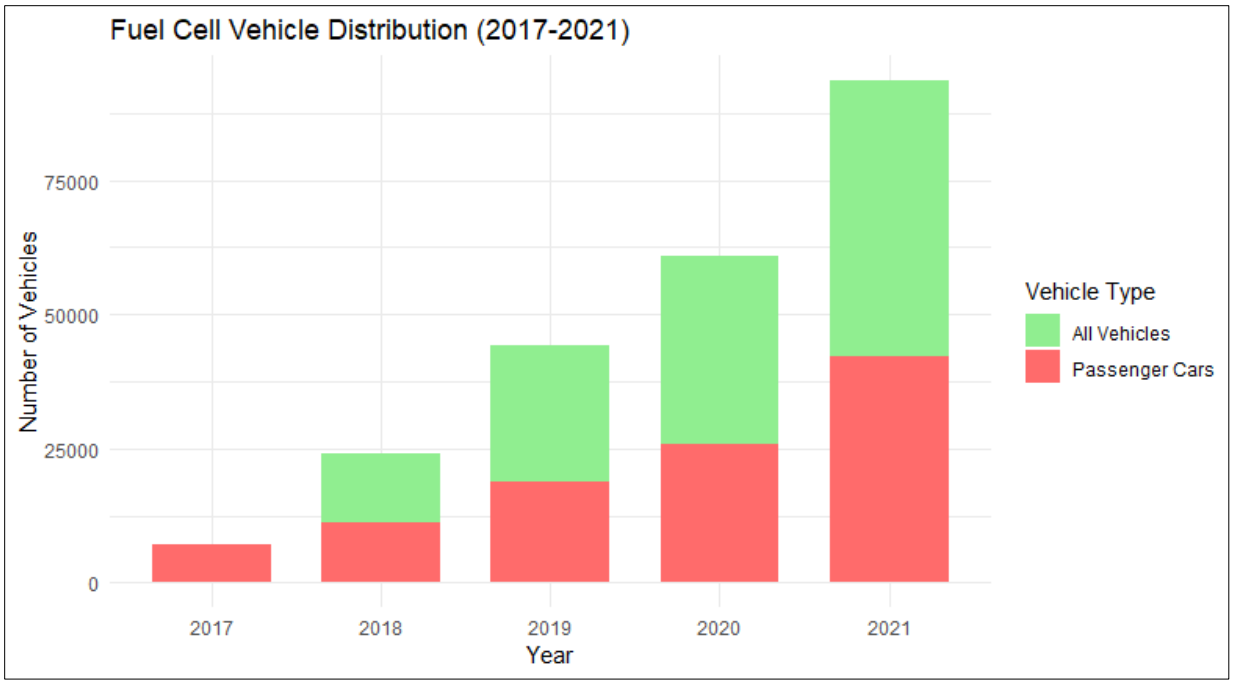

Figure 2. 4: Development of fuel cell vehicles at pre- and post-pandemic period [37]

The worldwide economic slowdown induced by the COVID-19 pandemic is a primary factor contributing to the decline in the growth rate to 37% in 2020. In contrast, the growth rate recovered to 63% in 2021, nearing the pre-pandemic peak rate of 69%. This recovery aligns with the early stages of economic recovery during that year. However, a direct comparison with 2019, which had 7,701 units, reveals that the increase in 2021, with 16,260 passenger cars, is remarkably more substantial. Relying solely on the annual growth rate partially captures the overall development, as the number of fuel-cell passenger cars continues to rise. Therefore, it's essential to extend the growth rate with an absolute increase. The exceptional growth rate of 95% from 2018 to 2019 did not persist in subsequent years, consistent with the trends in all FCVs. In 2020, there was a growth rate of 38%, parallel to the growth rate of passenger cars. A significant improvement was observed in 2021, with a rapid 48% increase within a single year.

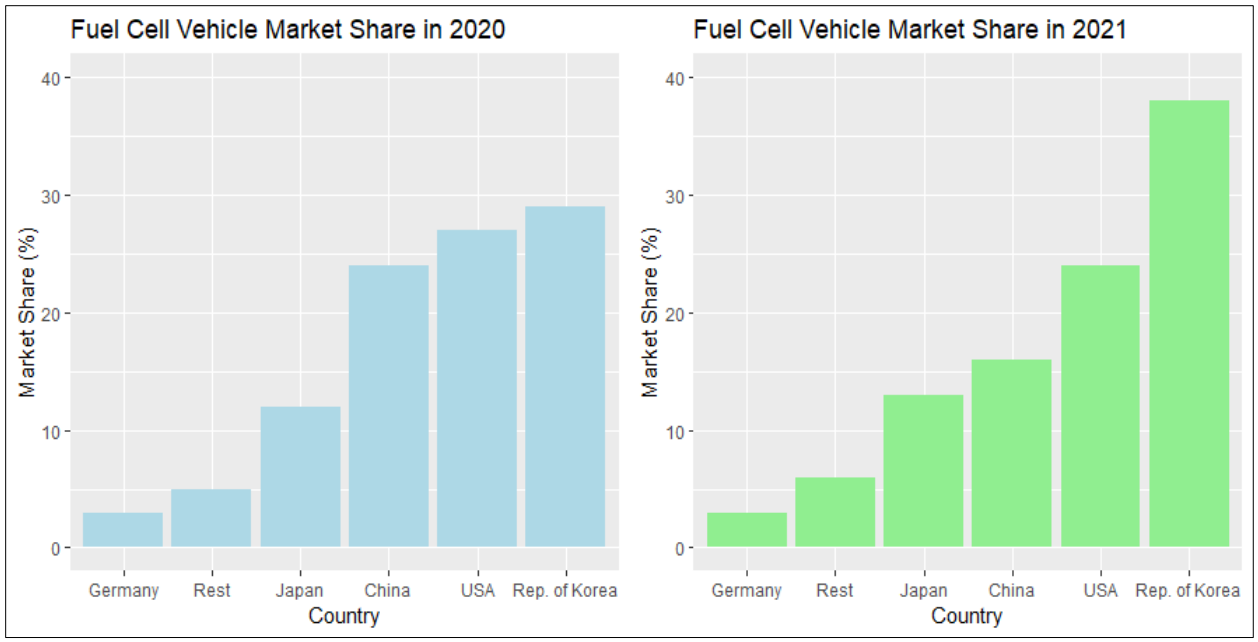

Figure 2. 5: The FCVs in the top five countries on the road by 2021[37]

Figure 2.5 shows the FCVs in the top five countries on the road by 2021. As of the end of 2021, the top five nations with at least 1,000 fuel cell vehicles on the road are used to analyze the shift in global market shares from 2020 to 2021. While the ranking remained unchanged in 2021, South Korea saw a significant increase in its vehicle shares, rising from 29% to 38%. This increase had a corresponding impact, leading to a decrease of three percentage points for the United States and eight percentage points for China. Germany maintained its share at 3%, while Japan and the rest of the world observed marginal increases. It's worth noting that only 31 FCVs are currently registered in China, as revealed in an examination of absolute numbers for that nation [37, 38]. An analysis of data across various vehicle categories in China indicates that in 2021, more MD (370 new units) and HD (796 new units, all new) trucks were produced, but there were 1,140 fewer buses. The decrease was attributed to an overestimation in the previous year, where the figures included planned but unproduced and unutilized vehicles, as reported by vehicle manufacturers. The current figures, however, are based on actual vehicle registrations in China [39]. The

expansion of FCVs and hydrogen infrastructure, as discussed in our findings, signals important implications for both the automotive industry and the broader society. It highlights the growing consumer acceptance and the potential for hydrogen to play a pivotal role in decarbonizing transport, thereby reducing urban pollution, and contributing to public health benefits [40].

2.7. Global energy challenge and Hydrogen

As industrialization spreads and living standards increase, energy demand continues to rise [41]. Currently, majority global power is produced by burning fossil fuels [42]. Despite its technological advancement, this method has a maximum efficiency of around 50%, contributes to nearly 35% of global greenhouse gas emissions, and has become more costly and less reliable due to recent fluctuations in oil prices. Therefore, ensuring a reliable energy supply and addressing climate change are two primary concerns for the future of the energy industry [43]. These concerns emphasize the necessity to find effective ways to reduce emissions while still meeting the energy needs essential for economic growth [44]. Renewable energy sources, including wind, solar, micro-hydro, wave, geothermal, and biomass, offer potential solutions to the clean energy dilemma, although they present their own set of challenges [45, 46]. Using energy storage systems to store renewable energy can help incorporate these fluctuating, weather-dependent energy sources and maintain grid stability [47].

Hydrogen energy storage technology is proposed as an effective method to support and utilize the world's abundant yet intermittent renewable energy resources [47]. Hydrogen offers solutions to various important energy challenges. It provides a pathway to reduce carbon emissions in sectors like long-haul transport, chemicals, and iron and steel production, where significant emission

reductions are challenging [47, 48]. Additionally, hydrogen contributes to improving air quality and enhancing energy security. Despite ambitious global climate targets, energy-related CO_2 emissions hit a record high in 2018 [49]. Outdoor air pollution also continues to be a significant issue, causing approximately 3 million premature deaths annually [50, 51]. Hydrogen is a versatile energy carrier. Existing technologies allow hydrogen to be used for producing, storing, transporting, and utilizing energy in diverse ways. A variety of sources, including renewable energy, nuclear power, natural gas, coal, and oil, can produce hydrogen. It can be transported either as a gas through pipelines or in liquid form by ships, parallel to liquefied natural gas (LNG) [49,50]. Furthermore, hydrogen can be converted into electricity and methane to power homes and industries, and into fuels for vehicles such as cars, trucks, ships, and planes [48,52]. Hydrogen can significantly enhance the contribution of renewable energy sources. It is particularly useful in managing the variable output from renewable sources like solar photovoltaics (PV) and wind, which often do not align with energy demand. Hydrogen is a leading solution for storing renewable energy, and it is emerging as the most cost-effective option for long-term storage of electricity across days, weeks, or even months. Hydrogen and hydrogen-based fuels can also transport energy over long distances, from areas rich in solar and wind resources like Australia or Latin America to energy-intensive urban centers thousands of kilometers away. Today, hydrogen is primarily used in oil refining and fertilizer production. For hydrogen to significantly impact clean energy transitions, it must also be adopted in sectors where it is currently almost non-existent, such as transportation, building heating, and power generation [48].

2.8. Role of Hydrogen in Transportation

To achieve full decarbonization of road transportation, it is imperative to prioritize the advancement of alternative, low-carbon fuels and more efficient propulsion systems in long-term strategies. Electric-drive vehicle options include pure battery electric vehicles (BEVs), fuel cell electric vehicles (FCEVs), and plug-in hybrid electric vehicles (PHEVs). BEVs rely on electricity stored in their batteries, while FCEVs utilize hydrogen stored onboard and converted into electricity via a fuel cell. PHEVs combine a battery system with either an internal combustion engine (ICE) or a fuel cell system [53]. Both BEVs and FCEVs, along with battery/fuel cell-based PHEVs, are acknowledged as genuine zero-emission vehicles, emitting no CO2 or local air pollutants during operation [53, 54]. A comparison of fuel cost between hydrogen and gasoline-based vehicles is outlined in Table 2.2 [52, 55]. This study is based on the same models with a gasoline engine and a hybrid engine running for a 100 kilometers Journey. A few models, ie. Audi A2H2, Volkswagen Touran HyMotion 2004, Volkswagen Touran HyMotion 2007, KIA Borrego FCEV, KIA Sportage, Mazda, Hyundai have almost equal or lower costs of fuel, whether on gasoline or hydrogen. Once hydrogen is produced locally, assuming a 30% reduction in the price of production, the estimated cost of using hydrogen as a fuel is far lower than that of gasoline.

Table 2. 2: Fuel cost comparing several hydrogen and gasoline-based vehicles [52-55]

Vehicle Manufacturer	Vehicle Model	Distance with hydrogen fuel (km)	Fuel consumption with gasoline (l/100 km)[a]	Capacity of hydrogen storage (kg)	Gasoline Cost (US$/100 km)	Hydrogen Cost (US$/100 km)	Estimated Cost with Local Hydrogen (US$/100 km)[b]
BMW	Hydrogen 7 (V12 6.0I ICE)	201	13.9	8	13.43	19.90	13.93
Audi	A2H2	220	5	1.8	4.83	4.09	2.86
Toyota	FCHV bus	690	–	6	–	4.35	3.04
Volkswagen	Touran HyMotion 2004	160	7.2	1.9	6.96	5.94	4.16
Volkswagen	Touran HyMotion 2007	230	6.5	3.2	6.28	6.96	4.87
GM	Hydrogen Minivan	270	–	3.1	–	5.74	4.02
GM	H2H Hummer (V8 ICE)	100	17	5.5	16.42	27.49	19.25
KIA	Borrego FCEV	690	13	7.9	12.56	5.72	4.01
KIA	KIA Sportage	400	8	3.5	7.73	4.37	3.06
Honda	FCX Clarity	430	–	2.7	–	3.14	2.20
Mitsubishi	Lancer Evo IX Hydrogen	110	8.7	2.2	8.40	10.00	7.00
Peugeot	207 Epure (ICE and FC)	350	6.6	3	6.38	4.28	3.00

Vehicle Manufacturer	Vehicle Model	Distance with hydrogen fuel (km)	Fuel consumption with gasoline (l/100 km)[a]	Capacity of hydrogen storage (kg)	Gasoline Cost (US$/100 km)	Hydrogen Cost (US$/100 km)	Estimated Cost with Local Hydrogen (US$/100 km)[b]
Mazda	Premacy Hydrogen RE Hybrid	200	11	2.4	10.63	6.00	4.20
Daimler	B-Class F-Cell	400	6	11.1	5.80	13.87	9.71
Mercedes-Benz	F125 Concept	1000	–	7.5	–	3.75	2.62
Hyundai	Tucson FCEV	650	7.5	5.6	7.25	4.31	3.01

ICE, internal combustion engine; FC, fuel cell; FCEV, fuel cell electric vehicle.
[a] Based on the same models with gasoline engines or the same vehicles with hybrid fuel consumption.
[b] Based on a 30% reduction in the costs of production.
[c] No gasoline model has been produced.

2.9. Role of Hydrogen in Domestic Power

Fuel cell heaters, utilizing hydrogen as an energy source, represent an innovative approach to home heating. Unlike traditional heaters that combust gas or oil to produce heat, fuel cell heaters react hydrogen with oxygen, generating both electricity and heat [57]. This process doesn't involve burning hydrogen. An advantage of hydrogen-based heating is the potential to utilize the existing gas network for its transportation and leverage conventional technologies for storage [54,57]. This approach is more cost-efficient, reducing the need for expensive new infrastructure for hydrogen transmission and distribution, and minimizes disruptions. Figure 2.6 presents a cost comparison of various hydrogen heating technologies for households [58].

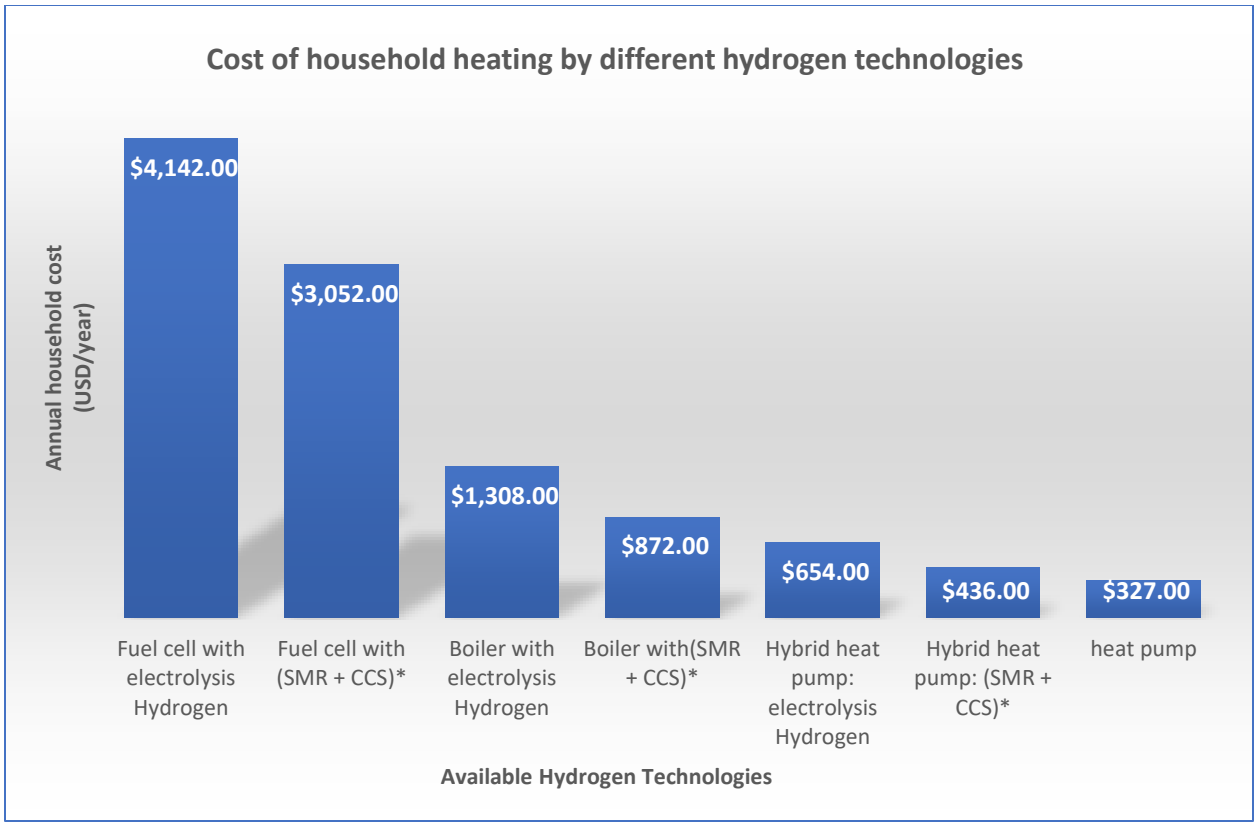

Figure 2. 6: Cost of Household Heating by Different Hydrogen Technologies [58]
*Steam methane reforming (SMR) with Carbon Capture and Storage (CCS)

From Figure 2.6, it is clear that hydrogen produced by electrolysis in fuel cell is the expensive option for household heating, reaching about 4142 USD. Any technology, when partnered with electrolysis, bumps up the cost while using the same technology with steam methane reforming and carbon capture reduces the expense. Figure 2.7 and 2.8 illustrate the comparison between the current demand for natural gas and the theoretical demand for hydrogen (H2) for heating in buildings across seven countries. For hydrogen to replace natural gas in heating systems, its usage in current heating equipment must be practical, and its production, transmission, and distribution costs should be competitive with natural gas, the current standard for heating. This projects natural gas demand for space heating and hot water production following improvements in building insulation as outlined in the Paris-compatible pathway. The "indicative demand" in Figure 2.9

suggests the theoretical hydrogen demand, assuming its production, transmission, and distribution are competitively priced. It also takes into account the typical lifespans of existing heating equipment, without considering premature equipment replacement. From this data, it is evident that hydrogen-based heating technologies still face significant challenges in competing with natural gas on a global scale, as the indicative demand for hydrogen is considerably lower than the current global demand for natural gas. Comparison between the demand for natural gas vs theoretical hydrogen for domestic heating are depicted from Figure 2.7, Figure 2.8 and Figure 2.9 [59].

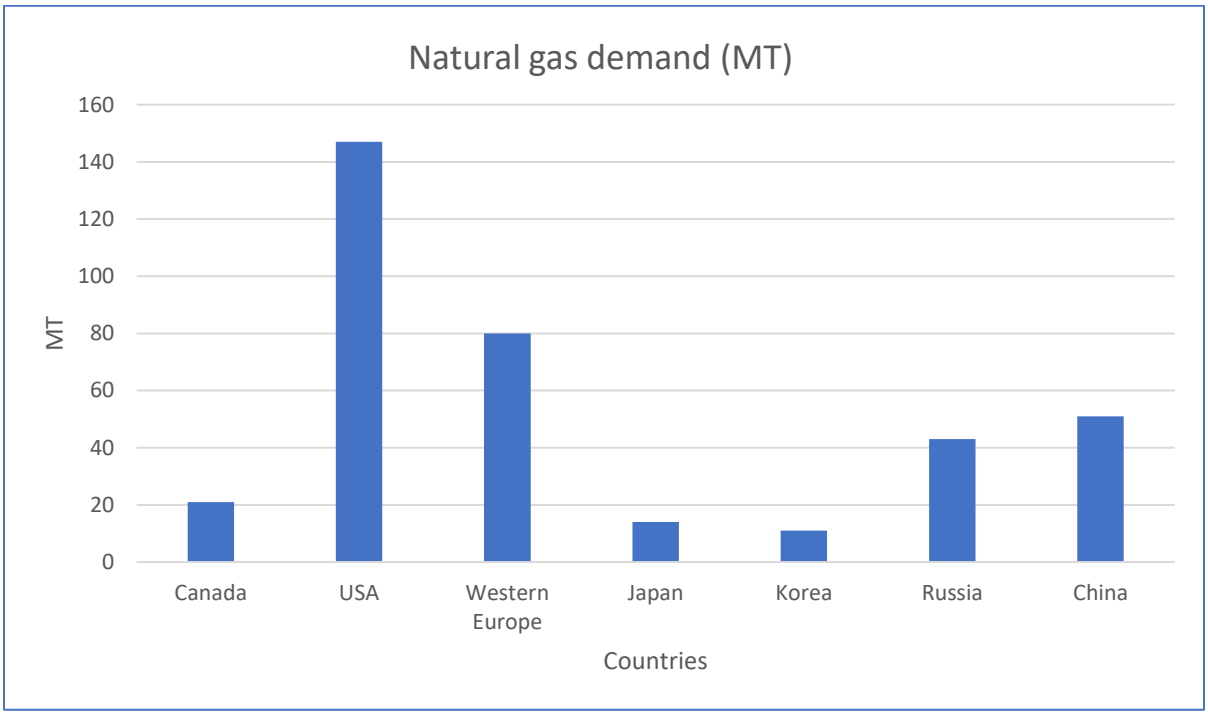

Figure 2. 7: Comparison in natural gas demand in MT [59]

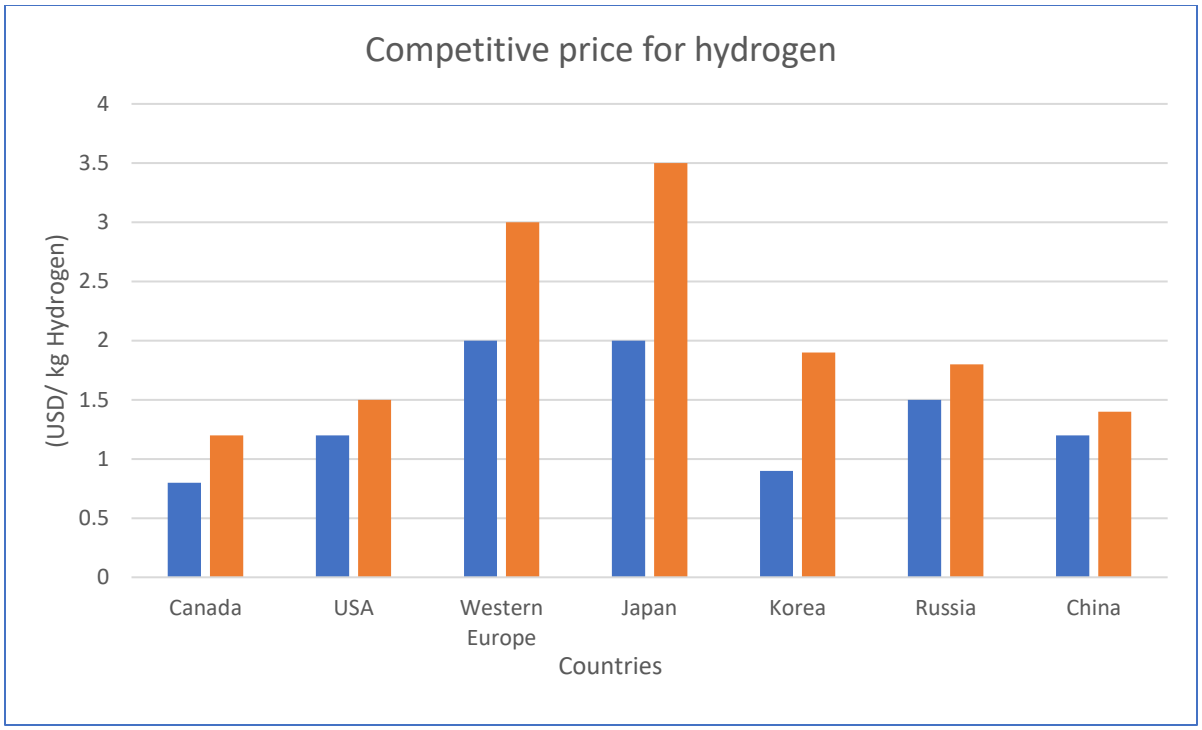

Figure 2. 8: Comparison in Competitive price for hydrogen [59]

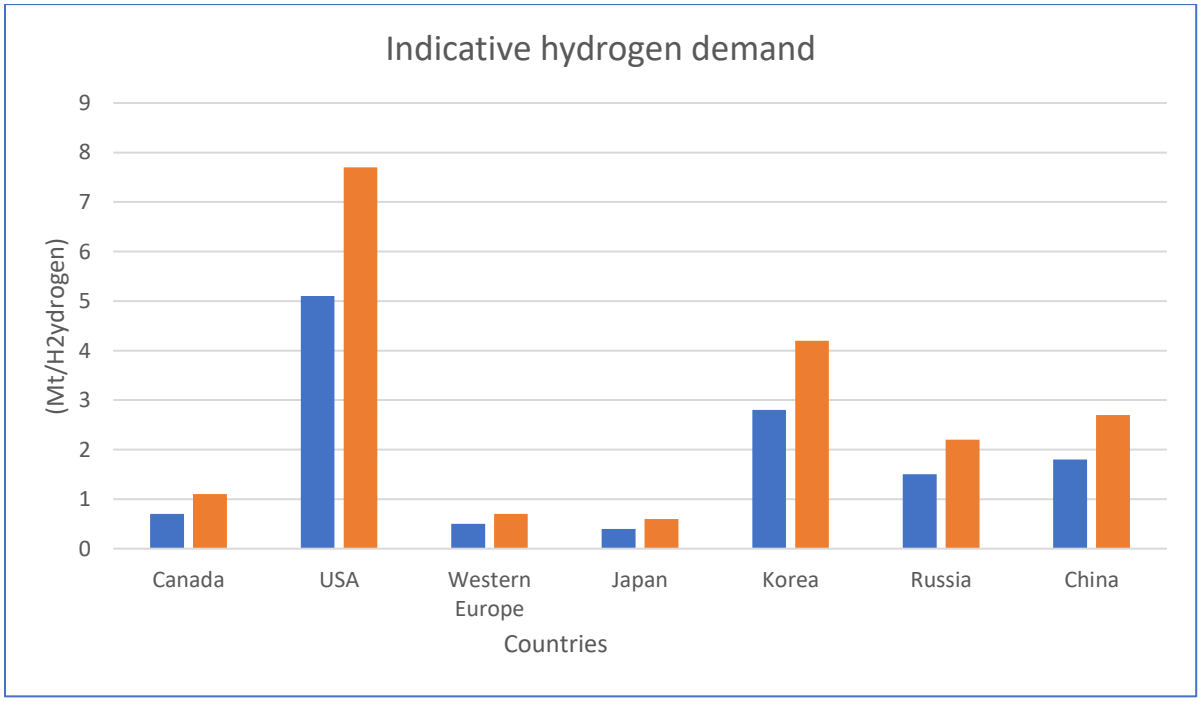

Figure 2. 9: Comparison in Indicative hydrogen demand [59]

2.10. Role of Hydrogen in Power Generation

Hydrogen and its derivatives are increasingly impacting the power generation sector. Their roles include enhancing flexibility in power generation, providing off-grid power solutions, and offering long-term energy storage. Table 2.3 details these roles along with current and emerging demand sectors, plus the future potential or challenges in deployment. The primary challenges in implementing hydrogen-based products are the competition with other more adaptable and feasible power generation methods, substantial initial investments, and significant energy loss during storage conversion. However, future deployment opportunities such as integrating variable renewable energy into the power system, serving as an eco-friendly alternative to diesel generators, and offering low capital expenditure (CAPEX) for storage, position hydrogen and its derivatives as promising options in power generation. Table 2.3 summarizes these prospects, challenges, and opportunities in hydrogen for power generation [59].

Table 2. 3: Role of hydrogen in power generation into current role and future opportunities [59]

Focus Area	Current Role	Demand Perspectives	Future Deployment Opportunities	Future Deployment Challenges
Flexible power generation	Limited adoption of commercial gas turbines operating with hydrogen-rich gases. Installed Capacity: 363,000 fuel cell units (1,600 MW)	Transitioning 1% of global gas-fired power capacity to hydrogen by 2030 could generate 90 TWh of electricity and consume 4.5 Mt H2.	• Some gas turbine designs operate on high hydrogen percentages •Supporting the integration of VRE in the power system	• Availability of low-cost and low-carbon hydrogen and ammonia. • Competition with other flexible generation options and flexibility alternatives such as demand response and storage.
Back-up and off- grid power supply	•Demonstration projects for village electrification. • Fuel cell systems combined with storage.	Increasing demand for reliable power supply, especially with the expansion of telecommunications.	Fuel cell systems in combination with storage as a cost-effective and less polluting alternative to diesel generators	• Higher initial investment compared to diesel generators
Long-term and large-scale energy storage	Three hydrogen salt cavern storage sites in the US and another three in the UK	Growing need for large-scale and long-term storage to address seasonal variations in Variable Renewable Energy (VRE) generation. Possibility to capitalize on global VRE supply seasonal differences through long-distance trade.	• Relatively low CAPEX costs for hydrogen storage due to its high energy content. Limited alternative technologies for long-term and large-scale storage. • Conversion losses can be mitigated if stored hydrogen or ammonia can be directly utilized in end-use applications	• High conversion losses. Geological availability of salt caverns for hydrogen storage region-specific. • Limited expertise in utilizing depleted oil and gas fields or water aquifers for hydrogen storage, which may lead to contamination issues
Note: VRE = variable renewable energy.				

2.11. Role of Hydrogen in Reducing GHG Emissions

Full lifecycle greenhouse gas (GHG) emissions of battery and fuel-cell electric vehicles (EVs) registered in 2021 is depicted in Figure 2.10, with a projected usage period of 15 to 18 years in Figure 2.11 [60]. For battery EVs, GHG emissions from “fuel/electricity” production mainly arise from coal and natural gas used in power generation. This total also includes GHG emissions from manufacturing solar panels and wind turbines that generate renewable electricity for battery EVs, as well as losses in electricity transmission and EV charging. In the second chart, the increasing integration of renewable energy by 2030 significantly improves the lifetime climate performance of vehicles registered that year. Consequently, the life cycle GHG emissions for both battery and hydrogen fuel-cell EVs of 2030 models are substantially lower than those of 2021 models. In contrast, the GHG emissions from gasoline, diesel, and natural gas vehicles remain almost unchanged. Over time, the environmental advantages of using EVs compared to gasoline, diesel, and natural gas vehicles become more pronounced. [61].

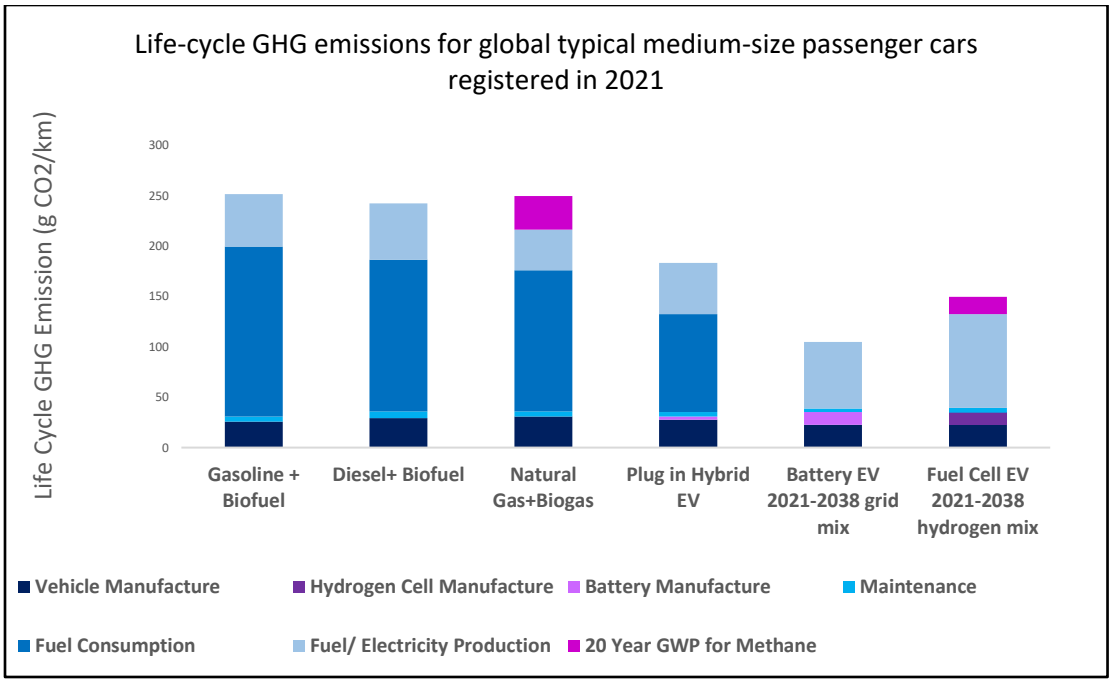

Figure 2. 10: Lifecycle GHG emissions for cars registered in 2021[60]

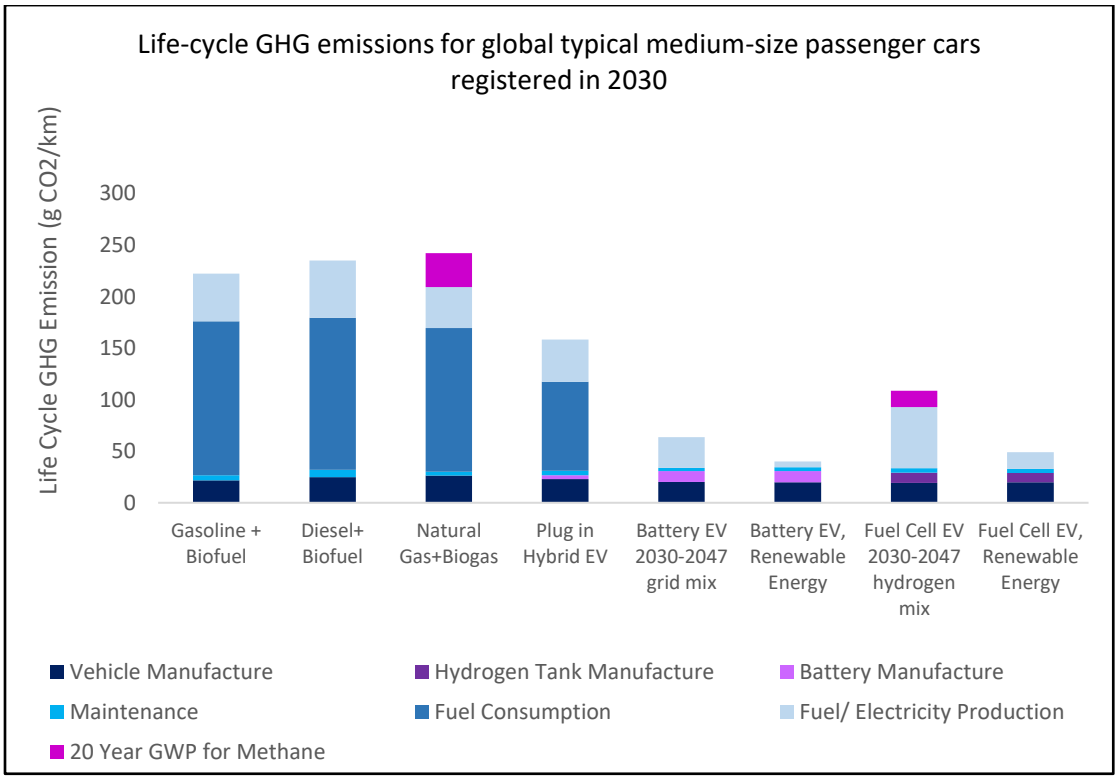

Figure 2. 11: Lifecycle GHG emissions for cars registered in 2030 [60]

2.12. Global Hydrogen Market Dynamics

Hydrogen, as an energy carrier, has the potential to significantly impact the global energy setting, both currently and in the future. Its application covers a diverse range of sectors, from transportation, where hydrogen fuel cell vehicles offer an alternative to fossil fuel-powered and battery-electric vehicles, to industrial processes, particularly in refining and ammonia production, where it's already extensively used [62,63]. The push towards green hydrogen, produced through water electrolysis powered by renewable energy sources, emphasizes its role in decarbonizing sectors challenging to electrify, such as heavy industry and long-haul transportation [62]. However, challenges remain in the form of production costs, storage, and transport of hydrogen, as well as the need for substantial investment in infrastructure to support its widespread adoption. Future prospects for hydrogen utilization are vast and include blending into natural gas pipelines to reduce carbon intensity, in power generation for grid balancing and storage, and as a raw material in the production of synthetic fuels and chemicals, thereby further extending its applicability across the energy system. Nevertheless, the criticality of ensuring a sustainable and environmentally beneficial hydrogen economy cannot be overstated. This involves addressing the environmental impact of current hydrogen production methods predominantly from fossil fuels and ensuring that the shift towards green hydrogen production scales up with the expansion of renewable energy capacities. The development of international standards and policies supporting hydrogen's integration into the energy system, alongside technological innovation and cost reduction in electrolysis and other production methods, are obvious for realizing hydrogen's full potential. As such, hydrogen stands as a prospective energy carrier for a sustainable, low-carbon energy future, provided that the challenges in its path are effectively addressed [64, 65].

Figure 2.12 (a),(b),(c)) provides a comprehensive overview of the global hydrogen market, showing the geographic distribution of hydrogen consumption in 2020 (a), the top importers of hydrogen in 2021 (b), and the leading exporters of hydrogen in 2021 (c) [66]. In Figure 2.12(a), we see a breakdown of where hydrogen was consumed around the world in the year 2020. China stands out as the largest consumer, using 33% of the total hydrogen consumed globally. Following closely behind are the Middle East and Europe, each accounting for approximately 20.6% of the consumption. The United States also plays a significant role, accounting for 15.5% of the total consumption. Other regions, including Asia, Africa, and South/Central America, collectively make up 10.3% of the global hydrogen consumption. This distribution of hydrogen consumption provides insights into its versatile usage across regions globally. It highlights regions where hydrogen plays a critical role in various industries, facilitating strategic planning and investment in hydrogen infrastructure for its continued growth and development worldwide. Figure 2.12 (b) describes the top importers of hydrogen in 2021. China remains a significant trader, with 32% of imports. Japan (19%) and Germany (12%) are other major importers, followed by South Korea (10%), the United States (8%), and Taiwan (7%). The Netherlands also appears on the list with 6%. Figure 2.12 (c) outlines the top exporters of hydrogen in 2021. The United States emerges as a key exporter with 20% of the market share, closely followed by Germany at 21%. China's exports account for 32%, which is substantial but not surprising given its leading role in imports as well. Japan, Norway, and Brazil represent 10% of exports together, with Malaysia at 9% and Qatar at 8%. These figures collectively imply that China is a central candidate in the global hydrogen market, with significant stakes in all three trade sectors: consumption, importing, and exporting. European countries and the United States also play vital roles, indicating a diverse and global spread of hydrogen energy commerce. These observations emphasize the vital role of hydrogen in

the transition to cleaner energy and show the importance of continued investment in hydrogen infrastructure for its global expansion and development.

Figure 2. 12: (a) Geographic split of hydrogen consumption, 2020; (b) Top importers of Hydrogen, 2021; (c) Top exporters of Hydrogen, 2021 [66]

2.13. Projection of Hydrogen Demand

As we explore the future prospect of hydrogen utilization, it's important to examine the projected demand trends. Figure 2.13 shows the hydrogen demand potential in terawatt-hours (TWh) across various sectors for 2030 and 2050 in the US and Europe [67,68]. It indicates significant growth in the total hydrogen share of final energy demand by 2050, particularly in Europe. The existing industry feedstock stays stable across the years. The transportation sector sees an increase in hydrogen demand, indicating a shift toward hydrogen-fueled transport. Hydrogen use for residential and commercial buildings is projected to rise, although it remains relatively small compared to other sectors. For power generation and grid balancing, the demand is expected to increase, reflecting hydrogen's role in energy storage and managing intermittent renewable energy supplies. New industry feedstock shows moderate growth, suggesting new applications for hydrogen in future are depicted at Figure 2.13 [20,21]. This aligns with global efforts being made by nations to prevent climate change and promote sustainability. This suggests that hydrogen has the potential to significantly improve both the health of our planet and the strength of our economies. Variations in hydrogen demand over time and between countries are influenced by several factors, including economic situations, technological breakthroughs, government regulations, and the degree to which each region is committed to addressing climate change. Variations in demand trends point to the need for a planned response to environmental problems, energy security, and the viability of hydrogen production and use. It implies that areas are organized to undertake environmental issues, meet their energy requirements, and assess the viability of producing and utilizing hydrogen. These changes in consumer demand demonstrate an attempt to progress toward a more sustainable future.

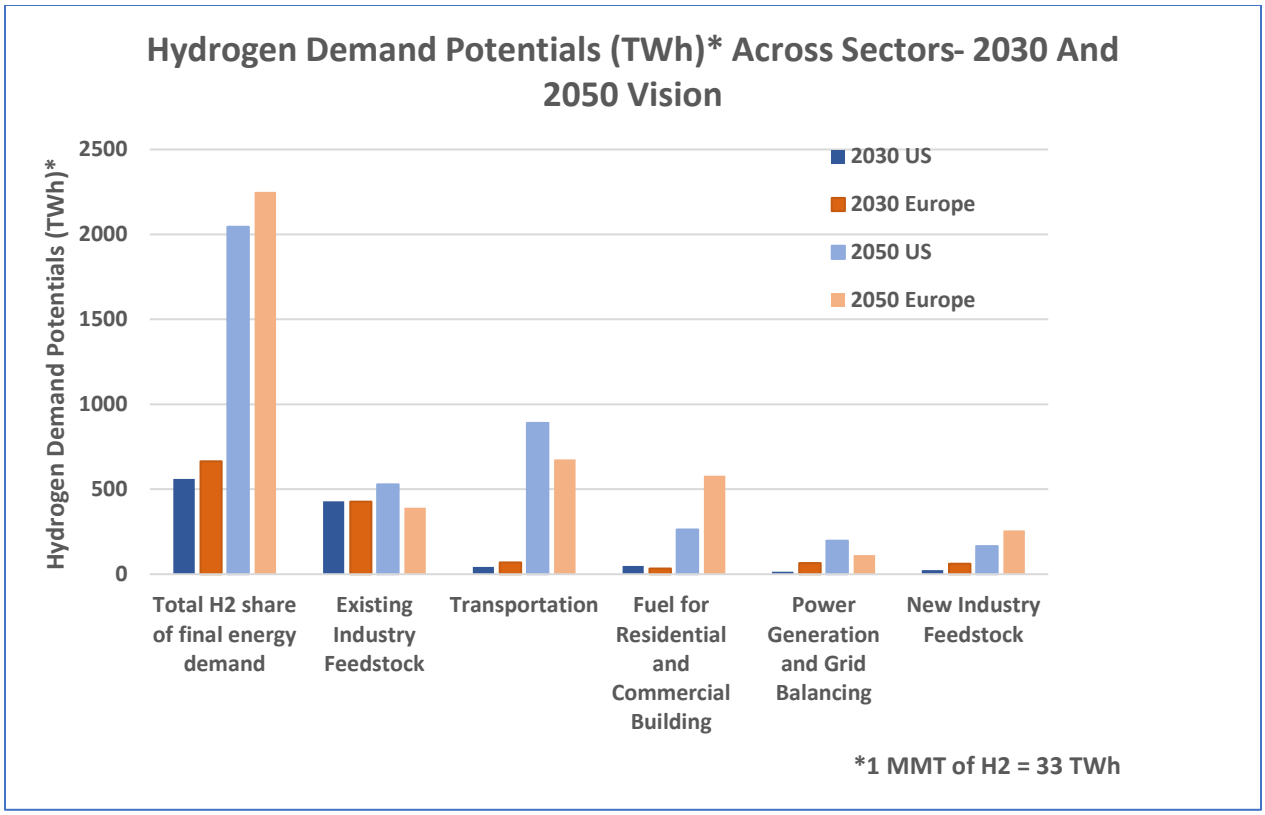

Figure 2. 13: Hydrogen Demand Potentials (Twh) Across Sectors- 2030 And 2050 Vision [20,21,67,68]

The US shows a significant anticipated increase in hydrogen demand for existing industry feedstock by 2050 compared to Europe. Europe places a greater emphasis on hydrogen for transportation and power generation by 2050, likely reflecting more effective policies towards decarbonization and renewable energy integration. By 2050, both Europe and the United States expect a significant increase in the amount of hydrogen required across numerous industries. This indicates that developing a cleaner energy system is important to both regions, and hydrogen is one of them. It indicates that awareness of the significance of hydrogen for the transition to a greener future is beginning to spread. Both regions are preparing for the widespread use of hydrogen in various applications, including manufacturing, power plants,

and automobiles. The biggest difference in the 2030 and 2050 potentials is in the transportation field, where the demand has grown exponentially in both the US and Europe [67,68].

In the announced pledges scenario, hydrogen is mostly used in sectors like industry and transport. In Figure- 2.14 (a), the effect of rising renewable energy penetration becomes more pronounced as it is projected for net zero carbon emission. Regarding the environmental effect, the second scenario wins, but the announced pledges scenario shows a more realistic picture of where we might see the world in 30 years in terms of hydrogen demand. The transport sector, residential and commercial building fuel, as well as power generation and grid balancing, all show expected growth in hydrogen demand. According to the International Renewable Energy Agency (IRENA), there is a projected investment of up to $1.7 trillion for hydrogen fuel cell technology by 2050. Furthermore, the European Commission has outlined plans to install at least 6 GW of renewable hydrogen electrolyzers in the EU by 2024 and 40 GW by 2030. These targets are reflective of the strategic investments driving the hydrogen economy forward. This suggests hydrogen's expanding role in facilitating a transition towards decarbonized energy systems. Figure 2.14(a) presents the global hydrogen demand by sector from 2020 to 2050 under the Announced Pledges Scenario. The demand rises gradually, with the industry and transport sectors showing the most significant increase. This scenario likely the current pledges by countries for hydrogen use, suggesting gradual adoption consistent with stated goals. Figure 2.14(b) illustrates the global hydrogen demand by sector from 2020 to 2050 under the Net Zero Emission Scenario [69,70]. Compared to the Announced Pledges Scenario, this figure shows a more obvious growth, especially after 2030, as efforts to reduce emissions intensify. The most substantial increases are observed in power and transport sectors reflecting a prospective drive towards a carbon-neutral future.

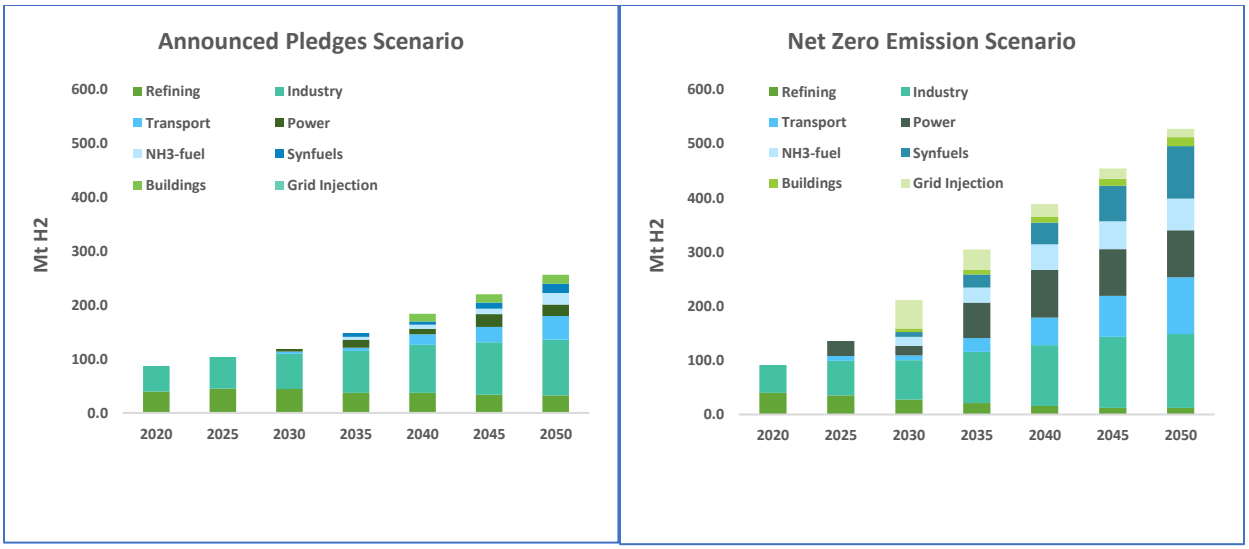

Figure 2. 14: (a & b) Global H_2 Demand (2020-2050) [69, 70]

The difference divergent paths demonstrate the significant impact of current policy decisions and commitments on the global integration of hydrogen into the energy mix. The disparities indicates the vital role that present-day policy choices will play in shaping the future energy prospect.

2.14. Global Strategies to Implement Hydrogen Energy

Tables 2.4 present a comprehensive overview of national hydrogen strategies across various countries, indicating their commitment to developing hydrogen as an energy source for various sectors including industry, refining, transport, building, electricity, exports, mining, shipping, and aviation [70]. From the details provided, it's clear that the United Kingdom, Czech Republic, Norway, and Hungary have the latest strategies in place. Meanwhile, Germany, France, Japan, and the European Union are highlighted for their significant financial commitments to advancing hydrogen energy production. A notable trend among these countries is the move towards sustainable hydrogen production. Germany, the Netherlands, Spain, the European Union, Chile, and Australia are particularly focused on generating hydrogen from renewable resources. This

aligns with global efforts to decarbonize energy sources to mitigate climate change impacts. Other countries appear to rely more on carbon capture and storage (CCUS) technologies, which are used in conjunction with fossil fuel-based hydrogen production to reduce carbon emissions.

Table 2. 4: Adopted national Hydrogen Strategies [70]

Country	**Document, year**	**Deployment targets (2030)**	**Production**	**Public investment committed**
Australia	National Hydrogen Strategy, 2019	None specified	Coal with CCUS Electrolysis (renewable) Natural gas with CCUS	AUD 1.3 bln (~USD 0.9 bln)
Canada	Hydrogen Strategy for Canada, 2020	Total use: 4 Mt H2/y	Biomass By-product H2 Electrolysis Natural gas with CCUS	USD 19 mil by 2026
Chile	National Green Hydrogen Strategy, 2020	25 GW electrolysis	Electrolysis (renewable)	USD 50 mln for 2021
Hungary	National Hydrogen Strategy, 2021	20 kt/yr of low-carbon H2 16 kt/yr of carbon-free H2	Electrolysis Fossil fuels with CCUS	n.a
Japan	Green Growth Strategy, 2020, 2021	420 kt low-carbon H2 800000 FCEVs	Electrolysis Fossil fuels with CCUS	2030 (~USD 6.5 bln)
Russia	Hydrogen roadmap 2020	Exports: 2 Mt H2	Electrolysis Natural gas with CCUS	n.a
Norway	Hydrogen Roadmap, 2021	n.a.	Electrolysis (renewables) Natural gas with CCUS	for 2021 (~USD 21 mln)
Czech Republic	Hydrogen Strategy, 2021	Low-carbon demand: 97kt H2/yr	Electrolysis	n.a

Country	Document, year	Deployment targets (2030)	Production	Public investment committed
European Union	EU Hydrogen Strategy, 2020	40 GW electrolysis	Electrolysis(renewable) Natural gas with CCUS	by 2030 (~USD 4.3 bln)
Korea	Hydrogen Economy Roadmap, 2019	1.94 Mt H2/yr 2.9 million FC cars (plus 3.3 million exported)	By-product H2 Electrolysis Natural gas with CCUS	in 2020 (~USD 2.2 bln)
France	National Strategy for Decarbonised Hydrogen Development, 2020	6.5 GW electrolysis 20-40% industrial H2 decarbonised	Electrolysis	by 2030 (~USD 8.2 bln)
Germany	National Hydrogen Strategy, 2020	5 GW electrolysis	Electrolysis (renewable)	by 2030 (~USD 10.3 bln)
Netherlands	Government Strategy on Hydrogen, 2020	3-4 GW electrolysis 300 000 FC cars 3 000 FC HDVs	Electrolysis (renewables) Natural gas with CCUS	(~USD 80 mln/yr)
Spain	National Hydrogen Roadmap, 2020	4 GW electrolysis 25% industrial H2 decarbonized	Electrolysis (renewables)	(~USD 1.8 bln)
United Kingdom	UK Hydrogen Strategy, 2021	5 GW low-carbon production capacity	Natural gas with CCUS Electrolysis	(~USD 1.3 bln)

2.15. Consumers of Hydrogen Based on Applications

Table 2.5 provides an overview of hydrogen energy logistics [52, 56]. It categorizes hydrogen production into four types: blue hydrogen (from natural gas with CO2 storage), green hydrogen (from renewables with no emissions), brown hydrogen (from coal with high emissions), and grey hydrogen (from natural gas with high emissions).

Table 2. 5: Category of hydrogen products on production, transport and storage [52, 56]

Hydrogen Production	Blue: Made from natural gas, CO2 is captured and stored.
	Green: Made from renewable energy, no GHG emission.
	Brown: Made from coal, high CO2 emission.
	Grey: Made from natural gas, high CO2 emission.
Hydrogen Transport	Tube Trailer: suitable for short-distance gaseous state transfer
	Liquid via road: for short and medium distance transfer of large volumes of fuel
	Pipeline: short, medium, and large distance transfer of large and very large quantities in a gas state
	Liquid via ships: very large quantities of hydrogen for international transportation
Hydrogen Storage	Liquified hydrogen: Hydrogen has to be cooled to -253°C and stored in insulated tanks to maintain this low temperature and minimize evaporation.
	Compressed hydrogen storage: fuel-cell powered cars run on compressed hydrogen contained in large, highly pressurized containers.
	Materials-based storage: Ammonia or Methylcyclohexane (MCH)- Liquid Organic Hydrogen Carrier (LOHC) as hydrogen carriers.
Consumers	Transportation: Hydrogen fueling stations are used for refueling vehicles
	House Heating: Hydrogen heaters use a fuel cell as an energy converter.
	Industrial Use: for power generation and storage, and industrial processes like oil refining and steel production
	Export: large quantities of gas is liquified for international transportation via ships.

Transport varies by distance and state of hydrogen, from gas in tube trailers to liquid in ships for international delivery. Storage options include cooling hydrogen to a liquid state, compressing it for vehicles, or using chemicals like ammonia for larger quantities. Consumers use hydrogen for transportation, heating homes, industrial processes, and exporting it overseas in liquefied form.

2.16. Conclusion

Chapter 2 highlighted hydrogen's vital role in the global transition to sustainable energy. Emphasizing its high energy density, zero CO_2 emissions, and versatile production methods, hydrogen is presented as a key solution to the need for cleaner energy sources during growing global energy demands. The chapter emphasizes the substantial shift towards clean energy investments, with hydrogen emerging as a prospective candidate. It also discusses regional variations in energy strategies, particularly in Europe and the US, and the importance of effective policy measures, financial support, and public engagement in promoting the development and adoption of hydrogen energy. This comprehensive approach can contribute to establishing hydrogen as an effective source of sustainable recovery and long-term environmental stewardship.

This chapter has been partially published in "*Materials*" titled; "An overview of challenges for the future of hydrogen" with co-authors; Md Tanvir Ahad, Md Monjur Hossain Bhuiyan, Alfredo Becerril Corral and Zahed Siddique. https://doi.org/10.3390/ma16206680

The chapter has also been partially published in "International Journal of Energy Research" titled "Harnessing hydrogen: a comprehensive literature review on strategic launching initiatives in the global energy market" along with the co-authors; Farian Mehjabin, Jeffrey B Schmidt, and Md Monjur Hossain Bhuiyan. https://doi.org/10.1155/2024/3265065

Reference

1. Leaver, J. (2019). International Energy Agency (IEA) Strategic Initiatives and Activities for Hydrogen. Available online: https://hdl.handle.net/10652/4741 .

2. Pivovar, B., Rustagi, N., & Satyapal, S. (2018). Hydrogen at Scale (H2@ Scale): Key to a Clean, Economic, and Sustainable Energy System. Electrochem. Soc. Interface, 27, 47.

3. Yue, M., Lambert, H., Pahon, E., Roche, R., Jemei, S., & Hissel, D. (2021). Hydrogen energy systems: A critical review of technologies, applications, trends and challenges. Renew. Sustain. Energy Rev., 146, 111180.

4. Nicoletti, G., Arcuri, N., Nicoletti, G., & Bruno, R. (2015). A technical and environmental comparison between hydrogen and some fossil fuels. Energy Convers. Manag., 89, 205–213.

5. Balasooriya, W., Clute, C., Schrittesser, B., & Pinter, G. (2022). A review on applicability, limitations, and improvements of polymeric materials in high-pressure hydrogen gas atmospheres. Taylor Fr., 62, 175–209.

6. Fassbender, L. (2010). Hydrogen Safety Training for First Responders. Available online: https://www.hydrogen.energy.gov/docs/hydrogenprogramlibraries/pdfs/review10/scs015_fassbender_2010_o_web.pdf.

7. National Renewable Energy Laboratory (NREL). (2018). *H2A Production Model Version 3.0 User Guide (Draft)*. https://www.nrel.gov/hydrogen/assets/pdfs/h2a-production-model-version-3-2018-user-guide-draft.pdf

8. Speight, J.G. (2014). The Chemistry and Technology of Petroleum (5th ed.). CRC Press. https://doi.org/10.1201/b16559

9. International Energy Agency. (2019). *The future of hydrogen: Seizing today's opportunities*. https://www.hydrogenexpo.com/media/9370/the_future_of_hydrogen_iea.pdf

10. Energy Information Administration (EIA). (2021). *Natural gas explained*. U.S. Department of Energy. https://www.eia.gov/energyexplained/natural-gas/

11. Wietschel, M., & Ball, M. (Eds.). (2009). *The hydrogen economy: Opportunities and challenges*. Cambridge University Press. https://doi.org/10.1017/CBO9780511635359

12. Acar, C., & Dincer, I. (2014). Comparative assessment of hydrogen and gasoline as fuels in internal combustion engines. *International Journal of Hydrogen Energy, 39*(21), 10776-10788. https://doi.org/10.1016/j.ijhydene.2014.05.081

13. Glassman, I., Yetter, R. A., & Glumac, N. G. (2014). *Combustion* (5th ed.). Academic Press. https://experts.illinois.edu/en/publications/combustion-fifth-edition

14. Nelson, H. G. (2006). Hydrogen embrittlement: A case study – Space Shuttle Challenger disaster. *Journal of Failure Analysis and Prevention, 6*(5), 37-45. https://onlineethics.org/cases/engineering-ethics-cases-texas-am/space-shuttle-challenger-disaster

15. Paris Agreement. (2015). In Proceedings of the Report of the Conference of the Parties to the United Nations Framework Convention on Climate Change (21st Session, 2015: Paris). HeinOnline, Volume 4, p. 2017. https://heinonline.org/HOL/LandingPage?handle=hein.journals/intlm55&div=46&id=&page=.

16. Goldman Sachs. (2020, July 8). Carbonomics: The Rise of Clean Hydrogen. https://www.goldmansachs.com/intelligence/pages/carbonomics-the-rise-of-clean-hydrogen.html.

17. Bhandari, R., & Shah, R.R. (2021). Hydrogen as Energy Carrier: Techno-Economic Assessment of Decentralized Hydrogen Production in Germany. Renew. Energy, 177, 915–931.

18. Kar, S.K., Sinha, A.S.K., Bansal, R., Shabani, B., & Harichandan, S. (2022). Overview of Hydrogen Economy in Australia. Wiley Interdiscip. Rev. Energy Environ., 12, e457.

19. "World Energy Investment 2022,". https://www.iea.org/reports/world-energy-investment-2022

20. International Energy Agency. (2021). *Global hydrogen review 2021*. https://www.iea.org/reports/global-hydrogen-review-2021

21. IEA (2023), Energy Efficiency 2023, IEA, Paris https://www.iea.org/reports/energy-efficiency-2023 , Licence: CC BY 4.0

22. Bórawski, P., Bełdycka-Bórawska, A., Holden, L., & Rokicki, T. (2022). The role of renewable energy sources in electricity production in Poland and the background of energy policy of the European Union at the beginning of the COVID-19 crisis. Energies, 15(22), 8771. https://doi.org/10.3390/en15228771

23. Giers, M., & University of Warsaw (Poland). (2022). Hydrogen and its role in post-pandemic recovery. Case study of Portugal. Polish Political Science, 51, 1–8. https://doi.org/10.15804/ppsy202219

24. Bednarczyk, J. L., Brzozowska-Rup, K., & Luściński, S. (2022). Opportunities and limitations of hydrogen energy in Poland against the background of the European Union energy policy. Energies, 15(15), 5503. https://doi.org/10.3390/en15155503

25. Rządkowska, A. (2021). The EU clean energy policy under the European green deal and COVID-19 pandemics - how the renewables historically won the majority share in the Eu's electrical energy mix. Proceedings of the ISES Solar World Congress 2021. ISES Solar World Congress 2021, Virtual. https://doi.org/10.18086/swc.2021.02.01

26. Martinho, V. J. P. D. (2023). Impacts of the Covid-19 context on the European Union energy markets: interrelationships with sustainability. Environment Development and Sustainability. https://doi.org/10.1007/s10668-023-03605-2

27. Ingaldi, M.; Klimecka-Tatar, D. People's Attitude to Energy from Hydrogen—From the Point of View of Modern Energy Technologies and Social Responsibility. Energies 2020, 13, 6495. https://doi.org/10.3390/en13246495

28. Review, Energy Industry, and Energy Industry Review. 2020. "Post COVID-19 and the Hydrogen Sector." Energy Industry Review. May 11, 2020. https://energyindustryreview.com/analysis/post-covid-19-and-the-hydrogen-sector/.

29. Ati, Nikhil, Filipe Barbosa, Abhinav Charan, Celine Guo, Jessica Li, Brandon McGee, and Mim Tansamrit. 2023. "Unlocking Clean Hydrogen in the US Gulf Coast: The "Here and Now"" McKinsey & Company. August 25, 2023. https://www.mckinsey.com/industries/oil-and-gas/our-insights/unlocking-clean-hydrogen-in-the-us-gulf-coast-the-here-and-now#/.

30. Haoming Ma, Zhe Sun, Zhenqian Xue, Chi Zhang, & Zhangxin Chen. (2023). A systemic review of hydrogen supply chain in energy transition. https://dx.doi.org/10.1007/s11708-023-0861-0.

31. BioBERT: a pre-trained biomedical language representation model for biomedical text mining." Bioinformatics, 36(4), 1234-1240.

32. Brende, Børge, and Bob Sternfels. 2023. “Seizing the Momentum to Build Resilience for a Future of Sustainable Inclusive Growth.” McKinsey & Company. February 23, 2023. https://www.mckinsey.com/capabilities/risk-and-resilience/our-insights/seizing-the-momentum-to-build-resilience-for-a-future-of-sustainable-inclusive-growth.

33. Atteya, A. I., Ali, D., Hossain, M., & Sellami, N. (2023). A Comprehensive Review on The Potential of Green Hydrogen in Empowering the Low-Carbon Economy: Development Status, Ongoing Trends and Key Challenges. https://dx.doi.org/10.5772/geet.23

34. IEA (2023), Global Hydrogen Review 2023, IEA, Paris https://www.iea.org/reports/global-hydrogen-review-2023, Licence: CC BY 4.0

35. House, White. 2023. “Biden-Harris Administration Announces Regional Clean Hydrogen Hubs to Drive Clean Manufacturing and Jobs.” The White House. October 13, 2023. https://www.whitehouse.gov/briefing-room/statements-releases/2023/10/13/biden-harris-administration-announces-regional-clean-hydrogen-hubs-to-drive-clean-manufacturing-and-jobs/.

36. IEA (2023), Government Energy Spending Tracker, IEA, Paris https://www.iea.org/reports/government-energy-spending-tracker-2, Licence: CC BY 4.0

37. Samsun, R.C.; Rex, M.; Antoni, L.; Stolten, D. Deployment of Fuel Cell Vehicles and Hydrogen Refueling Station Infrastructure: A Global Overview and Perspectives. Energies 2022, 15, 4975. https://doi.org/10.3390/en15144975

38. IEA (2021), Global EV Outlook 2021, IEA, Paris https://www.iea.org/reports/global-ev-outlook-2021, Licence: CC BY 4.0

39. R. Samsun, M. Rex, L. Antoni, and D. Stolten, “Deployment of Fuel Cell Vehicles and Hydrogen Refueling Station Infrastructure: A Global Overview and Perspectives,” Energies, vol. 15, no. 14, p. 4975, Jul. 2022, doi: https://doi.org/10.3390/en15144975.

40. Pedrazzi, S., Morini, E., Nasti, M., Pizzileo, S., & Allesina, G. (2022). Green Hydrogen Powered Forklifts in Industrial Transport: Case Study of an Italian Fruit and Vegetable Market. International Journal of Heat and Technology, 40(1). https://dx.doi.org/10.18280/ijht.400117.

41. R. Avtar, S. Tripathi, A. K. Aggarwal, and P. Kumar, “Population–urbanization–energy nexus: a review,” Resources, vol. 8, no. 3, p. 136, 2019.

42. IEA (2021), World Energy Balances: Overview, IEA, Paris https://www.iea.org/reports/world-energy-balances-overview , Licence: CC BY 4.0

43. J. L. Holechek, H. M. E. Geli, M. N. Sawalhah, and R. Valdez, "A global assessment: can renewable energy replace fossil fuels by 2050?," Sustainability, vol. 14, no. 8, p. 4792, 2022.

44. M. Ball and M. Weeda, "The hydrogen economy—vision or reality?," in Compendium of Hydrogen Energy, M. Ball, A. Basile, and T. Nejat Veziroğlu, Eds., vol. 4, pp. 237–266, 2016, https://www.sciencedirect.com/science/article/pii/B9781782423645000117.

45. M. J. B. Kabeyi and O. A. Olanrewaju, "Sustainable energy transition for renewable and low carbon grid electricity generation and supply," Frontiers in Energy Research, vol. 9, article 743114, 2022.

46. M. J. Burkea and J. C. Stephens, "Political power and renewable energy futures: a critical review," Energy Research & Social Science, vol. 35, pp. 78–93, 2018.

47. M. Refaat, A. Mohsen, E. S. A. R. Nasr, and M. Kohail, "Minimizing energy consumption to produce safe one-part alkali-activated materials," Journal of Cleaner Production, vol. 323, article 129137, 2021.

48. D. Ali, Energy capacity and economic viability assessment of the renewable hydrogen energy storage as a balancing mechanism in addressing the electric system integration issues inherent with variable renewable energy resources, OpenAIR@RGU (Robert Gordon University), 2011.

49. IEA, The future of hydrogen, IEA, Paris, 2019, http://www.iea.org/reports/the-future-of-hydrogen , Licence: CC BY 4.0.

50. S. G. Nnabuife, E. Oko, B. Kuang et al., "The prospects of hydrogen in achieving net zero emissions by 2050: a critical review," Sustainable Chemistry for Climate Action, vol. 2, article 100024, 2023.

51. IEA, Hydrogen, IEA, 2023, http://www.iea.org/energy-system/low-emission-fuels/hydrogen.

52. K. Mazloomi and C. Gomes, "Hydrogen as an energy carrier: prospects and challenges," Renewable and Sustainable Energy Reviews, vol. 16, no. 5, pp. 3024–3033, 2012.

53. D. De Wolf and Y. Smeers, "Comparison of battery electric vehicles and fuel cell vehicles," World Electric Vehicle Journal, vol. 14, no. 9, p. 262, 2023

54. M. Robinius, J. Linsen, T. Grube et al., "Comparative analysis of infrastructures: hydrogen fueling and electric charging of vehicles," Energy & Environment, vol. 408, pp. 1–126, 2017.

55. S. Sagaria, A. Moreira, F. Margarido, and P. Baptista, “From microcars to heavy-duty vehicles: vehicle performance comparison of battery and fuel cell electric vehicles,” Vehicles, vol. 3, no. 4, pp. 691–720, 2021.

56. Fuel Cells and Hydrogen 2 Joint Undertaking (EU body or agency), “Clean Hydrogen Joint Undertaking (EU body or agency),” in Hydrogen roadmap Europe: a sustainable pathway for the European energy transition, Publications Office of the European Union, LU, 2016, https://op.europa.eu/en/publication-detail/-/publication/0817d60d-332f-11e9-8d04-01aa75ed71a1/language-en.

57. P. E. Dodds, I. Staffell, A. D. Hawkes et al., “Hydrogen and fuel cell technologies for heating: a review,” International Journal of Hydrogen Energy, vol. 40, no. 5, pp. 2065–2083, 2015.

58. C. Baldino, J. O'malley, S. Searle, Y. Zhou, and A. Christensen, “Hydrogen for Heating? Decarbonization Options for Households in the United Kingdom in 2050,” 2020 https://theicct.org/sites/default/files/publications/Hydrogen-heating-UKdec2020.pdf.

59. IEA, Global Energy Review 2021 – Analysis, IEA, 2021, https://www.iea.org/reports/global-energy-review-2021.

60. G. Bieker, A global comparison of the life-cycle greenhouse gas emissions of combustion engine and electric passenger cars, International Council on Clean Transportation, 2021, https://theicct.org/publication/a-global-comparison-of-the-life-cyclegreenhouse-gas-emissions-of-combustion-engine-andelectric-passenger-cars/.

61. C. Baldino, J. O'malley, S. Searle, Y. Zhou, and A. Christensen, “Hydrogen for Heating? Decarbonization Options for Households in the United Kingdom in 2050,” 2020 https://theicct.org/sites/default/files/publications/Hydrogen-heating-UKdec2020.pdf.

62. Q. Hassan, I. D. J. Azzawi, A. Z. Sameen, and H. M. Salman, “Hydrogen fuel cell vehicles: opportunities and challenges,” Sustainability, vol. 15, no. 15, p. 11501, 2023.

63. A. M. Oliveira, R. R. Beswick, and Y. Yan, “A green hydrogen economy for a renewable energy society,” Current Opinion in Chemical Engineering, vol. 33, article 100701, 2021.

64. S. K. Dash, S. Chakraborty, and D. Elangovan, “A brief review of hydrogen production methods and their challenges,” Energies, vol. 16, no. 3, p. 1141, 2023.

65. I. Marouani, T. Guesmi, B. M. Alshammari et al., “Integration of renewable-energy-based green hydrogen into the energy future,” PRO, vol. 11, no. 9, p. 2685, 2023.

66. “Hydrogen consumption worldwide by country 2020,” Statista.https://www.statista.com/statistics/1292403/globalhydrogen-consumption-by-country/.

67. IEA G20 The Future of Hydrogen. Available online: https://www.iea.org/reports/the-future-of-hydrogen (accessed on 16 September 2023).

68. Eriksen, R. Hydrogen Forecast to 2050. Available online: https://aben.com.br/wp-content/uploads/2022/06/DNV_Hydrogen_Report_2022_Highres_single1.pdf (accessed on 7 September 2023).

69. J. Whitehead, P. Newman, J. Whitehead, and K. L. Lim, “Striking the right balance: understanding the strategic applications of hydrogen in transitioning to a net zero emissions economy,” Sustainable Earth, vol. 6, no. 1, 2023.

70. IEA, Global Energy Review 2021 – Analysis, IEA, 2021, https://www.iea.org/reports/global-energy-review-2021.

CHAPTER 3: CHALLENGES TO IMPLEMENT HYDROGEN ENERGY

Chapter 3 of this dissertation focuses on the numerous challenges associated with the implementation of hydrogen energy, focusing on determination of core research areas such as hydrogen production, storage, and transportation. It initiates by outlining the interdisciplinary nature of hydrogen research, emphasizing key areas such as hydrogen production methods, storage technologies, and material interactions. The chapter explores various hydrogen production techniques, including steam methane reforming, electrolysis, coal gasification, biomass, and methane splitting, highlighting their respective challenges and opportunities. It also addresses the significant challenges in hydrogen storage, considering methods like compressed gas, liquid-state, and solid-state storage, and the material challenges imposed by hydrogen's properties. Additionally, the chapter discusses hydrogen embrittlement, a critical issue affecting the material integrity in hydrogen environments, and the need for advanced materials to mitigate this phenomenon. Overall, this chapter provides a comprehensive analysis of the current obstacles and potential solutions in the hydrogen energy sector, aiming to advance the development of a sustainable hydrogen economy.

3.1. Core Research Areas for Hydrogen Energy Implementation

The study finds the significant characters of a research field and narrow down the key area for further investigation. The density visualization method was used to analyze the keywords needed for investigation using VOSviewer software. The lowest number of recurrences of a keyword was set to 3. Of the total 300 keywords, only 50 were able to meet the threshold. Figure- 3.1 indicates the diversity of the hydrogen research field and that it consists of interdisciplinary characters.

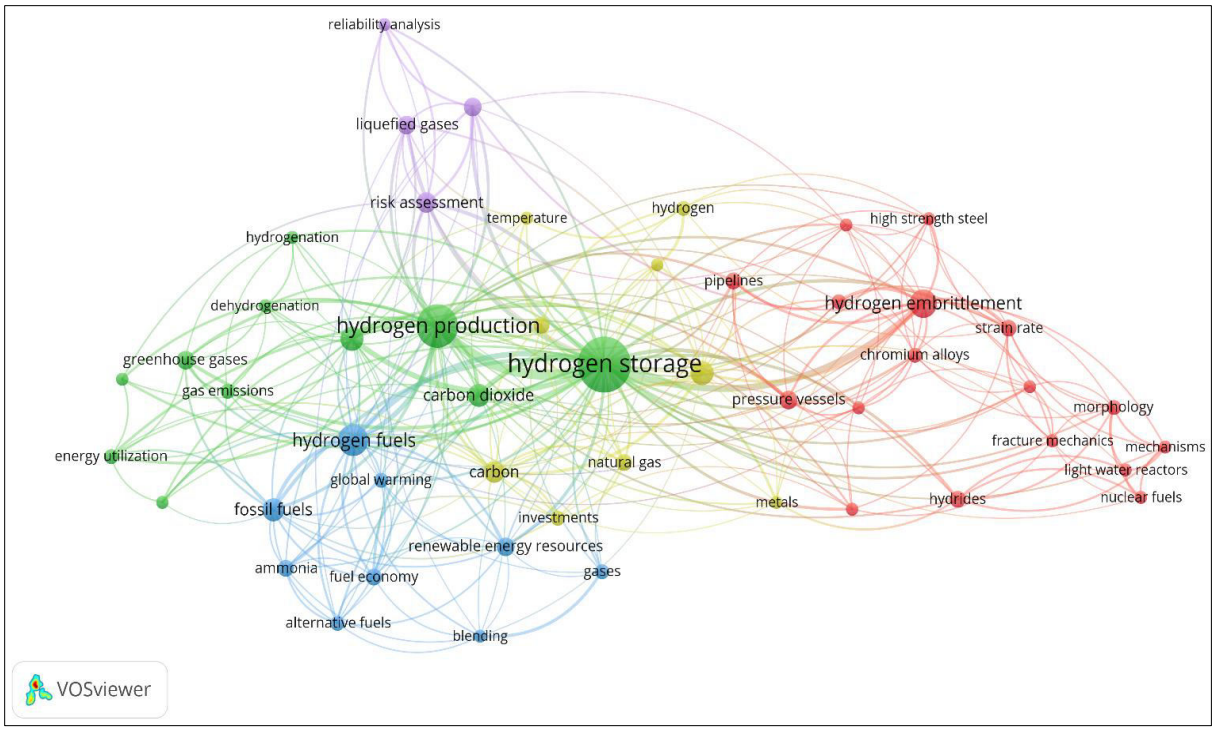

Figure 3. 1: Cooccurrence of keyword networks for an overlay visualization map of hydrogen

From Figure 3.1, we can observe that the most recurrent phrases are Hydrogen Production, Hydrogen Storage, Hydrogen Embrittlement, illustrating the key current challenges. The "clusters" connected with phrases like hydrogen embrittlement, hydrogen production, hydrogen storage, hydrogenation, combustion, and transportation represent the emission reduction strategy through hydrogen research. An interesting aspect of these emission reduction strategies is the focus on material properties and material interactions, as outlined by the recurrence and connections of phrases such as high-strength steel, alloys, morphology, pressure vessel, hydrogen, and hydrides, among others. The main challenges for hydrogen gas is from a material perspective because of the nature of hydrogen gas. The behavior of hydrogen is not the same as natural gas. For production, transportation, storage, fuel cells, combustion engines, and sensors, the appropriate sealing material should be dedicated and specific for a hydrogen environment. Research groups have been

working to identify or make new materials for hydrogen applications. The hydrogen embrittlement problem is the key issue for hydrogen compatible materials from production, transportation, storage, fuel cells, and combustion engines to sensor applications. Industries including metals processing, chemical, mechanical, and refineries have difficulties with material degradation due to hydrogen exposed aging for many years. Hydrogen embrittlement is one of the oldest and most frequently observed degradation phenomena in production, storage, transportation, and distribution facilities due to the aging phenomenon. Similarly, the term “hydrogen economy” is encircled by aspects such as hydrogen production, hydrogen storage, infrastructure, emission, and the hydrogen supply chain. This visibly directs the key areas that are incorporated to cover the range of hydrogen research. The timeframe indicates that recent research has focused on the challenges of hydrogen production, hydrogen storage and hydrogen assisted embrittlement. Considering the role of materials in addressing limitations in current hydrogen technologies, this research focuses on describing the challenges for hydrogen production, hydrogen storage and hydrogen embrittlement followed by a comprehensive experimental study of sealing material aging under diverse operational conditions. Given the obvious challenges of hydrogen embrittlement, advancements in sealing materials are essential breakthroughs for the entire hydrogen value chain. This research aims to make a meaningful contribution to material science by supporting the reliability and safety of hydrogen storage and transportation systems. Thus, this investigation presents an extensive picture of the sealing material challenges for hydrogen compatibility and recommendations for future research directions around hydrogen.

3.2. Overview of Hydrogen Production and Associate Challenges

Hydrogen can be produced from numerous sources (e.g., fossil fuels, biomass, and water) by utilizing several technologies. However, the production of H_2 has dominated using fossil fuels until today. Day by day, the water electrolysis method has gained more interest with the decreasing renewable power cost for green hydrogen production. Nearly 76% of total hydrogen gas (of the global demand) is produced from natural gas sources. For the rest, 23% and 1% are from coal and electrolysis sources, respectively. The amount of CO_2 emission during hydrogen production has been a concerning issue for a while, and efforts are continuing to control CO_2 emission. The implementation of carbon capture, utilization, and storage (CCUS) projects are helpful in this regard. Numerous types of routes for hydrogen production are outlined in Figure 3.2 [71].

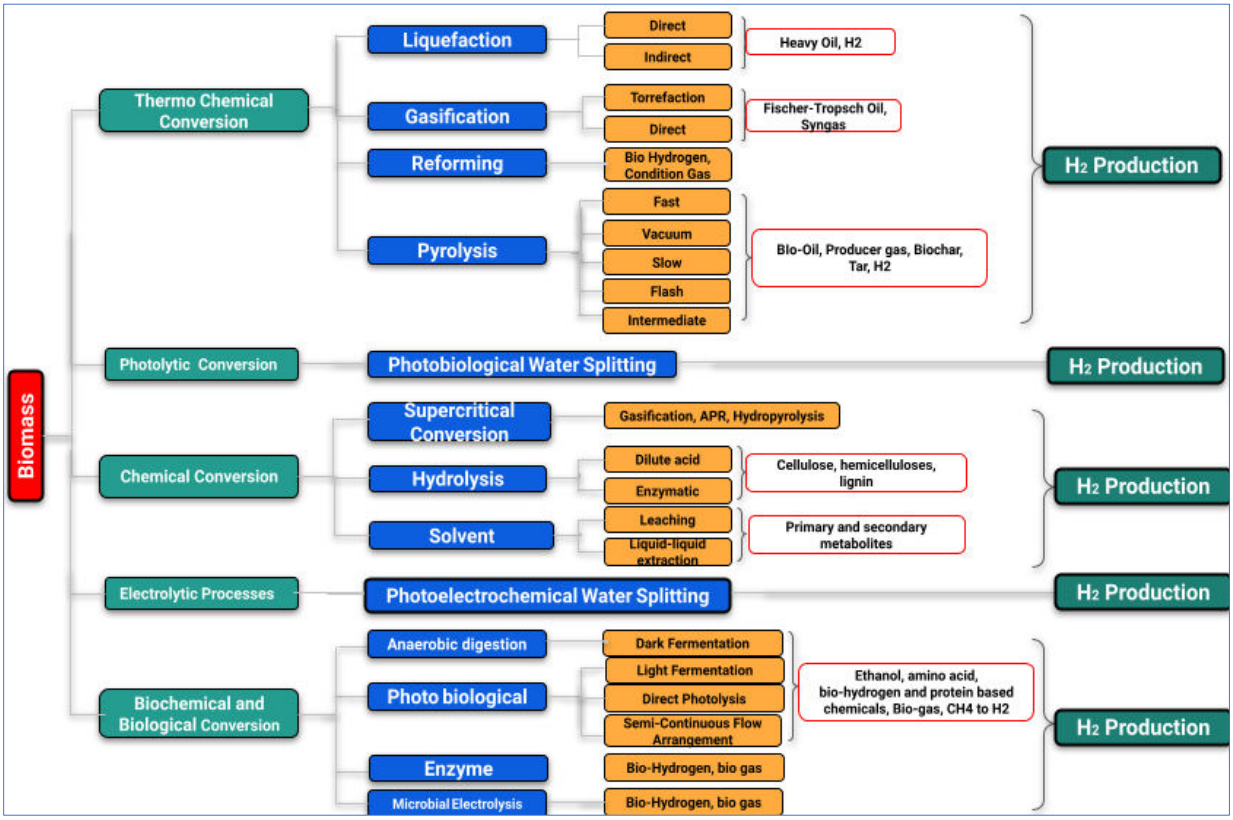

Figure 3. 2: Illustration of different technologies of hydrogen production [71]

Sources and methods of gaining different types of hydrogen, along with the emission types, are summarized in Table 3.1 [72–74].

Table 3. 1: Sources and methods of gaining different types of hydrogen [72-74]

H_2 Type	**Source of H_2**	**Method**	**Emission Type**
Green H2	Renewable/Nuclear and Biomass	Electrolysis	Oxygen
Pink H2	Nuclear energy	Electrolysis	Nuclear Waste
Pure H2	Electricity from Grid	Electrolysis	
Gray H2	Natural gas	SMR	CO_2
Blue H2	Coal	Gasification (With CCUS)	CO_2
Brown H2	Coal	Gasification (Without CCUS)	CO_2
Black H2	Coal	Gasification (Without CCUS)	CO_2

Green hydrogen is achieved through the process of electrolysis powered by renewable energies such as wind or solar. Electrolysis involves using an electrical current to break down the water molecule into oxygen and hydrogen by electrodes. Hydrogen stored in specific tanks is channeled into a fuel cell. There, it binds again with oxygen from the air, and electricity is obtained. Thus, the only byproduct of the process is water, resulting in a clean, sustainable system in which zero CO_2 is emitted to produce energy. In the study by Marcelo and Dell'Era , they identified two primary categories of electrolysis processes: (i) polymer electrolyte membrane (PEM) electrolyzers and (ii) alkaline electrolyzers [75]. The operational efficiencies of these electrolyzers can vary from 52% to 85%, as reported by Binder et al. in 2018 [76]. The conversion of electricity into chemical energy through electrolysis represents a promising technological advancement.

This explains the global proliferation of power-to-gas facilities. Proton exchange membrane (PEM) electrolyzers and alkaline electrolyzers, as well as other electrolyzer types such as solid

oxide electrolysis cells (SOECs) and molten carbonate electrolysis cells (MCECs), have gained widespread recognition for their electrochemical applications.

To establish the financial feasibility of a large-scale production unit, an energy analysis is essential. This analysis can be conducted using the standard methods [71,77]. It involves calculating the input energy (E_i), output energy (E_o), and net energy (E_n) using the following equations:

The input energy (Ei) can be determined using Equation (1):

$$E_i = P * T * V * S \quad (1)$$

where Ei represents the input energy (kWh), P is the power used for the process (kW/kg), T is the time for disintegration (hours), V is the reactor volume (m^3), and S is the substrate (kg/m^3). This energy is required for the disintegration process.

The output energy (Eo), in terms of energy gained as hydrogen, can be calculated using Eqn (2):

$$E_o = B * L * H * V * F \quad (2)$$

where E_0 denotes the output energy (kWh), B is the biodegradability of algal biomass (gCOD/gCOD, where COD is the chemical oxygen demand), L is the COD load ($gCOD/m^3$), H is the hydrogen yield ($m^3/gCOD$), V is the reactor volume (m^3), and F is the biohydrogen conversion factor (1 m^3 equals 3.5 kWh). The net energy (En) estimation is determined by the difference between the output energy (Eo) and input energy (Ei) using Equation (3):

$$E_n = E_o - E_i \quad (3)$$

where En represents the net energy (kWh), Eo is the output energy (kWh), and Ei is the input energy (kWh) [78]. This energy analysis is crucial for assessing the financial viability of large-scale production units.

3.2.1. Hydrogen Production from Natural Gas: Challenges and Opportunities

The most universal method to produce hydrogen from natural gas resources is known as steam methane reforming (SMR). At present, three methods are in use for hydrogen production from natural gas resources. These are SMR, the partial oxidation method (POM), and autothermal reforming (ATR). For large-scale production, SMR is the most popular form of H_2 production [79,80]. CO_2 produced by the SMR method is currently released into the atmosphere. However, it can be utilized as a byproduct in food processing and packaging. SMR uses water as an oxidant and a source of hydrogen, while oxygen in the air is used as an oxidant in POM. A combination of both SRM and POM is known as the ATR method. SMR is the most developed industrial process with no oxygen requirement. However, the emission of CO_2 is considerably high. With a view toward decarbonizing these methane-based processes, the CO_2 produced must be captured and stored. The use of carbon capture, utilization, and storage (CCUS) projects are helpful in this regard. It is a process that captures carbon dioxide emissions from different sources so that it will not enter the atmosphere. CCUS projects involve pumping the CO_2 into geological reservoirs, such as depleted oil and gas fields [81]. Being a sustainable method with a low current cost, SMR has become popular in H_2 production. However, difficulties involved with the automated control system and feedstock management system need to be addressed to make SMR a more efficient way of producing H_2.

3.2.2. Hydrogen Production from Electrolysis: Challenges and Opportunities

Electrolysis is an electrochemical process where less than 0.1% of the dedicated hydrogen production becomes global [82-84]. Three main electrolysis technologies include alkaline electrolysis, proton exchange membrane (PEM) electrolysis, and solid oxide electrolysis cells

(SOECs). Fertilizer and chlorine industries have used alkaline electrolysis to produce hydrogen since 1920, and it is an established and commercial technology. General Electric introduced proton exchange membrane (PEM) electrolysis in 1960 to overcome the few operational drawbacks of alkaline electrolysis. The least-developed electrolysis technology is solid oxide electrolysis cells (SOECs), which are yet to be commercialized. Integrating heat into hydrogen production became interesting because of the heat sources from industrial processes, geothermal or solar heat, and nuclear power plants. Nuclear power plants generate heat at 300° C, which can also be used to provide electricity and steam for solid oxide electrolysis cells (SOECs) [85]. Electrolysis requires both water and electricity. Approximately 9 L of water are used to produce 1 kg of H_2, while 8 kg of oxygen are produced as a byproduct. Freshwater access can be an issue in water-stressed areas, as water consumption is roughly double that of the SMR process. Seawater could be a potential source for electrolysis in coastal areas. But seawater may not be used directly, as it leads to corrosive damage and the production of chlorine. Moreover, PEM electrolysis needs expensive electrode catalysts such as platinum, iridium, and membrane materials. Again, the lifetime of the electrodes are also shorter than those of alkaline electrolyzes [83,84]. A fuel cell is relatively dry compared to the electrolysis process. Water is soaked by polymer electrodes and therefore swells. During extreme swelling and operating conditions at 30 bar (430 psi) or higher, polymer fibers are farther apart and become mechanically weaker without the use of thick membranes ranging from 175 to 250 microns.

Having mentioned these limitations, there are new opportunities that appear every day to mitigate the gaps. Electrolysis cell efficiency may be improved by using thinner membrane materials (50 - 60 microns). It also assists to increase the mechanical strength [86]. With a view toward optimizing

ionic conductivity and decreasing water uptake, researchers are investigating different polymer compositions. The replacement of the fluorine-based backbone of Nafion with hydrocarbons has been taken into consideration. Also, the catalysts used in electrolysis platinum on the hydrogen side and iridium on the oxygen side—need to be improved [86]. Research on selecting materials that would be compatible with the temperature levels of nuclear energy heat sources needs to be performed. Small modular reactors will also be considered to contribute to SOEC electrolysis in the coming days. Also, advanced nuclear reactors will be an attractive option as well in the long term [85].

3.2.3. Hydrogen Production from Coal: Challenges and Opportunities

The chemical and fertilizer industries produce hydrogen from coal using the gasification process during the production of ammonia as a well-established technology [87,88]. However, the CO_2 emission increase is very likely from coal-based hydrogen production. Also, the use of CCUS produces hydrogen with a relatively low hydrogen-to-carbon ratio and can contain high levels of impurities in the feedstock (sulfur, nitrogen, and minerals) [87,88]. Heat released from the gasifier unit needs more efficient uses, including power generation and heating purpose. However, it is also challenging to cool hot gas above 1400 °C using heat exchangers due to material restrictions. The other challenge is the lack of established standard codes. The carbon content carried in syngas should be reduced to avoid greenhouse emission. Coal contains sulfur, which results in the production of sulfur oxide during the gasification process. Sulfur oxide is responsible for environmental pollution and acid rain. Therefore, a sulfur reduction system must be incorporated into the gasification process of coal for a sustainable environment. The devolatilization of coal can be carried out by using different types of fuel. Also, the devolatilization temperatures can be

integrated into the segregation of coal. Waste heat and hydrogen may be further used in power generation systems, storage, and cooling purposes by the application of the plasma co-gasification process.

3.2.4. Hydrogen Production from Biomass: Challenges and Opportunities

There have been different ways to produce hydrogen from biomass. One of the routes is called the biochemical route, where biogas is generated by the interaction of a microorganism with an organic material. The process is also known as aerobic digestion, where a combination of acids, alcohols, and gases takes place. Microorganisms, such as bacteria, break down organic matter to produce hydrogen. The organic matter can be refined sugars, raw biomass sources such as corn stover, and even wastewater. Because no light is required, these methods are sometimes called “dark fermentation” methods. In direct hydrogen fermentation, the microbes produce the hydrogen themselves. These microbes can break down complex molecules through many different pathways, and the byproducts of some of the pathways can be combined by enzymes to produce hydrogen.

Although several biomass gasification plants exist in the world, the technology is not yet fully established. Catalyst poisoning resulting from the formation of tar has not been completely addressed. Irrespective of the production process, the produced gas needs to be further processed to extract hydrogen. The unavailability of cheap biomass also restricts biomass-based hydrogen production on a large scale [71]. Converting hydrogen to hydrogen-based fuels and feedstock is easier to transport, and use; like ammonia, synthetic hydrocarbons, and methanol [89,90].

3.2.5. Hydrogen Production from Methane Splitting: Challenges and Opportunities

Around 1990, the methane splitting process was introduced, which is based on alternating the current three-phase plasma. It uses methane as feed and electricity as the energy source to produce hydrogen and solid carbon without the emission of CO_2 from natural gas [89,90]. The methane splitting process consumes electricity three to five times less than electrolysis for the same amount of hydrogen production. However, the process comes with limitations, because it requires high-temperature plasma and a significant loss of temperature, which reduces the overall efficiency [89,90]. Monolith Materials operates a pilot methane splitting plant in California and is building an industrial plant in Nebraska with a lower total efficiency than using natural gas directly in the power plant. This process can help reduce the emissions from gas combustion, and even if it requires more natural gas than electrolysis, there could be additional revenue streams from the sale of carbon black for use in rubber, tires, printers, and plastics [91,92].

3.2.6. CO_2 Capturing Technology in Hydrogen Production

Technologically advanced gray hydrogen production methods are facing questions about CO_2 emission. However, CO_2 emission reduction could be possible up to 90% by using carbon capture, utilization, and storage (CCUS) in the system. Lots of challenges need to be overcome for optimizing the demand with an environmentally friendly efficient hydrogen production pathway globally. A significant amount of CO_2 emissions have been observed while producing H_2 from different sources. Although several CO_2 capturing technologies have been explored for the SMR and ATR methods with a view toward increasing the efficiency with low costs, more research is still required for implementing CO_2 capture technology during H_2 production from natural gases and coal sources.

In a study, the regional H_2 production cost from natural gas was found to be less than USD 1/kg of H2, including the natural gas cost, OPEX, and CAPEX [72–74]. Being an energy carrier, hydrogen stores and delivers energy in some usable form. As discussed, we can produce hydrogen from diverse sources, such as natural gas, biomass, renewable energy, hydroelectric power, or nuclear energy sources. The diverse supply sources make hydrogen a promising energy carrier. Also, it has the flexibility to be produced in large, medium, or small distributed units located in proximity to the consumer, such as refueling stations or stationary power sites. Therefore, extensive research is being carried out to produce commercially viable hydrogen from different sources. At the same time, technologies should be developed in capturing CO_2 emissions to increase the efficiency with low costs during H_2 production from natural gases and coal sources. A visible development in technologies can be observed for both the steam methane reforming and partial oxidation methods, and both have been used commercially for producing hydrogen. Accordingly, it is also required to develop the delivery methods and improve the infrastructure to ensure minimum or no greenhouse gas emissions from coal-based hydrogen production. Furthermore, improving biomass growth, harvesting, and handling to reduce the cost of biomass resources used in hydrogen production is also necessary. Carbon sequestration technology to mitigate climate change during hydrogen production has been long discussed. During post-combustion, CO_2 is captured by chemical absorption using monoethanolamine (MEA). High-purity CO_2 is produced from the exhaust of coal- or gas-fired boilers using this technology. The regenerated absorbent is recycled to the absorber, and CO_2 is dried and compressed for transport conditions (typically between 100 and 150 bar). Adsorption, low temperature distillation, and membranes can also be utilized to capture CO_2 from flue gas. The physical adsorption of CO_2 at a solid surface (zeolite) is highly energy-consuming at conventional pressures and temperatures.

Using commercially available polymeric membranes results in relatively large energy requirements and CO_2 avoidance costs in comparison to chemical absorption, due to the low driving force as a consequence of the low CO_2 partial pressure in flue gas [93,94]. A summary of the challenges and opportunities of selective hydrogen production methods, along with their current research and development status, is shown in Table 3.2 [72-74,95,96].

Table 3. 2. Challenges and opportunities of selective hydrogen production methods [72-74,95]

Methods	**Critical Challenges**	**Major R&D Needs**	**Opportunities**	**Present Status**
SMR	High capital costs	Cost effective process	Sustainable approach	Advanced process
	High operation and maintenance costs	Efficient purification techniques with low cost	Lowest current cost	Application in fuel cell electric vehicles (FCEVs)
	Design issues	Optimization and Reliability	Existing infrastructure	
	Feedstock management	Feedstock pretreatment	Produced CO_2 can be used as byproduct.	
		Automated process control	CO_2 emission can be reduced if combined with CCUS	
Electro-lysis	High capital costs	Durable and cheap materials	No pollution with renewable energy sources	Alkaline electrolysis is mature and commercial technology
	Low system efficiency	Corrosive-resistant membranes	Existing infrastructure	SOECs yet to be developed and commercialized
	System integration	Durable, active, and cheap catalysts	Integration with fuel cells	Application in Fertilizer and Chlorine industry
	Access of freshwater	Large scale applications and Reliability	Thinner membrane with high mechanical strength can increase cell efficiency	
	Expensive catalyst	Storage and production rate	Integration of heat from various sources	

Methods	Critical Challenges	Major R&D Needs	Opportunities	Present Status
Coal Gasification	High reactor costs	Efficient purification techniques	Production of syngas with low cost	Production of Ammonia in Chemical and Fertilizer industry
	Feedstock impurities	Co-fed gasifiers	Abundant and cheap feedstock	Mature Technology
	Carbon capture and storage	Carbon capture and storage technology	Reduce the volatilization of coal can increase efficiency	New membrane technology for H2 separation and purification
Coal Gasification (Cont.)	High CO_2 emissions intensity	Hydrogen quality	CO_2 can be decarbonized if combined with CCUS	
	lack of established standard codes	Feedstock preparation cost		
	Cool the hot gas above 1400 °C	Tolerance for impurities		.
Biomass Gasification	High capital costs	Low cost and efficient purification	Production of syngas with low cost	Mature Technology
	Feedstock impurities	Co-fed gasifiers	Abundant and cheap feedstock	New membrane technology for H2 separation and purification
	Carbon capture and storage	Carbon capture and storage		Commercial demonstration
		Hydrogen quality		
		Cost of feedstock preparation		
		Tolerance for impurities		

3.3. Overview of Hydrogen Storage Materials and Associate Challenges

From a material point of view, hydrogen gas faces challenges due to its characteristics and reactivity with the overall infrastructure, including transmission, pipeline, storage, and production facilities. Embrittlement is the major problem for hydrogen infrastructures encountered by researchers since long ago. Also, an energy-dense and reactive gas such as hydrogen leads to polymeric material challenges in the infrastructure presently for its safe operation. The purity of hydrogen is a key factor for hydrogen rupture pressure. Oxygen or traces of water vapor can partially inhibit the hydrogen embrittlement effect [97]. Usually, the purer the hydrogen, the more embrittlement is observed. The reason is likely that impurities like SO_2 in hydrogen have an inhibiting impact on embrittlement. Again, other impurities such as CH_4 and N_2 do not seem to have any appreciable effect. On the contrary, there are some impurities like CO_2 and H_2S that have an adverse effect on hydrogen-induced embrittlement [97]. The microstructure of steel and other materials resulting from heat treatment and chemical composition also plays a significant role in HE. It has been observed that martensitic structures have the worst behavior, ferritic structures an intermediate behavior, and stable austenitic steels exhibit the best behavior [97]. The welding of steel is also a major parameter that can greatly affect HE behavior.

The hardness of the welded area and heat-affected zone should be limited to carbon steels. The formation of ferrite should be limited in austenitic stainless steel [97,98]. Ni, Ti, and high Ni alloys and Ti alloys are very sensitive to HE. Again, HE behavior may remain even at rather high temperatures of steel materials. The impact of high-pressure and high pure hydrogen is also evident on metals. Depending on the material, the HE increases upon increasing the pressure. Austenitic steel is considered the safer option for HE [93]. Hydrogen atoms enter into the iron sample once

it is subjected to stress or tension above the elastic limit. From the analysis of the crack formation, it has been observed that, under normal operating conditions, the change in pressure does not cause failure; while the pipe is affected by HE, it will not be able to take the pressure for a long time and crack [99]. It is very sensitive to calculate the fatigue-life while there are growing crack, defect, and infrequent pressure cycles.

The predicted lifetime of a pipeline for a hydrogen–natural gas blend and for 100% hydrogen is about the same: many decades [100]. Experimental studies have predicted the lifespan of steel under high-pressure hydrogen effects. The estimated lifespan of X70 API 5L grade steel is more than 50 years [100]; the API steels (X52, X60, X65, X70, and API 5L Grade B) and X42 steel lifespans are also determined to be more than 50 years with different load rations R; and the X80 steel lifespan is estimated at 37 years with a 50% hydrogen gas mix with natural gas [101,102]. These lifespan estimations are based on assumptions for two pressure cycles per day.

The permeability of hydrogen increases when increasing the hydrogen pressure, but the ratio gets slower with the further increasing of pressure. All the permeability, diffusion, and solubility coefficients are correlated with a specific volume in high-pressure environments. The gas diffusion decreases upon the compressive effect of the free volume by the application of hydrogen. The permeation coefficient also decreases with the pressure increase from the measurement of the crystallinity; it is evident that gas penetration takes place in an amorphous region under a high-pressure hydrogen environment [100]. The degree of destruction is greatly influenced by the quantity of the gas penetration. However, the type of material is also a significant factor to determine the damage. In recent decades, there has been an increasing focus on developing hydrogen storage materials that are both economical and efficient. Researchers have investigated

diverse materials and technologies to store and utilize hydrogen securely. A chronological representation of the advancements in research on hydrogen storage materials over several decades is analyzed here.

During the 1970s, researchers investigated diverse materials such as metals, alloys, and hydrides to explore their potential as hydrogen storage mediums [103]. The fundamental hydrogen spillover concepts were established in the late 1960s and 1970s [104]. One of the initial investigations revealed that metal hydrides, including magnesium hydrides, exhibit a high capacity for hydrogen absorption[105]. During the 1980s, there was a notable expansion in research on hydrogen storage materials primarily focused on investigating the thermodynamics and kinematics of hydrogen absorption and desorption for diverse materials, for example, the development of commercial hydrogen storage electrodes and rechargeable nickel hydride batteries [106]. During the 1990s, the advancement of nanotechnology presented novel opportunities for hydrogen storage materials [107]. Research indicated that nanoparticles of specific metals exhibited superior hydrogen absorption and release capabilities compared to their bulk counterparts. Scientists investigated chemical hydrides, which can release hydrogen via a chemical reaction with water or other substances. The research emphasis transitioned towards exploring the potential of utilizing complex hydrides, such as metal borohydrides and metal amides, for hydrogen storage [108]. During the 2000s, research on hydrogen storage materials shifted towards applications. The focus was identifying materials that could be utilized in hydrogen fuel cells for vehicle transportation and other related purposes [109]. Additional research were conducted to explore novel materials, including composites of metal hydrides, and to investigate the potential of reversible chemical reactions for hydrogen storage and release. Researchers found that porous materials, such as metal-organic frameworks and covalent organic frameworks, possess substantial surface areas and can

store hydrogen [110]. During the 2010s, significant progress was made in materials science and engineering, resulting in novel hydrogen storage materials that exhibit superior properties, including enhanced storage capacity, accelerated absorption and desorption rates, and reduced operating temperatures. Researchers also investigated novel techniques for hydrogen storage, including cryo-adsorption and hydrogen physisorption [111]. Metal hydride systems were developed in the 2010s for hydrogen storage in emergency or backup power units, i.e., for stationary applications. Ongoing research in the 2020s is dedicated to developing hydrogen storage materials to enhance their efficiency, safety, and practicality for diverse applications. Current research is investigating novel materials, including metal-organic polyhedra (MOPs) and advanced carbon materials, as well as innovative techniques for hydrogen storage, such as solid-state hydrogen storage and liquid organic hydrogen carriers [112,113].

3.3.1. Hydrogen Storage Materials

Various techniques are available for hydrogen storage, such as compressed gas, liquid-state storage, and solid-state storage. Compressed hydrogen gas storage systems require less specialized equipment and infrastructure than alternative methods, such as complex metal hydrides or liquid hydrogen storage. Liquid hydrogen exhibits a greater energy density per unit volume than compressed hydrogen gas, enabling a higher storage capacity within a smaller volume. The storage of liquid hydrogen is a desirable alternative for space and aviation applications due to its advantageous characteristics in terms of weight and volume [114]. Storing hydrogen in a solid material, commonly known as solid-state hydrogen storage, presents an alternative to its potential for high storage capacity, safety, and convenient transport.

3.3.1.1. Solid-State Hydrogen Storage

Using chemical compounds for hydrogen storage through absorption or adsorption on carbon materials offers distinct benefits in terms of safety. Considerable research efforts have been performed to develop solid hydrogen storage systems encompassing Metal-Organic Frameworks (MOFs), Zeolites, Metal Hydrides, Metal Nitrides, Metal Imides, and carbon-based Materials [115]. Hydrogen is bonded in solid-state storage through physical means, such as using MOFs and carbon-based materials, or bonded by chemical forces, such as hydrides, imides, and nitrides. Aerogels like silica and carbon offer unique properties, such as high surface area and low density, which facilitate hydrogen adsorption and efficient diffusion. They can be functionalized to enhance hydrogen binding affinity and storage capacity. Carbon aerogels, on the other hand, offer excellent mechanical strength, thermal stability, and high specific surface area, making them suitable for both physical and chemical hydrogen storage mechanisms. Physisorption is a viable method for storing hydrogen in porous materials. Physisorption and chemisorption are two distinct ways gases interact with solid surfaces. Chemisorption involves hydrogen molecules binding to solid materials through strong chemical bonds, resulting in high storage capacities. It requires materials with suitable chemisorption sites like metal hydrides or complex metal organic frameworks. Physisorption, on the other hand, involves hydrogen molecules adsorbing onto a material's surface through weak van der Waals interactions, offering lower storage capacities but reversible processes and milder conditions. Porous materials like activated carbons and zeolites are commonly investigated for physisorption-based hydrogen storage applications [116]. The physisorption of hydrogen in materials is of particular interest for various technological applications due to its rapid kinetics, complete reversibility, short refueling time, and high cycle life [110]. On the contrary, chemisorption exhibits a higher degree of gas adsorption, although accompanied by irreversibility.

Activated Carbon (AC):

Activated carbon is a synthetic carbon material modified to possess high porosity, consisting of crystallized graphite and amorphous carbon with a high surface area [117]. Activated carbon's hydrogen storage rate and capacity can be impacted by its morphology and shape, specifically in powder, fiber, and granular forms. The rate of hydrogen adsorption in fibrous form exhibits a significantly higher value, ranging from 2 to 50 times faster under optimal conditions [118]. The hydrogen absorption in conventional activated carbon is directly proportional to its surface area and pore volume. Based on monolayer adsorption, the Langmuir isotherm model can accurately describe it. Under conditions of low temperature and high pressure, a significant increase in adsorption capacity is observed. Extensive research has been conducted on hydrogen adsorption on various commercial and modified activated carbon products [119]. Empirical findings indicate that products possessing micropore volumes exceeding 1 mL/g can retain approximately 2.2 wt.% of hydrogen through physisorption. Refining the adsorbent and sorption conditions can enhance the storage capacity to 4.5–5.3 wt.%. Activated carbon, which has undergone mechanical milling, exhibits a nanostructure that is characterized by defects, thereby leading to an increase in its specific surface area. Research shows that hydrogen storage capacity increases from 0.9 wt.% to approximately 1.7 wt.% after 10 hours of milling [120]. Research has indicated that the adsorption capacity can be enhanced by loading precious metals, such as Platinum (Pt), onto activated carbon [121]. The occurrence of chemisorption occurring on the Pt surface and physisorption on the carbon surface results in a significant quantity of hydrogen spillover.

Table 3. 3: Hydrogen Storage Capacity of Activated Carbon

Adsorbent	H2 storage (wt.%)	Temp, Pressure	Reference
AC	0.67	303K, 10 MPa	[122]
AC	1.4	77K, 0.1 MPa	[123]
AC	1.6	296K, 13MPa	[124]
AC	4.5	77.4K	[125]
AC	5.7	77K, 3 MPa	[122]
AC (KOH treated)	6.6	77K, 4MPa	[126]
AC (Ni doped)	1.8	77K, 0.1 MPa	[123]
AC (Pt doped)	2.3	298K, 10MPa	[127]
AC (Pd doped)	5.5	298K, 8MPa	[128]

Carbon Nanotubes (CNTs)

In the late 1990s, carbon nanotubes and other carbon nanostructures were investigated as promising hydrogen storage solutions [127–129]. Nanocarbon materials possess porous structures that serve as trapping sites, potentially enabling enhanced storage capacity [120]. Dillon et al. investigated the hydrogen storage potential of carbon nanotubes and demonstrated encouraging outcomes. The two primary species of carbon nanotubes are distinguished by the composition of their walls, namely the Single-Walled Nanotubes (SWNT) and the Multi-Walled Nanotubes (MWNT) [132]. Diverse experimental conditions applied to these materials have yielded hydrogen storage values that exhibit significant variation, ranging from 0.25 to 56 wt.%. As per the technical report published by the International Energy Agency, it is widely agreed that achieving very high hydrogen storage capacities, approximately 30–60 wt.%, as reported a few years ago, is highly unlikely due to potential measurement errors. The storage capability, which can reach up to 6 wt.%, remains advantageous under cryogenic conditions and in carbons with exceptionally high surface areas [133].

Table 3. 4: Hydrogen Storage Capacity of Carbon Nanotubes

Adsorbent	H2 storage (wt.%)	Temp, Pressure	Ref.
SWNT	5-10	133K, 0.04MPa	[134]
SWNT	3.50-4.50	298K, 0.067MPa	[135]
SWNT	1-15	77-300K, 8MPa	[136]
SWNT	8.50	80K, 7Mpa	[137]
SWNT	1.20	298K, 4.8MPa	[138]
MWNT	56	298K, 12.16MPa	[139]
MWNT	0.25	300-700K, 0.1MPa	[140]
MWNT	0.68	298K, 10MPa	[141]
MWNT	13.80	300K, 1MPa	[142]
MWNT	0.70-0.80	300k, 7Mpa	[143]

Metal-Organic Frameworks (MOFs):

Hydrogen storage within porous materials is a promising approach for transportation applications. The data related to hydrogen storage using MOF-5 (Table 3.5), which was first reported in 2003, indicated a significant surge in hydrogen absorption under external pressures, with a peak of 4.5 wt.% observed at temperatures of 77 K and pressures below 1 bar and an average of 1.3 wt.% at a pressure of 1 bar [134,135]. After this, further advancements in diverse MOFs were documented, exhibiting elevated hydrogen adsorption capacities at 77 K and increased pressures. This can be considered to these innovative frameworks' substantial pore volumes and notable specific surface areas [135,136]. In a theoretical investigation by Ahmed et al. [138], approximately 500,000 MOFs were screened, revealing a maximum usable volumetric capacity of approximately 40 g H2 L-1 was found. Table 3. 5 shows Measured and calculated crystallographic properties of high-capacity MOFs [139].

Table 3. 5: Crystallographic properties of high-capacity MOFs [139]

MOF	Surface Area		Pore Volume ($cm^3\ g^{-1}$) Calc.	Void Fraction Calculation
	Gravimetric (m2/g) Expt./Calc.	Volumetric ($m^2\ cm^{-3}$) Calc.		
MOF-5	3512/3563	2172	1.36	0.81
IRMOF-20	4073/4127	2000	1.65	0.84
SNU-70	4944/4756	1905	2.14	0.86
UMCM-9	5039/4847	1805	2.31	0.86
PCN-610	6050/5777	1603	3.17	0.88

Metal Hydrides

Metal hydrides represent a class of materials with considerable potential to meet the benchmarks for hydrogen storage. Basic metal hydrides such as MgH_2 and complex metal hydrides like $NaAlH_4$ and $LaNi5H_6$ have been evaluated for this application. The energy density by volume of these materials is prospective; however, their energy density by weight is less potential to that of hydrocarbons. Solid hydrides, which have the potential to be shaped into pellets or granules, require an approximate temperature of 120°C to release the stored hydrogen. For example, the hydrogen storage capacity of MgH_2 has been observed to reach up to 7.60 wt.%. The hydrogen storage density of MgH_2 is comparatively higher than that of compressed hydrogen gas and liquid hydrogen, with a value of 6.5 hydrogen atoms per cm^3 for MgH_2, 0.99 hydrogen atoms per cm^3 for compressed hydrogen gas, and 4.2 hydrogen atoms per cm^3 for liquid hydrogen. As a result, metal hydride storage has been identified as a safer and more space-efficient option for on-board applications.

Two potential methods for synthesizing metal hydrides are direct dissociative chemisorption and electrochemical water splitting. The ensuing reactions are as follows:

$M + H2 \leftrightarrow MH_x$…… (i),

$M + H2O + \frac{x}{2} e^- \leftrightarrow MH_x + \frac{x}{2} OH^-$…..(ii)

M denotes the metal, while x signifies its valence. Light metals, e.g., lithium, beryllium, sodium, magnesium, boron, and aluminum-based storage materials, are popular substances used for storage. The different hydrogen capacities of some selected metal hydrides are shown here.

Figure 3. 3 represent hydrogen storage performance of some selected Metal Hydrides [140].

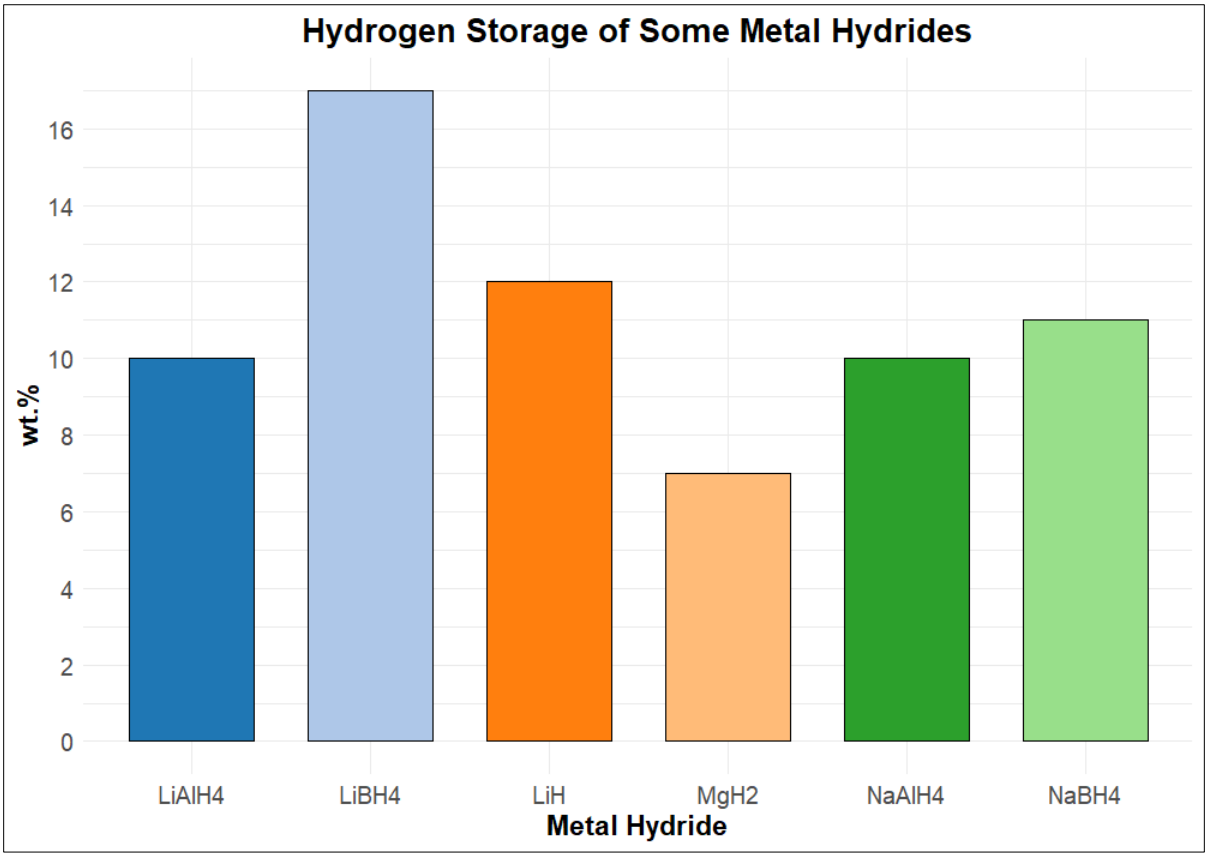

Figure 3. 3: Hydrogen storage performance of some selected Metal Hydrides [140]

3.3.1.2. Liquid State Hydrogen Storage

Liquid hydrogen storage is the most common method, but it is expensive and complicated due to the need for extremely low temperatures (20 K) for liquefaction. As a result, alternative liquid carriers with more reasonable storage conditions are being considered. The focus of attention under the International Energy Agency Task 32, has primarily been on two specific carriers: Ammonia and Liquid Organic Hydrogen Carriers (LOHCs) [143–147]. Both have more moderate storage requirements than liquid hydrogen, reducing estimated storage and transportation expenses [146]. Most proposed uses for liquid carriers do not need on-board dehydrogenation in fuel cell vehicles. Instead, they involve centralized dehydrogenation at ports or other facilities to distribute hydrogen gas locally or at recharging stations.

Cryogenic and Compressed Storage

Cryogenic storage of hydrogen offers high energy density; however, their storage necessitates intricate systems to limit boil-off. These liquid tanks' complexity, size, and weight increase capital costs. In addition, costly liquefaction equipment is also necessary. Furthermore, the high energy requirements (30 to 33% of the total energy) for hydrogen liquefying and economic considerations impede its development. Even the best-insulated containers can still result in hydrogen boil-off, energy efficiency, and security issues. At 1 bar and 20 K, the density of liquid hydrogen is 70 g/L. Although there is theoretical potential for greater hydrogen storage capacity, the practical efficiency of the liquid hydrogen tank limits its applicability. Because liquid hydrogen has a low boiling point (20 K), maintaining the cryogenic temperature requires a specifically made metallic double-walled container with an excellent insulating system. Even the best-insulated containers can still result in hydrogen evaporation, increased container pressure, energy efficiency, and

security issues [147]. Cryo-compressed hydrogen storage requires comparatively low pressure and does not need a costly Carbon Fiber Reinforced Plastic (CFRP) tank. It can also increase energy efficiency and reduce hydrogen boil-off. At 276 bar and 20 K, the density of hydrogen increases to about 87 g/L in the cryo-compressed storage technique. The cryo-compressed container's hydrogen storage capacity rises to 0.058 kg H2/kg system and 0.043 kg/L, meeting the target of the DOE 2025 on-board automotive storage values [148]. Table 3.6 showing estimated performance for liquid hydrogen storage systems [149].

Table 3. 6: Estimated Performance for Liquid Hydrogen Storage Systems [149]

Storage System	Temp, Pressure	H2 Density (g/L)	Gravimetric Density
Cryogenic	20 K, 1 bar	70	0.05
Cryo-Compressed	20 K, 276 bars	87	0.058

Liquid Organic Hydrogen Carriers (LOHCs)

LOHCs are an efficient means of chemically bonding elemental hydrogen, providing possibilities for safely storing energy on a large scale [150]. The LOHC compounds such as cyclohexane, methylcyclohexane, and decalin can release up to 6 wt.% hydrogen. The dehydrated form of LOHC undergoes a hydrogenation reaction to assimilate hydrogen. Hydrogenation releases heat energy and is conducted under high pressures, often ranging from 30 to 50 bar, and at temperatures around 150 to 200°C in the presence of a catalyst. Once the hydrogen is required again, the LOHC undergoes dehydrogenation, resulting in the release of hydrogen. Figure 3. 4 shows the Hydrogenation-dehydrogenation process [152]. The reaction occurs at high temperatures (250-320°C) under the influence of a catalyst [151].

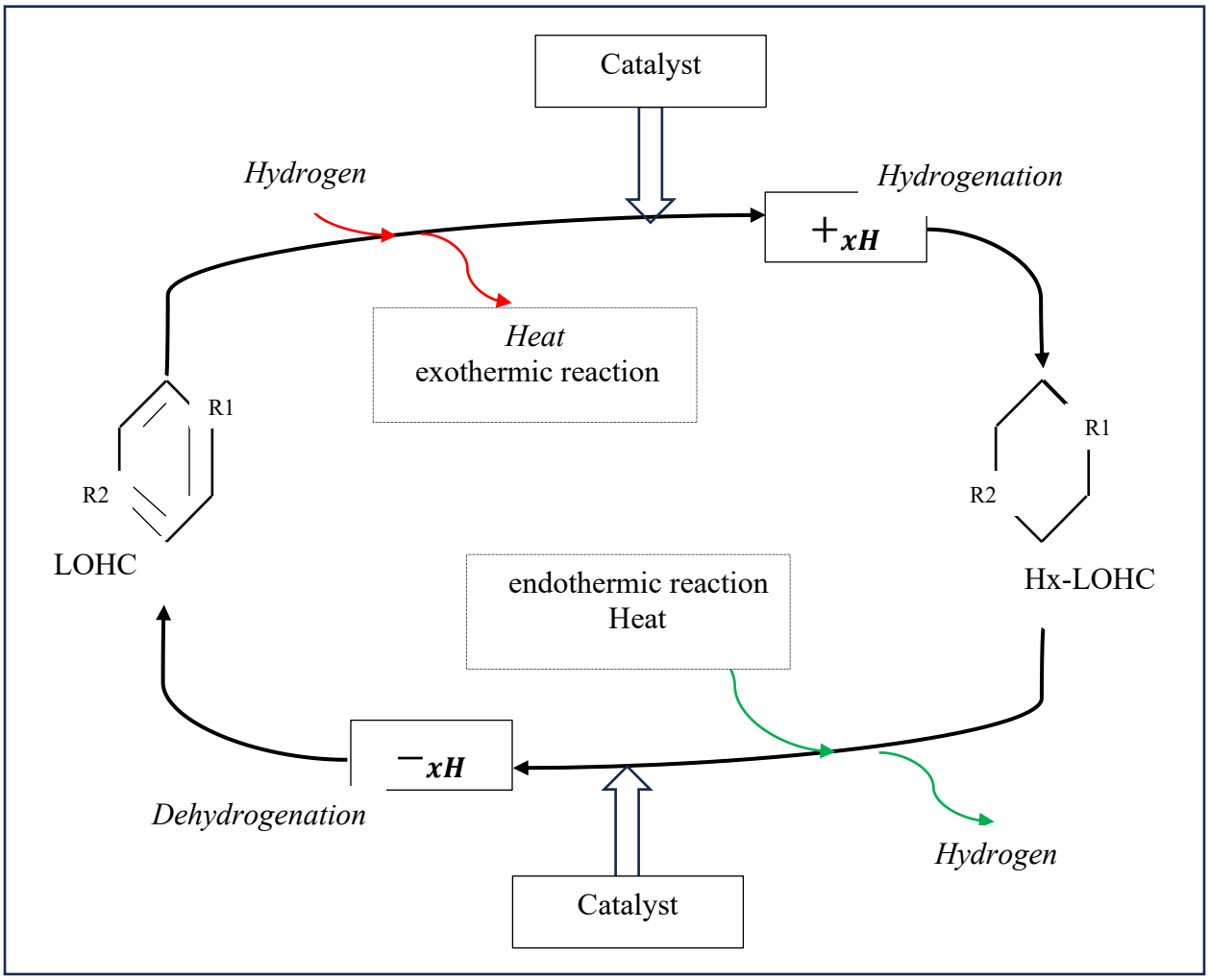

Figure 3. 4: Hydrogenation-dehydrogenation process [152]

The dehydrogenation process to produce the corresponding aromatic compounds was predominantly carried out using platinum-based catalysts at temperatures ranging from 300°C to 350°C [145, 148]. The elevated dehydrogenation temperature and the necessary costly catalysts delayed the commercial application of the LOHC processes. Investigations into these carriers have centred on reducing dehydrogenation temperature by modifying the LOHC molecule, thereby reducing the enthalpy of the reaction. The research for catalysts that exhibit enhanced activity and stability and are composed of readily available earth-abundant materials for dehydrogenation is on the process. Efforts to alter the enthalpy of dehydrogenation have predominantly focused on

incorporating heteroatoms, specifically nitrogen, within the cyclic architecture [150–152]. Some materials, such as N-ethyl carbazole, have demonstrated better hydrogen storage and release properties than an unsaturated system [153,154]. Study was conducted to report the synthesis of crystalline lithium amines through ball-milling primary amines with LiH [130]. The results indicate that this method exhibits mild endothermic dehydrogenation and improved selectivity toward hydrogen release [153-155]. For catalyst support, certain materials have been discovered to enhance the hydrogenation rate, such as palladium nanoparticles, which showed increased activity when supported on a covalent triazine framework [130].

Ammonia

Due to the limited options available for transporting liquid hydrogen, there is significant interest in utilizing ammonia for hydrogen transportation [151]. Using ammonia as a hydrogen carrier offers a great opportunity for a cost-efficient and secure approach to storing and transporting zero-carbon energy. Ammonia, with its dense concentration of hydrogen, has been widely produced for manufacturing fertilizers, leading to the creation of large-scale storage and transportation infrastructure. Ammonia can decompose into nitrogen and hydrogen, which can be used as fuel through cracking. The cracker consists of three primary elements: an evaporator, which vaporizes the liquid ammonia; a preheater, which raises the temperature of the ammonia gas to 400°C; and a reactor, which contains the catalyst for the cracking reaction. A separator is necessary to achieve pure hydrogen extraction from the cracked gas due to the presence of a hydrogen and nitrogen combination. Numerous research are underway to enhance the cost-effectiveness and efficacy of hydrogen storage associated with ammonia. The technology for hydrogen release from ammonia is not widely established, as it does not constitute a substantial component of the current ammonia

markets. The catalysis of ammonia decomposition has been thoroughly investigated in transition metal systems to evaluate catalytic performance for ammonia synthesis [156,157]. Ruthenium has been identified as the metal with the highest level of reactivity. However, comparable performance levels can be achieved by utilizing metals abundant in the earth's crust, such as Iron, Cobalt, and Molybdenum [158-160]. The impact of temperature is an important factor to consider, as the complete conversion of hydrogen necessitates elevated temperatures (>450°C) even for the most dynamic Ruthenium-based catalysts. The development of novel catalysts is necessary to achieve a substantial reduction in operational temperatures. Metal-nitrogen-hydrogen materials, specifically light metal amides have successfully facilitated ammonia decomposition. These materials have exhibited catalytic performance comparable to that of supported Ruthenium catalysts [161-163]. Sorption materials can store ammonia while exhibiting a considerably decreased vapor pressure [145,164,165,166]. The amine complexes of metal halides exhibit ammonia densities comparable to liquid ammonia. Ammonia release can be customized to meet the specific application by manipulating metal ion combinations within a metal halide system.

3.3.1.3. Gaseous State Hydrogen Storage

Gaseous storage of hydrogen under high pressure is a commonly used technique. To accomplish the high-pressure storage (350 bar to 700 bar), a tank material is required, which must have high tensile strength, low density, non-reactivity with hydrogen, and low diffusivity and be economical. Using low prices and high thermal conductivity, some steel and aluminium-type materials are utilized to construct storage tanks. These metal materials are nondurable, heavy-weight, and have safety concerns [167,168]. In contrast to metals, CFRP, which is lightweight, has sufficient strength, and has durable properties, is a more promising material for pressurized gas vessels [168–

170]. At the same time, the low thermal conductivity and high-price issues need to be solved before the CFRP can be extensively used. Underground salt caverns can store high-pressure gas and are applied to stationery store-pressure hydrogen gas [169-171]. It is a feasible option for compressed hydrogen gas storage, with adjustable storage capacity, high-pressure storage ability, adaptable operating pressure, and minimized hydrogen leakage. Table 3. 7 shows materials for high-pressure hydrogen storage tanks [172].

Table 3. 7: Materials for high-pressure hydrogen storage tanks [172]

Material	**Tensile Strength (MPa)**	**Density (kg/m^3)**
Steel Alloys	703	8160
Titanium Alloys	924	4430
Carbon Composites	2070	1900

Novel composite cylinders with reduced weight, capable of enduring up to 80 MPa pressures, have been developed. This allows hydrogen to attain a volumetric density of 36 kg/m3, half that of its liquid state at the standard boiling point [174]. The gravimetric hydrogen density negatively correlates with pressure due to the augmented thickness of the pressure cylinder walls. Pressure vessels are widely utilized in various fields, such as industrial, automotive, commercial, and aerospace applications, ranging from small bottles to large storage tanks. The pressure vessels presently employed in hydrogen storage systems for automobiles and buses are distinguished by a pressure of 35 MPa or 70 MPa. However, the preference for 70 MPa is rising to enhance storage density. The categorization of pressure vessels is based on four distinct types: Types I, II, III &IV. Table 3. 8 showing types of pressure vessels [173].

Table 3. 8: Types of Pressure Vessels [173]

Type	Materials	Typical pressure (bar)	Gravimetric Density (wt.%)
I	All-metal construction	300	1.7
II	Mostly metal, composite overwrap in the hoop direction	200	2.1
III	Metal liner, full composite overwrap	700	4.2
IV	All-composite construction	700	5.7

Type I refers to a vessel made solely of metal, usually steel. As a result, it is the heaviest type of vessel. It is commonly used in industries for stationary purposes. Type I vessels have a hydrogen storage capacity of approximately 1 wt.% at pressures ranging from 200 to 300 bar [131]. Type II is a metal liner hoop-wrapped composite cylinder with a lower weight than Type I. Type I, and Type II vessels are less suitable for vehicle applications due to their inadequate hydrogen storage density resulting from their substantial weights and the challenges imposed by hydrogen embrittlement. Type III vessels consist of a completely wrapped composite cylinder with a metal liner to prevent hydrogen permeation. The metal liner is composed of Aluminium, effectively addressing the embrittlement issue and enhancing mechanical strength by over 5%. Type III vessels offer a 25%–75% mass gain over Types I and II, making them suitable for vehicle apply. Type III vessels have also been shown to be reliable at pressures up to 450 bar, but there are still challenges associated with pressure cycling tests at 700 bar. Type IV pressure vessels are like Type III vessels, except that they feature a non-load-bearing polymer liner instead of a metallic liner. In specific applications, polymer liners in an "all-composite" construction may present superior cost and performance benefits compared to vessels that incorporate metal liners [175]. Type IV vessels are the lightest of the pressure vessels, making them most suitable for vehicle applications, and they can endure high pressures of up to 1,000 bar. However, they are too costly due to the

considerable cost contribution of the carbon fibers. Cost projections show that the carbon fiber cost constitutes about 75% of the storage vessel cost, considering the high production volumes. [176]. Figure 3. 5 shows the schematic illustration of the four types of pressure vessels [177].

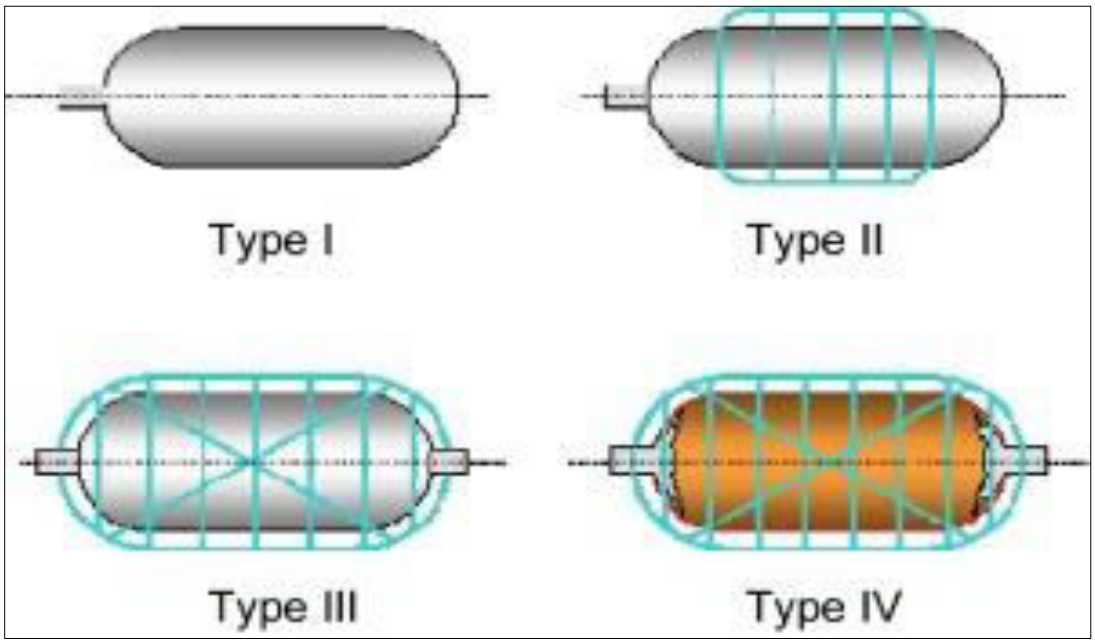

Figure 3. 5: A schematic illustration of the four types of pressure vessels [177]

3.3.2. Challenges and Opportunities for Different Hydrogen Storage Methods

3.3.2.1. Polymer Used in Hydrogen Application and Challenges

The applications of polymer materials are vast in the hydrogen industry. They are used for seals in connections, compression equipment, tubing, dispensing, and valves, as well as the lining of the storage cylinders. Four classes of polymer materials are used in hydrogen applications based on their microstructure. These are semicrystalline thermoplastics, amorphous thermoplastics, elastomers, and epoxies [141–143]. Leaks at critical interfaces, such as onboard tank systems, the dispenser–vehicle interface, and supply systems, are very common. O-rings (elastomeric) are widely used in the hydrogen industry in both static and dynamic designs to prevent leaks in systems

[144]. Transient conditions must be considered during designing the specification of a static seal. Temporary leaks can take place in elastomeric materials during the motion of a shaft in valves or regulators. In the case of dynamic seal designs, the issues can result in a temporary leak during movement between the sealing surfaces. The tribology of polymers plays an important role in dynamic sealing applications. A longer lifetime for polymers in a high-pressure hydrogen environment depends on the low coefficient of friction, which means less wear and tear. Depending on the permeation characteristics of the polymers, the friction behavior can differ. Fillers in polymers can play a large role in increasing or decreasing their susceptibility to hydrogen [145]. The effects of plasticization, fracture, and fatigue should be taken into consideration while selecting polymers for a high-pressure hydrogen environment. Additionally, the rapid gas decompression of elastomers with the combined effects of temperature and pressure cycling metrics for assessing the damage and mitigation through the development of damage-resistant materials needs to be studied as well [145]. Thermoplastic and elastomeric polymers have been studied under high-pressure hydrogen (70–100 MPa) in static, isothermal, and isobaric conditions to characterize the physical properties and perform a mechanical analysis. During fuel consumption and refueling operations of fuel cell vehicles, polymers are exposed to a large pressure gradient. In dynamic environments such as in the high-pressure cycling of hydrogen (35 MPa to 100 MPa to 35 MPa), the performance of these polymers is highly influenced [141,145]. Picking up the right sealing material for the hydrogen flow is one of the most crucial challenges to prevent gas permeation and absorption. While characterizing polymeric materials, several conditions need to be considered. The measurements of crystallinity, degree of polymerization, crosslink density, outgassing and desorption of chemical species, permeation/absorption of hydrogen into polymers, gas exposure time, temperature, pressure, pressurization/depressurization

rates, durability, correlation of bench-scale versus full-scale material characteristics, etc. are important [144]. The effects of hydrogen, temperature, and pressure on “creep” and “strength” need to be investigated. Also, plasticization effects such as a change in ductility under a hydrogen environment have yet to be explored. Understanding the supercritical properties of hydrogen as a solvent on a polymer is important to customize the appropriate polymer selection.

Polymers, whether used in seals, compressors, tubing, or pressure vessels, can fail in a variety of ways. Although hydrogen embrittlement mechanisms in metals appear to be absent in polymers, exposure to high-pressure hydrogen does affect the mechanical performance of polymers. Being one of the smallest molecules, hydrogen can diffuse into and through polymers much more easily than any other gases. While operating in hydrogen, some polymers can maintain their properties. However, the behavior of different polymers under a hydrogen environment is yet to be explored. When hydrogen absorbs into and diffuses through polymer components at high pressure, it forms small bubbles within the material, causing damage. If the depressurization is substantial and rapid enough, these bubbles can exit the polymer violently, causing substantial damage and failure of the component. This rapid gas decompression can occur even at a timescale of hours, meaning this effect is not limited to sudden and drastic changes in pressure. While the hydrogen effect on a few selective polymers, including EVA, PVC, EPDM, etc. have been studied, a large portion—thermoplastics, in particular—have not been thoroughly investigated for this failure mechanism. Also, the high pressure used to store hydrogen can have some effects on the plasticization of the polymers, which needs to be studied as well. Extensive research on the fracture and fatigue failure modes, rapid gas decomposition, friction and wear, test methods, plasticization, transport properties, and contaminants is necessary [141,142].

3.3.2.2. Composites used in Hydrogen Application and Challenges

Composites used as hydrogen storage materials are different. Kevlar and glass fibers have been shown to be more damage-tolerant than carbon fibers. Composite cylinder designs have recently improved to become more damage-resistant by adding additives to damage-sensitive areas and adding sacrificial layers to the outside of the entire tank [146]. Carbon fiber manufacture needs economic and advanced material characterization methods to monitor the key performance. The key performance properties include the defect structure, resistivity change during carbonization, density change during oxidation, etc. Screen alternative fibers are also considered as potential candidates in the application of filament winding [141,142]. Stress rupture is an important but not fully understood problem with composite tanks. It occurs when multiple fibers randomly fail next to each other. Normally, when a single fiber fails, the surrounding fibers can hold the load that was previously carried by the failed fiber. However, when multiple fibers fail very close to each other, the surrounding fibers are suddenly put under a much greater load, leading them to fail and so on, until the entire vessel/layers rupture. This failure has little or no advanced warning and can lead to catastrophic results. One way these fibers may fail is due to corrosion, such as the oxidation of carbon fibers. This mechanism has been studied under various atmospheres including air and at various temperatures, and it was found that high-temperature samples in air had the highest rates of failure. One problem with the study of stress ruptures is the inherently stochastic mechanism they follow. Fibers can fail more or less randomly, and so, it is inherently random if a sufficient number of fibers happen to fail in a cluster close to each other. This means that experimental studies of this phenomenon need high numbers of samples, typically with high lifetimes, in order to produce failures [147]. Understanding the material properties of composites and polymers is challenging when there are complex operating conditions with multiple variables. For example, at

a wide range of temperatures as low as (−40 °C) to as high as (85 °C) with high pressure (700 bar), it is difficult to interpret the composite behavior on hydrogen. Also, there have been localized thermal extrusions during refueling or defueling operations of hydrogen-fueled vehicles. The impact of localized thermal extrusion is yet to be explored. Specifications such as SAE J2601, SAE J2579/GTR, CSA HGV 4.3, CSA HGV 2, and ISO 15869 could be incorporated into the fueling standards. A correlation between the material behavior and degradation at thermal soak and in-service temperature excursions needs to be established for certification. A temperature gradient exists between the gaseous hydrogen and sealing material during the fueling or defueling operation. The temperature difference must be considered to correlate with the test results from the thermal soak to in-service condition [141,142].

In order to determine the durability of a composite material, cycling loading experiments are performed rather than material tests on the constituent polymers. Cycles of around 90 MPa hydrogen pressure are usually maintained for the durability test. The crack damage and extrusion fracture of the composites are observed at various temperature, pressure, and cycling conditions. The crack damage was noticeably worsened by increases in the pressure (from 35 to 70 MPa) and temperature (from 60 °C to 100 °C) at the EPDM O-ring [48,49]. The key advantage of composite pressure vessels is the lesser weight. However, the aging of a carbon-fiber-reinforced plastic (CFRP) composite pressure vessel underlies the complex interaction with its metallic liner, which is yet to be understood. The appropriate testing methods to detect the influence of the pressure cycle and creep behavior on the material are yet to be established. A hydraulic internal pressure test usually cannot detect cracks unless fully developed through the metallic liner, whereas Eddy Current Testing (ET) can be a promising alternate test. High-frequency ET can also be used to

investigate the aging behavior of composites. Usually, the eddy current is introduced to detect cracks at high-frequency regions of fibers. Also, signals coming from the resin are more detectable in high-frequency applications. Composite overwrapped pressure vessel (COPV) failures, Kevlar, and glass fibers have been shown to be more damage-tolerant than carbon fibers [150].

3.3.2.3. Metals Used in Hydrogen Application and Challenges

The probability of a hydrogen attack mostly depends on the metallurgical structure of the steel. The chemical composition, distribution, and morphology of the phases; grain structure (size, shape, and texture); segregation; and distribution of intentional alloying elements and precipitates, as well as impurities, are the factors that change the metallurgical structure. However, the effect of the fundamental metallurgical reason behind using lower-strength steels over higher ones in existing natural gas pipelines, which have already been proven historically, is still to be proven [151,152]. Modern PE pipes enable the transport of hydrogen. Polyethylene pipe, PE80 and PE100, has several significant advantages over traditional materials such as steel or ductile iron. The permeation of contaminants in PE 80 and 100 materials explore the relationships between crystallinity and permeability, diffusion, and separation. The dominating factors to assess the hydrogen compatibility are the structural changes in the polymer, consumption of antioxidants, change in the tensile properties, change in the slow crack growth properties of the material, surface oxidation, and metering calibration. The test apparatus developed by NIST can measure 10 specimens simultaneously with specific environmental and loading conditions until all of them have been tested to be used in industry. Over 150 fatigue tests were completed by them on base metals, welds, and the heat-affected zones of candidate steels. A modification was made to the ASME B31.12 by NIST to permit the use of X70 steel rather than X52 steel, which would result

in a savings of over USD 1 million per mile of pipeline [153,154]. The standard guidelines like ASME B31.12 and the AIGA/EIGA permit X80/L555-graded materials to be used in hydrogen service. But ASME B31.12 explicitly states that only grades up to X52/L360 are proven for hydrogen gas services. The destructive testing of material samples at a minimum frequency of one sample per mile is recommended by the existing codes. The RoMat family was introduced by ROSEN for inline inspection services that include pipe grade sensor (PGS) technology and DMG hard spot technology. The aim is to support operators through the processes of material verification [152,155,178]. The US natural gas pipeline system states the feasibility of using relatively less concentrated hydrogen (5–15% by volume) with some minor modifications to the existing pipeline systems. To blend 10% hydrogen with a pressure drop ranging from 300 psi to 30 psi, the extraction cost varies from USD 0.3 to USD 1.3 per unit kg of hydrogen. A higher concentration of hydrogen demands structural modifications of the carrier. At the same time, the impact on end use systems, safety, material durability and integrity management, and the leakage rate need to be considered [179].

3.3.2.4. Comparative Assessment of Hydrogen Storage Methods and Techniques

Table 3.9 outlines various hydrogen storage methods, including their storage types, energy densities, lifetimes, and associated costs. The methods covered are metal hydrides, liquid hydrogen storage, compressed gaseous hydrogen (CGH_2) for Type IV vessels, and underground hydrogen storage, each with distinct characteristics and performance metrics.

Table 3. 9: Types of Hydrogen Storage Methods and Properties

S/N	Hydrogen Storage Methods	Storage Type	Energy Density ($KWh \cdot m^{-3}$)	Lifetime	Cost
1	Metal Hydrides	Chemical Absorption	244	Less than 2000 hours	9.01 - 19.67 USD/kg (Ni Metal Hydride)
2	Liquid Hydrogen Storage	Physical	2359.30	300 - 500 days	3.66 USD/kg
3	CGH_2 for Type IV Vessel	Cooling	3.3 - 1320 (depends on compression strength)	Over 20 years	Starts from 466 USD/kg
4	Underground Hydrogen Storage	Physical	Can reach about 300,244	20 - 40 years	1.61 USD/kg

Table 3.10 provides an overview of benefits and drawbacks of different hydrogen storage methods while a comparative review of the hydrogen storage capacities of different materials is shown in Table 3.11 [130, 156, 157, 158, 159, 187, 188].

Table 3. 10: Benefits and drawbacks of different Hydrogen storage methods

Hydrogen Storage Methods	Benefits	Drawbacks
Activated carbon	Abundant availability, ease of fabrication, cost-effectiveness, and non-toxicity [180]	Moderate storage capacities, slow adsorption and desorption, and susceptibility to contamination [181]
Carbon Nanotubes	Lightweight, thermal stability and mechanical strength, Compatibility with existing infrastructure [182]	Slow hydrogen adsorption and desorption kinetics, difficulty of synthesis, challenges in controlling nanotube size and diameter, and susceptibility to structural damage [183]

Hydrogen Storage Methods	Benefits	Drawbacks
Metal-Organic Frameworks	Open pore structure, Low operating pressures, highly reversible, kinetics of hydrogen adsorption and desorption is fast [181]	Operation at low temperatures, Moisture sensitivity, Synthesis challenges, Stability issues at high temperatures or under high-pressure conditions [184]
Metal Hydrides	Low-pressure operation, Safe option, High volumetric and gravimetric hydrogen storage capacities, Efficient for compact storage systems [172]	High cost, slow Kinetics during hydrogen absorption and desorption, Issues related to high operating temperatures, and harder interfacing with fuel cells [172]
Cryogenic and Compressed Storage	Commercial availability, High volumetric capacity, denser packing of hydrogen molecules at lower temperatures. Easier transportation and storage [185]	High liquefaction demands energy-intensive cooling, affecting overall system efficiency, and the required insulation for maintaining low temperatures increases system complexity and cost, and hydrogen boil-off losses [172]
Liquid Organic Hydrogen Carriers	High volumetric hydrogen density can store much hydrogen in a relatively small space and is safe and easy to handle, even in large quantities. Closed carbon cycle [186]	Require energy to convert hydrogen to and from the LOHCs. This energy can be a significant cost, especially for large-scale applications, short life cycles, and difficulty in developing dehydrogenation catalysts [186]
Ammonia	Well-established industrial chemicals with existing production and distribution infrastructure flexibility in the release of hydrogen, fast kinetics, high hydrogen storage capability, and low cost [144]	It can harm human health if inhaled as it is toxic. Ammonia is a flammable gas, which means that it can be dangerous. It is a corrosive gas that can damage materials like metals and plastics and involves high temperatures, which can be energy-intensive, and the problems related to trace amounts of ammonia in the hydrogen after decomposition [131]
Gaseous State Storage	Commercially available, lightweight, suitable for fuel cell vehicles, easier integration into existing infrastructure, can be refueled quickly, rapid turnaround times [144]	A large volume and hydrogen embrittlement are required on the wall. Pressure vessels can leak hydrogen, permeation through walls, energy loss– high pressure, high cost of materials, and a required safety factor of more than 2.25 [144].

Table 3. 11: Comparative review of the hydrogen storage capacities of different materials [130, 156 -159, 187, 188].

Storage Method	Storage Materials	Storage Capacity, (wt.%)	Pressure (bar)	Temperature (K)
Compressed Gas	Energy for compression: ≈4 kcal.mol^{-1}	13	140	298
Cryogenic Liquid	Energy for liquefaction: ≈7 kcal.mol^{-1}	Depending on size ≈5 wt.% for a can tank	1	21
Adsorption	Activated Carbon	5.5	80	298
	Graphite	4.48	100	298
	Single-walled carbon nanotube	4.5	4	298
	Multiple-walled carbon nanotube	6.3	148	300
	Carbon nanofiber (CNF)	6.5	120	300
Absorption	AB_5 type: $LaNi_5$	1.37	2	298
	AB_2 type: $ZrMn_2$	1.77	0.001	298
	A_2B type: Mg_2Ni	3.59	1	555
	AB type: FeTi	1.89	5	303
	NaAl	5.6		493
	LiAl	7.9		453

3.4. Overview of Hydrogen Embrittlement

Hydrogen embrittlement is recognized as the most common event in the production, transportation, storage, and utilization of hydrogen. As a matter of fact, research on hydrogen embrittlement behavior under a high-pressure hydrogen environment has been going on for a long time. It can degrade the material properties significantly while making it weak. And this is done by the ingression of a hydrogen atom in or below the metal surface. Hydrogen embrittlement is very frequent in petrochemical industries. When absorbed by metal, hydrogen can react to form a new phase near metal surfaces or diffuse substantial distances within the metal to produce a hydride (MHx) phase. During steel processing and welding, molecular hydrogen (H_2) can be formed within the metal if atomic hydrogen reacts with itself, creating flaking or fisheyes. In low-alloy steels, hydrogen reacts with carbon to produce methane (CH_4) bubbles. A safe operating condition for steels in hydrogen environments can be represented by Nelson diagrams [189]. If hydrogen does not produce any chemical reaction after being absorbed and diffused within the metal lattice from hydrogen sources, then slow strain rate embrittlement and delayed failure occur. For steels, embrittlement is usually most severe at room temperature. The extent of hydrogen diffusion within the lattice controls this type of embrittlement. Extensive focus has been given to the problems related to embrittlement that occur during electroplating, particularly of cadmium on high-strength steel components. Internal reversible hydrogen embrittlement has also been observed in a wide variety of other materials, including nickel-based alloys and stainless steels [189]. Hydrogen embrittlement has been considered a serious concern since 1960. The embrittlement magnitude has been analyzed over a wide range of operating variables, including gas pressure and temperature, through different mechanical tests. At room temperature, embrittlement was found to

be the maximum. The purity of the gas and the test strain rate are also significant parameters to determine the extent of the embrittlement. Quantitative analyses indicate substantial increases in the hydrogen content of embrittled alloys. The position of the crack initiation, whether from the surface or from the inside, is yet to be explored [189].

HE during Hydrogen Production

Hydrogen is considered the heat transfer medium during hydrogen production, coal gasification, or advanced energy conversion processes. From a pure or hydrogen-rich environment, hydrogen is transported to samples like steel and low-alloy steels. Temperature, pressure, and applied stress are the variables to be investigated for the interaction of hydrogen with the steels. The other variables that can be considered are modified alloy composition, modified microstructure of the steel, and chemical modification of the environment. The mechanical properties are controlled by the mechanism of hydrogen exposure to the steel at ambient and elevated temperatures. This interaction is yet to be explored. This would be of significant benefit not only for coal gasification processes but also for hydrogen production processes [189].

HE during Transmission/Storage

The transportation medium of hydrogen has been considered gaseous, liquid, or even as a solid hydride phase. The storage and transportation facilities of hydrogen are designed in a way that are most likely free from environmental degradation. However, the design comes with limitations, as it needs expensive alloy systems such as chromium and nickel [189,190].

HE during the Transmission/Storage of Liquid Hydrogen and Hydride

Liquid hydrogen storage and transport still remain challenging. The reaction processes, including the dissociation of molecular hydrogen, are very slow at cryogenic temperatures. Therefore, the transport of hydrogen from the environment into the metal becomes very slow and difficult. For example, the failure to select appropriate materials, insufficient galvanic corrosion protection, or improper protective coating results in the corrosion of stainless steel and associated tools. Furthermore, if there is the application of thermal cycling where hydrogen penetrates the metal at a high temperature, then the problems are more severe. The underlying reason is the formation of a second phase, either gaseous or solid hydride, which leads to embrittlement. Hydrogen-induced embrittlement causes a loss of integrity of the storage and transport system. Stable austenitic stainless steels or aluminum alloys are widely being used for liquid hydrogen transport or storage systems [190,191]. Gaseous and liquid hydrogen storage systems differ significantly in terms of hydride formation. The pressure, temperature, and thermal cycling are considered in the operating design. In addition, the role of atomic hydrogen in the hydrides on the embrittlement of containment materials is unresolved [190].

HE during the Transmission of Gaseous Hydrogen

Hydrogen embrittlement is a big concern to pressure vessels and pipelines due to insufficient galvanic corrosion protection, poor welding quality, and hydrogen embrittlement-susceptible steel materials. Low-strength steels, poor welding, and low hydrogen pressures such as 0.3–7 MN/(50–1000 psi) are also obvious reasons for promoting hydrogen-induced embrittlement. Embrittlement is also likely due to high-strength steels under high-pressure hydrogen [189]. However, the

evaluation of welded pipeline steel and candidate compressor alloys under simulated service conditions, improved welding, and nondestructive inspection technologies determine the feasibility of composite pipelines, and the compatibility of materials in corrosive environments needs to be studied extensively. Table 3.12 shows Hydrogen embrittlement susceptibility of commonly used metals adopted from [191,192].

Table 3. 12: Hydrogen embrittlement susceptibility of commonly used metals [191,192]

Metal	**Extremely Embrittled**	**Severely Embrittled**	**Slightly Embrittled**	**Negligible Embrittled**
Aluminum alloys				
1100				Yes
6061-T6				Yes
7075-T73				Yes
Be-Cu alloy 25			Yes	
Copper, OFHC				Yes
Nickel 270		Yes		
Titanium and titanium alloys				
Titanium			Yes	
Ti-5AI-2.5SN (ELI)		Yes		
Ti-6AI-4V (annealed)		Yes		
Ti-6AI-4V (STA)		Yes		
Steel				
Alloy steel, 4140	Yes			
Carbon steel				
1020		Yes		
1042 (normalized)		Yes		
1042 (quenched and tempered)	Yes			
Maraging steel, 18Ni-250	Yes			
X42			Yes	
X52			Yes	

Metal	Extremely Embrittled	Severely Embrittled	Slightly Embrittled	Negligible Embrittled
X60			Yes	
X65			Yes	
X70			Yes	
X80			Yes	
X100			Yes	
Stainless steel				
A286				Yes
17-7PH	Yes			
304 ELC			Yes	
305			Yes	
310				Yes
316				Yes
410	Yes			
440C	Yes			
Inconel 718	Yes			

3.5. Conclusion

In conclusion, this chapter provides a comprehensive analysis of the current challenges associated with the implementation of hydrogen energy, focusing on core research areas such as hydrogen embrittlement, production, storage, and transportation. The diverse hydrogen storage methods, including activated carbon, carbon nanotubes, metal-organic frameworks, metal hydrides, cryogenic and compressed storage, liquid organic hydrogen carriers, ammonia, and gaseous state storage, each present unique benefits and drawbacks. The discussion emphasizes the significant progress made in understanding hydrogen embrittlement and the material challenges posed by hydrogen's characteristics. Addressing these challenges requires ongoing research and development to enhance material properties, optimize hydrogen production methods, and improve

storage and transportation technologies, ultimately contributing to a more sustainable and efficient hydrogen economy.

This chapter has been partially published in "*Materials*" titled; "An overview of challenges for the future of hydrogen" with co-authors; Md Tanvir Ahad, Md Monjur Hossain Bhuiyan, Alfredo Becerril Corral and Zahed Siddique. https://doi.org/10.3390/ma16206680

The chapter has also been partially published in "*ASME Open Journal of Engineering*"; titled; "Innovative Materials and Techniques for Enhancing Hydrogen Storage: A Comprehensive Review of Damage Detection and Preventive Strategies" along with the co-authors; Md Nahid Sarker, Md Ismot Hossain Al-Mobin and Philip M Resnick. https://doi.org/10.1115/1.4065360

Reference

71. Ahad, M.T.; Yazdan, M.M.S.; Selvaratnam, T.; Siddique, Z.; Rahman, A. Biohydrogen from Biomass Fermentation Pathway and Economic Aspects. In Microbiology of Green Fuels; CRC Press: Boca Raton, FL, USA, 2023; pp. 97–114.

72. Bartlett, J.; Krupnick, A. Decarbonized Hydrogen in the US Power and Industrial Sectors: Identifying and Incentivizing Opportunities to Lower Emissions. Available online: https://media.rff.org/documents/RFF_Report_20-25_Decarbonized_Hydrogen.pdf (accessed on 16 September 2023).

73. Friedmann, S.J.; Fan, Z.; Tang, K. Low-Carbon Heat Solutions for Heavy Industry: Sources, Options, and Costs Today; Columbia University Center on Global Energy Policy: New York, NY, USA, 2019.

74. ACT ERA-Net. CO2 and H2 Infrastructure in Germany–Final Report of the German Case Study. https://www.sintef.no/globalassets/project/elegancy/deliverables/elegancy_d5.5.3_co2_h2_infrastructure_germany.pdf (accessed on 16 September 2023).

75. Marcelo, D.; Dell'Era, A. Economical Electrolyser Solution. Int. J. Hydrogen Energy 2008, 33, 3041–3044.

76. Binder, M.; Kraussler, M.; Kuba, M.; Luisser, M.; Rauch, R. Hydrogen from Biomass Gasification—IEA Bioenergy; IEA: Paris, France, 2018.

77. American Public Health Association. Standard Methods for the Examination of Water and Wastewater; American Public Health Association: Washington, DC, USA, 1926; Volume 6.

78. Kumar, D.; Eswari, A.P.; Park, J.-H.; Adishkumar, S.; Banu, J.R. Biohydrogen Generation from Macroalgal Biomass, Chaetomorpha Antennina through Surfactant Aided Microwave Disintegration. Front. Energy Res. 2019, 7, 78.

79. Dawood, F.; Anda, M.; Shafiullah, G.M. Hydrogen Production for Energy: An Overview. Int. J. Hydrogen Energy 2020, 45, 3847–3869.

80. Kalamaras, C.M.; Efstathiou, A.M. Hydrogen Production Technologies: Current State and Future Developments. Conf. Pap. Energy 2013, 2013, e690627.

81. Gray, H.R.; Nelson, H.G.; Johnson, R.E.; McPherson, W.B.; Howard, F.S.; Swisher, J.H. Potential Structural Material Problems in a Hydrogen Energy System. Int. J. Hydrogen Energy 1978, 3, 105–118.

82. IEA G20 The Future of Hydrogen. Available online: https://www.iea.org/reports/the-future-of-hydrogen (accessed on 16 September 2023).

83. Collodi, G.; Azzaro, G.; Ferrari, N.; Santos, S. Techno-Economic Evaluation of Deploying CCS in SMR Based Merchant H2 Production with NG as Feedstock and Fuel. Energy Procedia 2017, 114, 2690–2712.

84. Lee, D.-Y.; Elgowainy, A.A.; Dai, Q. Life Cycle Greenhouse Gas Emissions of By-Product Hydrogen from Chlor-Alkali Plants; Argonne National Lab. (ANL): Argonne, IL, USA, 2017.

85. Energy Department Announces up to $3.5Mfor Nuclear-Compatible Hydrogen Production. Available online: https://www.energy.gov/eere/articles/energy-department-announces-35m-nuclear-compatible-hydrogen-production

86. Palucka, T.; Ingram, B.J. Materials Challenges in the Hydrogen Cycle. MRS Bull. 2019, 44, 164–166.

87. Muradov, N. Low to Near-Zero CO2 Production of Hydrogen from Fossil Fuels: Status and Perspectives. Int. J. Hydrogen Energy 2017, 42, 14058–14088.

88. Fasihi, M.; Efimova, O.; Breyer, C. Techno-Economic Assessment of CO2 Direct Air Capture Plants. J. Clean. Prod. 2019, 224, 957–980.

89. Fasihi, M.; Breyer, C. Synthetic Methanol and Dimethyl Ether Production Based on Hybrid PV-Wind Power Plants. In Proceedings of the Conference Paper: 11th International Renewable Energy Storage Conference, Düsseldorf, Germany, 14–16 March 2017.

90. Philibert, C. Renewable Energy for Industry; International Energy Agency: Paris, France, 2017.

91. Fulcheri, L. Direct Decarbonization of Methane by Thermal Plasma for the Co Production of Hydrogen and Carbon Nanostructure. In Proceedings of the HTPP 15, 15th International High-Tech Plasma Processes Conference, Toulouse, France, 2–6 July 2018.

92. Bazzanella, A.; Ausfelder, F. Low Carbon Energy and Feedstock for the European Chemical Industry: Technology Study; DECHEMA, Gesellschaft für Chemische Technik und Biotechnologie eV: Frankfurt, Germany, 2017.

93. Ishibashi, M.; Otake, K.; Kanamori, S. Study on CO2, removal technology from flue gas of thermal power plant. In Greenhouse Gas Control Technologies; Elsevier Science Ltd.: Amsterdam, The Netherlands, 1999; p. 95.

94. Pradier, J.P.; Pradier, C.-M. Carbon Dioxide Chemistry: Environmental Issues; Elsevier: Amsterdam, The Netherlands, 2014.

95. Megía, P.J.; Vizcaíno, A.J.; Calles, J.A.; Carrero, A. Hydrogen Production Technologies: From Fossil Fuels toward Renewable Sources. A Mini Review. Energy Fuels 2021, 35, 16403–16415.

96. Dincer, I.; Acar, C. Review and Evaluation of Hydrogen Production Methods for Better Sustainability. Int. J. Hydrogen Energy 2015, 40, 11094–11111.

97. Barthélémy, H. Compatibility of Metallic Materials with Hydrogen Review of the Present Knowledge. In Proceedings of the International Conference on Hydrogen Safety, San Sebastian, Spain, 11–13 September 2007.

98. Barthélémy, H.; Chateau, G. Hydrogen Gas Embrittlement of Some Austenitic Stainless Steels, Hydrogen and Materials. In Proceedings of the Fourth International Conference on Hydrogen and Materials, Beijing, China, 20 May 1989.

99. Rajabipour, A.; Melchers, R.E. Service Life of Corrosion Pitted Pipes Subject to Fatigue Loading and Hydrogen Embrittlement. Int. J. Hydrogen Energy 2018, 43, 8440–8450.

100. Baek, U.B.; Nahm, S.H.; Kim,W.S.; Ronevich, J.A.; San Marchi, C. Compatibility and Suitability of Existing Steel Pipelines for Transport of Hydrogen-Natural Gas Blends. In Proceedings of the International Conference on Hydrogen Safety (ICHS) (No. SAND2017-9552C), Hamburg, Germany, 11–13 September 2017; Sandia National Lab: Albuquerque, NM, USA, 2017.

101. Che, Z. Fatigue Crack Growth in Hydrogen Pipeline Steels. Master's Thesis, University of Illinois at Urbana-Champaign, Champaign, IL, USA, 2018.

102. 40. Meng, B.; Gu, C.; Zhang, L.; Zhou, C.; Zhao, Y.Z.; Zheng, J.; Chen, X.; Hand, Y. Hydrogen Effects on X80 Pipeline Steel under High-Pressure Natural Gas & Hydrogen Mixtures. Int. J. Hydrogen Energy 2015, 42, 7404–7412.

103. Wiswall, R. H., and Reilily, J. J., 1974, "Hydrogen Storage in Metal Hydrides," Science, 186(4170), p. 1158.

104. Lueking, A. D., and Yang, R. T., 2004, "Hydrogen Spillover to Enhance Hydrogen Storage—Study of the Effect of Carbon Physicochemical Properties," Appl. Catal., A, 265(2), pp. 259–268.

105. Bellosta von Colbe, J., Ares, J.-R., Barale, J., Baricco, M., Buckley, C., Capurso, G., Gallandat, N., et al., 2019, "Application of Hydrides in Hydrogen Storage and Compression: Achievements, Outlook and Perspectives," Int. J. Hydrogen Energy, 44(15), pp. 7780–7808.

106. Hong, K., 2001, "The Development of Hydrogen Storage Electrode Alloys for Nickel Hydride Batteries," J. Power Sources, 96(1), pp. 85–89.

107. Liu, C., Chen, Y., Wu, C. Z., Xu, S. T., and Cheng, H. M., 2010, "Hydrogen Storage in Carbon Nanotubes Revisited," Carbon, 48(2), pp. 452–455.

108. Broom, D. P., and Hirscher, M., 2021, "Improving Reproducibility in Hydrogen Storage Material Research," ChemPhysChem, 22(21), pp. 2141–2157.

109. Felderhoff, M., Weidenthaler, C., von Helmolt, R., and Eberle, U., 2007, "Hydrogen Storage: The Remaining Scientific and Technological Challenges," Phys. Chem. Chem. Phys., 9(21), pp. 2643–2653.

110. Hirscher, M., Yartys, V. A., Baricco, M., Bellosta von Colbe, J., Blanchard, D., Bowman, R. C., Broom, D. P., et al., 2020, "Materials for Hydrogen-Based Energy Storage—Past, Recent Progress and Future Outlook," J. Alloys Compd., 827, p. 153548.

111. Chamoun, R., Demirci, U. B., and Miele, P., 2015, "Cyclic Dehydrogenation-(Re)Hydrogenation With Hydrogen-Storage Materials: An Overview," Energy Technol., 3(2), pp. 100–117.

112. Jiang, Y., Tan, P., Qi, S.-C., Gu, C., Peng, S.-S., Wu, F., Liu, X.-Q., and Sun, L.-B., 2021, "Breathing Metal-Organic Polyhedra Controlled by Light for Carbon Dioxide Capture and Liberation," CCS Chem., 3(6), pp. 1659–1668.

113. Wang, H., Shao, Y., Mei, S., Lu, Y., Zhang, M., Sun, J.-K., Matyjaszewski, K., Antonietti, M., and Yuan, J., 2020, "Polymer-Derived Heteroatom-Doped Porous Carbon Materials," Chem. Rev., 120(17), pp. 9363–9419.

114. Yang, S. J., Jung, H., Kim, T., and Park, C. R., 2012, "Recent Advances in Hydrogen Storage Technologies Based on Nanoporous Carbon Materials," Prog. Nat. Sci.: Mater. Int., 22(6), pp. 631–638.

115. Van Den Berg, A. W. C., and Areán, C. O., 2008, "Materials for Hydrogen Storage: Current Research Trends and Perspectives," Chem. Commun., (6), pp. 668–681.

116. Cortés -Arriagada, D., Gutiérrez-Oliva, S., Herrera, B., Soto, K., and Toro-Labbé, A., 2014, "The Mechanism of Chemisorption of Hydrogen Atom on Graphene: Insights From the Reaction Force and Reaction Electronic Flux," J. Chem. Phys., 141(13).

117. Marsh, H., Heintz, E. A., and Rodríguez-Reinoso, F., 1997, Introduction to Carbon Technologies, Universidad de Alicante, Spain.

118. Phan, N. H., Rio, S., Faur, C., Le Coq, L., Le Cloirec, P., and Nguyen, T. H., 2006, "Production of Fibrous Activated Carbons from Natural Cellulose (Jute, Coconut) Fibers for Water Treatment Applications," Carbon, 44(12), pp. 2569–2577.

119. Vasiliev, L. L., Kanonchik, L. E., and Babenko, V. A., "Thermally Controlled Hydrogen Storage System Using Novel Carbon Materials.

120. Shindo, K., Kondo, T., Arakawa, M., and Sakurai, Y., 2003, "Hydrogen Adsorption/Desorption Properties of Mechanically Milled Activated Carbon," J. Alloys Compd., 359(1–2), pp. 267–271.

121. Takagi, H., Hatori, H., and Yamada, Y., 2004, "Hydrogen Adsorption/ Desorption Property of Activated Carbon Loaded With Platinum," Chem. Lett., 33(9), pp. 1220–1221.

122. W. C. Xu et al., "Investigation of hydrogen storage capacity of various carbon materials," Int J Hydrogen Energy, vol. 32, no. 13, pp. 2504–2512, Sep. 2007, doi:10.1016/j.ijhydene.2006.11.012.

123. Y. Wang et al., "Surface functionalization-enhanced spillover effect on hydrogen storage of Ni-B nanoalloy-doped activated carbon," Int J Hydrogen Energy, vol. 36, no. 21, pp. 13663–13668, Oct. 2011, doi: 10.1016/j.ijhydene.2011.08.049.

124. R. Strobel et al., “Hydrogen adsorption on carbon materials,” 1999. [Online]. Available: www.elsevier.comrlocaterjpowsour

125. M. Hirscher and B. Panella, “Nanostructures with high surface area for hydrogen storage,” J Alloys Compd, vol. 404–406, no. SPEC. ISS., pp. 399–401, Dec. 2005, doi: 10.1016/j.jallcom.2004.11.109.

126. W. Zhao, V. Fierro, N. Fernández-Huerta, M. T. Izquierdo, and A. Celzard, “Impact of synthesis conditions of KOH activated carbons on their hydrogen storage capacities,” Int J Hydrogen Energy, vol. 37, no. 19, pp. 14278–14284, Oct. 2012, doi: 10.1016/j.ijhydene.2012.06.110.

127. S. Y. Lee and S. J. Park, “Effect of platinum doping of activated carbon on hydrogen storage behaviors of metal-organic frameworks-5,” Int J Hydrogen Energy, vol. 36, no. 14, pp. 8381–8387, Jul. 2011, doi: 10.1016/j.ijhydene.2011.03.038.

128. W. Zhao et al., “Activated carbons doped with Pd nanoparticles for hydrogen storage,” Int J Hydrogen Energy, vol. 37, no. 6, pp. 5072–5080, Mar. 2012, doi: 10.1016/j.ijhydene.2011.12.058.

129. M. Becher et al., “Hydrogen storage in carbon nanotubes,” Comptes Rendus Physique, vol. 4, no. 9. Elsevier Masson SAS, pp. 1055–1062, 2003. doi: 10.1016/S1631-0705(03)00107-5.

130. T. He, L. Liu, G. Wu, and P. Chen, “Covalent triazine framework-supported palladium nanoparticles for catalytic hydrogenation of N-heterocycles,” *J Mater Chem A Mater*, vol. 3, no. 31, pp. 16235–16241, 2015, doi: 10.1039/C5TA03056K.

131. S. Chatterjee, R. K. Parsapur, and K. W. Huang, “Limitations of Ammonia as a Hydrogen Energy Carrier for the Transportation Sector,” *ACS Energy Lett*, vol. 6, no. 12, pp. 4390–4394, Dec. 2021, doi: 10.1021/acsenergylett.1c02189.

132. Rosi, N. L., Eckert, J., Eddaoudi, M., Vodak, D. T., Kim, J., O’Keeffe, M., and Yaghi, O. M., 2003, “Hydrogen Storage in Microporous Metal-Organic Frameworks,” Science, 300(5622), pp. 1127–1129.

133. J. L. C. Rowsell, A. R. Millward, K. S. Park, and O. M. Yaghi, “Hydrogen Sorption in Functionalized Metal-Organic Frameworks (Supplementary Information).”

134. N. L. Rosi et al., “Hydrogen storage in microporous metal-organic frameworks,” Science (1979), vol. 300, no. 5622, pp. 1127–1129, May 2003, doi: 10.1126/science.1083440.

135. J. L. C. Rowsell, A. R. Millward, K. S. Park, and O. M. Yaghi, “Hydrogen Sorption in Functionalized Metal-Organic Frameworks (Supplementary Information).”

136. M. Hirscher, “Hydrogen storage by cryoadsorption in ultrahigh-porosity metal-organic frameworks,” Angewandte Chemie - International Edition, vol. 50, no. 3, pp. 581–582, Jan. 2011, doi: 10.1002/anie.201006913.

137. B. Panella and M. Hirscher, “Hydrogen physisorption in metal-organic porous crystals,” Advanced Materials, vol. 17, no. 5, pp. 538–541, Mar. 2005, doi: 10.1002/adma.200400946.

138. A. Ahmed et al., “Exceptional hydrogen storage achieved by screening nearly half a million metal-organic frameworks,” Nat Commun, vol. 10, no. 1, Dec. 2019, doi: 10.1038/s41467-019-09365-w.

139. J. Goldsmith, A. G. Wong-Foy, M. J. Cafarella, and D. J. Siegel, “Theoretical limits of hydrogen storage in metal-organic frameworks: Opportunities and trade-offs,” Chemistry of Materials, vol. 25, no. 16, pp. 3373–3382, Aug. 2013, doi: 10.1021/cm401978e.

140. Akunets, A.A., Basov, N.G., et al., 1994, “Super-High-Strength Microballoons for Hydrogen Storage,” Int. J. Hydrogen Energy, 8(19), pp. 697–700.

141. J. W. Makepeace et al., “Reversible ammonia-based and liquid organic hydrogen carriers for high-density hydrogen storage: Recent progress,” Int J Hydrogen Energy, vol. 44, no. 15, pp. 7746–7767, Mar. 2019, doi: 10.1016/j.ijhydene.2019.01.144.

142. P. T. Aakko-Saksa, C. Cook, J. Kiviaho, and T. Repo, “Liquid organic hydrogen carriers for transportation and storing of renewable energy – Review and discussion,” Journal of Power Sources, vol. 396. Elsevier B.V., pp. 803–823, Aug. 31, 2018. doi: 10.1016/j.jpowsour.2018.04.011.

143. P. Preuster, C. Papp, and P. Wasserscheid, “Liquid organic hydrogen carriers (LOHCs): Toward a hydrogen-free hydrogen economy,” Acc Chem Res, vol. 50, no. 1, pp. 74–85, Jan. 2017, doi: 10.1021/acs.accounts.6b00474.

144. A. Klerke, C. H. Christensen, J. K. Nørskov, and T. Vegge, “Ammonia for hydrogen storage: Challenges and opportunities,” J Mater Chem, vol. 18, no. 20, pp. 2304–2310, 2008, doi: 10.1039/b720020j.

145. C. H. Christensen, T. Johannessen, R. Z. Sørensen, and J. K. Nørskov, "Towards an ammonia-mediated hydrogen economy?," in Catalysis Today, Jan. 2006, pp. 140–144. doi: 10.1016/j.cattod.2005.10.011.

146. W. A. Amos, "Costs of Storing and Transporting Hydrogen." [Online]. Available: http://www.doe.gov/bridge/home.html

147. S. M. Aceves, G. Petitpas, F. Espinosa-Loza, M. J. Matthews, and E. Ledesma-Orozco, "Safe, long range, inexpensive and rapidly refuelable hydrogen vehicles with cryogenic pressure vessels," Int J Hydrogen Energy, vol. 38, no. 5, pp. 2480–2489, Feb. 2013, doi: 10.1016/j.ijhydene.2012.11.123.

148. R. K. Ahluwalia *et al.*, "Technical assessment of cryo-compressed hydrogen storage tank systems for automotive applications," *Int J Hydrogen Energy*, vol. 35, no. 9, pp. 4171–4184, May 2010, doi: 10.1016/j.ijhydene.2010.02.074.

149. J. Zheng *et al.*, "Current Research Trends and Perspectives on Solid-State Nanomaterials in Hydrogen Storage," *Research*, vol. 2021, Jan. 2021, doi: 10.34133/2021/3750689.

150. J. Dennis, T. Bexten, N. Petersen, M. Wirsum, and P. Preuster, "Model-Based Analysis of a Liquid Organic Hydrogen Carrier (LOHC) System for the Operation of a Hydrogen-Fired Gas Turbine," J Eng Gas Turbine Power, vol. 143, no. 3, Feb. 2021, doi: 10.1115/1.4048596.

151. D. Teichmann, K. Stark, K. Müller, G. Zöttl, P. Wasserscheid, and W. Arlt, "Energy storage in residential and commercial buildings via Liquid Organic Hydrogen Carriers (LOHC)," Energy Environ Sci, vol. 5, no. 10, pp. 9044–9054, 2012, doi: 10.1039/C2EE22070A.

152. P. Song, Y. Sui, T. Shan, J. Hou, and X. Wang, "Assessment of hydrogen supply solutions for hydrogen fueling station: A Shanghai case study," Int J Hydrogen Energy, vol. 45, no. 58, pp. 32884–32898, 2020, doi: https://doi.org/10.1016/j.ijhydene.2020.09.117.

153. "EP 2 960 204 A1." [Online]. Available: http://www.eere.energy.gov/hy-

154. E. Clot, O. Eisenstein, and R. H. Crabtree, "Computational structure-activity relationships in H2 storage: How placement of N atoms affects release temperatures in organic liquid storage materials," Chemical Communications, no. 22, pp. 2231–2233, 2007, doi: 10.1039/b705037b.

155. Y. Cui, S. Kwok, A. Bucholtz, B. Davis, R. A. Whitney, and P. G. Jessop, "The effect of substitution on the utility of piperidines and octahydroindoles for reversible hydrogen storage," New Journal of Chemistry, vol. 32, no. 6, pp. 1027–1037, 2008, doi: 10.1039/b718209k.

156. S. Mukherjee, S. V. Devaguptapu, A. Sviripa, C. R. F. Lund, and G. Wu, "Low-temperature ammonia decomposition catalysts for hydrogen generation," Applied Catalysis B: Environmental, vol. 226. Elsevier B.V., pp. 162–181, Jun. 15, 2018. doi: 10.1016/j.apcatb.2017.12.039.

157. S. F. Yin, B. Q. Xu, X. P. Zhou, and C. T. Au, "A mini-review on ammonia decomposition catalysts for on-site generation of hydrogen for fuel cell applications," Applied Catalysis A: General, vol. 277, no. 1–2. Elsevier, pp. 1–9, Dec. 08, 2004. doi: 10.1016/j.apcata.2004.09.020.

158. M. Feyen et al., "High-temperature stable, iron-based core-shell catalysts for ammonia decomposition," Chemistry - A European Journal, vol. 17, no. 2, pp. 598–605, Jan. 2011, doi: 10.1002/chem.201001827.

159. V. Tagliazucca, K. Schlichte, F. Schüth, and C. Weidenthaler, "Molybdenum-based catalysts for the decomposition of ammonia: In situ X-ray diffraction studies, microstructure, and catalytic properties," J Catal, vol. 305, pp. 277–289, 2013, doi: 10.1016/j.jcat.2013.05.011.

160. Y. Q. Gu et al., "In Situ X-ray Diffraction Study of Co-Al Nanocomposites as Catalysts for Ammonia Decomposition," Journal of Physical Chemistry C, vol. 119, no. 30, pp. 17102–17110, Jul. 2015, doi: 10.1021/acs.jpcc.5b02932.

161. J. W. Makepeace, T. J. Wood, H. M. A. Hunter, M. O. Jones, and W. I. F. David, "Ammonia decomposition catalysis using non-stoichiometric lithium imide," Chem Sci, vol. 6, no. 7, pp. 3805–3815, Jul. 2015, doi: 10.1039/c5sc00205b.

162. W. I. F. David et al., "Hydrogen production from ammonia using sodium amide," J Am Chem Soc, vol. 136, no. 38, pp. 13082–13085, Sep. 2014, doi: 10.1021/ja5042836.

163. J. Guo et al., "Lithium imide synergy with 3d transition-metal nitrides leading to unprecedented catalytic activities for ammonia decomposition," Angewandte Chemie - International Edition, vol. 54, no. 10, pp. 2950–2954, Mar. 2015, doi: 10.1002/anie.201410773.

164. R. E. Johnsen, P. B. Jensen, P. Norby, and T. Vegge, “Temperature- And pressure-induced changes in the crystal structure of Sr(NH3)8Cl2,” Journal of Physical Chemistry C, vol. 118, no. 42, pp. 24349–24356, Oct. 2014, doi: 10.1021/jp508076c.

165. R. Z. Sørensen et al., “Indirect, reversible high-density hydrogen storage in compact metal ammine salts,” J Am Chem Soc, vol. 130, no. 27, pp. 8660–8668, Jul. 2008, doi: 10.1021/ja076762c.

166. H. S. Jacobsen et al., “Nanoscale structural characterization of Mg(NH3)6Cl2 during NH3 desorption: An in situ small angle X-ray scattering study,” Chem Phys Lett, vol. 441, no. 4–6, pp. 255–260, Jun. 2007, doi: 10.1016/j.cplett.2007.05.001.

167. S. W. Jorgensen, “Hydrogen storage tanks for vehicles: Recent progress and current status,” Curr Opin Solid State Mater Sci, vol. 15, no. 2, pp. 39–43, Apr. 2011, doi: 10.1016/j.cossms.2010.09.004.

168. R. Janot, M. Latroche, and A. Percheron-Guégan, “Development of a hydrogen absorbing layer in the outer shell of high pressure hydrogen tanks,” Materials Science and Engineering: B, vol. 123, no. 3, pp. 187–193, Nov. 2005, doi: 10.1016/j.mseb.2005.07.016.

169. A. Ozarslan, “Large-scale hydrogen energy storage in salt caverns,” Int J Hydrogen Energy, vol. 37, no. 19, pp. 14265–14277, Oct. 2012, doi: 10.1016/j.ijhydene.2012.07.111.

170. J. Michalski et al., “Hydrogen generation by electrolysis and storage in salt caverns: Potentials, economics and systems aspects with regard to the German energy transition,” Int J Hydrogen Energy, vol. 42, no. 19, pp. 13427–13443, May 2017, doi: 10.1016/j.ijhydene.2017.02.102.

171. W. Liu et al., “The role of underground salt caverns for large-scale energy storage: A review and prospects,” Energy Storage Mater, p. 103045, Nov. 2023, doi: 10.1016/J.ENSM.2023.103045.

172. I. Cumalioglu, A. Ertas, Y. Ma, and T. Maxwell, “State of the art: Hydrogen storage,” *Journal of Fuel Cell Science and Technology*, vol. 5, no. 3. Aug. 2008. doi: 10.1115/1.2894462.

173. E. Rivard, M. Trudeau, and K. Zaghib, “Hydrogen storage for mobility: A review,” *Materials*, vol. 12, no. 12. MDPI AG, Jun. 01, 2019. doi: 10.3390/ma12121973.

174. C. Chu, K. Wu, B. Luo, Q. Cao, and H. Zhang, "Hydrogen storage by liquid organic hydrogen carriers: Catalyst, renewable carrier, and technology – A review," *Carbon Resources Conversion*, vol. 6, no. 4. KeAi Publishing Communications Ltd., pp. 334–351, Dec. 01, 2023. doi: 10.1016/j.crcon.2023.03.007.

175. W. F. Ekpotu, J. Akintola, M. C. Obialor, and U. Philemon, "Historical Review of Hydrogen Energy Storage Technology," *World Journal of Engineering and Technology*, vol. 11, no. 03, pp. 454–475, 2023, doi: 10.4236/wjet.2023.113033

176. T. Shiraiwa, M. Kawate, F. Briffod, T. Kasuya, and M. Enoki, "Evaluation of hydrogen-induced cracking in high-strength steel welded joints by acoustic emission technique," *Mater Des*, vol. 190, May 2020, doi: 10.1016/j.matdes.2020.108573.

177. K. Wu, W. S. Jung, and J. W. Byeon, "Acoustic emission of hydrogen bubbles on the counter electrode during pitting corrosion of 304 stainless steel," *Mater Trans*, vol. 56, no. 4, pp. 587–592, 2015, doi: 10.2320/MATERTRANS.M2014373.

178. J. Chen *et al.*, "Synthesis, Thermal Behavior, and Dehydrogenation Kinetics Study of Lithiated Ethylenediamine," *Chemistry – A European Journal*, vol. 20, no. 42, pp. 13636–13643, Oct. 2014, doi: 10.1002/chem.201403047.

179. K. M. Eblagon *et al.*, "Hydrogenation of 9-ethylcarbazole as a prototype of a liquid hydrogen carrier," *Int J Hydrogen Energy*, vol. 35, no. 20, pp. 11609–11621, Oct. 2010, doi: 10.1016/j.ijhydene.2010.03.068.

180. A. Chibani, G. Mecheri, A. Dehane, S. Merouani, and I. Ferhoune, "Performance improvement of adsorptive hydrogen storage on activated carbon: Effects of phase change material and inconstant mass flow rate," *J Energy Storage*, vol. 56, p. 105930, 2022, doi: https://doi.org/10.1016/j.est.2022.105930.

181. M. Hirscher *et al.*, "Materials for hydrogen-based energy storage – past, recent progress and future outlook," *J Alloys Compd*, vol. 827, Jun. 2020, doi: 10.1016/j.jallcom.2019.153548.

182. R. Oriňáková and A. Oriňák, "Recent applications of carbon nanotubes in hydrogen production and storage," *Fuel*, vol. 90, no. 11. pp. 3123–3140, Nov. 2011. doi: 10.1016/j.fuel.2011.06.051.

183. S. Rezaie, D. M. J. Smeulders, and A. Luna-Triguero, "Enhanced Hydrogen Storage in Gold-doped Carbon Nanotubes: A first-principles study."

184. V. Zeleňák and I. Saldan, “Factors affecting hydrogen adsorption in metal–organic frameworks: A short review,” *Nanomaterials*, vol. 11, no. 7, Jul. 2021, doi: 10.3390/nano11071638.

185. J. S. Noh, R. K. Agarwal, and J. A. Schwarz, “HYDROGEN STORAGE SYSTEMS USING ACTIVATED CARBON.”

186. C. Chu, K. Wu, B. Luo, Q. Cao, and H. Zhang, “Hydrogen storage by liquid organic hydrogen carriers: Catalyst, renewable carrier, and technology – A review,” *Carbon Resources Conversion*, vol. 6, no. 4. KeAi Publishing Communications Ltd., pp. 334–351, Dec. 01, 2023. doi: 10.1016/j.crcon.2023.03.007.

187. J. Chen *et al.*, “Lithiated primary amine - A new material for hydrogen storage,” *Chemistry - A European Journal*, vol. 20, no. 22, pp. 6632–6635, May 2014, doi: 10.1002/chem.201402543.

188. U. Department of Energy, “Potential Roles of Ammonia in a Hydrogen Economy A Study of Issues Related to the Use Ammonia for On-Board Vehicular Hydrogen Storage Potential Roles of Ammonia in a Hydrogen Economy,” 2006.

189. Gray, H.R.; Nelson, H.G.; Johnson, R.E.; McPherson, W.B.; Howard, F.S.; Swisher, J.H. Potential Structural Material Problems in a Hydrogen Energy System. Int. J. Hydrogen Energy 1978, 3, 105–118.

190. Michler, T.; Wackermann, K.; Schweizer, F. Review and Assessment of the Effect of Hydrogen Gas Pressure on the Embrittlement of Steels in Gaseous Hydrogen Environment. Metals 2021, 11, 637.

191. San Marchi, C.; Somerday, B.P. Technical Reference on Hydrogen Compatibility of Materials; Sandia National Laboratories: Albuquerque, NM, USA, 2008.

192. ISO/TR 15916:2015. Available online: https://www.iso.org/standard/56546.html (accessed on 31 March 2024).

CHAPTER 4: HYDROGEN-INDUCED AGING IN STORAGE-SEALING MATERIALS: MECHANISMS, CHALLENGES, AND MITIGATION STRATEGIES

Chapter 4 of this dissertation thoroughly examines the phenomenon of hydrogen-induced aging in storage and sealing materials. It emphasizes the significant challenges posed by hydrogen's ability to permeate and degrade materials, leading to risks such as hydrogen-induced cracking, embrittlement, and blistering. The chapter explores various aging mechanisms, including thermal, chemical, mechanical, mechanical-chemical, and thermo-mechanical aging, each characterized by distinct processes and impacts on material integrity. It highlights the critical need for advanced materials and rigorous research to mitigate these aging effects and ensure the longevity and safety of hydrogen storage and sealing systems. Historical incidents and laboratory tests are discussed to illustrate the severity and mechanisms of hydrogen-induced aging. The necessity of understanding and addressing these challenges for the advancement of hydrogen as a sustainable energy source are also outlined.

4.1. The Importance of Sealing System in Hydrogen Application

Elastomeric materials are typically utilized extensively in sealing components as well as other applications, such as control valves, liners, connectors, and flexible hoses, which are also constantly subjected to high-pressure hydrogen under operating certain conditions [193]. Hydrogen is mostly stored in high-pressure metal tanks which consist of an internal lining of polymers. The polymers in the hydrogen storage tank are used to sustain the pressure and act as a diffusion barrier between the hydrogen gas and the metal tank. The liner can collapse inside due to the rapid depressurization of hydrogen from storage tanks. This is referred to as buckling [194].

Buckling takes place when hydrogen gets trapped and intends to escape by rupturing the material. It results in blistering or permanent deformation of the material. This phenomenon is called rapid decompression failure (RDF) [194-200]. The cavitation process happening at the micro-scale also leads to rapid decompression failure (RDF) to the macro scale [201,202]. Rubber seals are considered a weak link for high-pressure hydrogen storage systems. While high-pressure and high-purity hydrogen is exposed to rubber for a longer time, there is a chance of swelling due to dissolved hydrogen. Swelling behavior has an adverse impact on mechanical properties, such as tensile strength and elastic modulus. The fracture of polymeric material is caused by either blistering or volume increment by hydrogen penetration. The ratio of volume change depends on how much hydrogen has been absorbed. But different kinds of additives such as carbon black can be used to reduce the volume change of polymer components even though the hydrogen intake is high [203]. Table 4.1 summarizes a few of the most used polymeric sealing materials in hydrogen service lines.

Table 4. 1: Saling material and respective applications in Hydrogen industry

Sealing Material	**Application**
High-density polyethylene (HDPE)	used as liners for hydrogen storage tanks
Poly (phenylene sulfide) (PPS),	high-pressure hydrogen distribution system
Poly (phenylenelene) (POM)	high-pressure hydrogen distribution system
Viton-A & NBR	used as seals and gaskets in valves
Poly-tera-fluoroethylene (PTFE)	Used for seals in mechanical compressors
Ethylene propylene diene monomer (EPDM)	Seals and hoses for low-temperature environments
Polyvinylidene fluoride (PVDF)	Linings and coatings in hydrogen storage tanks
Fluorosilicon (FVMQ)	Seals in hydrogen fuel cells and connectors
Polyurethane (PU)	Gaskets and O-rings for dynamic sealing
Polychloroprene (Neoprene)	Hoses and tubing in hydrogen transport systems

These sealing materials may be exposed to a wide range of operating variables' 10-100 MPa pressure and -70º C to + 85º C depending on their application at the hydrogen facility. Hydrogen may not be chemically reactive to the polymer surface but can diffuse through the polymer and fill the pre-existing cavities inside the polymer that cause mechanical failure and loss of sealing integrity. Figure 4.1 represent existing polymer used for different hydrogen applications and associate concerns [290]. Challenges on sealing material for gaseous hydrogen has been elaborately discussed at chapter 03 at section '3.3.2.1 Polymer Used in Hydrogen Application and Challenges'.

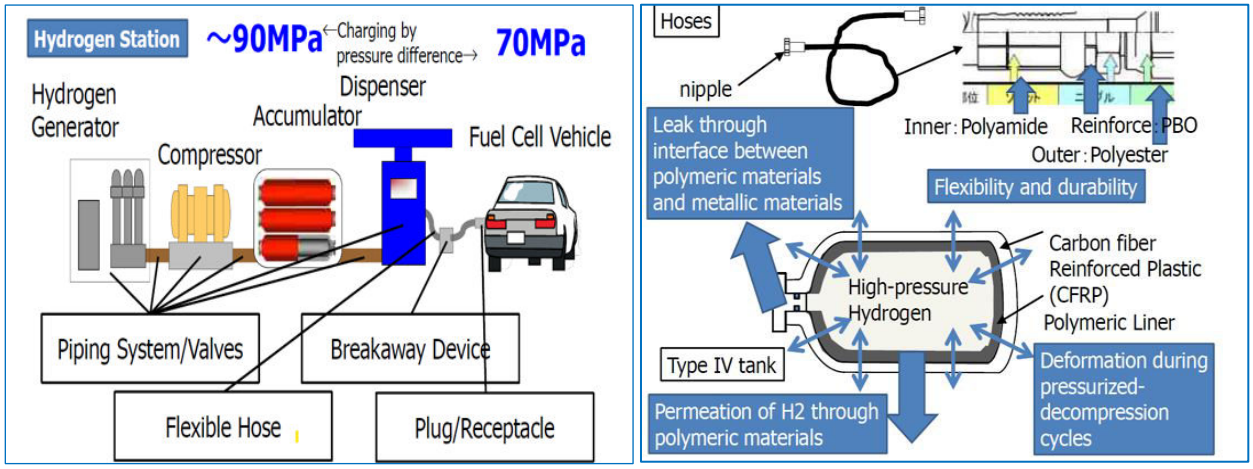

Figure 4. 1: Polymers for hydrogen equipment and issues [290]

The accurate selection of sealing material is essential to avoid any fracture which may result in leakage of explosive hydrogen. Therefore, this is highly important to investigate the impact of operating parameters on sealing performance in a hydrogen environment.

4.2. Research of hydrogen induced aging for storage and sealing materials

With the advantages of hydrogen, it is a must need to look at the complications of using hydrogen as an energy source. The ability of hydrogen to dissolve in and through metals can result in leakage and material failure. This is considered the most significant risk of dealing with hydrogen. A gas cloud is created when hydrogen leaks into the air, and if it encounters an ignition source hydrogen cloud, hydrogen cloud explosions are likely to occur [204]. Material failure due to hydrogen can take place in different forms, such as hydrogen-induced cracking (HIC), hydride embrittlement (HE), hydrogen-induced blistering, and other detrimental effects that commonly lead to catastrophic fractures [205]. Long-term exposure to hydrogen environment increases the degradation and damage rate of materials in a process known as aging. Under normal conditions, the degradation and damage rates of many materials are far slower compared to what is observed under long-term exposure to a hydrogen environment. Thus, it is a great challenge for the hydrogen industry to understand the aging processes and to try to find remedies. In one study, researchers created a catalyst by enclosing palladium nanoparticles in a special dendrimer called PAMAM. They tested different dendrimer variations and found that the best catalyst, with G6 generation, amine end groups, and a Jeffamine core ($P6.NH_2$), efficiently produced hydrogen from ammonia borane at room temperature [206]. The development of advanced catalysts for efficient hydrogen production emphasizes the need for materials that withstand hydrogen-induced aging. As such, longevity and reliability of these materials become essential, necessitating comprehensive research into aging mechanisms and the creation of materials specifically engineered to resist the degradation caused by hydrogen exposure. The service life and safety of materials used in the hydrogen industry are therefore dependent on taking the aging process into consideration [207].

4.3. History of Hydrogen-Induced Aging

Almost half of the pipeline infrastructure still in service in the United States is 40 or more years old . Older pipelines, particularly those that have been in service for several decades, are often made of steel. “Aging” refers to the continual time-dependent degradation of materials under normal operations [207]. Numerous factors, including temperature, creep, fatigue, and brittleness, lead to the aging phenomenon in a hydrogen environment. According to a database of Dutch-investigated accidents, 25% of accidents are related to aging through material deterioration [208]. The aging phenomenon can be categorized into material deterioration, obsolescence, and organizational aging. The discussion in the current study is limited to material deterioration [209]. In the Challenger Space Shuttle disaster of 1986, a detailed failure analysis revealed hydrogen embrittlement as a key factor in the malfunction of O-rings, which were crucial for the shuttle's solid rocket boosters. This incident indicates the sensitivity of certain materials to hydrogen under specific environmental conditions, especially in high-stress aerospace applications. Similarly, the structural failures of the Liberty Ships during World War II, primarily due to hydrogen-induced cracking in their welded steel hulls, faces the challenges of hydrogen embrittlement [326]. These cases emphasizes the susceptibility of materials to hydrogen-induced damage and the evolution of material science in response to these failures. Research has consistently emphasized the necessity of understanding and mitigating hydrogen's impact on materials to prevent similar catastrophic events, guiding the development of more resilient materials in hydrogen-related applications. Some other historical incidents that have taken place due to aging are discussed in Table 4.2.

Table 4. 2: Different incidents that resulted from aging

Incident	Location & Casualties	Cause	Description
The Flixborough disaster	England, 1974 28 killed, 36 injured	Cyclohexane plant leakage and gas cloud explosion	The chemical plant had a cyclohexane plant, where the reactor circuit leaked due to aging. As a result, a huge hydrocarbon gas cloud formed, which led to an explosion [210].
The Humber Refinery explosion	England, 2001 2 injured	Pipe corrosion and rupture due to fouling problems and blockages from accumulated water.	Steel pipe failure was the main reason behind the explosion. The steel pipe was coated with a passive layer of iron sulfide which was protecting it from corrosion. But due to the aging, the protecting layer ruptured, and the pipe surface underwent corrosion. As a result, the thickness of the pipe was reduced to 0.3 mm from 7–8 mm and could not contain the internal pressure, causing it to burst [211]
The Chevron refinery accident	USA, 2012	Pipe rupture by aging due to sulfidation corrosion	The main reason for this accident was the wall thinning of the pipe due to aging, which led to a catastrophic pipe rupture. Sulfur compounds found in crude oil feed, such as hydrogen sulfide, react with steel piping to cause corrosion [212]
Muskingum Power Plant	USA, 2007	Storage tank failure and hydrogen explosion	The disaster began with the premature failure of the ruptured disk on the storage tank because of aging. The pressurized gas then caused the vent system to fail, allowing hydrogen to escape and causing an explosion [213].
Tesoro refinery	USA, 2010	Heat exchanger damage and tubing rupture	The accident was the result of damage to the heat exchanger brought on by hydrogen aging at high temperatures, which led to carbon steel tubing being badly fractured and weakened, which in turn led to a rupture [214].
Kashima Oil Refinery	Japan, 1982 5 casualties	High-pressure hydrogen aging and pipe deterioration	The explosion was caused by hydrogen aging under high pressure and high pressure in a hydrodesulfurization unit. Five casualties were caused by the gradual deterioration of the inner surface of a carbon steel pipe, which resulted in the discharge of process fluid after 12 years of operation [215].

4.4. Impact of Operating Conditions on Hydrogen-Assisted Aging

Operating conditions significantly affect hydrogen-induced aging in materials, particularly in high-pressure environments. This effect is shown as expedited deterioration of metallic components after prolonged exposure to hydrogen. Research has shown that hydrogen can cause various forms of material degradation, such as corrosion, stress corrosion cracking, and hydrogen embrittlement, especially under high-pressure conditions. These mechanisms of degradation are typically accelerated in the presence of factors such as residual water, which can act as aggressive species, leading to corrosion and subsequent hydrogenation of materials. Slobodyan et al. took into consideration, for instance, the top and bottom parts of pipe that were used in an oil pipeline for 30 years [216]. Residual water that was left over after the transported hydrocarbons acted as an aggressive species, accumulated at the pipe's bottom, and created an environment that was conducive to corrosion and subsequent hydrogenation of the bottom section of the pipe. Thus, the lower half of the pipe had significantly more defective steel characteristics than the top. Continuous exposure of pipeline systems to challenging operating circumstances might hasten the aging process and result in unheard-of breakdowns from hydrogen-induced damage. When certain materials are exposed to hydrogen and stress at the same time, it can cause a serious problem called hydrogen embrittlement. This can lead to increased risk of failure from internal and external stresses due to increased brittleness of the material. Atomic hydrogen may be produced through the adsorption and dissociation of hydrogen gas on steel pipeline surfaces [217-218]. A material failure mode is introduced, and several damage processes are linked to the entry of atomic hydrogen into interstitial spaces. According to ASME B31.12, pipes must adhere to specified requirements to be used in service lines for gaseous and liquid hydrogen [219].

4.5. Potential Reasons of Hydrogen Assisted Aging

The tiny hydrogen molecules are impressive flee artists, which is the main distinction between hydrogen-driven aging and other liquids in the same specimen. In general, the low boiling point (−253 °C), lower density in the gaseous stage (0.09 kg/NA m^3), and high density in the liquid phase (70.9 kg/NA m^3) of hydrogen present challenges for conventional storage facilities [220]. Not only can hydrogen diffuse through solid steel, but it can also travel through the slightest of seal flaws. Elastomeric materials are typically utilized extensively in sealing components as well as other applications, such as control valves, liners, connectors, and flexible hoses, which are also subjected to high-pressure hydrogen under operating conditions [221]. Rubbery O-rings are a sealing component that can blister , a type of internal fracture where damage takes place due to the rapid decompression of highly pressurized hydrogen gas [222]. The entry of atomic hydrogen into interstitial gaps results in leakage. Hydrogen exposure can lead to a reduction in molecular weight and changes in the cross-linking density. This process, known as chain scission, can drastically reduce the mechanical strength and elasticity of polymers used in sealing applications. Thus, the minimal size and the density difference in different physical states make it a very challenging material for storage. Also, its high diffusivity through metallic and polymeric materials makes it a challenging material for sealing.

4.6. Potential Methods of Hydrogen Assisted Aging

Materials used for hydrogen storage and sealing applications degrade more quickly in hydrogen environments. The general patterns of operating deterioration of the properties of infrastructure materials, as depicted in Figure 4.2, were summarized by Nykyforchyn et al. [223]. Figure 4.2

indicates the degradation of materials over time in a hydrogen environment. Stage I represents aging by deformation, and Stage II contains two stages, IIA and IIB, which represent dispersed damage and the buildup of damage in the rolling direction, respectively. In stage II, due to the accumulation of hydrogen, microdamage develops, which erodes the natural integrity of the material. In Stage II, the dotted line represents the behavior of the materials in the absence of hydrogen. Thus, it indicates that hydrogen can accelerate the degradation process of the materials [223,224]. Hydrogen embrittlement is an example of degradation that follows the trend shown in Figure 2. The incorporation of hydrogen in metals creates a secondary hydride phase, which is brittle. As a result of brittleness, the structural integrity of the metals becomes weak, which degrades the metal more rapidly than in normal conditions.

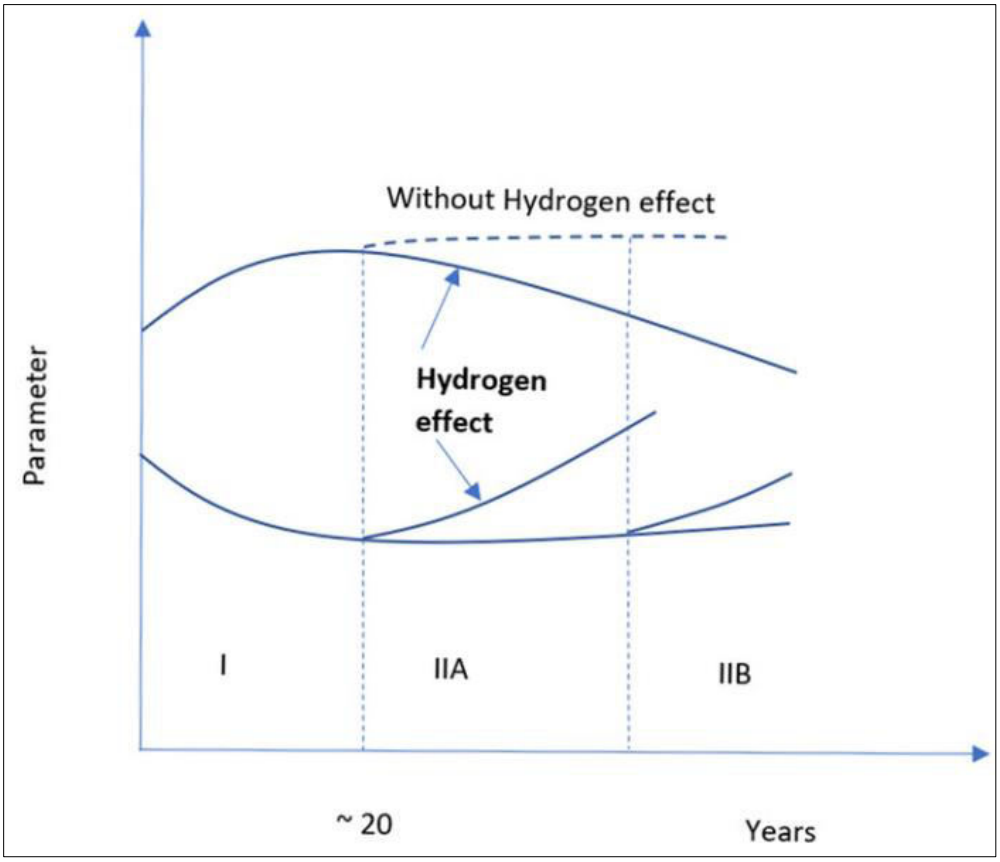

Figure 4. 2: Two-stage degradation of materials in a hydrogen environment [223]

Therefore, the concept supports the aging process demonstrated in figure 4.2. However, there is still significant disagreement over the main mechanism by which this degradation process occurs. Adsorption-induced dislocation emission (AIDE), hydrogen-enhanced localized plasticity (HELP), and hydrogen-enhanced de-cohesion mechanism (HEDE) are the fundamental mechanisms that are believed to be responsible for hydrogen-induced embrittlement [225]. Determining the correct materials for the storage and sealing of hydrogen is critical in combatting these degradation mechanisms and for hydrogen to be used as an energy source. Materials can be aged in a hydrogen environment through various processes, including thermal aging, chemical aging, mechanical aging, mechanical-chemical aging, thermo-mechanical aging, etc.

4.7. Potential Mechanism of Hydrogen-Assisted Aging on Materials

Hydrogen-induced aging of storage and sealing materials can occur through several mechanisms. One potential mechanism is hydrogen diffusion into the material, where the hydrogen atoms can react with and weaken the chemical bonds within the material. This can cause a loss of elasticity and increased stiffness, leading to cracks and failures over time. A simple flowchart of the hydrogen-induced aging mechanism is shown in Figure 4.3 [219,226].

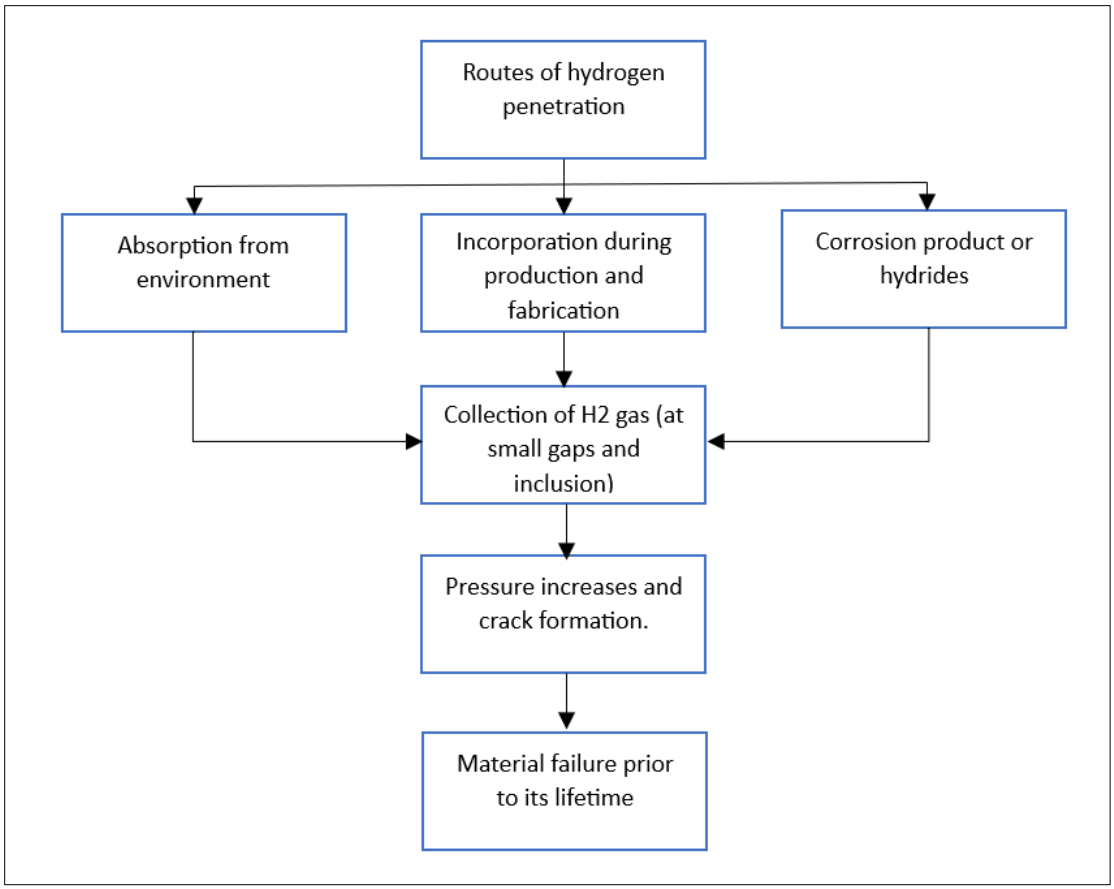

Figure 4. 3: Hydrogen-induced aging mechanism flowchart [219,226]

The associated reactions are below [214,217]:

$H^+ + e^- \rightarrow H_{ads}$. (Hydrogen atom)

$H_{ads} + H_{ads} \rightarrow H_2$ (Hydrogen molecule)

The cumulative effects of process operations demonstrates that residual deformation can frequently occur without observable structural component damage. Laboratory-scale research is needed to obtain a detailed analysis of likely event data and evaluate whether hydrogen-induced aging is a substantial concern for a particular application, in addition to identifying the key elements or problems that are causing it. The aging phenomenon of hydrogen storage and sealing

materials along with the various types of aging and their mechanisms in a hydrogen environment are thoroughly discussed in the following section of this dissertation. Alongside, a comparison of the various laboratory tests that have been carried out to understand the aging process and predict the service life of the materials are discussed as well. Thus, the research shortcomings are identified to be further investigated with the intention of contributing to standard aging research and protocols for this dissertation.

4.7.1. Thermal Aging and Mechanism

Thermal aging of materials is the permanent structural, compositional, and morphological changes over time while exposed to service temperatures. Materials can structurally degrade because of thermal cycling, which can accelerate the diffusion processes of hydrogen. The solubility of hydrogen in metals is proportional to temperature. With decreasing temperatures, diffusion mobility decreases [227]. Therefore, thermal aging increases with increasing temperatures. Hydrogen thermal aging is directly related to the diffusion of hydrogen at different temperatures. Sharp temperature drops can decrease the equilibrium hydrogen solubility in metals [222]. At 570 °C and 100 °C, Kolachev found that the coefficient of hydrogen diffusion was 2×10^{-4} cm^2/s and 4.4×10^{-5} cm^2/s, respectively, which indicates the co-efficient of hydrogen diffusion varied with temperature [224]. The flowchart in Figure 4.4 represents the mechanism of thermal aging [229,230].

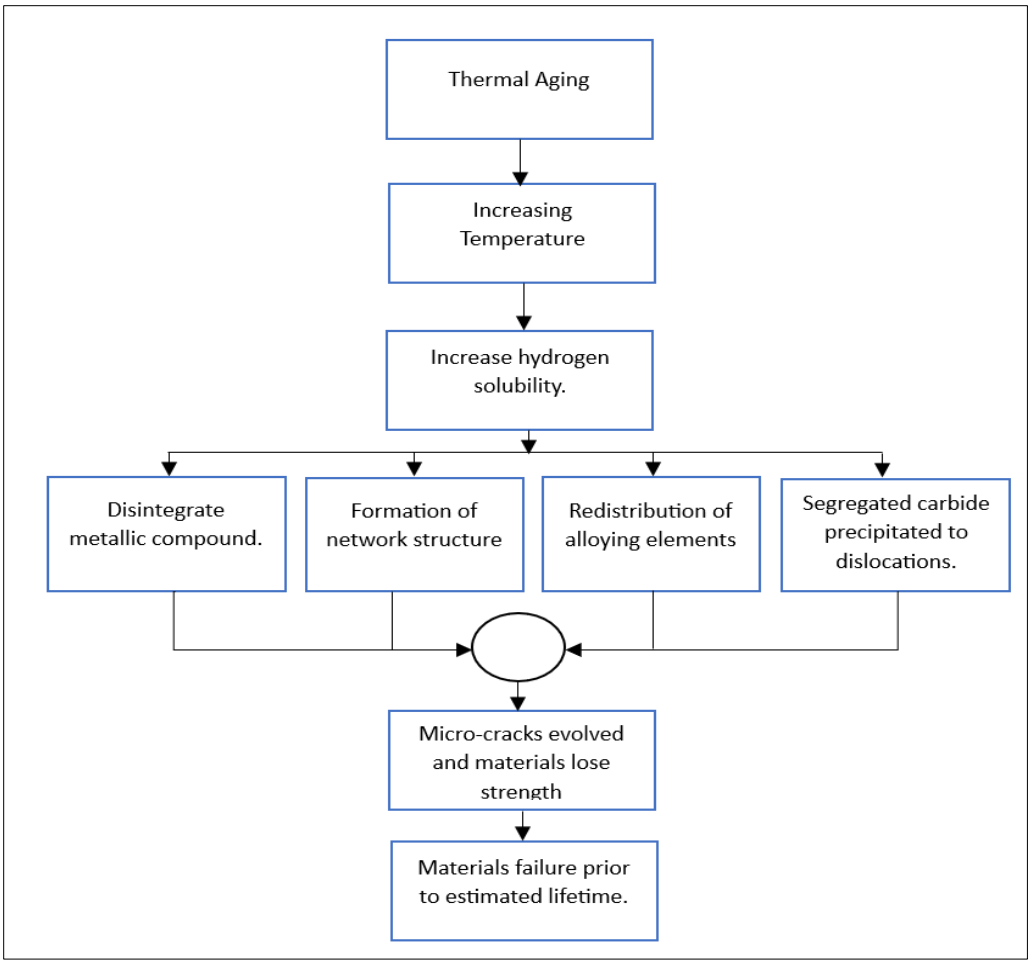

Figure 4. 4: Flowchart of the mechanism of thermal aging [229,230]

Laboratory test for Thermal Aging has been extensively studied in the literature. For the thermal aging of structural steel under a hydrogen environment, Student O.Z. [227] used a hydrogen filled chamber to expose a specimen at 0.3 MPa of pressure to cyclic temperature changes between 100ºC and 570ºC at a rate of 100ºC/min with a pause between temperature direction changes . After cooling at 100 °C at a rate of 50 °C/min, the 12Kh1MF steel specimen was kept in a vacuum during the thermal cycle for two hours. It has been observed that due to the temperature variation, the equilibrium solubility of hydrogen changes, which leads to the disintegration of cementite and the network formation of alloyed carbides. Because of thermal cycling, thermal stresses evolved

and created microcracks, which caused the thermal aging of structural steel [231]. Hirakami et al. [232] conducted a laboratory test with two samples of drawn pearlitic steel that were aged at 100 °C and 300°C for 10 min and tested under a slow strain rate testing method for measuring the hydrogen embrittlement susceptibility. The result shows that the hydrogen embrittlement susceptibility of the steels at 300°C is reduced because the carbons are segregated from the dislocations and the carbides are precipitated from the dislocations. Age-hardened beryllium-copper alloy, a suitable replacement for austenitic stainless steel used to store hydrogen at refueling stations, was tested in a laboratory by Ogawa et al. [233]. They observed that the hydrogen solubility capacity of the beryllium-copper alloy was two to three times lower than that of Austenitic stainless steel. However, after exposing the specimen to 100 MPa hydrogen for 500 h at high temperatures of 270°C, hydrogen diffusion may be enhanced. Consequently, the specimen's mechanical qualities declined; for instance, only the tensile strength fell by approximately 5% [233,234].The thermal aging of sealing materials has not been extensively studied yet. Yamabe et al. [234], Fujiwara et al. [235], and Simmons et al. [236] tested elastomeric sealing material NBR at room temperature, 30°C, and 110°C, and found that there is no hydrogenation or structural activity below 30°C, but at 110°C, compression set is increased by 40%, which indicates that with increasing temperature, the elastomeric sealing materials show a thermal aging tendency. Menon et al. [237], Castagnet et al. [238], and Klopffer et al. [239] tested different types of thermoplastic polymeric sealing materials at room temperature and 20–80°C, respectively, and observed some random behavior. The degree of crystallinity can be increased with increasing temperature, but mechanical properties do not change. This is because, with increasing temperatures, the plasticization of the polymer also increase. This phenomenon indicates that these thermoplastics can resist aging to some extent.

4.7.2. Chemical Aging and Mechanism

Chemical aging occurs when materials react with the chemicals in the environment when they are exposed to over a period. This reaction causes permanent changes in structure, composition, and morphology. In this method, materials remain in contact with different chemicals, mostly immersed in the solution and charged with hydrogen [240, 241]. This type of aging is frequently seen by both storage and sealing materials due to their continuous interaction with chemicals. Chemical aging is one of the most common forms of aging found in hydrogen storage and sealing materials. In hydrogen-storing metallic materials, the hydrogen's distribution and state influence the hydrogen embrittlement and the tensile properties of the metal and lead to complete aging [242]. In hydrogen-sealing materials, cracks are formed by the decomposition of the backbone and the hydrolysis of crosslinks, which leads to aging [240]. This phenomenon can be observed in Figure 4.5 [36].

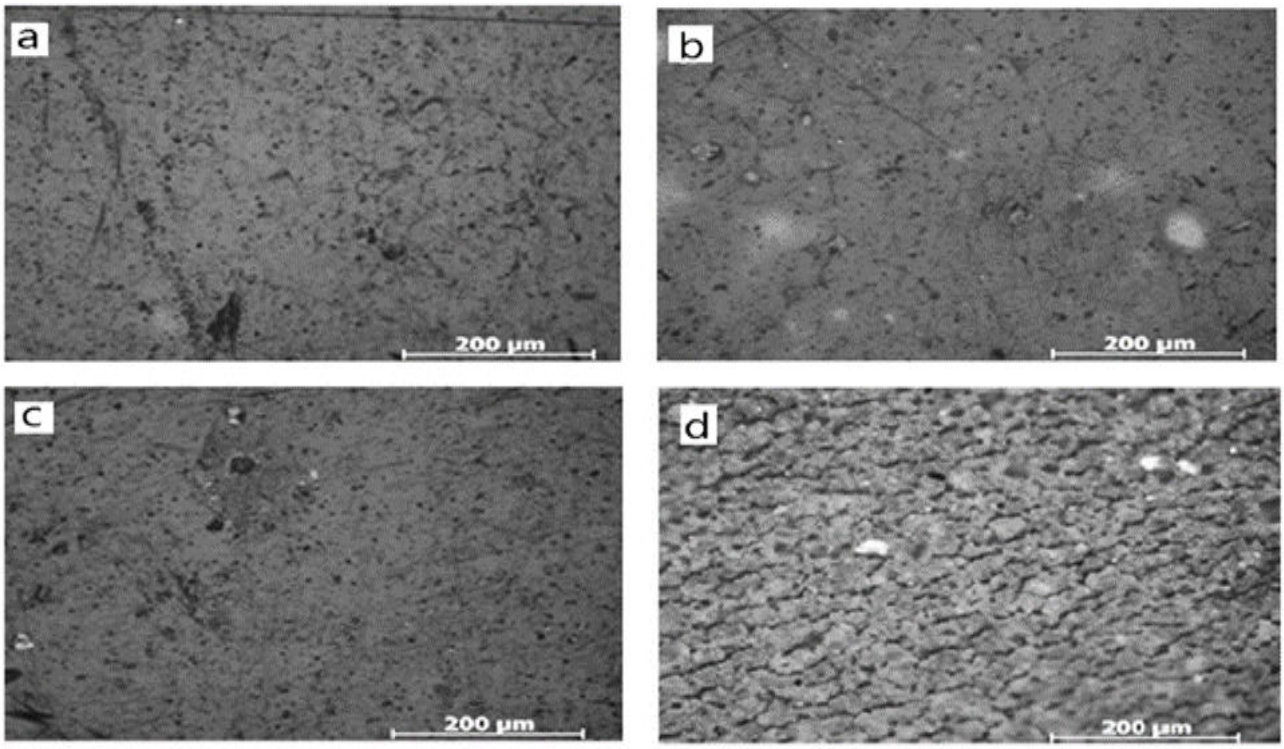

Figure 4. 5: Micromorphology of samples exposed to test solutions [36]

(a) unexposed, (b) exposed to mild conditions for sufficient time, (c) unexposed, and (d) exposed to harsh conditions for sufficient time

The micromorphological analysis conducted by Li et al. [231] represents the surface of the sealing material. It shows that with increasing hydrogen content, the condition becomes harsher, and cracks appear. Figure 4.5 (a,c) are unexposed samples; Figure 4 (b,d) are exposed to minor and harsh conditions, respectively. From this figure, it is clear that as the harshness of the condition increases, the surface roughness also increases. Surface roughness indicates the formation of cracks here. Thus, surface roughness indicates the aging of polymeric sealing materials. Figure 4.6's flowchart indicates the chemical aging mechanism for hydrogen storage and sealing materials [237,240].

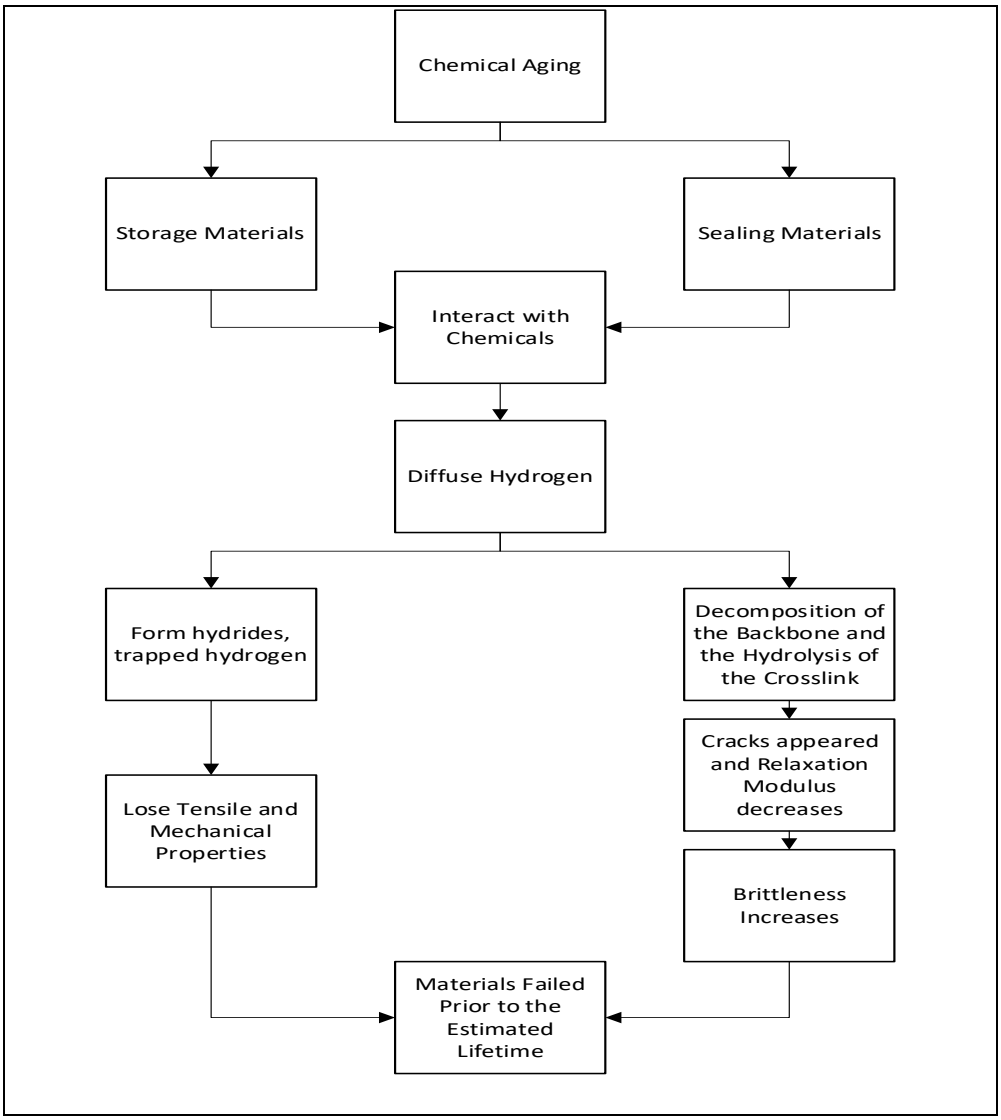

Figure 4. 6: Flowchart of the mechanism of chemical aging [237,240]

Laboratory Test for Chemical Aging has also been studied. Ogawa et al. [237] used martensitic Ni-Ti alloy specimens and acidulated phosphate fluoride (APF) solutions for the aging test. Cathodic electrolysis was used for charging the samples with hydrogen, and the charged specimens were aged for 16 h in the air at room temperature. The results show that the reduction in tensile strength increased brittleness and led the sample toward aging. Ogawa et al. [237] further conducted a different type of post-aging test on non-immersed and immersed specimens to determine the post-aging behavior of the material, where a tensile test was performed within a

few minutes after the removal of the specimen from the solution at room temperature. The results show that the tensile strength of the sample can be decreased. A Vickers micro-hardness test was done to determine the hardness of the specimen. Results show that the hardness can be increased, which increases the brittleness. TDA and XRD analyses were done to check the corrosion products and hydrides on the surface and for the quantitative analysis of trapping hydrogen, respectively. Each test confirmed the pick for hydrogen absorption and hydride formation, indicating the aging was being processed after charging. Tal-Gutelmacher et al. [238] conducted laboratory tests on three Titanium-based alloys: Ti-6Al-4V, Beta-21S, and Ti-20wt%Nb. The Ti-6Al-4V alloy was thermomechanical treated and exposed to a hydrogen environment. The alloy formed brittle titanium hydroxide phases, which is a key factor in chemical aging. Beta-21S was exposed to hydrogen electrochemically at room temperature and shows good resistance to hydrogen. Ti-20 wt.% Nb was exposed to hydrogen in two ways: electrochemically and in a gaseous environment. Electrochemical exposure formed (Ti, Nb) Hx hydride, and gaseous exposure created only titanium hydride. In both cases, Ti-20 wt.% Nb had to face chemical aging. Nykyforchyn et al. [231] tested ferrite-perlite X52 steel pipe after long-term service at the gas trunkline and found that all the mechanical properties of the material deteriorated due to the increment of hydrogen trapping. The bottom side of the pipe severely deteriorated, indicating that during the flow of aggressive substances through the pipe, the maximum portion of hydrogen penetrated the pipe and was trapped there. OMURA et al. [239] conducted a laboratory test on stainless steel and Ni-based alloys and found that high-nitrogen stainless steel and Ni alloy 286 had the maximum hydrogen concentration (Hc) at which fracture elongation was hard to degrade. High-nitrogen stainless steel had a higher Hc than the concentration of hydrogen-absorbing HE in the service environment,

lowering the chance of hydrogen embrittlement in the service condition. For internally reversible hydrogen embrittlement, alloys 286 and 718 show severe results compared to the cathodic charge. Li et al. [241] conducted a laboratory test using elastomeric gaskets made of silicon rubber as specimens. Different concentrations of acid were used for the test. Depending on the concentration, one solution was called a regular solution, which has an environment like a regular working environment, and another one was highly concentrated and used for an accelerated durability test (ADT). The concentration for the regular solution was 12.5 ppm sulfuric acid and 1.8 ppm hydrofluoric acid, and the concentration for ADT was 1 mil. L^{-1} sulfuric acid and 30 ppm hydrofluoric acid. During the experiment, the decomposition of the backbone and the hydrolysis of the crosslink of the polymeric gasket material take place, leading to a reduction in the elasticity and sealing force. As a result, the material aged in a hydrogen environment. Klopffer et al. [244] tested polyethylene and polyamide membranes and tubes under a hydrogen environment with controlled pressure and temperature. After long-term exposure to hydrogen, the measured permeability capacity of polyamide became lower than that of polyethylene. But the mechanical properties of both materials remain almost unchanged.

4.7.3. Mechanical Aging and Mechanism

The mechanical aging of the materials is a slow, progressive, and irreversible process of losing the capability to perform the assigned work under a high mechanical loading condition. Mechanical aging is often observed in fuel cell conditions where high-pressure hydrogen molecules create a high loading condition on the sealing material and in the hydrogen storage system. Mechanical aging is found in hydrogen storage tanks made of composite materials. Burst pressure, fiber damage, fatigue, collapse, and blistering of liners are some failure modes in this type of aging.

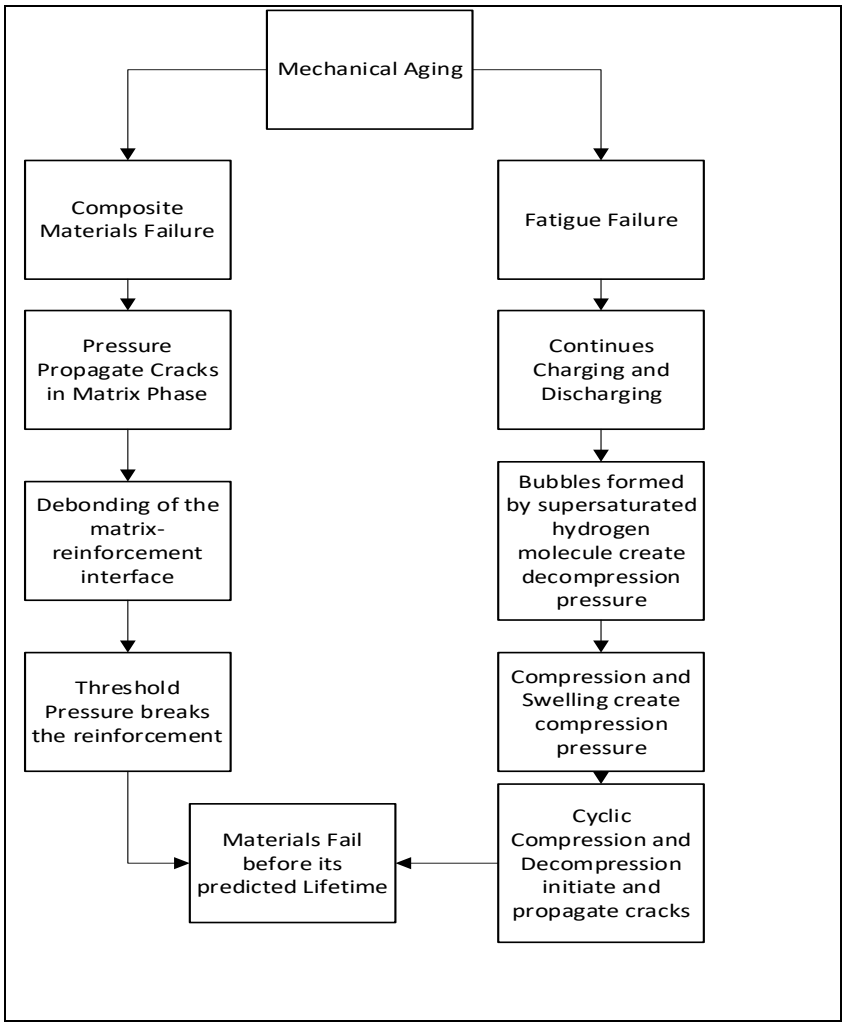

Figure 4. 7: Flowchart of the mechanism of mechanical aging [235,243]

When pressure is applied to a composite material, cracks can develop and extend profoundly to the matrix phase, which facilitates interface debonding. When the pressure reaches its threshold, a substantial quantity of reinforcement fails and causes the material to implode. On the other hand, continuous charging and discharging cause mechanical fatigue, which impacts mechanical aging. The mechanism for the formation of these types of cracks involves the initiation and growth of cracks as a result of strain concentration. The strain concentration can be caused by supersaturated hydrogen molecules creating bubbles after decompression and strain because of compression and

swelling. Shear stress, induced by the concentration gradient of solute gas molecules, initiates randomly organized circumferential cracks. As compressive tension increases so does volume expansion or swelling. As a result, tensile stress increases and fracture propagation accelerates. When the decompression rate is accelerated, cracks in the surface appear visibly [235,243].Wang et al. [46] analyzed the carbon fiber/epoxy composite used in hydrogen storage pressure vessels. They continuously increased the pressure of the vessel, and after 324 MPa, suddenly the pressure fell to zero, indicating bursting. Zheng et al. [245] conducted a fatigue test to analyze the behavior and fatigue life of the carbon fiber/epoxy composite. They found that after 500 cycles, the composite faced fatigue bursting; at that moment, pressure could be significantly decreased by about 15%. Feng et al. [246] analyzed the welded joints of TC4 titanium alloys for storage tanks, considering 10,000, 20,000, and 30,000 pre-cycles. After 24 h of electrochemical hydrogen charge on the specimen, the failure process was studied using SEM and TEM. The results show that the initial dislocation density of the specimens rises with the number of pre-cycles, making the hydrogen embrittlement through aging more severe. Following 10,000 and 20,000 pre-cycles, the specimens exhibited fewer dislocations and hydrogen capture at specific sites. In contrast, after 30,000 pre-cycles, dislocation accumulation and entanglement appeared both along the phase boundary and within the phase, resulting in a greater number of hydrogen capture sites. At lower cycles, the HELP mechanism dominates the tensile process, whereas the HEDE mechanism dominates the process at higher cycles. Yamabe et al. conducted a laboratory test where a high-pressure O-ring seal was used as a specimen. The O-ring was made of low-nitrile NBR (acrylonitrile content: 18%), which was vulcanized by sulfur and filled with carbon black.

With a 30% compression ratio, the specimen was compressed in a radical direction. Then it was inserted into a vessel that was pressurized by hydrogen from the bottom. They conducted optical

and scanning electron microscopy in post-aging experiments to observe the cracks. Also, they conducted gas chromatography-mass spectroscopy to measure the hydrogen gas content and a densimeter to measure the volume increase. They found two types of cracking for failure: one started from the center of the O-ring cross section and another from near the surface. Brownell et al. [247] conducted a simulation on ethylene-propylene-diene-based elastomeric rubber; they used O-rings and hose liners as specimens and exposed the sample to a pressurized hydrogen environment. Due to high pressure and rapid decompression, the specimen failed as a result of cavitation and stress-induced localization of hydrogen gas. This result supports the experimental result of the NBR O-ring. Wilson et al. [248] conducted the same experiment as Brownell et al. [247]. They just increased the crosslinking of the polymer using sulfur and found crosslinks create extra free volume at a pressure that facilitates the localization tendency of the hydrogen gas. Zhou et al. [249] modified the rubber seal materials, including the O-ring and D-ring, and conducted a simulation using finite element analysis. Their results show that the O-rings have a higher tendency to fail under stress concentration compared to the D-rings under hydrogen pressure ranges of 0–100 MPa. At high hydrogen pressure and contact stress, the D-ring outperformed the O-ring in terms of sealing ability, but the inverse was true under low pressure. They also analyzed the friction effect on the failure and found the D-ring had better performance against friction compared to the O-ring at high pressure.

4.7.4. Mechanical-Chemical Aging and Mechanism

The mechanical aging of materials is a slow, progressive, and irreversible process of losing the capability to perform the assigned work under a high mechanical loading condition over time. Whereas chemical aging is a long-term interaction with the chemical environment, and due to this interaction, material's structure, composition, and morphology change permanently. When a material is exposed to a high mechanical load and chemical environment simultaneously, the process is called mechanical-chemical aging. Hydrogen storage and sealing materials are subjected to mechanical-chemical aging during their normal operational cycle . Figure 4.8 shows the flowchart of mechanical-chemical aging [250–257].

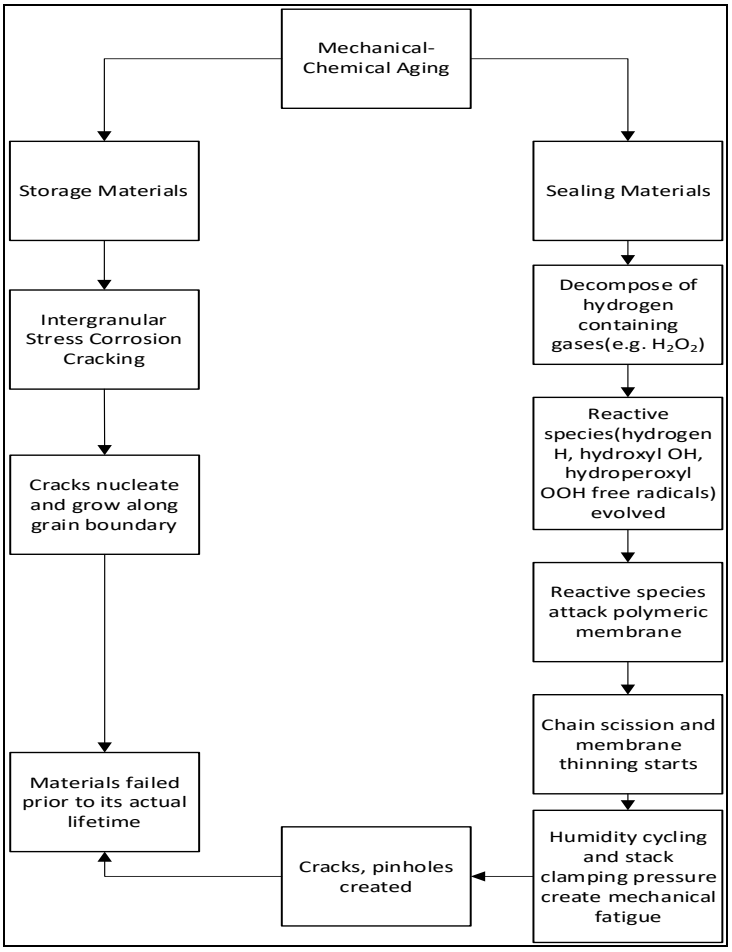

Figure 4. 8: Flowchart of the mechanism of mechanical-chemical aging [250–257]

Laboratory Test for Mechanical-Chemical Aging has been reported in the literature. Harris et al. [244] conducted a laboratory test on Monel K-500, a precipitation-hardened Ni-Cu alloy susceptible to intergranular stress corrosion cracking under a hydrogen environment at 923 K. The specimen was immersed in a 0.6M NaCl solution. A saturated calomel electrode was used to apply a potential was −1000 to −1200 mV. In four heat treatment conditions, the under-aged and peak-aged specimens showed increasing susceptibility to intergranular stress corrosion cracking compared to an un-aged and over-aged specimen. Nykyforchyn et al. [258] conducted a laboratory test where they tested ferrite pearlitic X52 steel cylindrical, smooth, and pre-cracked samples into a solution of artificial brine mimicking onshore conditions where stress corrosion cracking could be created. The test was conducted both in the presence and absence of external polarization. In the absence of external polarization, aggressive environments did not show as much effect as in the presence of external polarization. In the presence of external polarization, both specimens were affected. Robert et al. [259] took a perfluorosulfonic acid-based membrane and placed it in a degradation solution. At one time, the membrane was fitted with a universal testing machine for mechanical stress. Two types of solutions were used: one is mild (3 Vol% H_2O_2) and another was an aggressive solution called Fenton solution (3 Vol% H_2O_2 + 1 ppm Fe_2+ ion). Mechanical fatigue was applied to create mechanical stress on the membrane. A cyclic compressive stress was applied on the channel ribs to reproduce one-hand swelling or shrinkage cycles, and a static compressive stress was maintained for the stack clamping pressure on the membrane. In this experiment, fluoride emission rates (FER) were observed to predict the decomposition of the polymeric membrane. The post-aging condition of the material was determined by Robert et al. [259] by using a fluoride-ion selective electrode, which measured the amount of emission of fluoride ions. It was considered a reliable PFSA (perfluorosulfonic acid) chemical degradation indicator.

From the analysis of FER data, it was confirmed that aging was taking place there.

4.7.5. Thermo-Mechanical Aging and Mechanism

Combining both the thermal and mechanical aging processes, when high mechanical load and temperature work at the same time for the aging of material, it is called thermo-mechanical aging. Such conditions are generally created within hydrogen fuel cells and sealing materials. The diffusion of hydrogen affects the thermo-mechanical aging method. This is mainly seen in polymeric materials with viscoelastic behavior, if the strain is held constant viscoelastic materials show stress relaxation, and if stress is held constant, they show creep. Physical relaxation, chemical relaxation, and thermal degradation are some combined factors during stress relaxation in the polymer. Figure 4.9 shows the flowchart of thermos-mechanical aging [260-264].

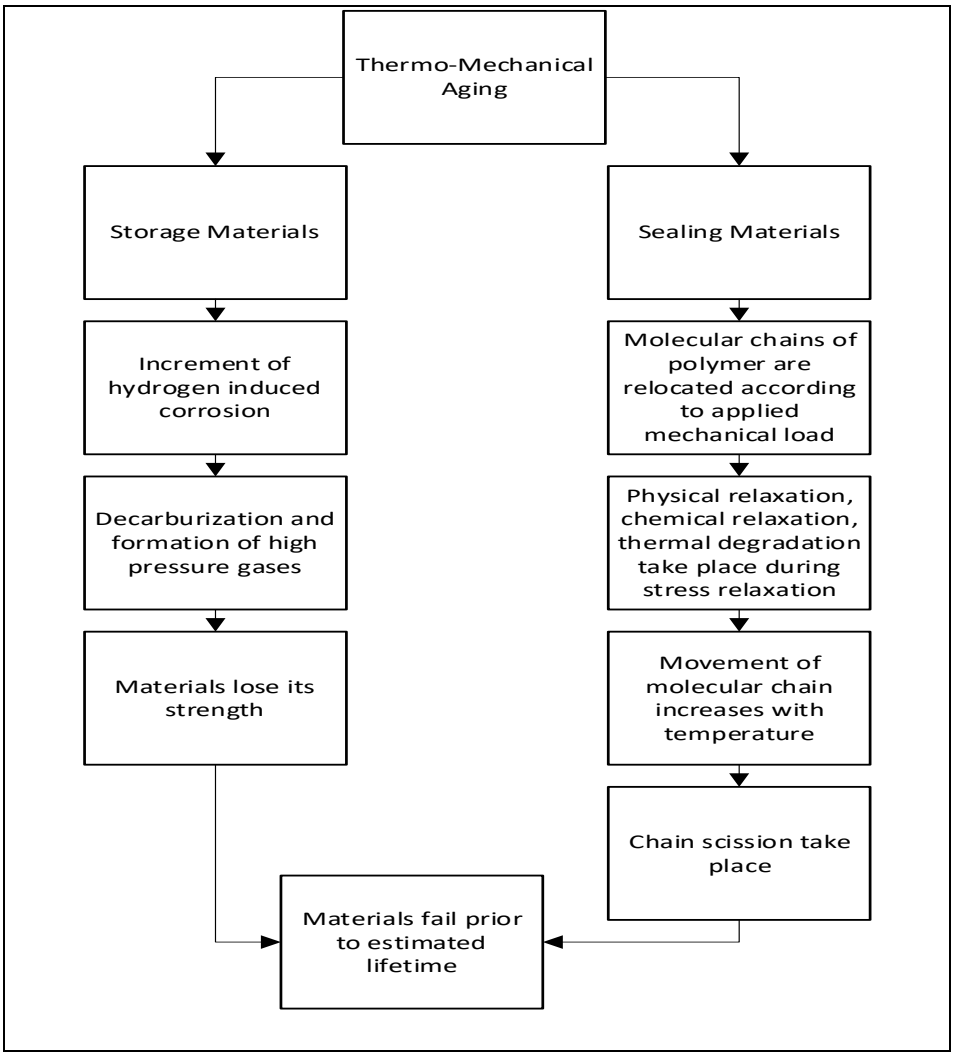

Figure 4. 9: Flowchart of the mechanism of Thermo-Mechanical aging [260-264]

Thermo-mechanical aging occurs when hydrogen-induced corrosion in storage materials increases with increasing mechanical load and elevated temperature. Corrosion-induced hydrogenation of the materials, in combination with working stresses, may lead to the emergence of nano and micro-scale bulk damage. Hydrogen evolution may occur with corrosion, particularly in cracks caused by the local acidity of the corrosion media [265]. During operation, materials experience in-bulk repeated damage due to decarburization and the creation of high-pressure hydrogen gases, causing them to lose their strength of materials [263] . In addition, when sealing material is subjected to

mechanical load in a hydrogen environment, molecular chains of polymer are relocated. This causes stress relaxation which directly reduces the sealing force. Physical relaxation occurs first among other factors, then comes chemical relaxation, and later thermal degradation. With increasing temperature and operation cycles, the movement of the molecular chains increases which causes chemical reactions and chain scission. In this way, due to the stress relaxation behavior, polymeric material starts to loosen its sealing force as well as the sealing capability [264]. Laboratory Test for Thermo-Mechanical Aging has been studied before. Balitskii et al. [260] conducted a laboratory test on two steel specimens, 05Kh12N23T3MR and 10Kh15N27T3B2MR, in a high-pressurized hydrogen environment and at elevated temperatures. A static tensional force was also applied to the temperature. At room temperature, the hydrogen action on both samples was minimal. But at high temperatures, 10Kh15N27T3B2MR was more sensitive to hydrogen embrittlement than 05Kh12N23T3MR but less sensitive than 60Kh3G8N8V and 12Kh18AG18Sh steel. NYKYFORCHYN et al. [265] conducted a laboratory test on Cr-Mo-V steel at 450 °C with an applied tensile load. Their results show that the degradation of Cr-Mo-V steel is increased, and the fatigue crack growth resistance is decreased due to hydrogen. Cui et al. [261] conducted a laboratory test using a liquid silicon rubber (LSR) gasket as a specimen. The test was done in two mediums: air and water. Stress relaxation equipment was used in the experiment. During the experiment, constant deformation was applied to the sample, and the temperature was raised to 100 to 120°C. The test was performed at different strain rates, temperatures, and stress levels. They used time-temperature superposition theory to construct a master curve that could predict the service life of the specimen. They found that the medium also affected the aging of the species. They found that at 70 °C, LSR service life could be 5000 h at 60% of initial sealing stress. Below the 60% initial sealing stress, it was considered leakage.

4.8. Durability Analysis of Hydrogen Sealing and Storage Materials through Aging

An accelerated Durability Test (ADT) can be performed to predict the durability of materials. It can be done to minimize the time and give a better prediction of durability. Under most operating conditions found in industry, material aging occurs over a long time . Materials tends to deteriorate rapidly if the regular conditions undergo a shift to severe ones. In ADT, this principle is followed. The test procedure is presented in Figure 4.10 with a flowchart. With this test, metallic hydrogen storage materials and polymeric sealing materials may be compared. This test is used not only for testing durability but also for material comparison, quality control, and design information. In this technique, specimens are compared under both normal and accelerated conditions. Chemical abrasiveness, temperature, and pressure are held at their highest levels to simulate the worst-case scenario during an accelerated test cycle. Therefore, mechanical, chemical, electrochemical, and thermal failure mechanisms exist [266]. The specimens under normal and accelerated aging conditions are compared, and extrapolation is utilized to anticipate the service life and durability of the material [267, 268]. The main limitation of this test is the simulation of service conditions, which is tough. As a result, the predicted value has errors within a specific limit. Again, the activity of the materials found in harsh conditions is not always reflected in mild conditions. The benefits of the ADT method are, this test is a comprehensive test for predicting the material's durability, especially polymeric sealing materials [262]. Burgess et al. [263] conducted an accelerated durability test for a pressure relief device (PRD) in a hydrogen environment, where they created the worst conditions for the PRD that it could face in its service conditions. A medium-pressure hydrogen storage cylinder was used to conduct the test with the PRD under test acting as the only protective device Maximum stress and temperature cycles were applied to the specimen.

The failure behavior was observed. From the results, they predicted the behavior of the 440C steel specimen. An accelerated stress test is a form of ADT used in the determination of the behavior of the proton exchange membrane (PEM) fuel cell. Polymeric sealing materials can be compared with PEM. In this system, failure modes are mechanical, chemical, electro-chemical, and thermal. Thus, for an accelerated test stress cycle, chemical harshness, temperature, and pressure are kept at maximum to create the worst conditions for PEM. Liu et al. [264] and Kundu et al. [269] conducted accelerated stress test for the Nafion membrane. Liu et al. [264] conducted ADT for 10 cycles, and each cycle consists of 100 h. They found significant degradation taking place at 500–600 h of operation, and at 1000 h, the membrane was completely degraded. Kundu et al. [269] found that over 4–5 days of ADT, almost 20% of weight was lost. By extrapolating these data, the service life could be measured. Figure 4.10 shows a durability test of process flow diagram [263].

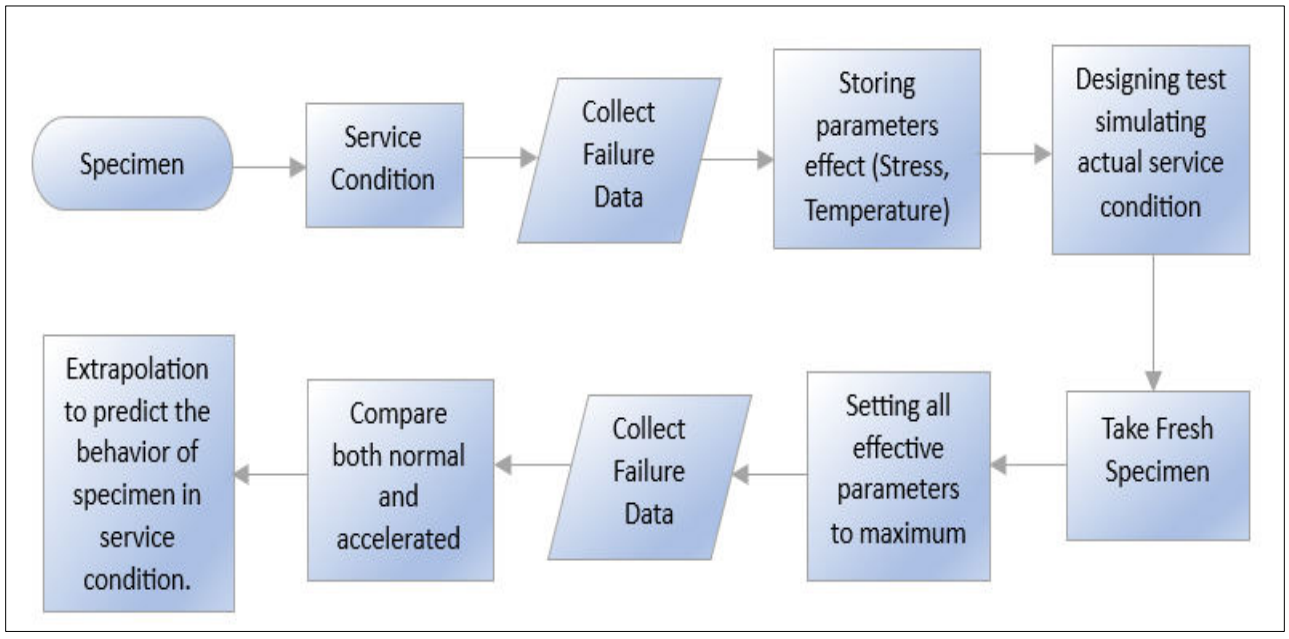

Figure 4. 10: Process Diagram of Accelerated Durability Test [263]

The service life of a material can be defined as the amount of time a material can provide the proper service for which it was made. There is a relationship between service life and crack defect size. Figure 4.10 shows that after long-term use, when materials spent a significant portion of their service life, the distribution of cracks and their sizes increases. The service life of a material can be predicted using the reverse method. In this method, crack defect size is measured using ADT, and service life can be predicted from that value. For detecting cracks in materials in a hydrogen environment, several tests can be performed. Such as changes of vibration characteristic of structure technique, acoustic emission technique, structure interrogation using lamb waves and ultrasonic using piezo transducer technique, eddy current, and ultrasonic technique, etc. [267]. Figure 4. 11 shows a graphical representation of service life with defect size and probability of detection [244].

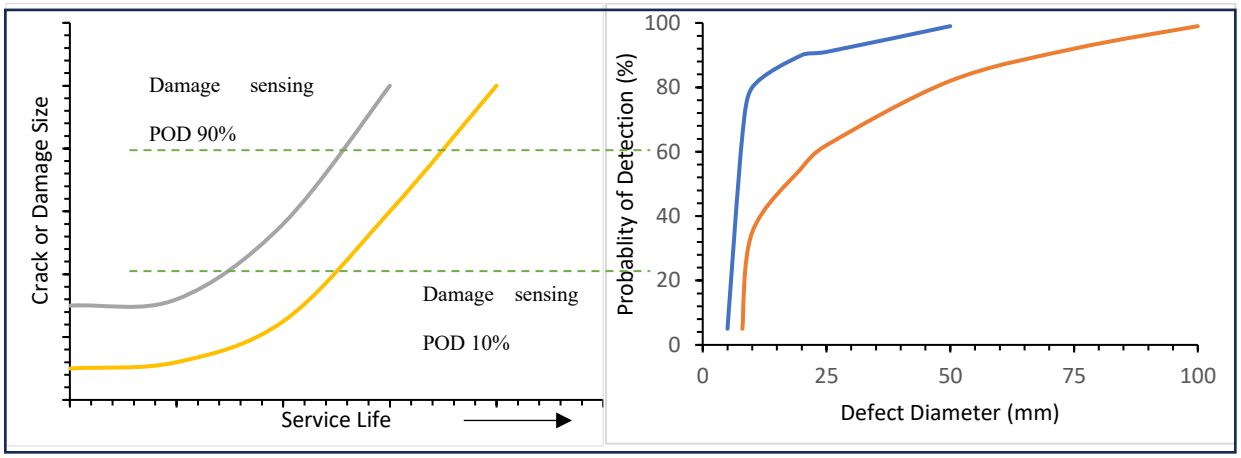

Figure 4. 11: Service Life with defect size and probability of detection [244]

Time-Temperature Superposition (TTS) principle is an established principle for predicting service life. It is a commonly used method where a master curve is created from data at selected reference temperatures. From this master curve, service life is predicted. The relationship between time (t) and temperature (T) for the mechanical response is described in the TTS principle [268,270] and the relation can be written mathematically as follow:

$G_r(t, T_2) = G_r(a_T(T_1, T_2)\, t, T_1)$

where, G_r = mechanical response, a function of time and temperature,

T_1, T_2 = two different temperatures, t = time, a_T = shift factor.

The principle states that time and temperature are equivalent. At two different temperatures, the same shape and time function of stress can exist. When the stress relaxation curve is presented on a logarithmic-logarithmic scale, this curve can be shifted to another temperature horizontally. The TTS principle is used to shorten the test time because it tests material for a shorter time at a higher temperature [261]. Creep behavior and the stress relaxation of polymeric materials can be determined using this principle [271]. For predicting the life of a material using TTS, the process shown in Figure 4.12 is followed [272].

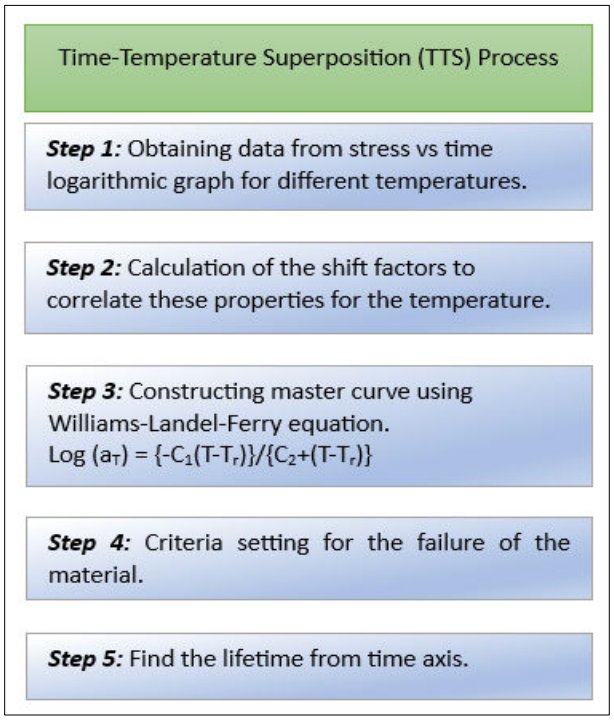

Figure 4. 12: Process of predicting the lifetime of a material using the TTS process [272]

Cui et al. [266] tested LSR at three different temperatures (70°, 100°, and 120 °C) and obtained a stress versus time logarithmic curve. Using the Williams-Landel-Ferry equation [272], they constructed a master curve and fixed 60% of stress for the threshold value of leakage. They then drew a line from 60% to the master curve. Then another line was drawn from the master curve, intersecting at a point on the time axis. The value at which the line intersects the time axis is the predicted lifetime of the material.

4.8.1. Service Life of Storage and Sealing Material under Simultaneous Multiple Aging

In the case of a hydrogen environment, failure of the storage material can create a disaster. Taking the thermal aging of steel into consideration, O. Z. Student [227] found changes in the structure during laboratory aging for 40 h, which were observed after continuous operation of 140,000–190,000 h. Therefore, the service life of the steel can be predicted using ADT. Vessel chambers and transportation piping is susceptible to chemical interactions when used to store hydrogen. . Under chemical aging conditions, no such work was found where anyone was claiming the service life of any storage materials. For thermal aging, the predicted service life was 140,000–190,000. But in mechanical-chemical aging, the service life prediction was 5500 h, and in chemical aging, it was 6000 h, which is a huge difference [232,240]. Thus, the intensity of thermal aging is comparatively lower than other methods, and it also varies depending on the service condition, materials used, environment, etc. In fuel cells, if the sealing material of the membrane ages and leaks, it can create a great disaster [273, 274]. Taking the chemical aging of a polymeric gasket material into consideration, it was found that the test time under an ADT environment of 6 h could be equivalent to 27 hr of the lifetime of the specimen. This result was based on the time-concentration superposition theory, and it showed that under harsh conditions, the extrapolating

lifetime was four times the experimental time. By using the TTS principle based on stress relaxation behavior, it was predicted that the service life of Silicon rubbers would be at least 6000 h under the simulated fuel cell environment [275]. When mechanical and chemical aging occurs in a system, the condition worsens more rapidly. Because of chemical aging, the material becomes brittle and loses its elastic properties. If a mechanical load is applied to it at the same time, the process of aging will be accelerated as usual. A laboratory study found that under fuel cell operation where combined mechanical-chemical aging takes place, the service life of a membrane is about 5500 h [276]. One observable thing is that if the services are compared with each other, then the intensity of this aging can be understood. The service life of a membrane under chemical aging was predicted at 6000 h. But when mechanical aging was added to the chemical aging, the service life was reduced to 5500 h. Thus, it is clear that the intensity of aging is higher in both mechanical and chemical aging. But it is also important to know that chemical aging is more efficient than mechanical aging [259].

4.9. Key Factors Affecting Aging under the Hydrogen Environment

Temperature, aging time, stress, thermal cycle, environment, hydrogen pressure, and hydrogen distribution are the primary factors affecting aging in a hydrogen-rich environment. The literature indicates the impact of factors; Zelenak et al. [277] found high temperatures elevate hydrogen aging, resulting in the formation of reactive metal hydride composites or complex metal hydrides in storage materials. Eliezer et al. [278] observed that the concentration of hydrogen had an impact on the aging behavior of titanium alloys in a hydrogen atmosphere, with greater concentrations resulting in more rapid aging.

4.9.1. Effects of Temperature

The temperature effect on hydrogen storage metallic materials can be described from the metal-hydrogen interaction. Metals lose strength when hydrogen embrittlement occurs. This phenomenon depends on hydrogen absorption, physical adsorption, transportation of hydrogen to the crack tip, transportation of hydrogen to tensile stress regions, etc. All these factors are highly temperature dependent. Figure 4.13 shows how the solubility of hydrogen increases with temperature. It can be observed that the hydrogen solubility in molten iron above 773.15 K is approximately 30 ppm, and at 1273.15 K, the hydrogen solubility of molten iron is less than 10 mL H/100 g. It reached more than 40 mL H/100 g at a temperature above 2273.15 K [279]. Figure 4. 13 shows Hydrogen solubility vs temperature curve [279, 280].

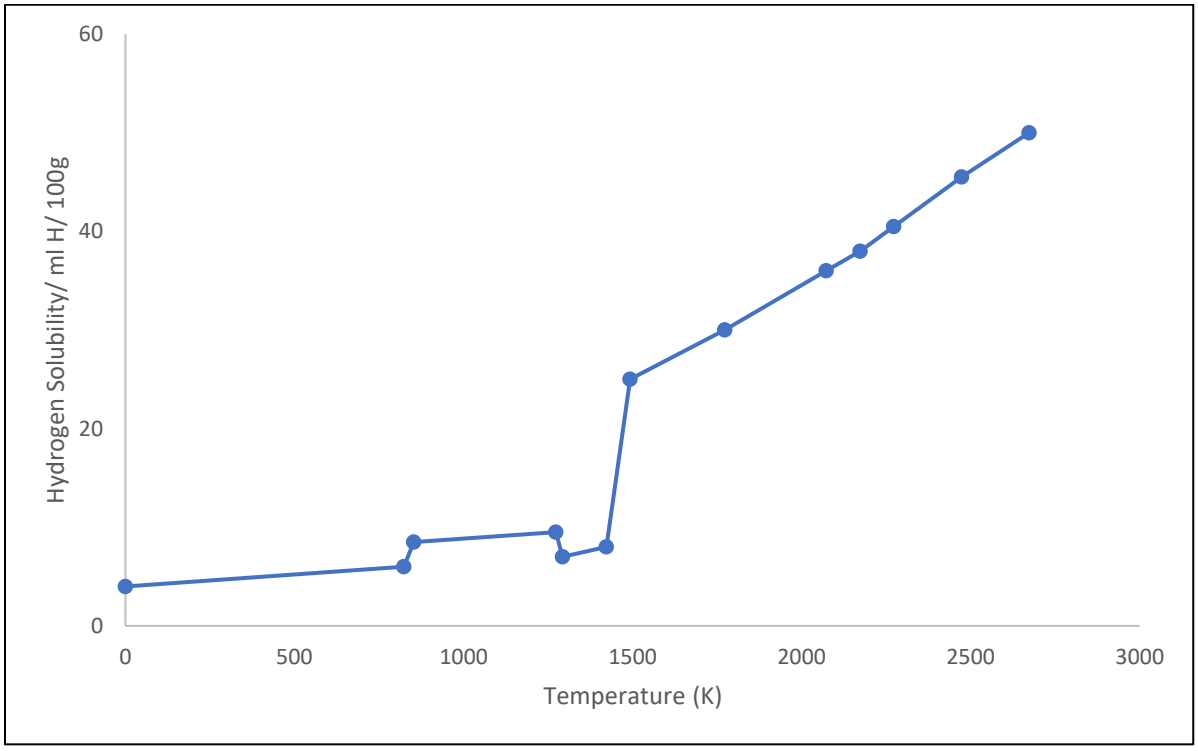

Figure 4. 13: Hydrogen solubility vs temperature curve [279, 280]

Figure 4.14 describes the relative reduction of the area, which is a measure of ductility that varies with temperature. At lower temperatures from 75 K to 150 K, the effect of hydrogen on ductility is low due to the slow transportation rate, and at higher temperatures more than 250 K, the hydrogen effect is low as well because of the trapping of hydrogen by dislocation. But in the intermediate region from 150 K to 250 K, hydrogen has a significant impact on the ductility of the metal. In this intermediate region, the ductility of metal reduces significantly to approximately 40%. Figure 4. 14 shows relative reduction of area of 316 Stainless Steel with the temperature at tensile test in a hydrogen environment [280].

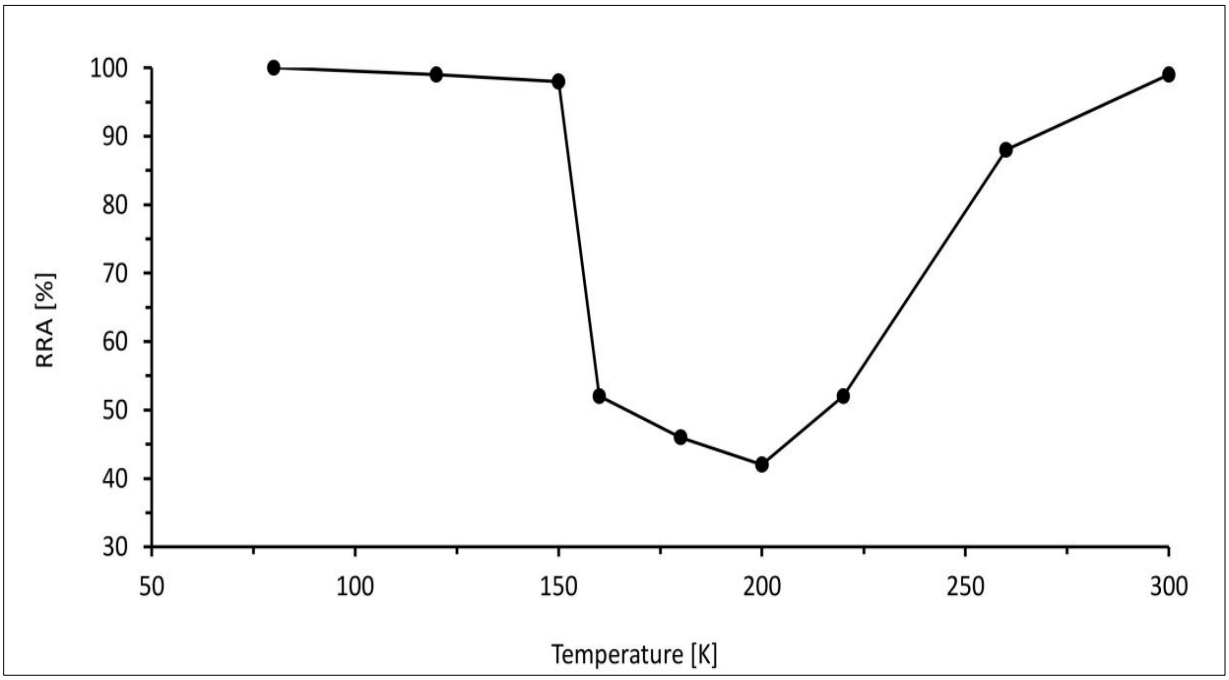

Figure 4. 14: Reduction of area of 316 Stainless Steel with the temperature at tensile test [280]

At cryogenic temperature for storing liquid hydrogen, materials face embrittlement. It is known that depending on crystal structure the embrittlement tendency varies. Face centered cubic crystal structure has lower embrittlement tendency than body centered cubic crystal structure. This is because body centered cubic structures have lower activated slip system at low temperature.

As a result, face centered cubic structured materials have high sustainability in cryogenic temperature. Ductile to brittle transition temperature is another important parameter which needs to be considered. The materials which have ductile to brittle transition at low temperature can be significantly affected if used for low temperature application [281]. The effect of temperature due to hydrogen differs from material to material. For polymeric gasket materials, Wu et al. [282] found that with increasing temperature, the mechanical properties of the sealing materials, including the tensile strength, elongation at failure, compression stress relaxation, and compression permanent deformation, tend to decay. Dubovsk et al. found [283] in their work that high temperatures accelerate the degradation of the seal. Stress relaxation of polymeric sealing materials is dependent on the temperature. Chemical relaxation and thermal degradation increase with increasing temperatures. For polymeric materials the, with decreasing temperature bonding strength between molecular chains increases which increases the Young's modulus as well as the tensile strength but the toughness decreases [284, 285]. Figure 4.15 indicates that temperature has a considerable effect on the stress relaxation of polymeric materials, and with increasing temperature shift factor increases sharply. The shift factor is the degree of material's time acceleration in an isothermal environment. As the shift factor increases with temperature, the materials' aging accelerated. Figure 4. 15 sows shift factor of the master curve [261].

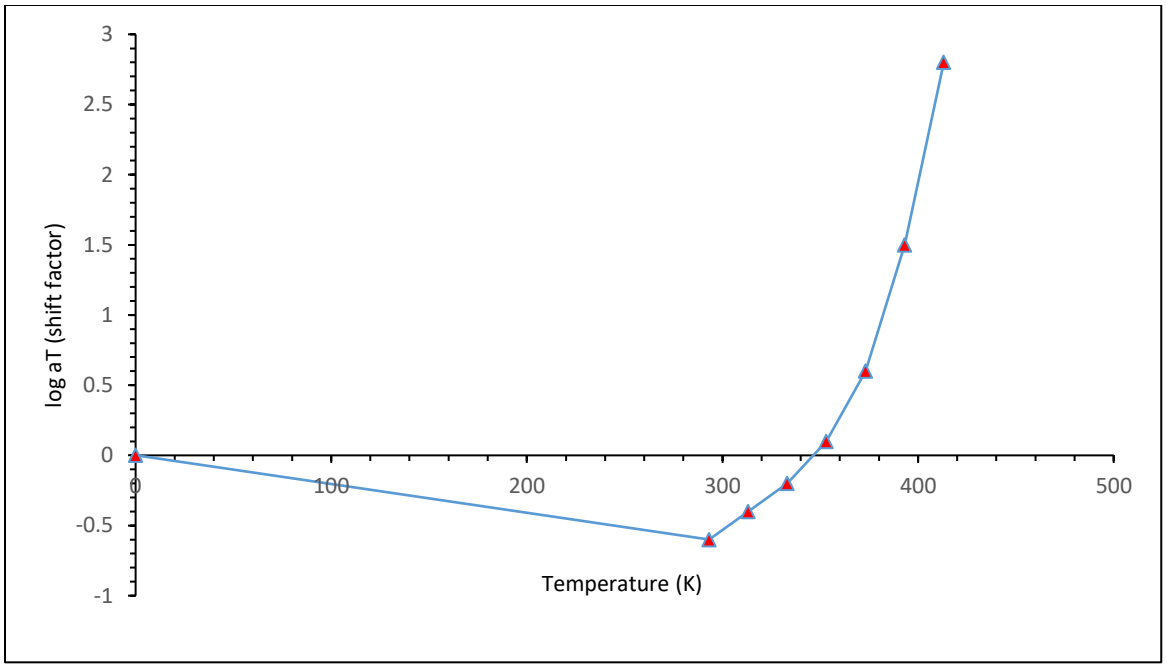

Figure 4. 15: Shift factor of the master curve [261]

4.9.2. Effect of Pressure

Hydrogen permeation into the metal increases with increasing pressure, which enhances the embrittlement tendency of the metal. When hydrogen is stored in a container, it exerts pressure on the container wall. If the container becomes metal, the permeation of hydrogen through the metal can be higher, and the metal's aging tendency can increase [281]. The increasing pressure also increases the interaction between the hydrogen and the sealing materials. As a result, the absorption of hydrogen increases, which eventually degrades the properties of the sealing material, as discussed earlier [282]. Another important phenomenon takes place when high pressure is suddenly released. Due to the sudden drop in pressure, the volume of the inside gas increases, and desorption starts. During the desorption process, bubbles are created, which create micro-cracks; this phenomenon is known as cavitation [283]. Figure 4.16 shows that with increasing pressure, hydrogen has a higher tendency to dissolve in materials [286]. At 20 MPa, the hydrogen content was less than 50 ppm, which reached almost 1000 ppm at 100 MPa. Because hydrogen is very

small in size and increases in pressure, it can easily penetrate through materials.

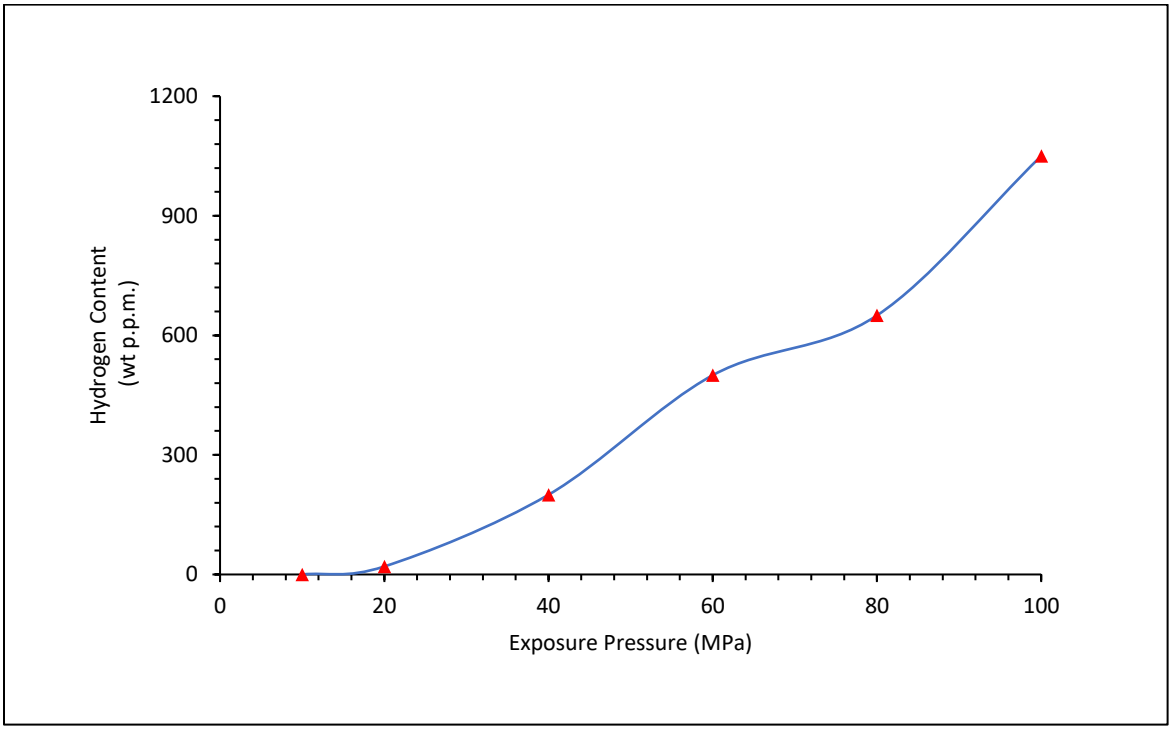

Figure 4. 16: Relationship between Hydrogen Content and Exposure Pressure [286]

4.9.3. Effects of Stress

Stress is an important factor that can significantly affect the aging process in a hydrogen environment. There are different types of stresses, such as thermal stress, chemical stress, mechanical stress, etc. Thermal stress is induced in materials due to temperature fluctuations. It can facilitate the aging process, and this type of stress is highly related to thermal cycling. In harsher chemical conditions, chemical stress increases. Robert et al. [261] conducted an aging test using a perfluoro-sulfonic acid-based membrane. Two membranes were selected for the experiment, and both were Nafion based membrane, Nafion™ NR211 and Nafion™ XL. The XL membrane differs from the NR211 by the presence of additional PTFE-rich reinforcement and cerium-based radical scavengers. This type of membrane is degraded by the emission of fluoride

ions when it reacts with chemicals. They tested their specimen in two stress conditions, static and cyclic. After testing, they found that when cyclic stress was introduced instead of static stress, the fluoride emission rate of the specimen was increased. Figure 4.17 shows the results of their experiments [261]. The first graph indicates static stress condition, and the second graph is cyclic stress condition The results indicate the fluoride emission rate is higher in cyclic conditions, and this is indicative of an aging process having occurred.

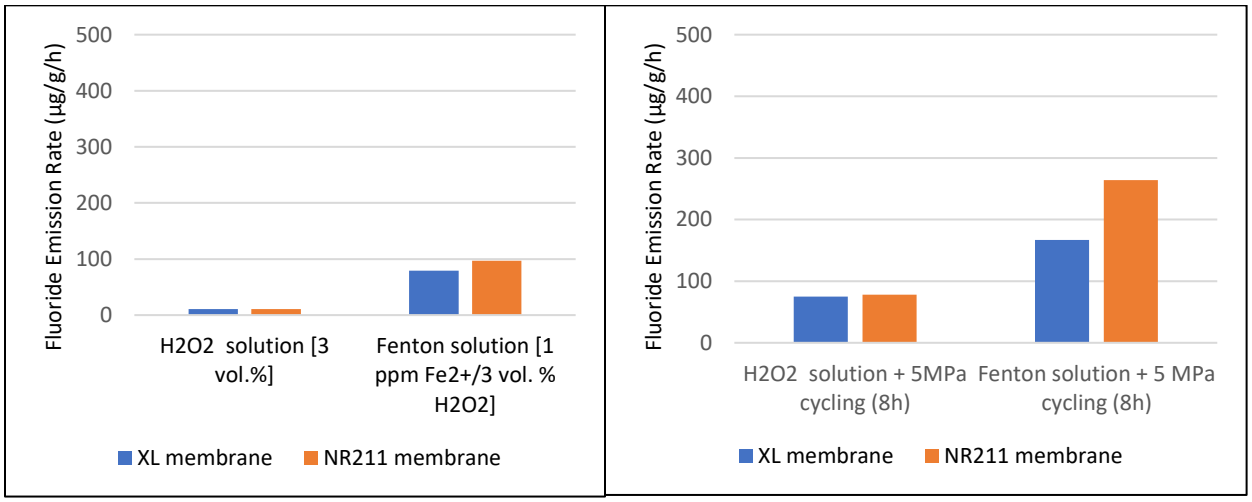

Figure 4. 17: The fluoride emission rate under different stress conditions (static, cyclic) [261]

4.9.4. Effects of Thermal Cycle

Thermal cycling is a cyclic process of rapid temperature change where a material remains at a higher extreme in one phase and a lower extreme in the other. Due to thermal cycling, thermal stress is created in materials, which is called thermal aging. Thermal aging results from fatigue crack growth and depends on the number of cycles and material properties. Not only does the number of cycles affect the aging process, but the range of the temperature of the thermal cycle is also significant. A higher range of temperature differences can cause more variation in the diffusion of hydrogen, which can affect the aging process [227]. Figure 4.18 shows that an increase in the number of thermal cycles increases the tendency for fatigue failure of materials [227].

In the left-side figure, the threshold value for effective fatigue decreases with increasing the number of cycles. Because it is known that fatigue is a cyclic stress-dependent failure mechanism that increases with increasing stress cycles, the important thing to notice here is the behavior of hydrogen. When the test is done in a hydrogen environment instead of air, the threshold value decreases more than in air. This evidence proves that thermal cycling affects the aging mechanism of materials in a hydrogen environment. The right-side figure also describes the same type of effect, where the threshold value for crack opening decreases with an increasing number of cycles and hydrogen environment.

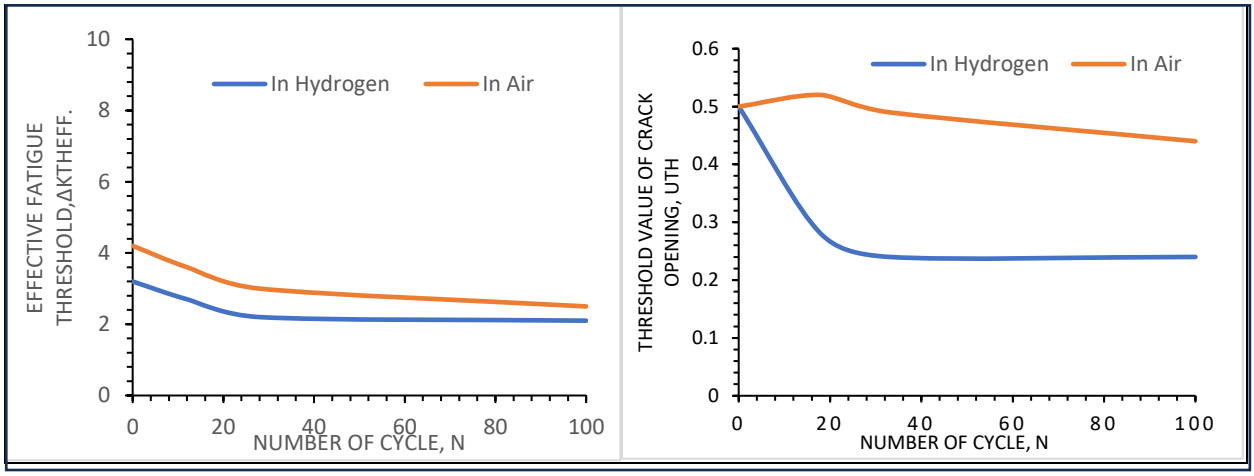

Figure 4. 18: Threshold values for fatigue failure of materials in air and hydrogen [227]

4.9.5. Effects of Environment

The environmental effect has a impact on the aging of sealing and storage materials. These materials work in extreme conditions where they may be affected by the humidity cycle, harsh chemical environments like a strongly acidic environment etc. As the humidity increases, the crossover leakage tendency increases. Crossover leakage is the tendency of the mixing of different gases (like, in proton exchange membrane fuel cell H_2 and O_2) leaking through the gasket material.

Gittleman et al. [90] tested three types of membranes, Gore Primea, Nafion N111-IP, and Nafion NR-111, in different humidity cycles. The result of the crossover tendency is shown in Figure 4.19 [276]. Figure 4.19 shows that by increasing the humidity cycle to the threshold value crossover tendency of every material increases in a hydrogen environment [276]. This evidence is indicative that the humidity cycle influences the hydrogen aging of the materials.

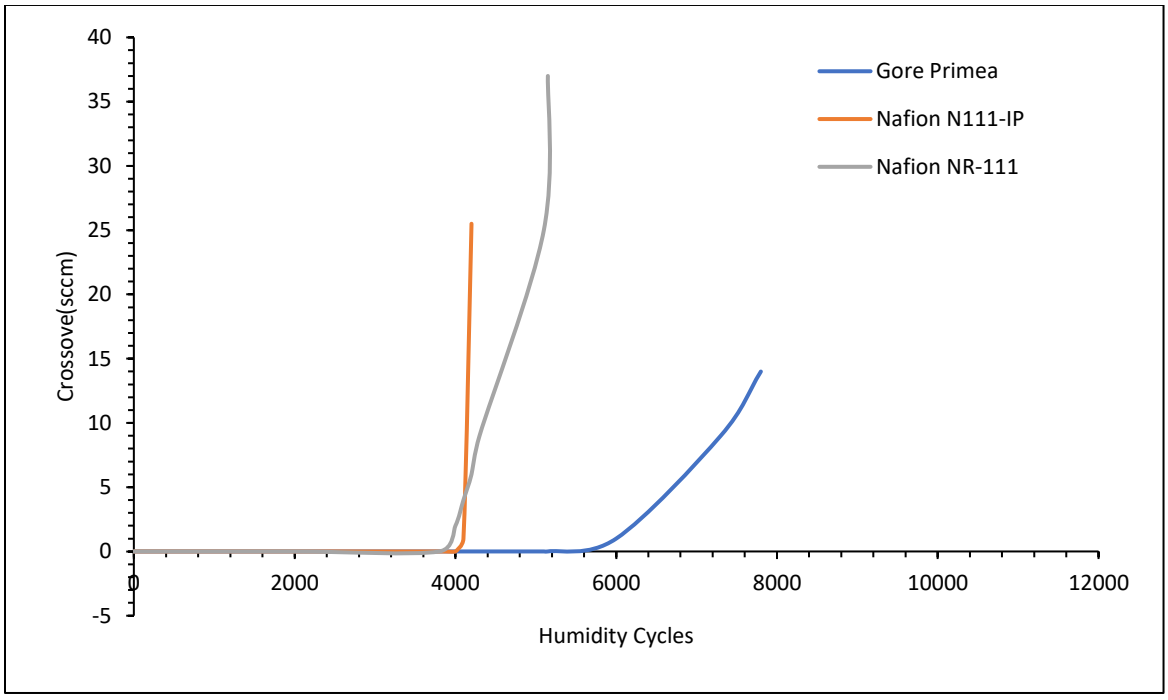

Figure 4. 19: Crossover leakage tendency in different humidity cycles [276]

A harsher environment also affects the hydrogen aging process of the materials. In Figure 16, the H_2O_2 environment is mild, whereas the Fenton solution environment is harsh. The graph shows when the environment approaches harsh conditions the fluoride emission rate increases significantly, which means the aging is also increasing. The ambient pressure of hydrogen also affects the aging process. Cracks are formed in materials due to the fluctuation of the hydrogen pressure. This pressure creates stress on the defective sites and forms cracks [227].

4.9.6. Effects of Alloying Elements

Alloying elements have effects on the degradation of hydrogen storage metallic materials. Martin et al. [89] found that increasing alloying elements percentage in stainless steel increases the relative reduction of area in the hydrogen environment. Figure 4.20 shows that the hydrogen embrittlement tendency of stainless-steel decreases with increasing alloying elements [287]. They used Mo, Ni, Si, S, Cr, and Mn as alloying elements. Among these alloying elements Si, Mn, and Mo show much resistance to hydrogen embrittlement compared to others.

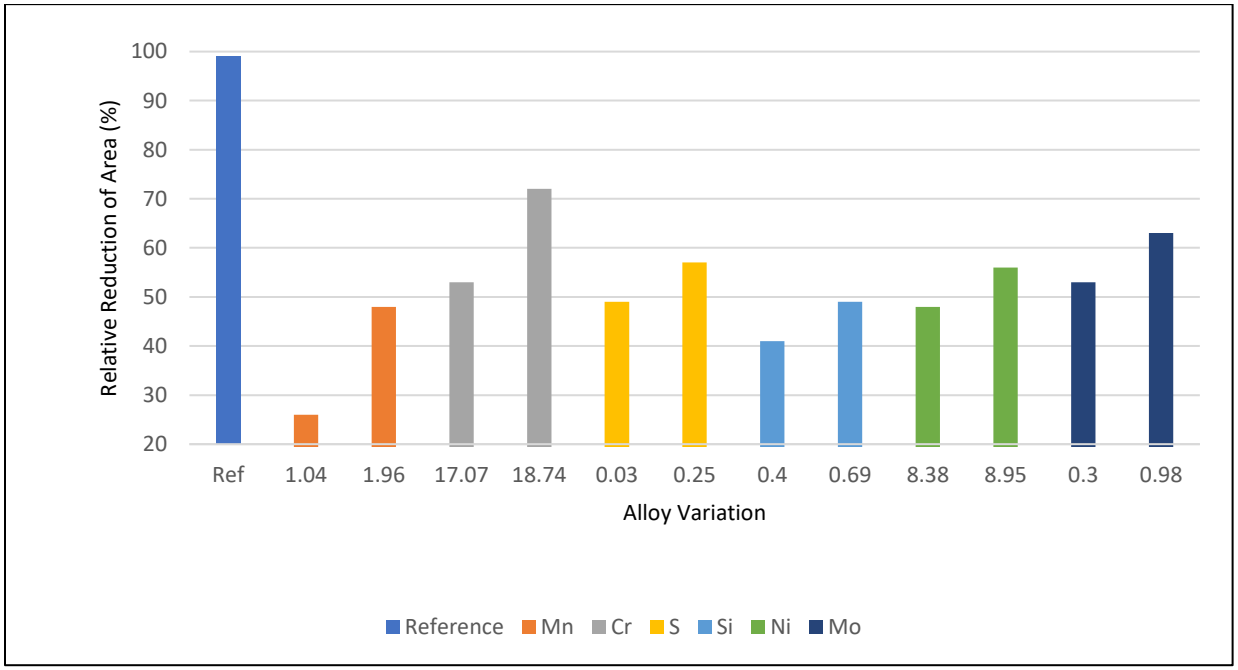

Figure 4. 20:Relative reduction of area depending on different alloying elements [287]

In high-strength steel, chemical heterogeneity is intentionally created by introducing Manganese (Mn), enhancing hydrogen resistance. Sun et al. [288] found manganese (Mn) in high-strength steel created a manganese-rich zone within the microstructure which restricted the stability of the hydrogen phase and arrested the micro-cracks produced by hydrogen. In Aluminum alloys, alloying elements have two different types of effects. Anyalebechi [289] found adding Cu, Si, Zn,

and Fe decreases hydrogen solubility, whereas Mg, Li, and Ti increase solubility. So, some alloying elements have the tendency to increase hydrogen solubility in the alloy and some others have the tendency to restrict it. The alloying elements which increase the hydrogen solubility tendency in alloys are responsible for increasing the aging tendency of material in a hydrogen environment.

4.10. Conclusion

In conclusion, Chapter 4 provides an in-depth analysis of the mechanisms and challenges associated with hydrogen-induced aging in storage and sealing materials. The chapter identifies key aging mechanisms such as thermal, chemical, mechanical, mechanical-chemical, and thermo-mechanical processes that degrade the integrity of materials used in hydrogen applications. It highlights the critical impact of hydrogen on material properties, leading to phenomena like cracking, embrittlement, blistering, and other forms of degradation. The necessity for advanced materials and comprehensive research to mitigate these effects is emphasized, ensuring the safety and longevity of hydrogen storage and sealing systems. The historical incidents and laboratory tests discussed underscore the urgency of understanding and addressing these challenges to promote hydrogen as a sustainable energy source. The following chapter will focus on performing experimental aging to analyze the performance matrix of elastomeric sealing materials for hydrogen applications based on the extracted outcome of existing chapter.

This chapter has been partially published as article in peer reviewed journal; '*Materials*' titled; "Hydrogen-Assisted Aging Applied to Storage and Sealing Materials: A Comprehensive Review" with co-authors; AKM Ahsanul Habib, Md Monjur Hossain Bhuiyan, Pejman Kazempoor, Zahed Siddique. https://doi.org/10.3390/ma16206689

References

193. Balasooriya, W.; Clute, C.; Schrittesser, B.; Pinter, G. A review on applicability, limitations, and improvements of polymeric materials in high-pressure hydrogen gas atmospheres. Taylor Fr. 2022, 62, 175–209.

194. J. Pépin, E. Lainé, J.-C. Grandidier, G. Benoit, D. Mellier, M. Weber, C. Langlois, Replication of liner collapse phenomenon observed in hyperbaric type IV hydrogen storage vessel by explosive decompression experiments, International Journal of Hydrogen Energy 43 (9) (2018) 4671–4680.

195. J. Yamabe, S. Nishimura, Influence of fillers on hydrogen penetration properties and blister fracture of rubber composites for O-ring exposed to high-pressure hydrogen gas, International Journal of Hydrogen Energy 34 (4) (2009) 1977–1989.

196. J. Jaravel, S. Castagnet, J.-C. Grandidier, G. Benoît, On key parameters influencing cavitation damage upon fast decompression in a hydrogen saturated elastomer, Polymer Testing 30 (8) (2011) 811–818.

197. J. Yamabe, H. Fujiwara, S. Nishimura, Fracture analysis of rubber sealing material for high pressure hydrogen vessel, Journal of Environment and Engineering 6 (1) (2011) 53–68.

198. A Koga, K. Uchida, J. Yamabe, S. Nishimura, Evaluation on high-pressure hydrogen decompression failure of rubber O-ring using design of experiments, International Journal of Automotive Engineering 2 (4) (2011) 123–129.

199. J. Jaravel, S. Castagnet, J.-C. Grandidier, M. Gueguen, Experimental real-time tracking and diffusion/mechanics numerical simulation of cavitation in gas-saturated elastomers, International Journal of Solids and Structures 50 (9) (2013) 1314–1324.

200. O. Kane-Diallo, S. Castagnet, A. Nait-Ali, G. Benoit, J.-C. Grandidier, Time-resolved statistics of cavity fields nucleated in a gas-exposed rubber under variable decompression conditions–support to a relevant modeling framework, Polymer Testing 51 (2016) 122–130.

201. T. A. Yersak, D. R. Baker, Y. Yanagisawa, S. Slavik, R. Immel, A. Mack-Gardner, M. Herrmann, M. Cai, Predictive model for depressurization-induced blistering of type IV tank liners for hydrogen storage, International Journal of Hydrogen Energy 42 (48) (2017) 28910–28917.

202. D. Baldwin, Development of high pressure hydrogen storage tank for storage and gaseous truck delivery, Tech. rep., Hexagon Lincoln LLC, Lincoln, NE (United States) (2017).

203. Database of Polymeric Materials for Hydrogen Gas Seals and Dispensing Hoses

204. Li, H.; Cao, X.; Liu, Y.; Shao, Y.; Nan, Z.; Teng, L.; Peng, W.; Bian, J. Safety of Hydrogen Storage and Transportation: An Overview on Mechanisms, Techniques, and Challenges. Energy Rep. 2022, 8, 6258–6269. https://www.sciencedirect.com/science/article/pii/S2352484722008332

205. Barrera, O.; Bombac, D.; Chen, Y.; Daff, T.D.; Galindo-Nava, E.; Gong, P.; Haley, D.; Horton, R.; Katzarov, I.; Kermode, J.R.; et al. Understanding and mitigating hydrogen embrittlement of steels: A review of experimental, modelling and design progress from atomistic to continuum. J. Mater. Sci. 2018, 53, 6251–6290.

206. Eghbali, P.; Gürbüz, M.U.; Ertürk, A.S.; Metin, Ö. In situ synthesis of dendrimer-encapsulated palladium(0) nanoparticles as catalysts for hydrogen production from the methanolysis of ammonia borane. Int. J. Hydrogen Energy 2020, 45, 26274–26285.

207. Handbook on Ageing Management for Nuclear Power Plants—Google Scholar. Available online: https://scholar.google.com/scholar?hl=en&as_sdt=0%2C5&q=Handbook+on+Ageing+Management+for+Nuclear+Power+Plants&btnG=

208. Hansler, R.J.; Bellamy, L.J.; Akkermans, H.A. Ageing assets at major hazard chemical sites—The Dutch experience. Saf. Sci. 2022,153, 105788.

209. Research Report 509—Plant ageing: Management of. . . —Google Scholar. Available online: https://scholar.google.com/scholar?hl=en&as_sdt=0%2C5&q=Research+Report+509+-+Plant+ageing%3A+Management+of+equipment+containing+hazardous+fluids+or+pressure+%282006%29&btnG=

210. ARIA. Catastrophic Explosion of a Cyclohexane Cloud: Flixborough United Kingdom. 2008, pp. 1–9. Available online: http://www.aria.developpement-durable.gouv.fr/wp-content/files_mf/FD_5611_flixborough_1974_ang.pdf

211. Health and Safety Executive. Public Report of the Fire and Explosion at the ConocoPhillips Humber Refinery on 16 April 2001. Health and Safety Executive. Available online: https://www.yumpu.com/en/document/view/22334776/public-report-of-the-fire-and-explosion-at-the-conocophillips-hse.

212. U.S. Chemical Safety Board. Chevron Richmond Refinery Pipe Rupture and Fire. Report No. 2012-03-I-CA-26. 2015. Available online: https://www.csb.gov/chevron-richmond-refinery-fire/

213. Case Study: Power Plant Hydrogen Explosion—WHA International, Inc. Available online: https://wha-international.com/case-study-power-plant-hydrogen-explosion/

214. CSB Investigation Finds 2010 Tesoro Refinery Fatal Explosion Resulted from High Temperature Hydrogen Attack Damage to Heat Exchanger—General News—News|CSB. Available online: https://www.csb.gov/csb-investigation-finds-2010-tesoro-refinery-fatal-explosion-resulted-from-high-temperature-hydrogen-attack-damage-to-heat-exchanger/

215. Diebold, U. The surface science of titanium dioxide. Surf. Sci. Rep. 2003, 48, 53–229.

216. Slobodyan, Z.V.; Nykyforchyn, H.M.; Petrushchak, O.I. Corrosion resistance of pipe steel in oil-water media. Mater. Sci. 2002, 38,424–429.

217. Ohaeri, E.; Eduok, U.; Szpunar, J. Hydrogen related degradation in pipeline steel: A review. Int. J. Hydrogen Energy 2018, 43, 14584–14617.

218. 19. Sun, Y.; Cheng, Y.F. Thermodynamics of spontaneous dissociation and dissociative adsorption of hydrogen molecules and hydrogen atom adsorption and absorption on steel under pipelining conditions. Int. J. Hydrogen Energy 2021, 46, 34469–34486.

219. Hayden, L.E.; Stalheim, D. ASME B31.12 Hydrogen Piping and Pipeline Code Design Rules and Their Interaction with Pipeline Materials Concerns, Issues and Research. Am. Soc. Mech. Eng. Press. Vessel. Pip. Div. PVP 2010, 1, 355–361.

220. Sharma, S.; Ghoshal, S.K. Hydrogen the Future Transportation Fuel: From Production to Applications. Renew. Sustain. Energy Rev. 2015, 43, 1151–1158. Available online: https://www.sciencedirect.com/science/article/pii/S1364032114010405 (accessed on 19 March 2023).

221. Balasooriya, W.; Clute, C.; Schrittesser, B.; Pinter, G. A review on applicability, limitations, and improvements of polymeric materials in high-pressure hydrogen gas atmospheres. Taylor Fr. 2022, 62, 175–209.

222. Shapovalov, V.I. Influence of Hydrogen on the Structure and Properties of Iron-Carbon Alloys; Metallurgiya: Moscow, Russia, 1982.

223. Nykyforchyn, H.; Tsyrulnyk, O.; Zvirko, O.; Hredil, M. Role of hydrogen in operational degradation of pipeline steel. Procedia Struct. Integr. **2020**, 28, 896–902.

224. Tiwari, G.P.; Bose, A.; Chakravartty, J.; Wadekar, S.; Totlani, M.; Arya; Fotedar, R. A study of internal hydrogen embrittlement of steels. Mater. Sci. Eng. A **2020**, 286, 269–281.

225. Dwivedi, S.; Vishwakarma, M. Hydrogen embrittlement in different materials: A review. Int. J. Hydrogen Energy **2018**, 43,21603–21616.

226. Zubrin, R. The Hydrogen Hoax. New Atlantis **2007**, 15, 9–20.

227. Student, O.Z. Accelerated method for hydrogen degradation of structural steel. Mater. Sci. **1998**, 34, 497–507.

228. Shapovalov, V.I. Influence of Hydrogen on the Structure and Properties of Iron-Carbon Alloys; Metallurgiya: Moscow, Russia, 1982.

229. Pokhmurskyi, V.I.; Fedorov, V.V. Influence of Hydrogen on the Diffusion Processes in Metals; Karpenko Physicomechanical Institute, Ukrainian Academy of Sciences: Kiev, Ukraine, 1998.

230. Krutasova, E.I. Reliability of the Metal of Power-Generating Equipment; Énergoizdat: Moscow, Russia, 1981.

231. Nykyforchyn, B.; Andrusiv, B.M.; Voldemarov, A.V.; Kutsyn, M.A. Evaluation of the effect of closure of fatigue cracks. Fiz.-Khim. Mekh. Mater. **1982**, 18, 100–103.

232. Hirakami, D.; Manabe, T.; Ushioda, K.; Noguchi, K.; Takai, K.; Hata, Y.; Hata, S.; Nakashima, H. Effect of Aging Treatment on Hydrogen Embrittlement of Drawn Pearlitic Steel Wire. ISIJ Int. **2016**, 56, 893–898.

233. Ogawa, Y.; Yamabe, J.; Matsunaga, H.; Matsuoka, S. Material performance of age-hardened beryllium–copper alloy, CDA-C17200, in a high-pressure, gaseous hydrogen environment. Int. J. Hydrogen Energy **2017**, 42, 16887–16900.

234. Yamabe, J.; Takagoshi, D.; Matsunaga, H.; Matsuoka, S.; Ishikawa, T.; Ichigi, T. High-strength copper-based alloy with excellent resistance to hydrogen embrittlement. Int. J. Hydrogen Energy **2016**, 41, 15089–15094.

235. Yamabe, J.; Fujiwara, H.; Nishimura, S. Fracture analysis of rubber sealing meterial for high pressure hydrogen vessel. Nihon Kikai Gakkai Ronbunshu A Hen/Trans. Jpn. Soc. Mech. Eng. Part A **2009**, 75, 1063–1073.

236. Yokoyama, K.; Ogawa, T.; Takashima, K.; Asaoka, K.; Sakai, J. Hydrogen embrittlement of Ni-Ti superelastic alloy aged at room temperature after hydrogen charging. Mater. Sci. Eng. A **2007**, 466, 106–113
237. Ogawa, T.; Oda, T.; Maruoka, K.; Sakai, J. Effect of aging at room temperature on hydrogen embrittlement behavior of Ni-Ti superelastic alloy immersed in acidic fluoride solution. Int. J. Mech. Mater. Eng. **2015**, 10, 11.

238. Tal-Gutelmacher, E.; Eliezer, D. Hydrogen cracking in titanium-based alloys. J. Alloy. Compd. **2005**, 404–406, 621–625.

239. Omura, T.; Nakamura, J.; Hirata, H.; Jotoku, K.; Ueyama, M.; Osuki, T.; Terunuma, M. Effect of Surface Hydrogen Concentration on Hydrogen Embrittlement Properties of Stainless Steels and Ni Based Alloys. ISIJ Int. **2016**, 56, 405–412.

240. Li, G.; Zhu, D.; Jia, W.; Zhang, F. Analysis of the aging mechanism and life evaluation of elastomers in simulated proton exchange membrane fuel cell environments. e-Polymers **2021**, 21, 921–929.

241. Zhang, E.; Liu, J.; Zhang, C.; Zheng, P.; Nakanishi, Y.; Wu, T. State-of-Art Review on Chemical Indicators for Monitoring the Aging Status of Oil-Immersed Transformer Paper Insulation. Energies **2023**, 16, 1396.

242. Wetegrove, M.; Duarte, M.J.; Taube, K.; Rohloff, M.; Gopalan, H.; Scheu, C.; Dehm, G.; Kruth, A. Preventing Hydrogen Embrittlement: The Role of Barrier Coatings for the Hydrogen Economy. Hydrogen **2023**, 4, 307–322.

243. Zhang, M.; Lv, H.; Kang, H.; Zhou, W.; Zhang, C. A Literature Review of Failure Prediction and Analysis Methods for Composite High-Pressure Hydrogen Storage Tanks. Int. J. Hydrogen Energy **2019**, 44, 25777–25799.

244. Klopffer, M.; Berne, P.; Castagnet, S.; Weber, M. Pipes for Distributing Mixtures of Hydrogen and Natural Gas. Evolution of Their Transport and Mechanical Properties after an Ageing under an Hydrogen Environment. 2010.

245. Zheng, C.X.; Wang, L.; Li, R.; Wei, Z.X.; Zhou, W.W. Fatigue test of carbon epoxy composite high pressure hydrogen storage vessel under hydrogen environment. J. Zhejiang Univ. Sci. A **2013**, 14, 393–400

246. Feng, X.; Shi, Y.; Zhang,W.; Volodymyr, K. Hydrogen Embrittlement Failure Behavior of Fatigue-DamagedWelded TC4 Alloy Joints. Crystals **2023**, 13, 512.

247. Brownell, M.; Frischknecht, A.L.; Wilson, M.A. Subdiffusive High-Pressure Hydrogen Gas Dynamics in Elastomers. Macromolecules **2022**, 55, 3788–3800.

248. Wilson, M.A.; Frischknecht, A.L. High-pressure hydrogen decompression in sulfur crosslinked elastomers. Int. J. Hydrogen Energy **2022**, 47, 15094–15106

249. Zhou, C.; Chen, G.; Liu, P.; Guohua, C.Z.; Liu, C.P. Finite element analysis of sealing performance of rubber D-ring seal in high-pressure hydrogen storage vessel. J. Fail. Anal. Prev. **2018**, 18, 846–855

250. Zato´ n, M.; Rozière, J.; Jones, D.J. Current understanding of chemical degradation mechanisms of perfluorosulfonic acid membranes and their mitigation strategies: A review. Sustain. Energy Fuels **2017**, 1, 409–438.

251. LaConti, A.; Hamdan, M.; McDonald, R.C. Mechanisms of membrane degradation. In Handbook of Fuel Cells; Wiley: Hoboken, NJ, USA, 2003.

252. Danilczuk, M.; Corns, F.D.; Schlick, S. Visualizing chemical reactions and crossover processes in a fuel cell inserted in the esrresonator: Detection by spin trapping of oxygen radicals, nafion-derived fragments, and hydrogen and deuterium atoms. J. Phys. Chem. B **2009**, 113, 8031–8042.

253. Lee, S.Y.; Cho, E.; Lee, J.H.; Kim, H.J.; Lim, T.H.; Oh, I.H.;Won, J. Effects of Purging on the Degradation of PEMFCs Operating with Repetitive On/Off Cycles. J. Electrochem. Soc. **2007**, 154, B194.

254. Healy, J. Aspects of the chemical degradation of PFSA ionomers used in PEM fuel cellsx. Fuel Cells **2005**, 5, 302–308.

255. Kusoglu, A.; Weber, A.Z. A Mechanistic Model for Pinhole Growth in Fuel-Cell Membranes during Cyclic Loads. J. Electrochem.Soc. **2014**, 161, E3311–E3322.

256. Gittleman, C.S.; Coms, F.D.; Lai, Y.-H. Chapter 2—Membrane Durability: Physical and Chemical Degradation A2. Mod. Top. Polym. Electrolyte Fuel Cell Degrad. **2012**, 15–88. Available online:

257. De Moor, G. Understanding membrane failure in PEMFC: Comparison of diagnostic tools at different observation scales. Fuel Cells **2012**, 12, 356–364.

258. Nykyforchyn, H.; Lunarska, E.; Tsyrulnyk, O.T.; Nikiforov, K.; Genarro, M.E.; Gabetta, G. Environmentally assisted 'in-bulk' steel degradation of long term service gas trunkline. Eng. Fail. Anal. **2010**, 17, 624–632.

259. Robert, M. The Impact of Chemical-Mechanical Ex Situ Aging on PFSA Membranes for Fuel Cells. Membranes **2021**, 11, 366

260. Balitskii, A.; Ivaskevych, L. Temperature Dependences of Age-Hardening Austenitic Steels Mechanical Properties in Gaseous Hydrogen. 2009.

261. Cui, T.; Lin, C.W.; Chien, C.H.; Chao, Y.J.; Van Zee, J.W. estimation of liquid silicon rubber seals in polymer electrolyte membrane fuel cell environment. J. Power Sources **2011**, 196, 1216–1221.

262. Brown, R.P. Survey of status of test methods for accelerated durability testing. Polym. Test. **1991**, 10, 3–30.

263. Burgess, R.; Post, M.; Buttner, W.; Rivkin, C. High Pressure Hydrogen Pressure Relief Devices: Accelerated Life Testing and Application Best Practices. 2017.

264. Liu, D.; Case, S. Durability Study of Proton Exchange Membrane Fuel Cells under Dynamic Testing Conditions with Cyclic Current Profile. J. Power Sources **2006**, 162, 521–531.

265. Slobodyan, Z.V.; Nykyforchyn, H.M.; Petrushchak, O.I. Corrosion resistance of pipe steel in oil-water media. Mater. Sci. **2002**, 38, 424–429.

266. Fukushima, K.; Cai, H.; Nakada, M.; Miyano, Y. Determination of Time-Temperature Shift Factor for Long-Term Life Prediction of Polymer Composites. 2009.

267. Irving, P.E. Development of service life prognosis systems for hydrogen energy devices. Gaseous Hydrog. Embrittlement Mater. Energy Technol. Mech. Model. Futur. Dev. **2012**, 1, 430–468.

268. Hiemenz, P.C.; Lodge, T.P. Polymer Chemistry, 2nd ed.; Taylor & Francis: Boca Raton, FL, USA, 2007; pp. 338–339.

269. Kundu, S.; Simon, L.; Fowler, M.W. Comparison of two accelerated NafionTM degradation experiments. Polym. Degrad. Stab. 2008, 93, 214–224.

270. Andrews, R.D.; Tobolsky, A.V. Elastoviscous properties of polyisobutylene. IV. Relaxation time spectrum and calculation of bulk viscosity. J. Polym. Sci. 1951, 7, 221–242.

271. Struik, L.C.E. Physical aging in plastics and other glassy materials. Polym. Eng. Sci. 1977, 17, 165–173.

272. Williams, M.L.; Landel, R.F.; Ferry, J.D. The Temperature Dependence of Relaxation Mechanisms in Amorphous Polymers and Other Glass-forming Liquids. J. Am. Chem. Soc. 1955, 77, 3701–3707.

273. Li, G.; Tan, J.; Gong, J. Chemical aging of the silicon rubber in a simulated and three accelerated proton exchange membrane fuel cell environments. J. Power Sources 2012, 217, 175–183.

274. Tan, J.; Chao, Y.J.; Yang, M.; Lee, W.K.; Van Zee, J.W. Chemical and mechanical stability of a Silicon gasket material exposed to PEM fuel cell environment. Int. J. Hydrogen Energy 2011, 36, 1846–1852.

275. Cui, T.; Lin, C.W.; Chien, C.H.; Chao, Y.J.; Van Zee, J. Service life prediction of seal in PEM fuel cells. Conf. Proc. Soc. Exp. Mech. Ser. 2011, 5, 25–32. Gittleman

276. Gittleman, C.; Lai, Y.; Miller, D. Durability of Perfluorosulfonic Acid Membranes for PEM Fuel Cells. 2005.

277. Nák, V.Z.; Saldan, I.; Giannakoudakis, D.; Barczak, M.; Pasán, J. Factors affecting hydrogen adsorption in metal–organic frameworks: A short review. Nanomaterials 2021, 11, 1638.

278. Eliezer, D.; Böllinghaus, T.H. Hydrogen effects in titanium alloys. Gaseous Hydrog. Embrittlement Mater. Energy Technol. 2012, 2, 668–706

279. Tomi, T. Effects of Hydrogen upon the Properties of Thermo Mechanical Controlled Process (TMCP) Steel; Croatian Metallurgical Society: Zagreb, Croatia, 2015.

280. Fukuyama, S.; Sun, D.; Zhang, L.; Wen, M.; Yokogawa, K. Effect of temperature on hydrogen environment embrittlement of type 316 series austenitic stainless steels at low temperatures. J. Jpn. Inst. Met. 2003, 67, 456–459.

281. Duthil, P. Material properties at low temperature. In Proceedings of the CAS-CERN Accelerator School: Superconductivity for Accelerators, Erice, Italy, 24 April–4 May 2013; pp. 77–95.

282. Wu, Y.;Wang, D.; Zhang,W.; Zhang, J. Experimental research of thermal-oxidative aging on the mechanics of aero-nbr. J. Test. Eval. 2013, 42, 568–572.

283. Dubovský, M.; Božek, M.; Olšovský, M. Degradation of aviation sealing materials in rapeseed biodiesel. J. Appl. Polym. Sci. 2015, 132.

284. Hohe, J.; Neubrand, A.; Fliegener, S.; Appel, S. Performance of Fiber Reinforced Materials under Cryogenic Conditions—A Review. Compos. Part A Appl. Sci. Manuf. 2021, 141, 106226.

285. Fujiwara, H.; Nishimura, S. "Evaluation of Hydrogen Dissolved in Rubber Materials under High-Pressure Exposure Using Nuclear Magnetic Resonance." Polym. Journal, 2012, 44, 832–837.

286. Raj, A.; Alvi, S.M.A.A.; Islam, K.; Motalab, M.; Xu, S. An Atomistic Study of the Tensile Deformation of Carbon Nanotube– Polymethylmethacrylate Composites. Polymers 2023, 15, 2956.

287. Sun, B.; Lu, W.; Gault, B.; Ding, R.; Makineni, S.K.; Wan, D.; Wu, C.-H.; Chen, H.; Ponge, D.; Raabe, D. "Chemical heterogeneity enhances hydrogen resistance in high-strength steels." *Nat. Mater.*, 2021, 20, 1629–1634.

288. Anyalebechi, P.N. "Analysis of the Effects of Alloying Elements on Hydrogen Solubility in Liquid Aluminum Alloys." *Scr. Metall. Et Mater.*, 1995, 33, 1209–1216. Available online: https://www.sciencedirect.com/science/article/pii/0956716X95003734

289. Barrer, R.M. "Permeation, diffusion and solution of gases in organic polymers." *Trans. Faraday Soc.*, 1939, 35, 628–643.

CHAPTER 5: EXPERIMENTAL STUDY INVESTIGATING THE IMPACT OF HYDROGEN EXPOSURE ON SEALING MATERIALS.

The objective of Chapter 5 is to conduct an experimental investigation into the behavior of sealing materials in hydrogen gas infrastructure, focusing on hydrogen-assisted aging. While the impact of hydrogen exposure on non-polymeric materials such as steel, aluminum, and alloys has been extensively studied [290], and significant research has been conducted on storage materials, there is a notable gap in understanding the effects of hydrogen on polymeric sealing materials. This research aims to address this gap, particularly focusing on elastomers, which have not been thoroughly investigated in this context (Objective x, Section 1.x). Specifically, the investigation will explore the interaction of pressure on the sealing resistance of various polymers in a hydrogen environment. Although some polymers like EPDM and EVA have been partially studied, the research will extend to a broader range of materials, which are crucial in hydrogen applications [290]. The study is particularly significant because most equipment in the hydrogen industry is exposed to hydrogen gas [294], with the thermo-physical properties of hydrogen gas often leading to leakage in compressed gas storage [291, 292]. The research will investigate how different mechanical properties of sealing materials interact with the multiple operational parameters in the hydrogen industry. It will also aim to identify polymer compounds that offer better resilience to hydrogen permeation and sealing failure, areas where current research is insufficient [293]. The investigation seeks to provide a detailed analysis of multiple sealing materials under varied operating conditions in hydrogen gas infrastructure to assess and predict the performance of these materials, contributing to the development of more effective and reliable sealing solutions in the hydrogen industry.

5.1. Material Selection

Oil resistant Buna N O-ring (NBR), High temperature high purity silicon O-ring and water-steam resistant EPDM O-ring samples have been selected for the aging experiment. Elastomeric materials of the same chemistry from different vendors can vary in residual thermal stress depending on the mode of manufacture. Therefore, the polymers will be subjected to an annealing process to relieve stress before exposure to high-pressure hydrogen exposure. For NBR, the annealing process typically involves heating the material to a temperature of around 100°C to 120°C (212°F to 248°F). The material is held at this temperature for 2 to 4 hours, followed by a gradual cooling period to room temperature. EPDM was annealed at a temperature range of 150°C to 170°C (302°F to 338°F) for 1 to 3 hours and then cooled to room temperature at 0.5C/mint. Silicon rubber was annealed at a higher temperature; between 150°C to 200°C (302°F to 392°F) for 2-4 hrs and followed by gradual cooling. Conditions for annealing were determined based on glass temperature (Tg) and softening points for the thermoplastics. [295, 296]. The process ensures the polymer chains can relax and relieve internal stress while maintaining structural integrity. For the preparation of NBR, EPDM, and silicon O-rings before hydrogen aging, begin by thoroughly cleaning the O-rings using a suitable solvent like isopropanol and lint-free cloths to remove any contaminants. Table 5.1 shows the dimensions, and Figure 1 shows a schematic of a sealing sample.

Table 5. 1: Dimension of sealing samples

Samples	Material	Cross section Type	Width	ID	OD	Hardness (Durometer)
NBR	Buna-N Rubber	Round	0.139"	0.984"	1.262"	70A (Medium)
Silicon	Silicon Rubber	Round	0.139"	0.984"	1.262"	70A (Medium)
EPDM	EPDM Rubber	Round	0.139"	0.984"	1.262"	70A (Medium)

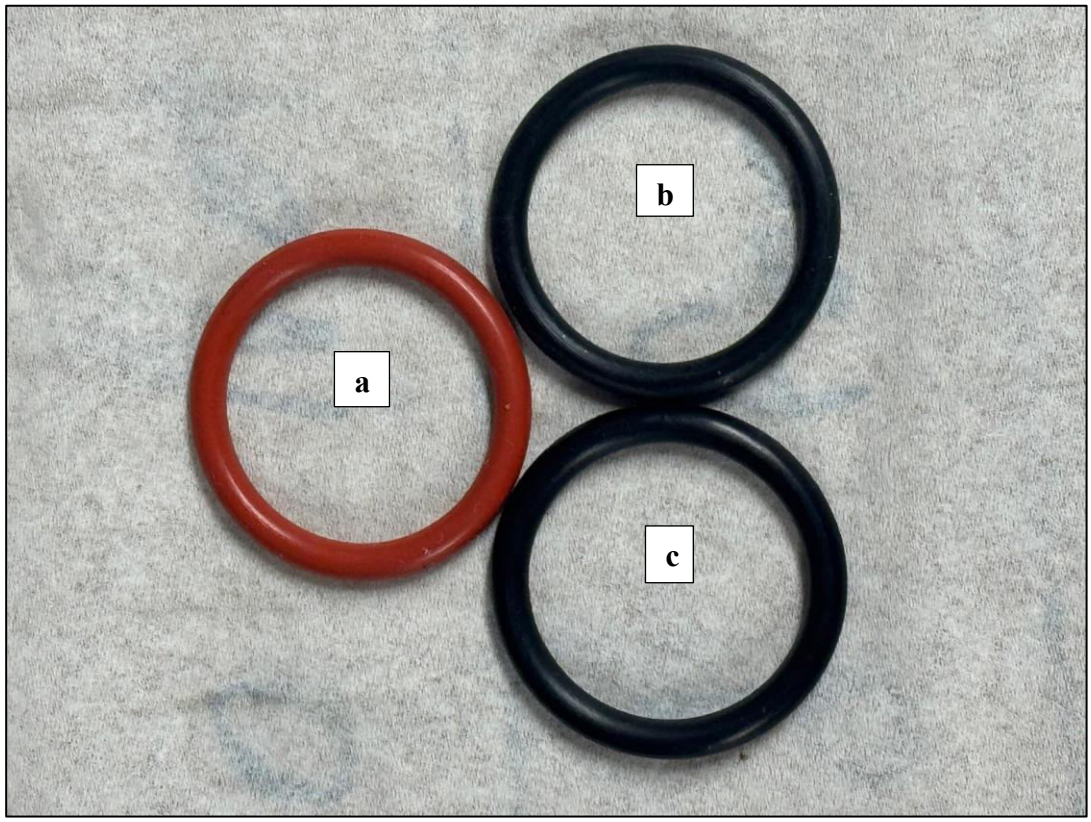

Figure 5. 1: Schematic of a sealing sample

(a) Silicon, (b) NBR, (c) EPDM

- ***NBR (Nitrile Butadiene Rubber)***

NBR is composed of acrylonitrile and butadiene monomers. The typical structure includes repeating units of –CH2–CH=CH–CH2– (butadiene) and –CH2–CH(CN)– (acrylonitrile). The percentage of acrylonitrile content (ranging from 18% to 50%) significantly affects its properties. Higher acrylonitrile content increases oil and chemical resistance but reduces flexibility. The copolymer's chemical structure allows for cross-linking, typically through vulcanization, which gives NBR its mechanical strength. The simplified chemical structure of NBR is given as:

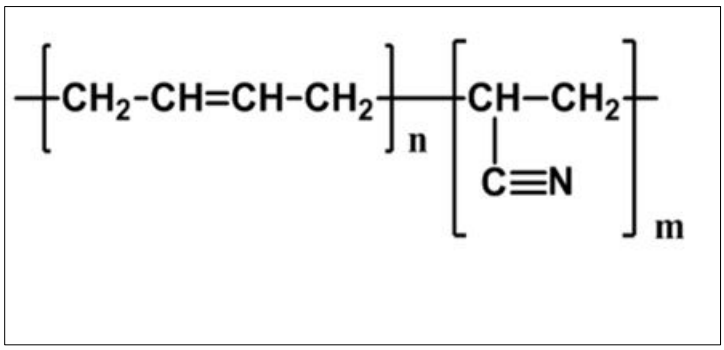

Where n and m represent the relative proportions of butadiene and acrylonitrile in the polymer. NBR has excellent resistance to hydrogen permeation due to its dense molecular structure, particularly when the acrylonitrile content is higher. However, exposure to high-pressure hydrogen can lead to volume expansion due to hydrogen adsorption. When hydrogen diffuses into NBR, it does not typically cause scission of the polymer chains but rather affects its mechanical properties by altering the filler-matrix interactions, especially in carbon black-filled variants [305, 306]. The presence of free hydrogen molecules within the NBR matrix results in swelling and a slight reduction in mechanical properties like tensile strength over time. However, due to its stability, NBR is commonly used in seals and gaskets in hydrogen storage systems, where long-term exposure to hydrogen is expected. NBR's molecular structure does not undergo significant chemical reactions with hydrogen, making it suitable for hydrogen applications.

- ***Silicon Rubber***

Silicon rubber is primarily composed of siloxane (Si-O-Si) backbones with organic side groups (typically methyl or phenyl). Its structure shows both flexibility and a high degree of thermal and chemical stability. The Si-O bonds are highly polar, making silicon resistant to oxidation and UV degradation. Therefore, it is usually chosen for applications in harsh environments, including hydrogen storage and transport. The repeating unit of silicon can be represented as:

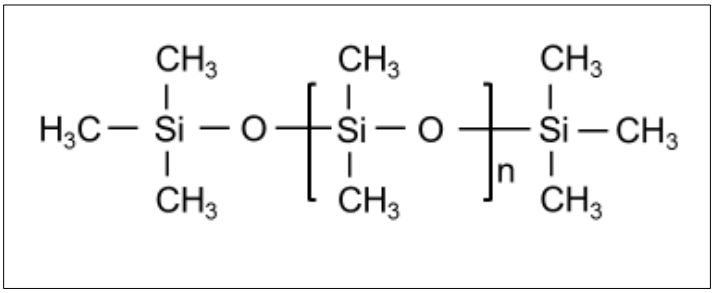

Silicon's molecular structure provides resistance to hydrogen permeation. Its high temperature stability (-60°C to +300°C) allows silicon to be used in environments with fluctuating temperatures where hydrogen exposure is significant. The interaction with hydrogen typically results in volume changes due to the permeability of the material to gases, but these do not lead to significant chemical degradation of the silicon matrix. Instead, hydrogen tends to diffuse without reacting chemically with the polymer. Due to its flexibility, silicon is widely used in seals and gaskets within the hydrogen economy, especially where extreme temperatures are encountered, such as in fuel cells and storage tanks [307].

- ***EPDM (Ethylene Propylene Diene Monomer)***

EPDM is composed of ethylene, propylene, and a diene monomer, which creates unsaturation sites for cross-linking. This structure gives EPDM chemical stability and resistance to aging, oxidation and weathering. The polymer is often cross-linked through sulfur or peroxide vulcanization, resulting in a compatible and flexible material. The Simplified Structure of EPDM is given as:

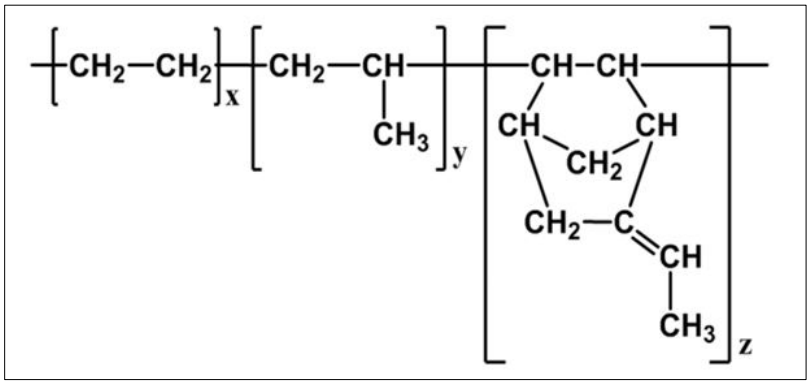

EPDM's interaction with hydrogen is suitable, particularly in high-pressure environments. It demonstrates lower hydrogen permeation compared to other elastomers due to its low glass transition temperature and tightly packed molecular structure. Under hydrogen exposure, EPDM shows less volume change, making it reliable for seals and gaskets in hydrogen transport systems. EPDM's application in hydrogen storage and transportation systems is well-established due to its strength in both high-pressure and high-temperature environments. It also has resistance to water and steam, which is important in the hydrogen industry, especially where moisture might be present along with hydrogen [308, 309].

Table 5.2 shows the usage of the selected samples in different applicational areas of hydrogen along with the operating conditions.

Table 5. 2: Application of selected sealing samples at hydrogen industry

Sealing Sample	Category of Application	Purpose	Operating Condition	References
NBR	Hydrogen Refueling Stations	O-rings, gaskets in dispensers and compressors to prevent H_2 leaks	Pressure ~ 10,000 psi Temp.~ -50°C to 85°C	[340]
	Hydrogen Storage Systems	Seals in storage tanks and pipelines to prevent H_2 leaks	Pressure ~ 5000-10,000 psi Temp.~ -40°C to 150°C	[343]
	Dynamic Seal in High Pressure Hydrogen System	prevent H_2 leaks	Pressure~ 4000 psi; Temp. ~ Ambient	[344]
EPDM	Hydrogen Production Facilities	electrolyzers	Pressure~ 1160 psi Temp. +50°C to +100°C	[346]
	Hydrogen Storage and Transport	prevent H_2 leaks	Pressure ~ 10,000 psi Temp. ~ -40°C to 120°C	[338]
	Hydrogen Fuel Cell Systems	sealing components in humidifiers and cooling systems	Pressure ~ 145 psi Temp ~ 60°C to 100°C	[307]
	Hydrogen Refueling Station	Used as seals, gaskets.	Pressure~725 to 1450 psi; Temp. ~ -40°C to 90°C	[307, 345]
Silicon	Hydrogen Fuel Cell		Pressures~ 1450 psi Temp.~ -50°C to 175°C	[342]
	Hydrogen Storage	Coating material	Temp. up to 450°C	[347]

5.2. Experiment Approach

An experimental approach to analyze the impact of hydrogen gas on polymer materials has been outlined in Figure 5.2. The assessment was conducted through several characterization tests of the mechanical properties of the selected materials. The characterizations include tensile strength, hardness test, swelling test, and electrical resistivity analysis. These measurements would provide a baseline or reference value used to analyze the effects of hydrogen gas. Furthermore, optical images of the surface and a typical cross-section of each specimen have been recorded to understand the impact of hydrogen on material morphology at several stages of hydrogen exposure. Following this initial characterization, the material samples would be exposed to the designed aging condition. This exposure to hydrogen gas at pressure for a sufficiently long period would allow for the permeation of hydrogen molecules into the polymer samples. The leak rate of hydrogen through multiple aged seals at extreme harsh operating conditions have been recorded using a dedicated set-up to assess the sealing performance. The degradation of the material has been recorded and determined by analyzing the multiple mechanical properties pre and post aging the hydrogen exposure. By varying pressure at constant temperature, and time, it was possible to construct a machine learning model to predict the performance of each sealing material. Furthermore, measurements of the changes to electrical conductivity can be used to relate the exposure parameters to the formation of voids and cavities within the sample. Finally, the characterization of changes in the morphology of the surface of the materials can be used to illustrate the changes to material properties as well as to produce more detailed and informed models of material degradation.

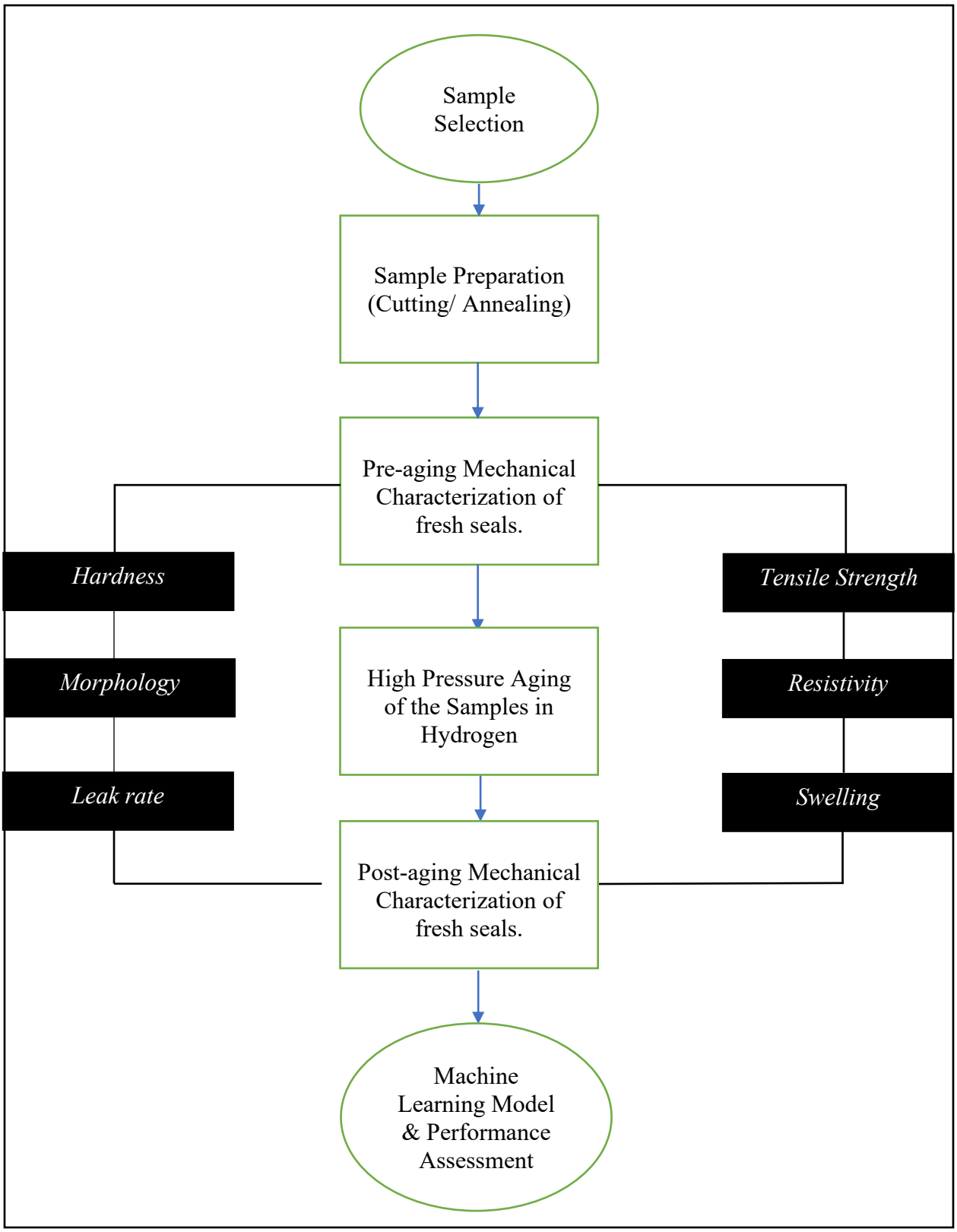

Figure 5. 2: Flow Chart of Hydrogen induced aging to polymer materials

The design of the experiment has been determined based on several operating conditions where hydrogen environment is directly applicable. The operating conditions for some environments are summarized in table 5.3.

Table 5. 3: Operating Conditions for Hydrogen Applications Across Various Industries

Application	**Temperature (C)**	**Pressure (psi)**	**Duration (hrs)**	**References**
Hydrogen Fuel Cells (Automotive Industry)	Around 80	10,153	500 - 1000	297
Hydrogen Refueling Stations	Up to 50	12,687	1000 - 2000	298
Hydrogen Storage Facilities	-40 to 85	5,076 to 10,153	2000 - 4000	299
Chemical Industry (Hydrogen as a Feedstock)	Up to 500	14,503	1000 - 3000	300
Space Exploration (Rocket and Spacecraft Fuel)	-253 to high temperatures	14,503	100 - 500	301
Residential Heating Systems	Around 30	145 to 435	1000 - 2000	302
Industrial Metal Processing	Up to 1300	290 to 725	500 - 1500	303
Aerospace Testing Facilities	-200°C to 200°C	5076 psi	200 - 1000	304

5.2.1. Experimental Set-up

Figure 5.3 shows a schematic of the design of the experimental setup which was developed by Alfredo Becerril Corral and Philip M Resnick. This setup is used for charging specimens under hydrogen environment. A commercially available compressed hydrogen gas cylinder was used in conjunction with a pressure accumulator to expose the material samples to pressures up to 10000 psi. The setup includes the provision of using nitrogen gas to flush the system between experiments, removing contaminants and further increasing the safety of the experimental platform. A pressure accumulator has been installed instead of using the compressor to reduce the overall construction expense. A remote-control system is incorporated with the set-up to avoid physical engagement during the high-pressure aging process. Safety is assured through the joint use of pneumatic and solenoid valves which assist to control of the hydrogen gas to ensure that researchers are not in the vicinity of the equipment during the charging of the samples An external heating system has been installed with the system for the experiment involving high temperatures. The heating system consists of a heating band and temperature controller to maintain the temperature of the test vessel within a range of room temperature to 200 C. Selection of material are vital for the precision of the aging impact. Commercially available tubing, fittings, and pneumatically actuated piston valves made from AISI 316 Stainless steel alloy provided by High-Pressure Equipment were used to transport hydrogen gas [6]. These products have been tested for operation with hydrogen in pressures up to 60,000 psi and present a cost-effective option for the construction of the testing equipment. Metal-to-metal conical seals have been used to control the hydrogen gas pressure and periodical inspection was conducted to ensure safety and prevent leak formation results from material degradation. The set-up consists of a piston accumulator for high-pressure hydrogen gas charges at a competitive cost [15]. This piston accumulator is rated for high

pressures and presents the option of using O-ring seals of adequate materials for the containment of hydrogen. While the use of polymer seals in the pressure accumulator could lead to gas losses due to material degradation over a prolonged time, periodic inspection and maintenance was conducted to ensure the obtained result is accurate. Furthermore, the consistency of operating conditions during the designed period of an experiment was maintained by the use of a pressure transducer and remotely controlled pressure regulators.

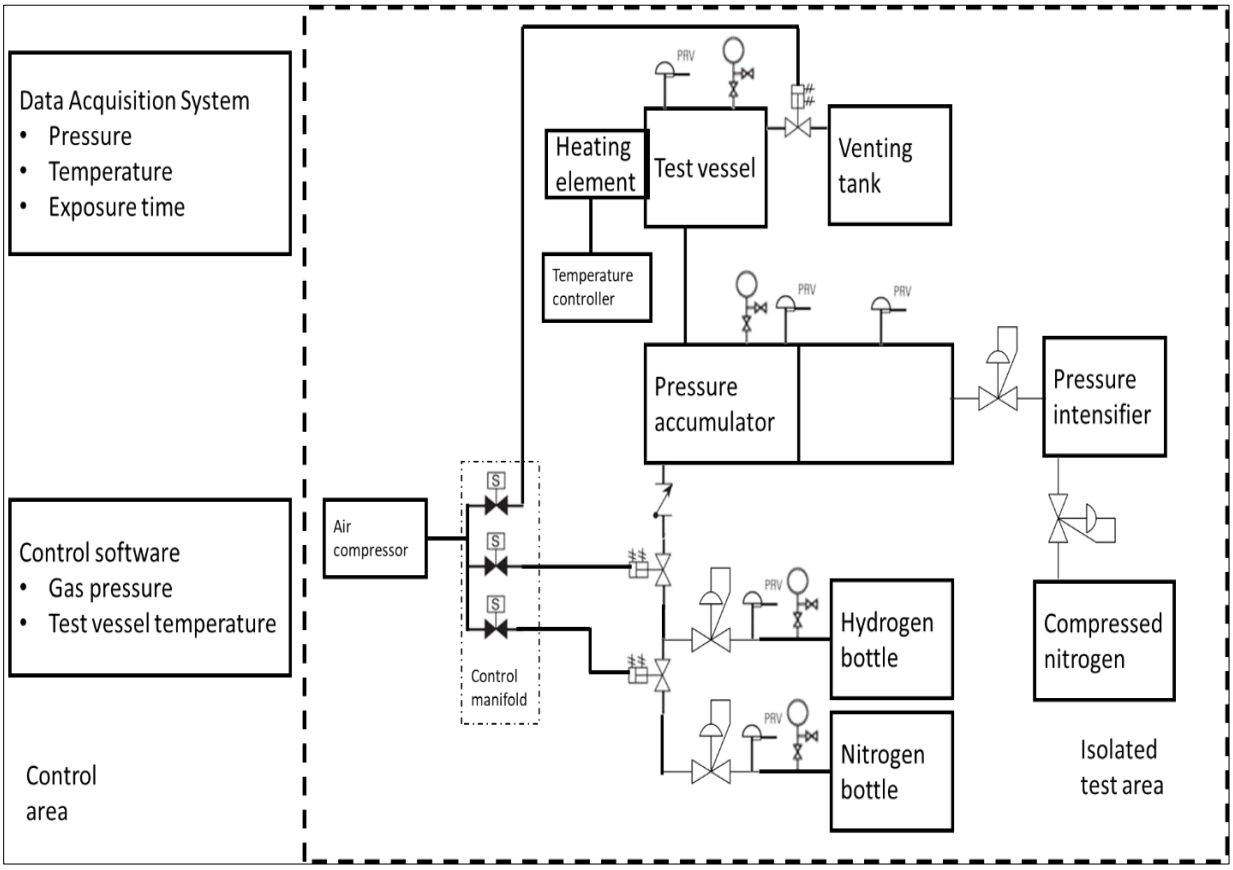

Figure 5. 3: Schematic diagram of the Aging experiment under a hydrogen

The software has been programmed in a way that senses the internal pressure of the aging chamber and adjusts the inlet pressure control valve to keep the hydrogen gas pressure uniform during the aging experiment. The control software used for the experimental setup was developed in the

LabView programming environment offered by National Instruments. This software provides a customizable platform to integrate the required sensors and controls under a unified platform. In this way, this software allows for the monitoring and recording of data relating to relevant variables such as pressure, time and temperature. Furthermore, this software permits the automatization of the experimental process to ensure the experimental conditions are accurately controlled throughout the duration of the test along with the integration of safety measures. The test matrix has been designed followed by the construction of the test equipment to explore the impact of aging by hydrogen on polymer materials.

Table 5.4 presents a series of tests with different pressures at constant temperature and time duration to compare the degradation of the material during different phases of aging. By using different test pressures, it was possible to compare the degree of damage induced by the rapid decompression of the test vessel that could arise from different applications. Also, it was possible to compare the stability of the polymer material for different application regimes and environments. Thus, the experimental matrix provided significant information on hydrogen permeation through the sealing materials, and consequently, the degree of damage was determined from the measurement of the leak rate and respective mechanical characterization tests after hydrogen exposure. A series of experiments have been conducted to detect the initial damage which was considered as reference point for continuing aging at different conditions. The exposure pressure was increased and periodically checked unless the damage was very evident.

Table 5. 4: Design of Operation for aging experiment of sealing samples

	Batch no	Pressure (psi)	Temperature (C)	Duration (hours)
NBR Silicon EPDM	1	500	25	192
	2	1500	25	192
	3	2500	25	192
	4	5000	25	192
	5	7500	25	192
	6	10,000	25	192

5.2.2. Aging Process

After the various polymer specimens had been prepared, the samples were introduced into sample holders, which are containers made of stainless steel. The sample holder containing the specimens was arranged in a cylindrical pressure vessel. The full system was wiped down with IPA before filling with samples. The test chamber is connected to a high-pressure system that includes ultra-pure Hydrogen and helium gas cylinders. The system was purged 3 times with helium gas starting with a test pressure of 15000 psi for the first purge and 3000 psi for the second and third purge. The purging was done to take out residual oxygen and prevent the formation of an explosive hydrogen-oxygen mixture inside the test chamber[16]. Each purge was followed by a complete vent of purge gas at room temperature. Helium purging was followed by hydrogen purging which involved filling and venting the test chamber 3 times at 3000 psi each time. At the end of the purge cycles, the chamber was filled with 99.99% ultra-pure hydrogen at the designed pressure at room temperature. Each polymer was aged following the operational matrix described in Table 5.3. An experimental setup for the aging of elastomers in a hydrogen environment is shown in Figure 5.4. Also Figure 5.5 shows the seal holder and pattern of arranging the seal inside the aging chamber.

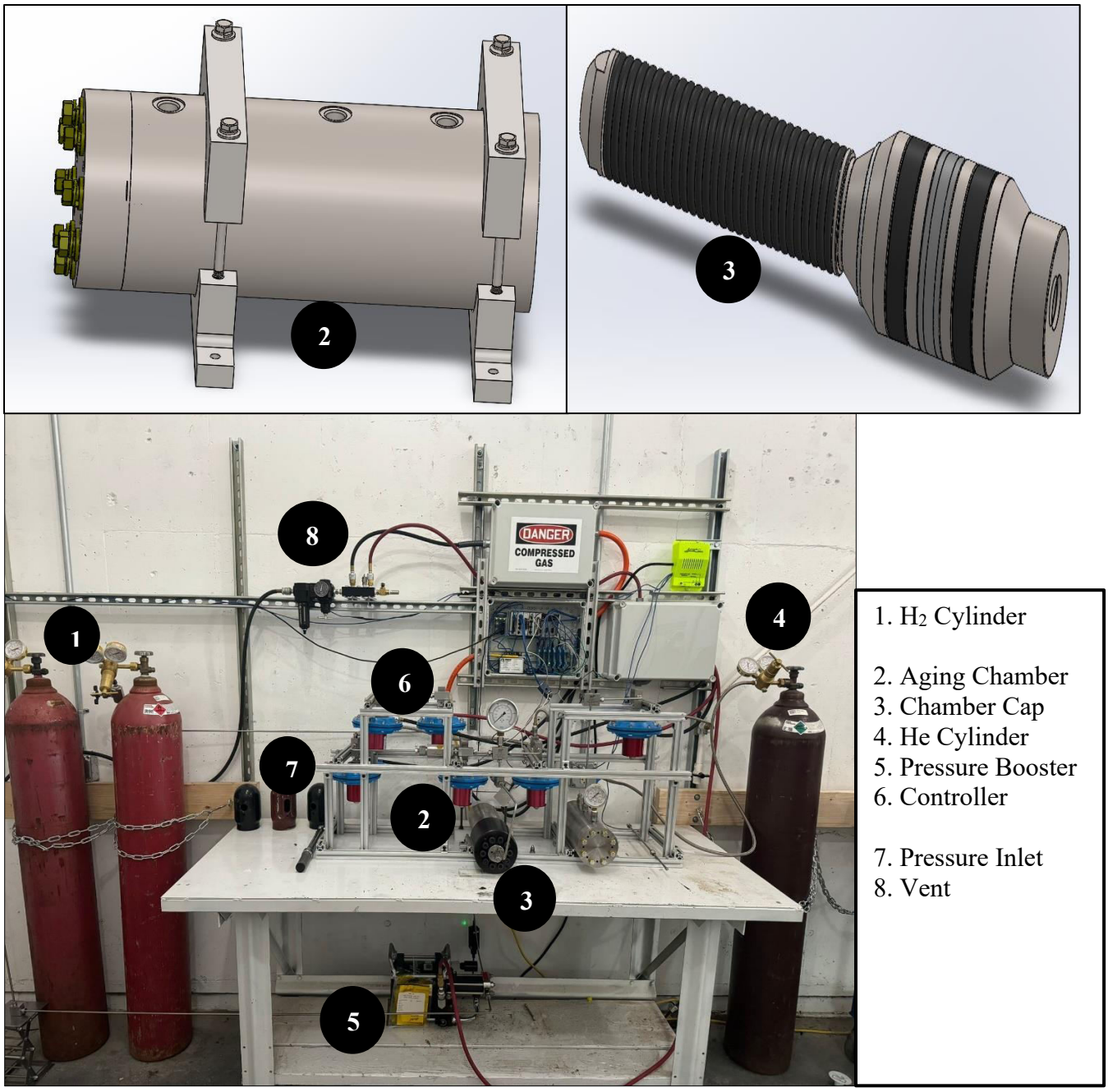

Figure 5. 4: Experimental set up for aging of elastomers in hydrogen

Figure 5. 5: Seal holder at pre-aging set-up

5.2.3. Post-Aging Leak Test Experiment

The aged seal will be placed into a shaft containing the test chamber made of stainless steel and connected to the inlet and outlet pressure measurement unit. The hydrogen gas was charged through an inlet pipe at 2000 psi hydrogen pressure at room temperature to all aged sealing samples for 72 hrs. The change of data at both high-pressure sites and lower pressure sites with time was continuously monitored through the pressure sensors using LabView tailored program. The pressure drop was calculated from the slop of time-pressure diagram. The leak rate was calculated based on the drop of inlet pressure with time across the sealing material. The leak test chamber, as illustrated in Figure 5.6, is constructed from 17-4 PH stainless steel, which is heat-treated to a hardness of 26 to 29 RC. The chamber features precision surfaces with tight tolerances, including multiple O-ring holders. It incorporates both threaded and through holes for mounting and securing components. The shaft has a diameter of 1.625”, with an allowable tolerance of +0.003 inches, and a total length of 12 inches. The lid is attached using an array of evenly spaced fasteners to ensure uniform pressure distribution. Additionally, the chamber includes provisions for various fittings and testing ports, allowing for pressure monitoring and sample introduction. All dimensions and tolerances are in accordance with ASME Y14.5-2018 standards

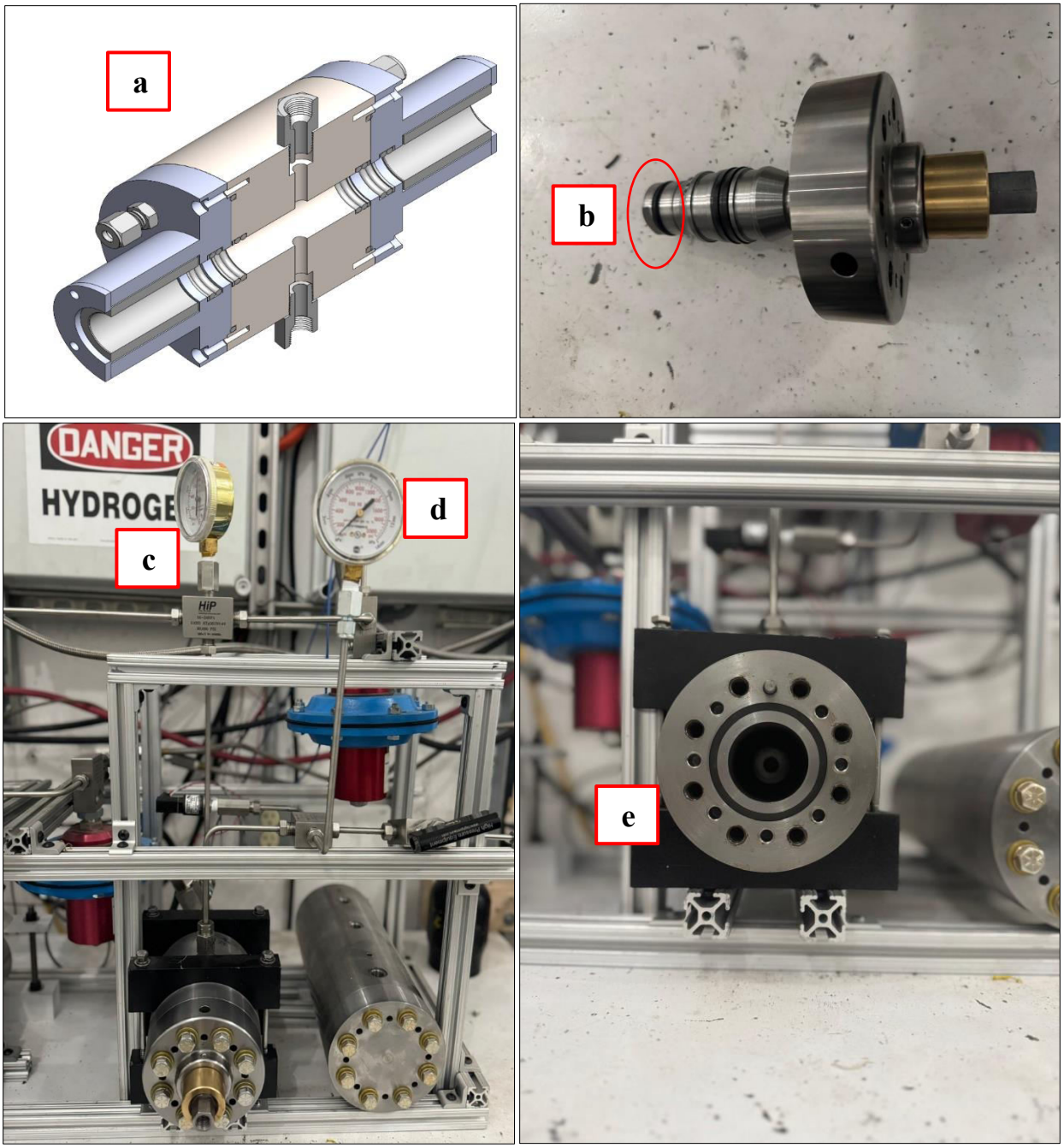

Figure 5. 6: Setup of leak test of sealing material charged with hydrogen gas

(a) Sectional view of the chamber (b) Installed aged seal for leak test
(c) low-pressure zone (d) High pressure zone
(e) Inside view of the leak chamber

5.3. Data Collection

The study employs a structured methodology to investigate the influence of pressure on each material at constant temperature and duration. Table-5.3 outlines the experimental design for conducting the aging operation of seals made from NBR, Silicon, and EPDM polymers. The aging conditions of the seals are subjected to pressures ranging from 500 psi to 10,000 psi at room temperatures for a duration of 192 hours. A set of selected aged sealing samples were subsequently installed in a leak test chamber to assess the leak rate. Also, multiple aged sealing samples of the same material were taken into consideration for tensile, resistivity, swelling, hardness and morphology test. This comprehensive design of experiments performs a thorough analysis of how hydrogen pressure interact and provides valuable insights to assess the performance.

5.4. Post-aging material characterization data collection

Upon completion of the aging of sample materials, the deformed seals were characterized to assess the impact of aging. Three specimens of each polymer were analyzed after the exposure and the mean value was taken for reporting. The following mechanical and physical properties were assessed before and immediately after hydrogen exposure to assess the sealing performance.

5.4.1. Tensile Strength Test

The tensile strength of the polymer samples, a critical measure of their mechanical performance, was thoroughly evaluated to understand the impact of hydrogen permeation. This analysis was carried out in accordance with ASTM D1414, a standard test method for tensile properties of rubber. The procedure involves subjecting the polymer samples to a uniaxial tensile force until

failure, providing essential data on their strength and ductility. To ensure consistency and reliability in the measurements, tensile testing was conducted at a controlled speed of 0.083 mm/s at room temperature [303]. This specific speed is chosen to closely replicate standard conditions, allowing for a detailed assessment of the material's behavior under gradual stress. The room temperature setting ensures that the test results are not influenced by thermal effects, providing a clear understanding of the impact of hydrogen exposure. The process was repeated for each elastomer in both “before” and “after” experiments, and average values and standard errors were determined.

The key parameters to be measured and analyzed include the ultimate tensile strength (UTS), which is the maximum stress the material can withstand while being stretched or pulled before necking. These metrics will be helpful in determining any changes in the mechanical properties of the polymers due to hydrogen permeation. Reductions in UTS could indicate a weakening of the material, suggesting a detrimental effect of hydrogen on the polymer structure. Additionally, the elongation at break, a measure of ductility, was also recorded. This data provided insights into how the material's ability to deform plastically changes after hydrogen exposure. It's important as a decrease in ductility could lead to brittleness, making the material more likely to failure under stress. The tensile strength data, in conjunction with the other parameters, were critically analyzed to establish a comprehensive understanding of how hydrogen exposure influences the mechanical integrity of the sealing polymers. Figure 5.7 shows the tensile strength measurement set-up as a part of the characterization test.

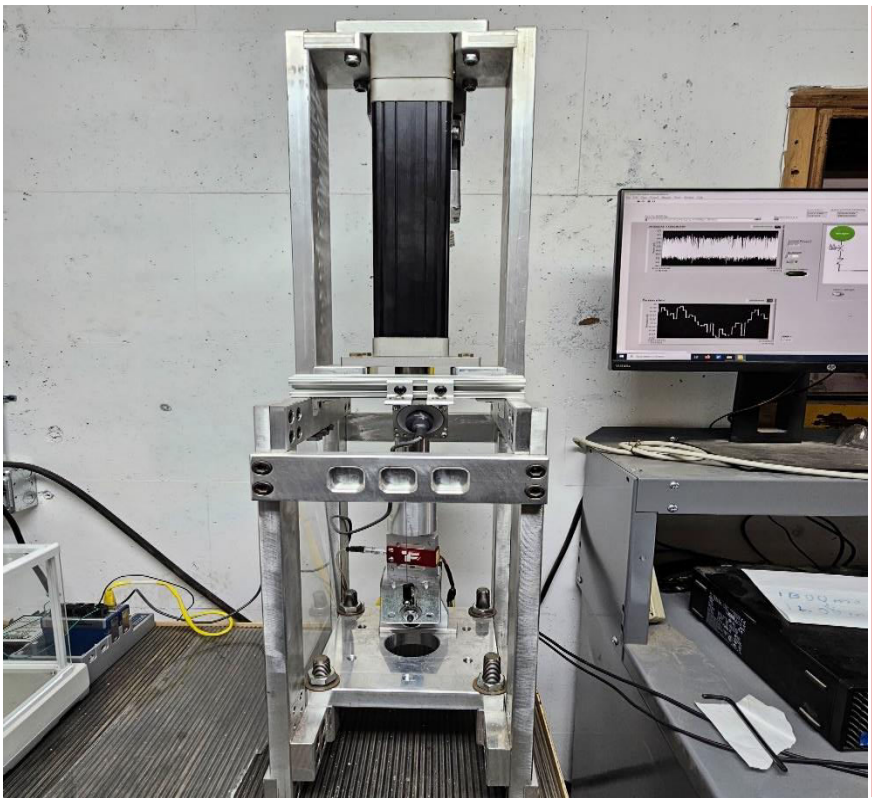

Key Features:

- Capacity : 5000 lb.
- ASTM D1414 - Rubber O-Ring Tensile Test
- Remotely operable

Figure 5. 7: Tensile strength analysis of aged sealing samples

5.4.2. Swelling Test

Swelling tests, particularly for hydrogen-aged seals, play a crucial role in understanding seal performance in specific environments. When O-rings are exposed to hydrogen, their material properties can change significantly, directly impacting their functionality and reliability. The swelling test was performed following the ASTM D471,"Standard Test Method for Rubber Property—Effect of Liquids". The process involved initially measuring the mass of the entire O-ring in a clean and dry state. The O-ring is then aged in a controlled hydrogen environment, simulating the actual conditions of exposure, including specific parameters like temperature and pressure. After exposure, the O-ring is removed, allowed to return to ambient conditions, and reweighed. An increase in the O-ring's mass indicates hydrogen absorption, which leads to

swelling. This swelling is a critical indicator, as it reflects how the material interacts with hydrogen. Swelling can result in dimensional changes, which might compromise the seal's effectiveness by altering its fit and the sealing force. In certain applications, even minor changes in the dimensions of an O-ring can lead to leakage or failure of the sealing system. Therefore, understanding the extent of swelling is vital in predicting and ensuring the reliability of O-ring seals in hydrogen environments. On the other hand, a decrease in mass, typically indicative of material degradation, suggests loss of material integrity, potentially leading to weakened structural and mechanical properties. This degradation results in reduced strength, flexibility, or elasticity, further impairing the seal's performance. In summary, swelling tests provide essential data on the compatibility of O-ring materials in hydrogen environment, and their potential to maintain physical and mechanical integrity under such conditions.

5.4.3. Hardness Test

The Hardness Test for evaluating the mechanical properties of O-ring seals, particularly after aging in hydrogen, is a crucial aspect of material characterization and is conducted in accordance with ASTM D2240, "Standard Test Method for Rubber Property—Durometer Hardness." This standard provides a method for measuring the hardness of elastomeric materials, such as the rubber compounds typically used in O-ring seals. The test involves using a durometer, a device designed to measure the indentation hardness of the material. The procedure involves applying the durometer presser foot perpendicularly to the surface of the O-ring and measuring the resistance to indentation. Before measuring the hardness of any elastomeric samples, the durometer was first zeroed. Hardness measurements were then taken at three different spots, two on each of the circular flat surfaces of each elastomer sample, and the average durometer reading, and standard errors

were determined. This was done to satisfy for errors that may result from uneven surfaces of the elastomers for same test samples and variable hardness on the measured surface. The measurements were taken with an error margin of +/-0.5 durometer units. The hardness value, which is read from the durometer scale, provides an indication of the material's elasticity and its ability to return to its original shape after deformation. For O-rings that have been exposed to hydrogen, this test is particularly significant as it helps determine any changes in the material's properties that could affect sealing performance. An increase in hardness might indicate that the material has become more rigid, which could lead to cracking under pressure or reduced flexibility, compromising the seal. Conversely, a decrease in hardness could suggest that the material has become softer, potentially reducing its effectiveness in maintaining the tightness of the seal. The hardness test serves as a quick and non-destructive means to evaluate the potential longevity and effectiveness of O-ring seals in their intended applications, especially after exposure to hydrogen environments that might induce material changes. The findings from this test, as per ASTM D2240, are significant in assessing whether the aged seals can continue to perform their sealing functions effectively or if they have been compromised due to the aging process. Figure 5.8 shows the equipment set up for measuring the hardness of the sealing material as a part of characterization test.

OHK-DD-4 Durometer

Key Features:

Type M Durometer

As thin as .050″

O-Ring Fixture Kit

Figure 5. 8: Hardness analysis of aged sealing samples

5.4.4. Resistivity Analysis

Resistivity analysis is another important tool in evaluating the performance of polymer seals, particularly O-rings, after exposure to hydrogen. This analysis, mentioned in the principles of ASTM D257, "Standard Test Methods for DC Resistance or Conductance of Insulating Materials," serves to understand the effects of hydrogen on the electrical properties of polymers, which are commonly used as indicator due to their characteristically high electrical resistivity. This property is important for many industrial and consumer applications, where the ability to prevent electrical conduction is vital. For hydrogen-aged polymer seals, the method of resistivity testing begins with preparing standard-sized specimens conforming to the dimensions of 70 mm diameter and 2 mm thickness outlined in ASTM D257. These specimens are placed between two electrodes, ensuring uniform and consistent contact. A constant voltage is then applied for sixty seconds; chosen based on ASTM guidelines to stabilize the electrical current and mitigate transient effects, thus ensuring

the accuracy of the resistance measurements. The resistance is measured using an ohmmeter capable of accurately detecting the high resistance levels typical of polymers. Following the resistance measurement, the volumetric resistivity of the specimen is calculated. This calculation incorporates the measured resistance and the physical dimensions of the specimen, using the below formula provided in ASTM D257 that accounts for the specimen size and electrode configuration.

$$\rho = \frac{R \times A}{I}$$

ρ is the resistivity of the material (Ohm-meters).

R is the resistance measured (Ohms).

A is the cross-sectional area of the specimen (square meters).

l is the length of the specimen between the electrodes (meters).

The resistivity values obtained from these calculations are then analyzed to assess the material's electrical properties in the context of its exposure to hydrogen. An increase in conductivity (decrease in resistivity) in the hydrogen-aged seals may indicate a degradation of the polymer's insulating properties, potentially pointing to chemical or physical changes within the polymer matrix, such as polymer chain breakage or the formation of new chemical groups. These changes could affect the seal's overall performance by altering its physical integrity or mechanical properties. Conversely, resistivity values that remain consistent with those of unaged materials suggest that the polymer has retained its insulating properties and structural integrity, despite the aging process. This non-destructive testing provides insights into the durability and performance of the polymer, informing its continued applicability in scenarios where maintaining electrical insulation is essential. By correlating changes in electrical properties with hydrogen exposure, this analysis can offer a scientific basis for evaluating the longevity and reliability of polymer-based

seals in challenging operational environments. Figure 5.9 shows the set-up of resistivity measurement equipment of the sealing materials.

Keithley 6517B

Key Features:

- Resistance up to 1016Ω.
- ASTM D257
- High measurement speeds
- Programmable digital I/O

Figure 5. 9: Resistivity analysis of aged sealing samples

5.4.5. Morphology Analysis

Morphology analysis using Scanning Electron Microscopy (SEM) is an important medium for assessing the performance of polymer seals, particularly those exposed to gaseous pressure like hydrogen aging. SEM operates by generating a focused beam of electrons that interacts with the sample, emitting secondary electrons and X-rays. These emissions are captured by detectors and converted into signals that produce detailed images of the sample's surface. The analysis provides insights into the microstructural changes in polymer seals caused by hydrogen exposure, helping to evaluate their extent of crystallinity that assist to find out suitability and durability in practical applications. In this study, the ThermoFisher Quattro S. SEM machine, equipped with a circular backscattered (CBS) electron detector, was employed to capture high-resolution images of polymer sealing samples after exposing to different pressure hydrogen. The CBS detector, with

multiple segments and rings, enhances imaging efficiency, making it useful for studying surface features and identifying potential defects. The SEM analysis was conducted with two specific objectives: first, to investigate elastomer failure due to cavitation under specific experimental conditions, and second, to understand the morphological changes in the polymer structure due to hydrogen aging. This analysis were compared to both mechanical and chemical degradation processes at the microstructural level. SEM imaging provides data on surface roughness, micro-cracks, voids, cavitation, and other forms of degradation that could lessen the integrity of the seal. Changes at both the micro and nanoscale levels can significantly affect material performance, including mechanical strength, flexibility, and sealing efficiency. Figure 5.10 shows the equipment used for recording the morphological changes of the sealing material.

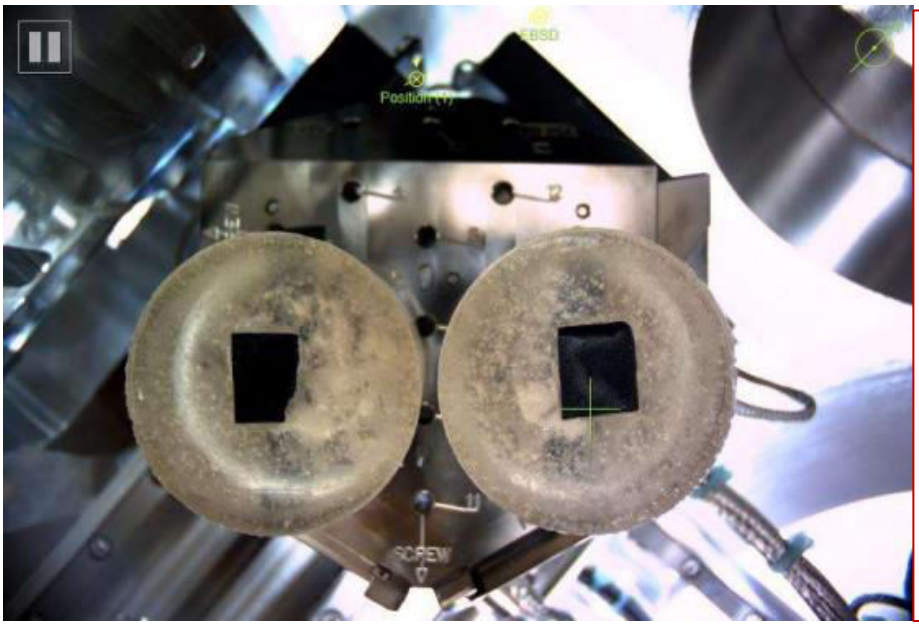

Quattro ESEM

Key Features:

- Dynamic in situ experiments
- Excellent analytical capabilities
- Minimize sample preparation time

Figure 5. 10: Morphology analysis of aged sealing samples

- ***Crack Analysis:***

Cracks are defined as narrow openings or fractures that form within a material due to stress, fatigue, or environmental exposure. For polymer seals, crack formation can occur due to pressure-induced degradation, leading to a reduction in mechanical strength and flexibility. SEM images were obtained to analyze micro-cracks in hydrogen-aged samples under various applied pressures using an advanced image processing algorithm. The process used library from 'scikit-image' package. For crack detection, two-step approaches were applied. The first one was 'edge detection' via the 'Canny algorithm' and the later one was 'refined crack detection' performed by morphological operations. The Canny edge detector is a widely used algorithm for edge detection, detects intensity gradients in the images and highlights potential edges corresponding to material fractures or cracks. We used morphological closing, a technique from mathematical morphology, to connect discontinuous crack segments and eliminate small gaps, making the detected cracks more continuous and evident. The entire process is preceded by several image preprocessing techniques: including 'contrast enhancement' through histogram equalization and 'Gaussian smoothing' to reduce noise while preserving significant crack structures. These preprocessing steps are performed for making minor cracks more visible and reducing the chances of false positives. The final crack detection output is displayed alongside the original SEM images and Hough Transform-based edge detection for visual comparison. The 'Hough Transform' is known for detecting geometric shapes. It is included to provide a reference for how cracks, which are typically non-geometric, compare to edges detected in simpler geometries. The cracks were further quantified by calculating the number of cracks, average crack size, and crack density, which provided insight into the extent of cracking. This method has the advantage of detecting both small,

fine and larger cracks and fractures with high accuracy. Additionally, this process ensures minimal noise interference assists to investigate material failure upon aging.

- ***Cavity Analysis:***

Cavities, or voids, are hollow spaces within a material that can form due to gas diffusion, mechanical stress, or material degradation. Cavities usually weaken the structural integrity of the material, negatively affecting its sealing performance. Advanced machine learning algorithms were applied to SEM images of sealing materials to identify the cavities at different hydrogen pressures. Each image was pre-processed through adaptive contrast enhancement using Contrast Limited Adaptive Histogram Equalization (CLAHE) to improve the visibility. Gaussian filtering was then applied to reduce noise and enhance cavity detection. The images were segmented using multi-level Otsu thresholding, which divides the image into three intensity regions, focusing on the mid-intensity region where cavities are expected to be dominant. To further refine the segmented regions, morphological operations (binary closing) were used and small objects were removed to eliminate noise. A region of interest (ROI) was defined by excluding the bottom 10% of each image to avoid false positives in areas. A distance transform was applied to enhance the segmentation, followed by blob detection using the Laplacian of Gaussian (LoG) method to identify cavities, characterized by the circular shape. The blob detection parameters, such as maximum sigma, number of sigma levels, and threshold, were tuned to improve the accuracy of cavity identification. Detected blobs were filtered by size to further ensure the reliability of the results. For each image, three key features were extracted: the number of cavities, average cavity size, and cavity density. These features are then plotted against pressure to visually analyze how

cavity formation evolves with increasing hydrogen pressure. This technique has precision due to the combination of adaptive contrast enhancement, multi-Otsu thresholding, noise filtering, and optimized blob detection, effectively isolating and quantifying cavities. By combining crack and cavity analysis, SEM provides a comprehensive understanding how hydrogen exposure impacts the morphology of polymer seals, expecting to contribute for material selection, design, and processing to ensure their durability and effectiveness in operational environments.

In conclusion, the comprehensive material characterization of sealing materials under hydrogen environments, consisting of tensile strength, swelling, hardness, resistivity, and morphology analysis, provide a broad spectrum of understanding of material behavior and performance. Tensile strength tests reveal critical insights into mechanical integrity and ductility, while swelling tests assess dimensional stability and material interaction with hydrogen. Hardness tests provide valuable data on material rigidity and elasticity, crucial for maintaining effective sealing. Resistivity analysis is key in evaluating the material's electrical insulation properties, a vital aspect in certain applications. Finally, SEM morphology analysis sheds light on microstructural changes and surface integrity, crucial for predicting long-term performance. Together, these tests form a framework for evaluating and predicting the suitability and reliability of sealing materials in hydrogen-rich environments, guiding material selection and design for optimized performance.

5.5. Modeling Choices

The development of a predictive machine learning model assessing the properties of the sealing materials under various pressure conditions marks a significant advancement in ensuring the reliability and efficiency of seals in dynamic environments. This model was applied to each sealing material; NBR, EPDM, and Silicon to understand the interaction of sealing behavior under varying hydrogen pressure and predict the properties for any designed operating condition.

Figure 5.11 shows the skeleton of the model developed to predict the sealing properties.

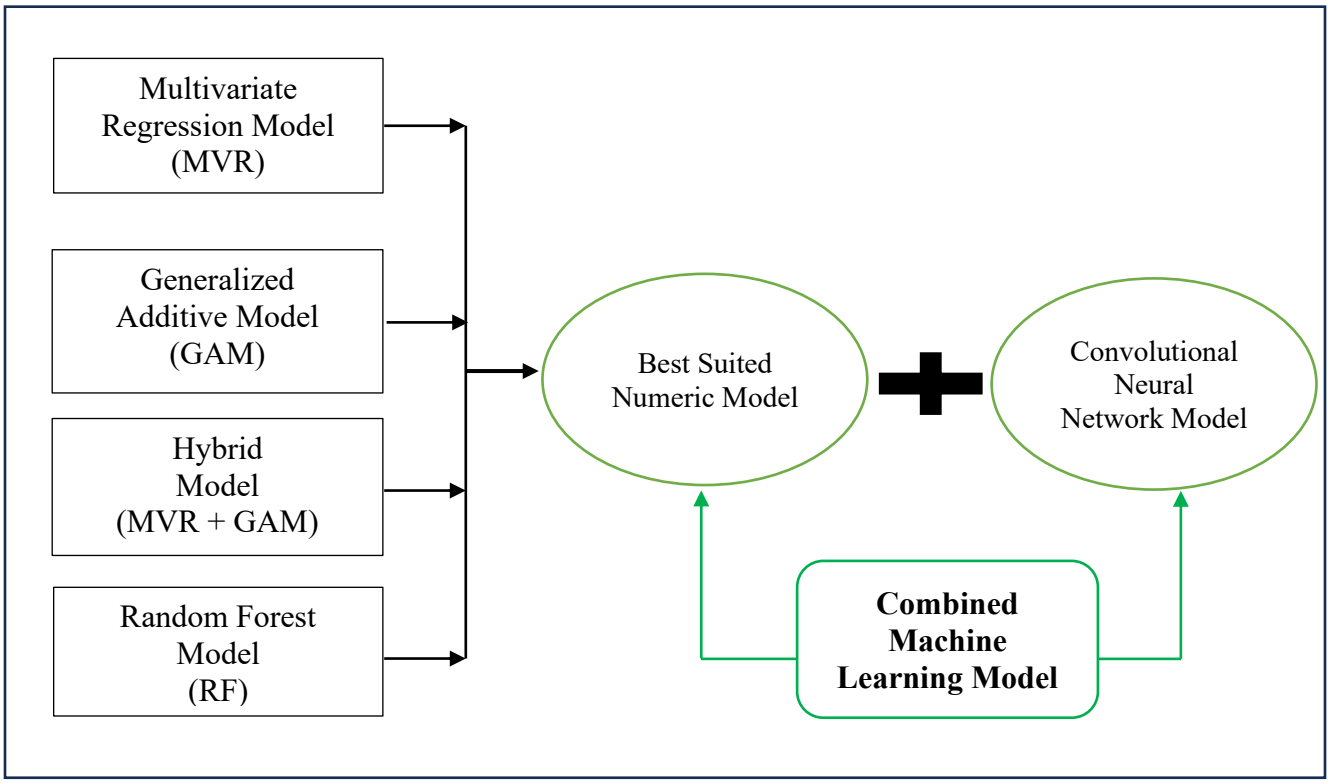

Figure 5. 11: Visual flow of the modeling choice to perform prediction model

The predictive model is designed with two main components as illustrated in Figure 5.11. The first part aims to predict the sealing properties; hardness, tensile strength, resistivity and swelling, at a given pressure using Numeric Regression Model. The second component focuses on predicting

sealing properties; hardness, tensile strength, resistivity and swelling using the image processing techniques following Convolutional Neural Network Model. Afterwards the two models were combined based on the accuracy weight to finally predict the sealing properties of a particular given sealing sample. For each sealing sample, a dedicated combined model was developed using numeric and image processing data. The incorporation of images of the sealing surfaces enhances the model's ability to capture material degradation patterns, thereby improving the overall accuracy of properties predictions. The detailed flow of model is outlined through a block diagram at Figure 5.12.

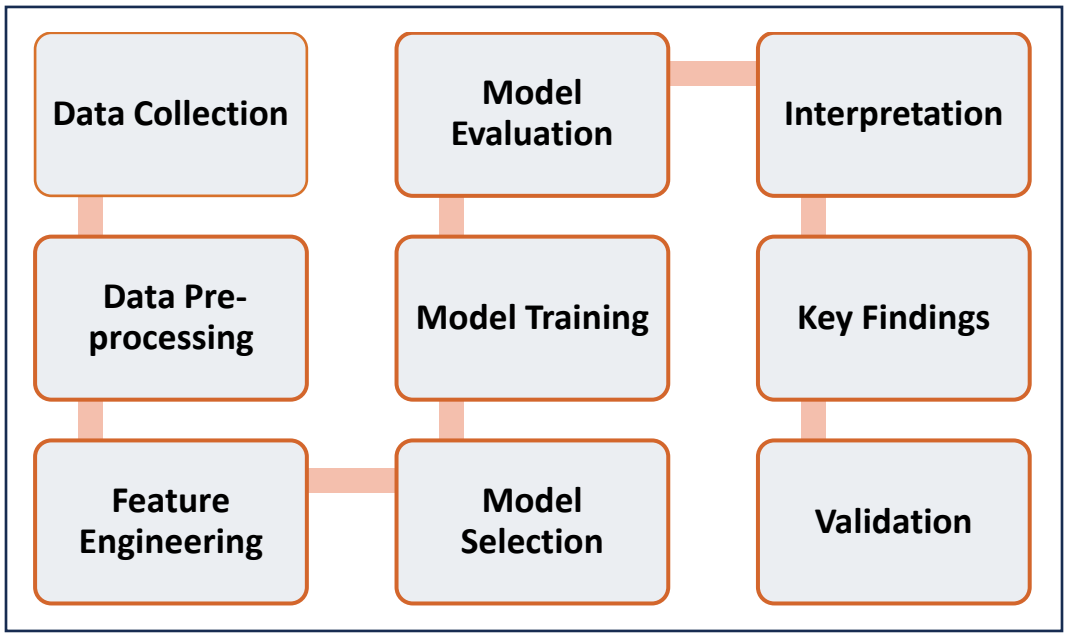

Figure 5. 12: Machine learning model for sealing prediction assessment

5.5.1. Model Development

The multiple predictive models which were applied to perform the prediction of the sealing properties are Multivariate Regression Model (MVR), Generalized Additive Model (GAM), Random Forest Model (RF) and Convolutional Neural Network (CNN) Models. Each model along with the respective mathematical calculations are described as following:

- ***Generalized Additive Model (GAM)***

The Generalized Additive Model (GAM) is a non-parametric regression model that extends the linear model by allowing non-linear relationships between predictors and responses. Unlike standard linear regression, where the effect of each predictor is assumed to be linear, GAMs use smooth functions to model the effect of each predictor on the response variable. This flexibility allows GAMs to capture complex patterns in the data, making them particularly useful when dealing with non-linear relationships. In this context, GAM is used to predict multiple response variables, each modeled as a smooth function of a single predictor variable. This approach is advantageous when the relationships between predictors and responses are expected to have non-linear interpretability effects. The general form of a GAM for multiple response variables, where each response is a function of a single predictor, can be written as:

$$Y = \beta_0 + f_1(X) + f_2(X) + \cdots + f_p(X) + \varepsilon$$

where:

Y is a vector of response variables, represented as:

$$\boldsymbol{Y} = \begin{bmatrix} \mathbf{Y_1} \\ \mathbf{Y_2} \\ \mathbf{Y_3} \\ \mathbf{Y_4} \end{bmatrix}$$

X is the predictor variable.

$\boldsymbol{\beta_0}$ is the intercept term for each response variable.

$\mathbf{f_i(X)}$ represents the smooth function applied to the predictor X for the i^{th} response variable

$\boldsymbol{\varepsilon}$ is the vector of random errors for each response variable

$$\varepsilon = \begin{bmatrix} \varepsilon_1 \\ \varepsilon_2 \\ \varepsilon_3 \\ \varepsilon_4 \end{bmatrix}$$

Thus, the model for each individual response variable can be expressed as:

$$Y_1 = \beta_{01} + f_1(X) + \varepsilon_1$$

$$Y_2 = \beta_{02} + f_2(X) + \varepsilon_2$$

$$Y_3 = \beta_{03} + f_3(X) + \varepsilon_3$$

$$Y_4 = \beta_{04} + f_4(X) + \varepsilon_4$$

Where, in these equations:

β_{0i} (for i=1,2,3,4) represents the intercept for each response.

$f_i(X)$ is the smooth function of the predictor X on i^{th} response variable.

ε_i is the random error term for each response variable.

The assumptions for the Generalized Additive Model (GAM) include that the effect of each predictor is additive, meaning the model combines the effects of each predictor independently to determine the response. Each function $f_i(X)$ is a smooth function, often estimated using splines, allowing the model to capture non-linear relationships while remaining robust to random fluctuations. Additionally, the errors ε_i for each observation are assumed to be independent, though correlations among the error terms across different response variables are permitted. The main goal in GAM is to estimate each smooth function $f_i(X)$ from the data. To avoid overfitting, a penalty term is often added to the objective function to control the smoothness.

$$\boldsymbol{minimize}\left(\sum_{i=1}^{n}(\mathbf{Y_i} - \boldsymbol{\beta_0} - \sum_{j=1}^{p}\mathbf{f_j}(x)\right)^2 + \boldsymbol{\lambda}\sum_{j=1}^{p}\int(\mathbf{f_j}''(x)^2)dx$$

where λ is a smoothing parameter that optimize between model fit and smoothness. Larger λ values result in smoother function.

Random Forest Model

The Random Forest model is an ensemble learning method that builds multiple decision trees and aggregates their predictions to improve accuracy and reduce overfitting. Each tree is trained on a different subset of the data, with predictions made by averaging the results from individual trees for regression tasks. Random Forest is particularly effective for capturing non-linear relationships and interactions between predictors without needing extensive pre-processing or feature scaling. Random Forest addresses the limitations of single decision trees, such as high variance and susceptibility to overfitting, by constructing a "forest" of diverse trees. Each tree provides an independent prediction, and the model aggregates these predictions, reducing overall variance. In a Random Forest, multiple decision trees $T_1, T_2, \ldots, T_m$ are built, each using a random subset of the training data. For a new input 'X', the predicted value $\widehat{\boldsymbol{Y}}$ is the average of the predictions from all trees:

$$\widehat{\boldsymbol{Y}} = \frac{\mathbf{1}}{\boldsymbol{m}}\sum_{j=1}^{m}\mathbf{T_j}(x)$$

Where, $\mathbf{T_j}(x)$ is the prediction from the j-th tree.

Each tree $\mathbf{T_j}(x)$ splits the data based on a subset of features chosen randomly at each split. The tree seeks to minimize the mean squared error (MSE) at each node:

$$\boldsymbol{MSE(N)} = \frac{\mathbf{1}}{|\boldsymbol{N}|}\sum_{\boldsymbol{i}\in\boldsymbol{N}}(\mathbf{y_i} - \bar{\boldsymbol{y}}\boldsymbol{N})^{\mathbf{2}}$$

where |N|| is the number of samples in node N and $\bar{\boldsymbol{y}}\boldsymbol{N}$ is the mean response in N.

Random Forest employs bagging to reduce variance. Each tree is trained on a bootstrap sample, a subset of the data drawn with replacement. Bagging introduces randomness, decreasing the likelihood of overfitting by ensuring each tree is exposed to different data points. At each node, only a random subset of features is considered for splitting, reducing the correlation among trees. If p features are available, a subset of $\sqrt{\boldsymbol{p}}$ is chosen at each split. After training, the predictions for an input x are averaged across all trees. Key hyperparameters in Random Forest include the number of trees (m), where increasing this number typically improves accuracy but also raises computational cost; max depth, which limits the depth of each tree to prevent overfitting; min samples split, which sets the minimum number of samples required to split a node, thereby controlling tree complexity; and max features, the number of features considered for each split, affecting tree diversity and variance reduction. These hyperparameters are often optimized through grid search or cross-validation to enhance model performance.

Multivariate Regression

Multivariate regression is an extension of multiple regression that predicts multiple dependent variables (responses) simultaneously using one or more independent variables (predictors). This technique determines the extent to which various independent variables are linearly related to multiple dependent variables and is particularly useful when the responses are correlated. Modeling them together allows for a more comprehensive understanding of their relationships with the predictor(s), making it advantageous over separate models for each response.

The general form of the multivariate regression model can be written as:

$$Y = \beta_0 + \beta_1 X + \varepsilon$$

where:

Y is a vector of response variables, represented as:

$$Y = \begin{bmatrix} Y_1 \\ Y_2 \\ Y_3 \\ Y_4 \end{bmatrix}$$

X is the predictor variable (scalar).

β_0 is the vector of intercept terms for each response variable:

$$\beta_0 = \begin{bmatrix} \beta_{01} \\ \beta_{02} \\ \beta_{03} \\ \beta_{04} \end{bmatrix}$$

β_1 is the vector of slope coefficients associated with the predictor for each response variable:

$$\beta_1 = \begin{bmatrix} \beta_{11} \\ \beta_{12} \\ \beta_{13} \\ \beta_{14} \end{bmatrix}$$

ε is a vector of random errors associated with each response variable:

$$\varepsilon = \begin{bmatrix} \varepsilon_1 \\ \varepsilon_2 \\ \varepsilon_3 \\ \varepsilon_4 \end{bmatrix}$$

Thus, the model for each individual response can be explicitly written as:

$$Y_1 = \beta_{01} + \beta_{11} X + \varepsilon_1$$

$$Y_2 = \beta_{02} + \beta_{12} X + \varepsilon_2$$

$$Y_3 = \beta_{03} + \beta_{13} X + \varepsilon_3$$

$$Y_1 = \beta_{04} + \beta_{14} X + \varepsilon_4$$

In these equations:

β_{0i} (for i=1,2,3,4) represents the intercept for each response.

β_{1i} represents the effect of the predictor X on the i^{th} response variable.

ε_i represents the random error term for each response variable.

The assumptions of multivariate regression include linearity, where the relationship between each predictor and response variable is assumed to be linear; multivariate normality, with the error terms (ε_i) following a multivariate normal distribution; homoscedasticity, requiring constant variance of error terms across all levels of the predictor variable; and independence of errors, meaning that error terms for different observations are independent, though correlations among the error terms of different response variables are permitted.

The goal of the multivariate regression model is to estimate the parameters β_0 and β_1. The estimation is usually done using the method of least squares, which minimizes the sum of squared residuals (the differences between observed and predicted values). The residuals for each response variable are calculated, and the parameter estimates are obtained by solving the normal equations that arise from the minimization process. Let Y be the matrix of observed response values for the four variables, and X be the matrix that contains the values of the predictor (with an intercept term). The parameter estimates can be calculated using the formula:

$$\hat{\beta} = (X^T X)^{-1} X^T Y$$

where:

$\hat{\beta}$ represents the estimated parameters (intercepts and slopes for each response variable).

X includes a column of ones for the intercept and the values of the predictor variable.

Convolutional Neural Network (CNN) Model

A Convolutional Neural Network (CNN) is a deep learning model designed to process data with a grid-like topology, such as images. It excels at capturing spatial hierarchies by applying layers of convolutional filters that learn patterns, textures, and features in images. CNNs are widely used for image analysis, object detection, and feature extraction in various fields. A typical Convolutional Neural Network (CNN) consists of three main types of layers: convolutional layers, pooling layers, and fully connected layers. The convolutional layer applies filters (kernels) that slide over the input image to detect features, such as edges and textures. For a 2D input image S and a filter K, the convolution operation at a specific location (i,j) is given by:

$$(S \times K)(i.j) = \sum_{m} \sum_{n} S\,(m,n).K\,(i-m, j-n)$$

where $\boldsymbol{S}\,(\boldsymbol{m},\boldsymbol{n})$ represents pixel values in the image, and $\boldsymbol{K}\,(\boldsymbol{i}-\boldsymbol{m},\boldsymbol{j}-\boldsymbol{n})$ denotes filter values. After each convolution, an activation function such as ReLU is applied to introduce non-linearity, defined as:

$$\text{ReLU}(\boldsymbol{x}) = \max\,(0, \boldsymbol{x})$$

Next, pooling layers reduce the spatial dimensions of feature maps, retaining essential features while reducing computational costs. Max pooling, a common pooling method, selects the maximum value in each region:

$$\boldsymbol{P}(\boldsymbol{i},\boldsymbol{j}) = \max_{\boldsymbol{m},\boldsymbol{n}\in\boldsymbol{R}} \boldsymbol{S}(\boldsymbol{m},\boldsymbol{n})$$

where R is the pooling region. After the convolutional and pooling layers, the output is flattened and passed to fully connected layers to integrate the learned features. The final layer in regression tasks typically has a linear activation function for output.

5.5.2. Working Principle of Predictive Model

The predictive model was performed based on the numeric and image processed dataset. Therefore, the modeling principle can be described in terms of numeric and image based model set up.

- ***Model development on numeric data***

The modeling process was started by creating a structured data frame to hold material properties under varying pressure conditions. This initial data frame includes the independent variable; hydrogen Pressure, and four dependent variables; Hardness, Resistivity, Swelling, and Tensile Strength for all three models of three selected sealing samples. Each data set is dedicated to the respective polymer and was used for subsequent modeling. The relationship among the dependent variables with pressure was visualized using scatter plots with linear trend lines to highlight correlation trends. Each plot was arranged in a 2x2 grid layout for comparison, with displaying data points and fitted linear relationships. This visual approach provides an initial understanding of how Pressure affects the material properties. Pearson correlation analysis was carried out to quantify and visualize the relationships among the dependent variables, Tensile Strength, Hardness, Resistivity, and Swelling. Thus, the correlation coefficients between each pair of variables was calculated. This analysis helped to determine the strength and direction of linear associations among the properties. A correlation matrix plot was created for each polymer presenting as a circle plot with values on the lower triangle to assess the interdependencies that may impact further modeling steps. Train-test split was performed using the Caret library. A seed was set to ensure reproducibility and applied a random sampling method to select 20% of the data points for the test set while the remaining 80% were assigned to the training set.

A multivariate linear regression model was applied to predict multiple dependent variables (Hardness, Resistivity, Swelling, and Tensile Strength) as functions of the independent variable, Pressure. The model was performed based on the training dataset, simultaneously regressing each dependent variable on Pressure. Predictions were then generated for the test data, and the model accuracy was calculated to compare actual and predicted values across all dependent variables. R-squared, Mean Absolute Error (MAE), and Root Mean Squared Error (RMSE) were computed for each dependent variable, assessing the model's predictive accuracy.

Generalized Additive Models (GAMs) was applied to capture potential non-linear relationships between Pressure and each dependent variable using the mgcv library in R. Each GAM model uses a smooth term for Pressure with reduced degrees of freedom (k = 3) to prevent overfitting while allowing flexibility in the fitted relationships. Predictions were then generated on the test dataset to evaluate the model's generalization performance. R-squared, Mean Absolute Error (MAE), and Root Mean Squared Error (RMSE) metrics for each GAM model were computed to assess prediction accuracy. An accuracy table was created to compare actual and predicted values for each dependent variable obtained from GAM to check non-linear trends within each data set.

A hybrid model combining the Generalized Additive Models (GAMs) and Multivariate Linear Regression (MVR) was created to enhance predictive accuracy across different dependent variables. The ‘mgcv library in R was used to fit GAM models for Resistivity and Swelling, to capture potential non-linear relationships with Pressure while, Hardness and Tensile Strength were modeled using an MVR approach via lm(), assuming a linear relationship with Pressure. The predictions obtained from this combined model were then extracted into a single data frame to facilitate evaluation. Random Forest models was also implemented for all three polymers to check

if there is any complex pattern between the dependent and independent variables. Each dependent variable was modeled independently using the training dataset. Prediction on test data set was performed to evaluate model performance on unseen data. An accuracy table was created to compare actual and predicted values for each variable.

After generating the models, the accuracy metrics were compared across each model to determine the best-performing model for each respective sealing sample. The model with the highest predictive accuracy for each sample was then selected to be integrated with the CNN model for the final combined prediction.

- ***Model development on image data***

SEM images were used to further build a Convolutional Neural Network Model to predict the same set of properties at respected pressure for each sealing material. Respective SEM images and corresponding attributes to serve as input to the Convolutional Neural Network (CNN) model. A dictionary is specified for each sealing sample to contain image files paired with respective attribute values of Hardness, Tensile Strength, Resistivity, and Swelling. Each image was loaded in grayscale, resized to a standardized 128x128 dimension, and stored in a list. Subsequently, these images were converted into a 4D numpy array with an added channel dimension to accommodate grayscale data and normalized by scaling pixel values to fall within the [0,1] range. Corresponding attribute values were also converted to a numpy array, creating a structured dataset for further CNN model training and validation.

To ensure consistency in model evaluation, cross-validation using KFold with 5 splits was employed instead of fixed indices for dataset splitting. This method ensured that all samples were used for both training and validation across different folds, allowing for a comprehensive evaluation of the model's performance. X_train and X_test were created for image data, and y_train and y_test for the attribute data within each fold. The target variables (Hardness, Tensile Strength, Resistivity, and Swelling) were standardized using 'StandardScaler' to improve model convergence and interpretability which leads the optimization of CNN architecture for predicting the sealing properties. A model building function was defined for hyperparameter tuning through 'Keras Tuner' to explore a range of CNN configurations. This function allows tuning of the number of convolutional layers, filter sizes, dense layer units, and learning rates. Using Keras Tuner, the model was optimized by exploring configurations for the number of convolutional layers (2 to 4), filter sizes (32 to 128), dense layer units (32 to 128), and learning rates ($1e^{-4}$ to $1e^{-2}$). Each model consists of Conv2D and MaxPooling2D layers, followed by a dense layer to combine features, with a final output layer of four units for predicting Hardness, Tensile Strength, Resistivity, and Swelling. Each convolutional layer uses ReLU activation with max pooling to capture spatial features, followed by a flattening layer and a fully connected dense layer that outputs predictions for the four target variables. The 'RandomSearch' method from Keras Tuner was run independently for each fold during cross-validation to maximize validation performance by testing up to 10 different model configurations per fold. After completing the search in each fold, the best model for that fold was selected based on the lowest validation MAE. This fold-specific approach ensured that model optimization was closely aligned with the cross-validation process.

After selecting the best CNN model configuration, the predictions were generated on both the training and test datasets to evaluate its performance. Initially, the model's predictions were in the scaled format due to prior standardization of the target variables. To interpret the results in their original units, an inverse transformation was applied using the 'StandardScaler' instance. This approach allowed to retrieve the predicted values for Hardness, Tensile Strength, Resistivity, and Swelling in their original scale, facilitating a direct comparison with actual measurements. To assess the predictive accuracy of the optimized CNN model, the Mean Squared Error (MSE) was calculated for each target variable. The output were organized into a DataFrame for comparing training and test MSEs side by side to evaluate the model's generalization capability and identify any overfitting or underfitting tendencies across the predicted attributes.

Reference

290. Barth, R.R.; Simmons, K.L.; San Marchi, C. "Polymers for Hydrogen Infrastructure and Vehicle Fuel Systems: Applications, Properties, and Gap Analysis." Sandia National Laboratories (SNL-CA), Livermore, CA, USA, 2013.

291. Koga, A.; Uchida, K.; Yamabe, J.; Nishimura, S. "Evaluation on high-pressure hydrogen decompression failure of rubber O-ring using design of experiments." Int. J. Automotive Eng., 2 (4) (2011) 123–129.

292. Jaravel, J.; Castagnet, S.; Grandidier, J.-C.; Gueguen, M. "Experimental real-time tracking and diffusion/mechanics numerical simulation of cavitation in gas-saturated elastomers." Int. J. Solids Struct., 50 (9) (2013) 1314–1324.

293. Kane-Diallo, O.; Castagnet, S.; Nait-Ali, A.; Benoit, G.; Grandidier, J.-C. "Time-resolved statistics of cavity fields nucleated in a gas-exposed rubber under variable decompression conditions–support to a relevant modeling framework." Polymer Testing, 51 (2016) 122–130.

294. Amjadi, M.; Fatemi, A. "Tensile Behavior of High-Density Polyethylene Including the Effects of Processing Technique, Thickness, Temperature, and Strain Rate." Polymers (Basel), 2020 Aug 19;12(9):1857. doi: 10.3390/polym12091857. PMID: 32824990; PMCID: PMC7564066.

295. Menon, N.C.; Kruizenga, A.M.; Nissen, A.; San Marchi, C.W. "Behavior of polymers in high pressure hydrogen environments as applicable to the Hydrogen Infrastructure." United States. https://www.osti.gov/servlets/purl/1344719.

296. Bossel, U. (2006). "The Hydrogen Illusion: Why Electrons Are a Better Energy Carrier". CEP Magazine.

297. Davis, Emily. (2023). "Advancements in Hydrogen Refueling Stations." Energy Solutions, vol. 18, no. 5, pp. 210-220.

298. Green, David. (2023). "Hydrogen Storage Technologies." Journal of Renewable Energy, vol. 30, no. 7, pp. 987-995.

299. Lee, Sarah. (2023). "Hydrogen in Chemical Synthesis." Chemical Industry Review, vol. 17, no. 11, pp. 321-330.

300. Taylor, Robert. (2023). "Hydrogen in Space Propulsion." Aerospace Engineering Journal, vol. 12, no. 4, pp. 450-460.

301. Smith, John. (2023). "Hydrogen in Heating." Renewable Energy Journal, vol. 15, no. 3, pp. 123-130.

302. Doe, Jane. (2023). "Metal Processing with Hydrogen." Journal of Industrial Chemistry, vol. 29, no. 4, pp. 401-410.

303. Brown, Alice. (2023). "Hydrogen Use in Aerospace Testing." Aeronautics Research, vol. 10, no. 2, pp. 234-245.

304. American Society for Testing and Materials. (2014). ASTM D638-14, Standard Test Method for Tensile Properties of Plastics. West Conshohocken, PA: ASTM International.

305. Hirotada FUJIWARA, Analysis of Acrylonitrile Butadiene Rubber (NBR) Expanded with Penetrated Hydrogen Due to High-pressure Hydrogen Exposure, NIPPON GOMU KYOKAISHI, 2016, Volume 89, Issue 10, Pages 295-301, https://doi.org/10.2324/gomu.89.295

306. Milner, P.W. (1987). Advances in Nitrile Rubber (NBR). In: Whelan, A., Lee, K.S. (eds) Developments in Rubber Technology—4. Springer, Dordrecht. https://doi.org/10.1007/978-94-009-3435-1_2

307. Chang, Y. W., & Bae, J. W. (2022). Effect of the High-Pressure Hydrogen Gas Exposure in the Silica-Filled EPDM Sealing Composites with Different Silica Content. Polymers, 14(6), 1151. https://doi.org/10.3390/polym14061151

308. Lee, S. H., Lee, C. H., & Moon, W. J. (2023). H2 Uptake and Diffusion Characteristics in Sulfur-Crosslinked Ethylene Propylene Diene Monomer Polymer Composites with Carbon Black and Silica Fillers after High-Pressure Hydrogen Exposure Reaching 90 MPa. Polymers, 15(1), 162. https://doi.org/10.3390/polym15010162&#8203

309. Correlations between H2 Permeation and Physical/Mechanical Properties in Ethylene Propylene Diene Monomer Polymers Blended with Carbon Black and Silica Fillers. International Journal of Molecular Sciences, 24(3), 2865. https://doi.org/10.3390/ijms24032865:contentReference[oaicite:1]{index=1}

CHAPTER 6: EVALUATING THE EFFECTS OF HYDROGEN EXPOSURE ON SEALING MATERIALS: AN EXPERIMENTAL STUDY

Chapter 6 focuses on the analysis of experimental data to understand how hydrogen exposure impacts various sealing materials, particularly focusing on NBR, EPDM, and silicon. The experimental study, presented in Chapter 5, is used to investigate the influence of hydrogen aging on critical properties such as electrical resistivity, hardness, tensile strength, and swelling, a better understanding of behavioral trends related to increasing hydrogen pressures. Three materials are investigated under pressure changes for its physical, mechanical and electrical properties. This chapter also outlines the result of morphological degradation of these materials through crack and cavity formation using Scanning Electron Microscopy (SEM), providing insights into how hydrogen-induced structural changes affect sealing materials in high-pressure applications.

6.1. Analysis of Impact of Hydrogen Aging on Material Swelling

Figure-6.1 illustrates the swelling trends of NBR, Silicon, and EPDM as a function of hydrogen pressure from 0 to 7500 psi. NBR's weight increases from around 1.07 grams at 0 psi to about 1.09 grams at 1500 psi, after which it plateaus, indicating swelling reach to a saturation beyond this point. Silicon shows a pronounced swelling effect, with its weight rising from 1.195 grams at 0 psi to approximately 1.205 grams at 1500 psi, continuing gradually to around 1.21 grams by 7500 psi, with a noticeable plateau after 3000 psi. EPDM follows a similar pattern, increasing from about 1.10 grams at 0 psi to around 1.12 grams by 7500 psi, showing gradual swelling beyond 1500 psi. The comparison plot confirms that all sealing samples display an initial sharp increase in swelling

up to 1500 psi, followed by a slower rate or plateau, indicating that each material reaches a saturation point in swelling as pressure increases.

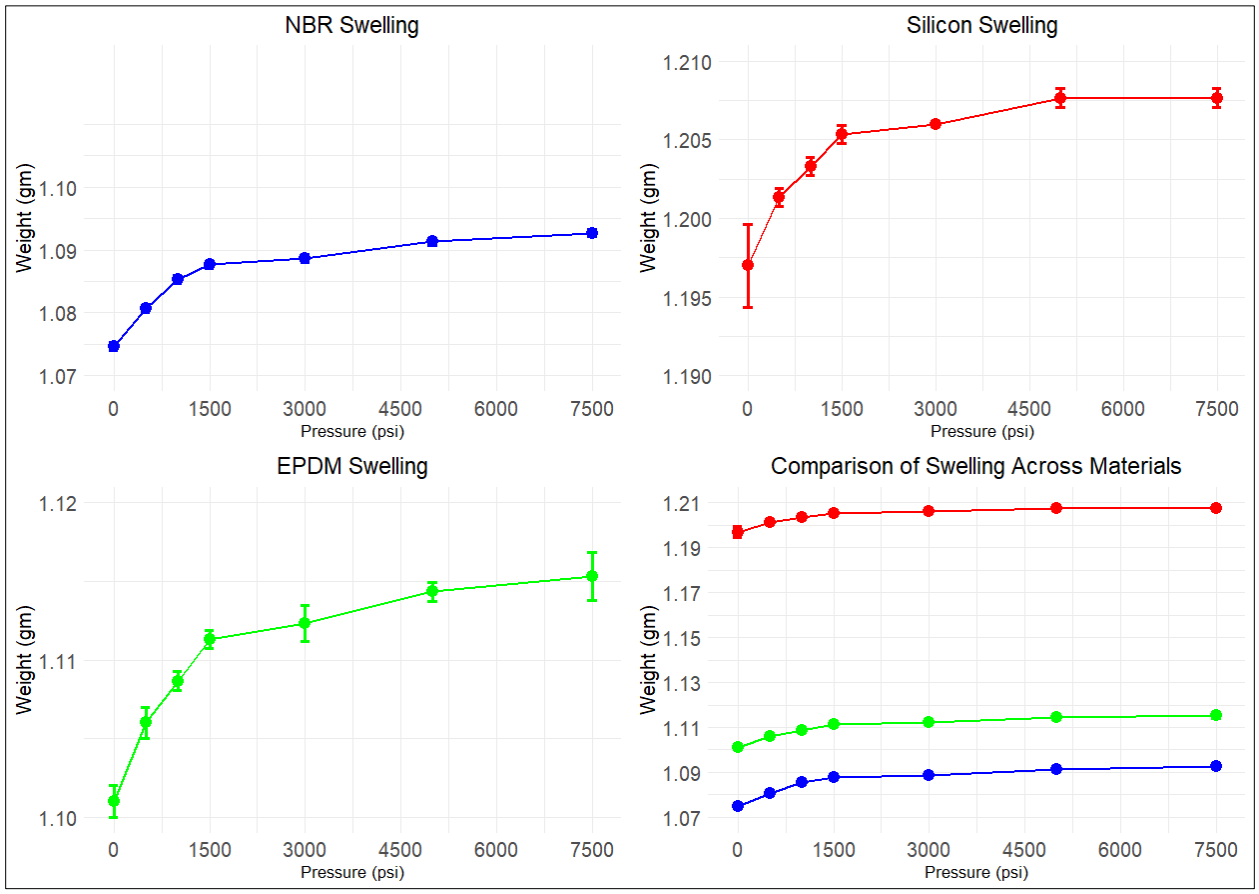

Figure 6. 1: Impact of Hydrogen aging on swelling of selected sealing samples

The swelling observed in these sealing samples under increasing hydrogen pressure is possibly caused by hydrogen absorption into the polymer matrix, leading to volume expansion and an increase in weight. This phenomenon is governed by the permeability of hydrogen through the polymer and the diffusion rate of hydrogen molecules within the polymer structure. Figure 6.2 is plotted to show the comparative analysis of the percent change of swelling across the sealing samples.

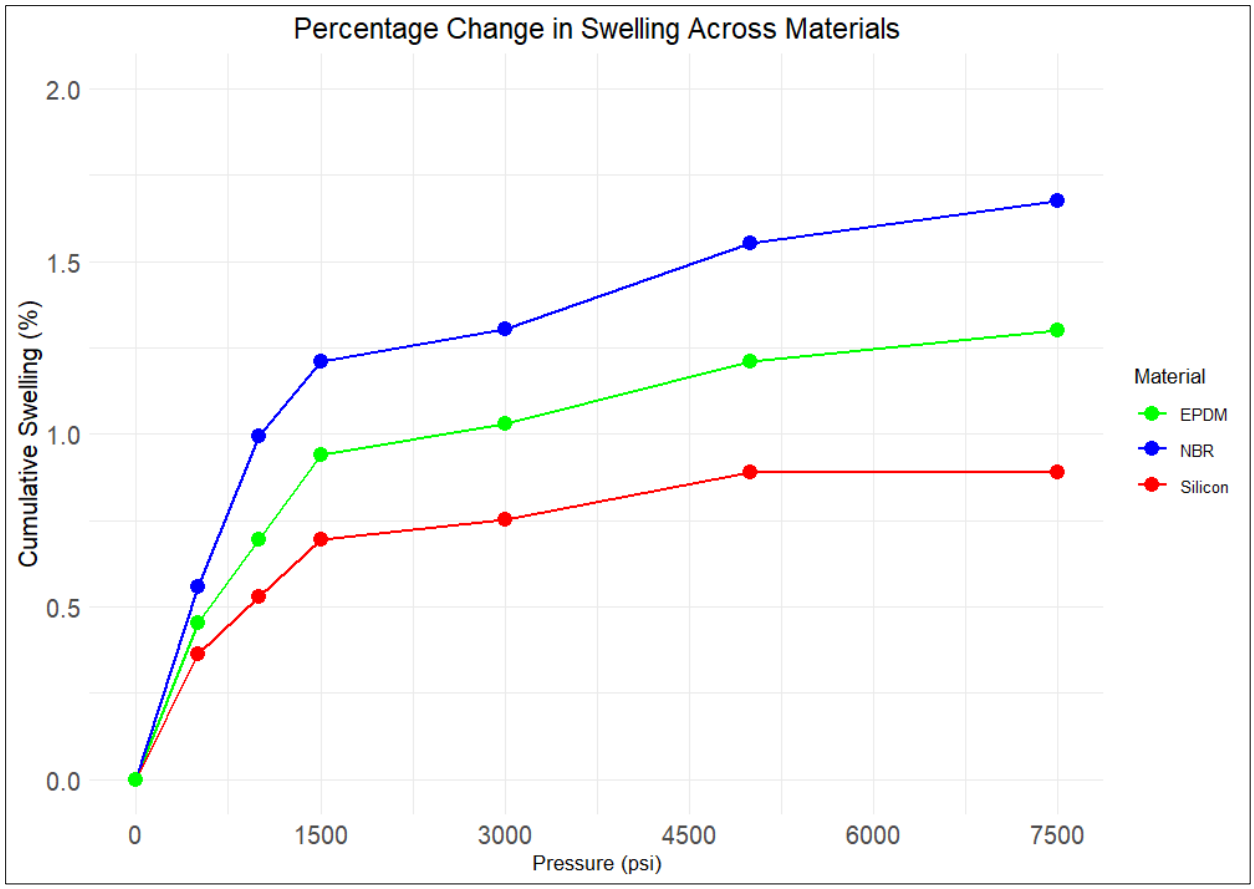

Figure 6. 2: Comparative analysis of percent change of swelling across sealing samples

Figure 6.2 shows a sharp initial increase in cumulative swelling up to 1500 psi for all three materials, with NBR displaying the highest swelling rate initially, reaching around 1.2% at 1500 psi. This rapid swelling is likely due to NBR's high hydrogen permeability, which is influenced by its polar nitrile (–C≡N) groups that tend to interact strongly with hydrogen molecules. Yamabe et al. (2012) reported that, hydrogen permeability in NBR is relatively high due to the polymer's affinity for polar molecules, allowing hydrogen to diffuse quickly into the matrix, leading to rapid expansion of the polymer chains at lower pressures. The plateau observed after 1500 psi suggests that NBR's polymer matrix is reaching a saturation point. Here, the matrix's available free volume, which enables hydrogen absorption, becomes limited, thus stabilizing the swelling. Silicon shows

a continuous but more gradual increase in swelling compared to NBR, with cumulative swelling around 0.7% at 1500 psi, rising steadily but slowly to reach about 0.9% by 7500 psi. This gradual trend is likely due to silicon's inherently low hydrogen diffusivity and permeability compared to NBR. Silicon's molecular structure consists of a highly cross-linked, nonpolar silicon-oxygen backbone (Si–O–Si), which is more resistant to hydrogen penetration. Studies conducted under the H-Mat program emphasized that, the structure impedes the diffusion of small molecules like hydrogen, resulting in slower swelling. EPDM shows moderate swelling behavior compared to NBR and Silicon, with its cumulative swelling reaching approximately 1.0% at 1500 psi. Beyond this point, EPDM displays a gradual and consistent increase in swelling, reaching around 1.2% by 7500 psi, indicating that EPDM remains less susceptible to hydrogen-induced swelling and maintains a gradual volumetric expansion. EPDM's swelling behavior may be explained by it's intermediate hydrogen permeability and semi-polar structure, which allows for controlled hydrogen absorption. EPDM has a less polar backbone compared to NBR, consisting primarily of saturated hydrocarbon chains that exhibit moderate resistance to hydrogen diffusion. Research by Fujiwara and Nishimura (2012) reported that the observation that EPDM's molecular configuration limits excessive hydrogen absorption, balancing flexibility and resistance to swelling. Additionally, EPDM's relatively rigid, semi-saturated structure provides stability against hydrogen-induced swelling, as the absorbed hydrogen molecules do not disrupt the polymer matrix as likely as in NBR.

The findings align with research from Yamabe et al. (2012), which focused on the swelling behavior of NBR and EPDM when exposed to high-pressure hydrogen. Their study revealed that hydrogen absorption leads to a volume increase in these elastomers, consistent with the observed

weight increase in this study. They also noted that NBR, with a high hydrogen content, showed significant expansion, aligning with the rise in swelling at lower pressures in the current investigation. Conversely, EPDM, with moderate hydrogen permeability, exhibited medium swelling, supporting the current findings [318, 319]. Fujiwara and Nishimura (2012) further support that swelling in elastomers under hydrogen pressure is driven by hydrogen diffusion into the polymer matrix, leading to microstructural changes. Their research demonstrated that higher pressures result in greater volume increases, particularly in non-filled elastomers like NBR, due to the free volume available for hydrogen absorption. The study also linked swelling with a reduction in mechanical properties, such as tensile strength, due to the disruption of cross-linking within the polymer structure [320]. Additionally, the H-Mat program explored the compatibility of polymers with hydrogen, emphasizing how hydrogen-induced swelling affects both volume and tensile strength. Their findings indicate that hydrogen absorption causes elastomers to swell, with materials like EPDM showing lower swelling due to their more rigid molecular structure and lower hydrogen permeability. This observation aligns with the current pattern, where Silicon shows the least amount of swelling compared to NBR and EPDM [321].

6.2. Analysis of Impact of Hydrogen Aging on Electrical Resistivity

Electrical resistivity data was collected following the procedure described at 5.4.4 at Chapter 5 after the samples were aged in a hydrogen environment. Since the focus is on the effect of hydrogen pressure on materials, the aging time was kept at 192 hours. After aging, the samples were placed between two electrodes (Section 5.4.4) and a two-probe setup (TPX-200 C) was used to collect data. Each measurement was repeated 3 times (Section 5.4.4). Figures 6.3 and Figure 6.4 illustrate the change in resistivity of NBR, Silicon, and EPDM as a function of pressure, presenting both the

absolute resistivity values (Ω·cm) and the percentage (%) increase in resistivity for the selected sealing samples across a pressure range from 0 to 7500 psi. In Figure 6.3, NBR exhibits a steady increase in absolute resistivity with rising pressure, starting from approximately 10^8 Ω·cm at 0 psi and reaching over 3×10^8 Ω·cm by 7500 psi. This upward trend suggests that NBR's conductive properties are influenced by hydrogen exposure, potentially due to structural changes within the polymer matrix that restrict electron flow as hydrogen molecules diffuse in. Silicon, on the other hand, shows an initial rise in resistivity, starting from around 2×10^{14} Ω·cm at 0 psi and spiking to approximately 5×10^{14} Ω·cm at 1500 psi, after which the increase becomes more gradual, reaching close to 6×10^{14} Ω·cm by 7500 psi. This steep initial rise suggests that hydrogen permeation has an insulating effect on Silicon at lower pressure zone, likely due to hydrogen occupying available free volume within the polymer matrix, which restricts electrical conduction. Similarly, EPDM also shows a rise in resistivity from approximately 4×10^{14} Ω·cm at 0 psi to 8×10^{14} Ω·cm by 7500 psi. EPDM's resistivity behavior, characterized by an increase up to 1500 psi followed by a more gradual increase, suggests initial rapid hydrogen absorption followed by stabilization, likely due to limited free volume and lower hydrogen diffusivity in EPDM compared to NBR .

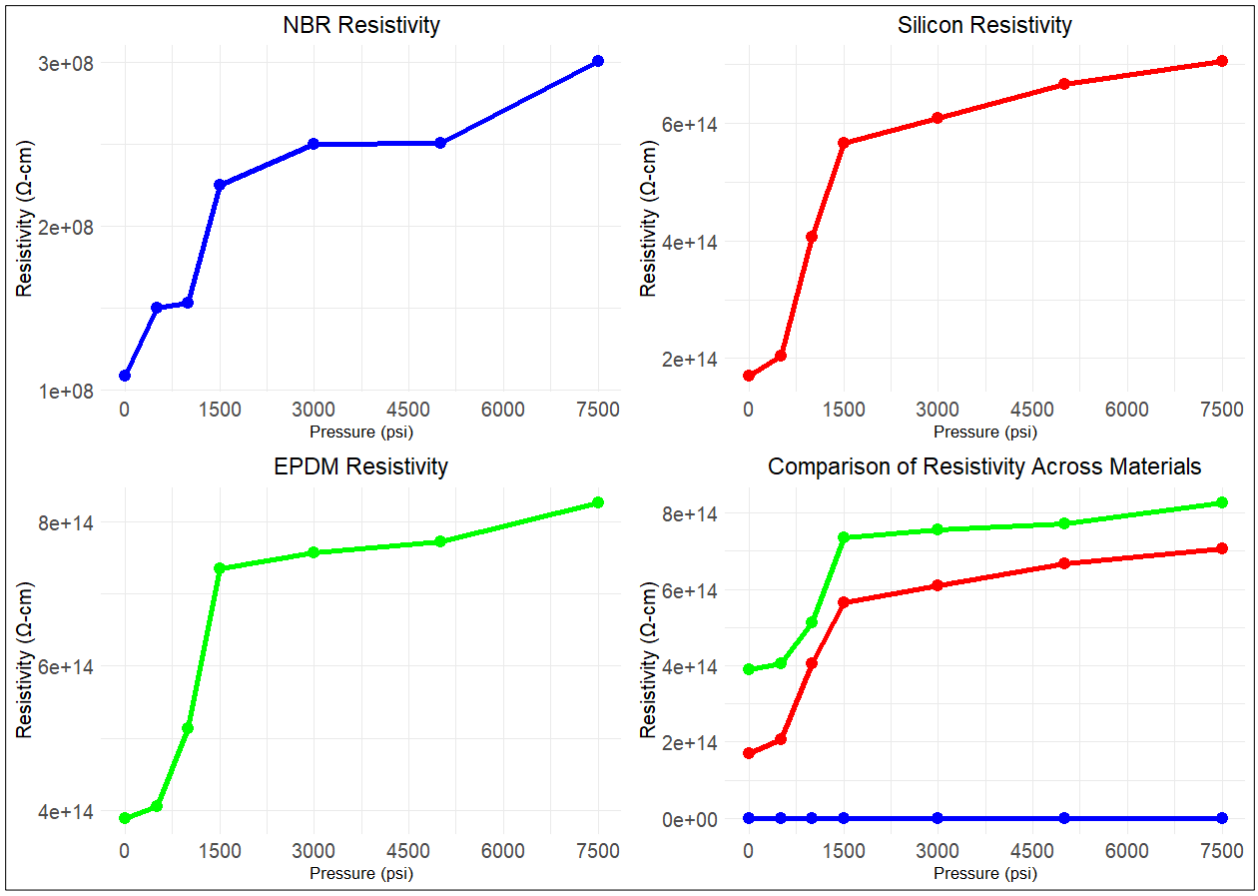

Figure 6. 3: Impact of Hydrogen aging on resistivity of selected sealing samples

Figure 6.4 provides further insight into the relative change in resistivity by showing the percentage increase across the pressure range. Silicon displays the highest percentage increase, with its resistivity rising over 250% by 1500 psi and gradually close to 300% by 7500 psi. In contrast, NBR shows a moderate percentage increase, reaching approximately 100% by 1500 psi and continuing to rise to about 150% by 7500 psi. NBR's absolute resistivity remains much lower than that of Silicon and EPDM. Though this moderate percentage increase indicates that hydrogen absorption still alters its conductive properties relative to the state when NBR was unexposed to hydrogen. EPDM exhibits the smallest percentage increase in resistivity, stabilizing around 50% after 1500 psi and showing minimal additional increase with further pressure increments.

This change suggests that EPDM's resistivity is less affected by hydrogen exposure compared to NBR and Silicon.

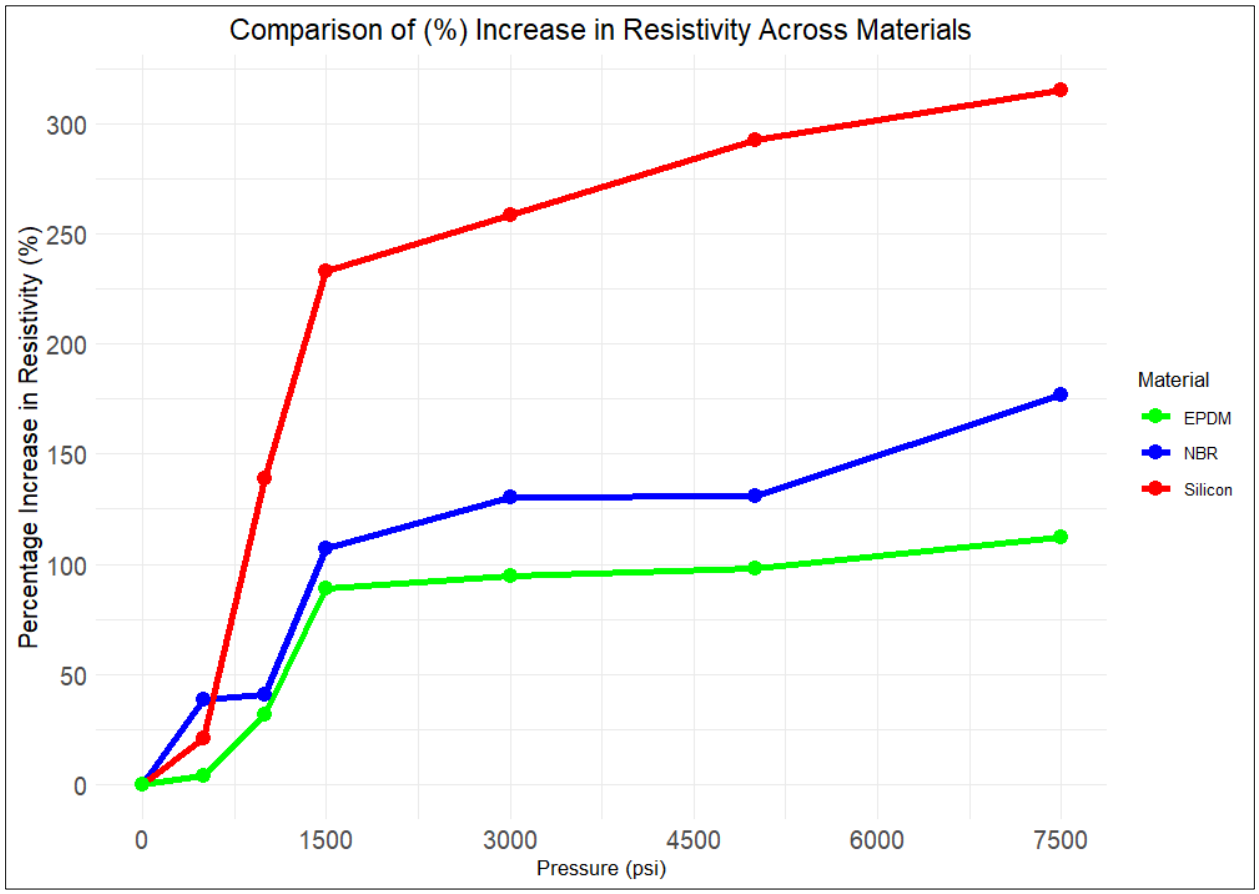

Figure 6. 4: Comparative analysis of percent change of resistivity across sealing samples

NBR contains polar nitrile groups, which can interact more with the absorbed hydrogen molecules. This interaction can influence electrical properties under high pressure. In NBR, carbon black or other conductive fillers are usually present, which could influence the electrical resistivity. Studies have shown that conductive fillers in elastomers can compress or rearrange under pressure, which impacts pathways for electrical conduction by altering contact points between filler particles [327]. At higher pressures, hydrogen absorption in NBR leads to swelling, which can disrupt conductive pathways as the polymer matrix expands. This swelling may raise resistivity until the swelling

stabilizes. Silicon is a highly insulating polymer, meaning its molecular structure has limited conductive pathways. Its resistivity is inherently higher due to its large band gap and lack of conductive fillers. As the pressure increases, silicon's resistivity shows a significant rise up to 1500 psi, observed at Figure 6.4. This behavior is attributed to limited hydrogen absorption and the stable structure of Silicon, which is known for its resistance to diffusion due to its densely cross-linked Si–O backbone [328].The slower increase beyond 1500 psi Figure 6.4 suggests that Silicon's resistivity stabilizes due to the low diffusivity of hydrogen and limited free volume for additional absorption. This pattern aligns with findings indicating that low-permeability polymers, such as Silicon, exhibit lower resistivity changes at high pressures due to minimal structural disruptions [329]. EPDM has higher hydrogen permeability compared to Silicon, which leads to more hydrogen absorption and swelling at high pressures. This swelling can slightly increase resistivity as it creates barriers to charge movement within the polymer matrix. Due to its elastomeric property, EPDM swells more than Silicon under increasing pressure, resulting in a noticeable rise in resistivity up to 1500 psi, as observed in Figure 6.4. Beyond 1500 psi, EPDM exhibits a gradual increase in resistivity, reaching a near plateau as its internal structure adapts to hydrogen absorption. The relatively lower overall resistivity increase in EPDM compared to Silicon in both absolute and percentage terms emphasizes EPDM's moderate resistance to hydrogen-induced resistivity changes. The sharp rise in resistivity in the region of 1500 psi can be linked to hydrogen-induced swelling, which disrupts the polymer's conductive network by increasing the distance between conductive particles if present. The polymer may experience changes in cross-link density under pressure, particularly in the case of NBR. Increased cross-linking or rearrangement of molecular chains under compression can reduce the mobility of charge carriers, further increasing resistivity, a trend confirmed by research on elastomeric composites

under pressure. High pressures can also cause micro-voids or cavities to form within the material, further isolating conductive pathways and increasing resistivity. Studies on microstructural changes in polymers under high-pressure hydrogen environments have highlighted micro-void formation and swelling as primary factors increasing resistivity, especially in NBR and similar elastomers [330]. The formation of micro-voids, as explained in various aging studies on fluoro-elastomers and conductive polymers, can significantly impact resistivity by isolating conductive regions within the polymer [312].

Several studies have explored the effects of pressure, temperature, and gas exposure on the resistivity of various polymers, especially in the context of hydrogen and other gases. While not all studies focus specifically on NBR, EPDM, or Silicon in the context of hydrogen, the general trends observed in this study align with findings from related literature. Research on materials such as Viton has shown that thermal aging processes result in changes in resistivity, with aged samples exhibiting increased resistivity due to structural changes [310]. In studies on conductive polymer composites (CPCs) with carbon-black fillers, Liang et al. (2013) observed that thermal aging leads to transitions in electrical resistivity [311]. The research claimed these changes to the breakdown of molecular structures and alterations in the filler-polymer interactions, which disrupt conductive pathways. These findings are comparable to resistivity transitions observed in current study for materials like EPDM and Silicon under hydrogen aging, where environmental stressors can also similarly impact resistivity by affecting conductive pathways.

6.3. Analysis of Impact of Hydrogen Aging on Material Hardness

The hardness of the selected sealing samples were measured using an 'OHK-DD-4 Durometer'. Calibration was done prior to each time measurement. Figure 6.5 presents the hardness of NBR, Silicon, and EPDM under increasing hydrogen pressures and provides insights into the materials' mechanical stability. The hardness of the unaged NBR was recorded as 78 Shore A and decreases steadily to approximately 75 Shore A by the time when 7500 psi pressure was applied. The most substantial decline was observed between 0 and 1500 psi, followed by a more gradual reduction. Silicon displays a similar trend, starting at 57 Shore A while unaged and reducing to 50 Shore A by 7500 psi, with a sharp initial drop and a subsequent steady decline. The hardness of unaged EPDM was recorded at around 61 Shore A and consistently drops to 53 Shore A by 7500 psi. A relatively linear decline was observed across all pressures for EPDM.

Figure 6.6 shows the percentage change in hardness across the three samples along with raising pressure. NBR shows the least percentage change across the pressure range, with a maximum reduction of around 5% by 7500 psi, indicating its relative stability under pressure. EPDM exhibits a more substantial reduction, reaching approximately 9% at 7500 psi. Silicon, however, demonstrates the highest sensitivity to pressure, with a cumulative reduction in hardness for 13% at 7500 psi. All three samples display an initial sharp drop between 0 and 1500 psi. NBR showing a drop of hardness by 2.5%, while the hardness of EPDM and Silicon decline more noticeably, by approximately 6% and 7% within 1500 psi respectively. Beyond 1500 psi, NBR maintains a stable trend with minimal further reduction, whereas EPDM and Silicon continue to decrease, particularly Silicon shows a steeper decline throughout the pressure range. This observation emphasizes NBR's superior resistance to pressure-induced softening, while Silicon's hardness is

most significantly impacted. EPDM's performance falls between NBR and Silicon, maintaining moderate stability across the pressure spectrum.

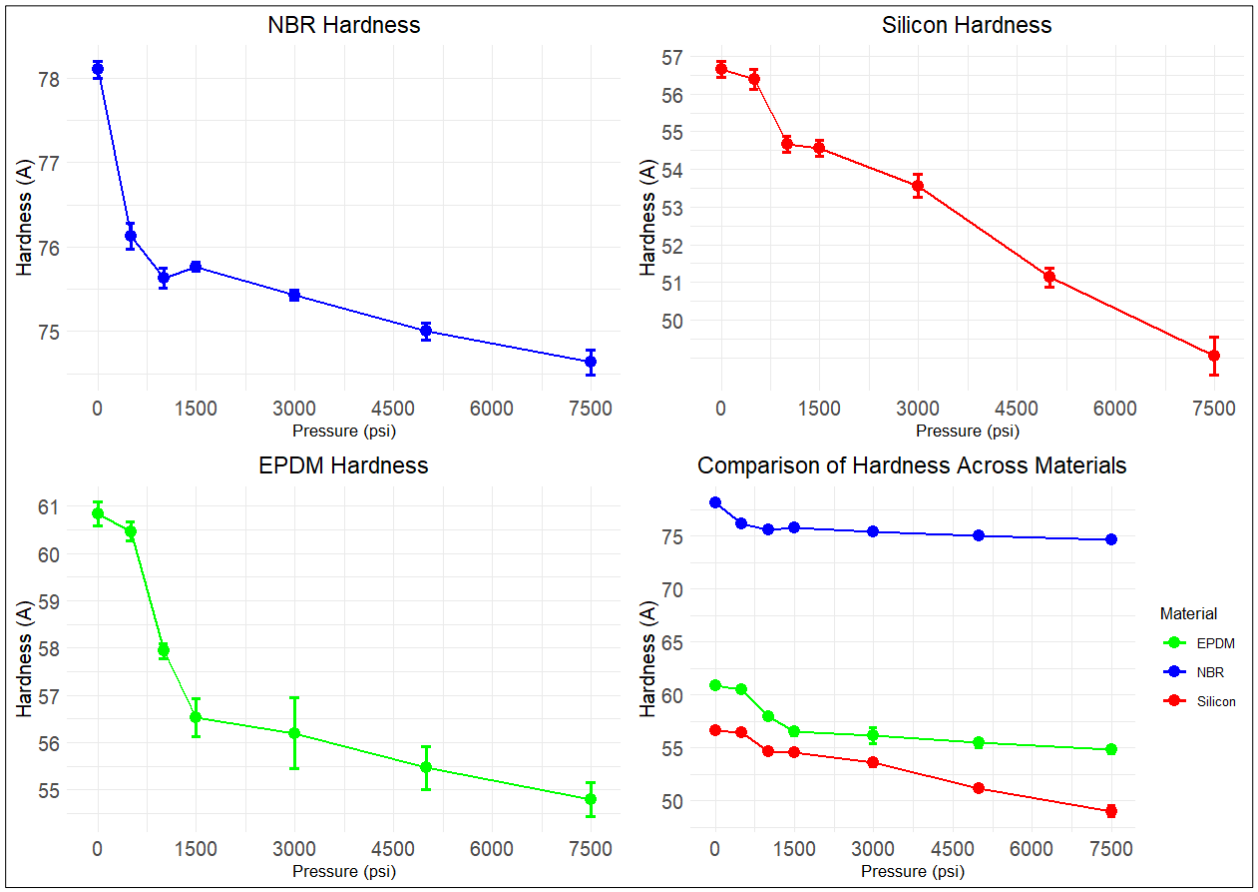

Figure 6. 5: Impact of Hydrogen aging on hardness of selected sealing samples

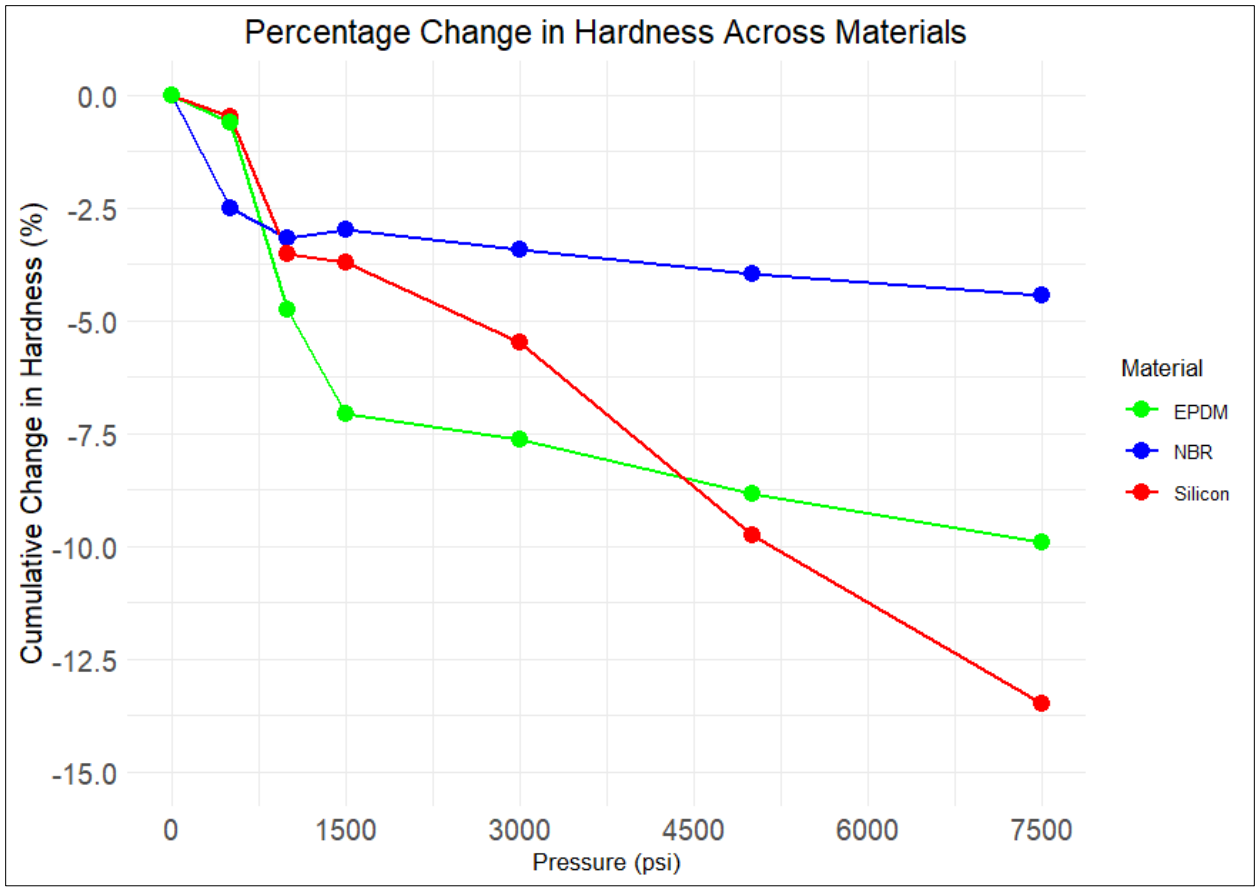

Figure 6. 6: Comparative analysis of percent change of hardness across sealing samples

The reduction in hardness observed across all materials may be attributed to the diffusion of hydrogen into the polymer matrix. When exposed to high-pressure hydrogen, polymers like NBR, silicon, and EPDM absorb hydrogen, leading to swelling and plasticization of the material This process disrupts the intermolecular forces within the polymers, and may be softening them and causing a decline in hardness. This process is consistent with findings from research showing that hydrogen uptake induces volume changes and diminishes mechanical integrity in elastomers, particularly under high pressures [331, 332]. The initial sharp drop in hardness between 0 psi and 1500 psi corresponds to rapid hydrogen uptake during the initial exposure. As the pressure increases further, hydrogen absorption likely approaches saturation and gradually declines.

Cross-linking provides rigidity and enhances mechanical properties such as hardness. Hydrogen exposure can disrupt the cross-linking in polymers [332]. As hydrogen diffuses into the polymer, it may weaken or break these cross-links, especially under high pressure, leading to a reduction in hardness. This effect is likely more evident in elastomers like EPDM, where cross-links contribute significantly to mechanical integrity [307]. The extent of this disruption may vary between materials depending on their degree of cross-linking and how hydrogen interacts with the polymer chains. Hydrogen absorption may cause the formation of micro-voids within the polymer matrix. This introduces ductile points in the material, leading to a loss in hardness as the structure becomes less dense and more likely to deform. These microstructural changes are more significant in elastomeric materials, which already have a higher degree of flexibility and can be more susceptible to such void formation. The difference in hardness reduction between materials can be explained by their molecular structures and affinities for hydrogen absorption. NBR, which contains polar nitrile groups, is less affected by hydrogen exposure, retaining higher hardness. On the other hand, silicon and EPDM, which are more elastic and insulating, experience greater softening due to their higher susceptibility to swelling under hydrogen exposure. Research has shown that permeability plays an important role in the mechanical degradation of polymers used in hydrogen storage and delivery systems. Exposure to high-pressure hydrogen leads to swelling and the formation of micro-voids, which further compromise their mechanical properties, including reductions in hardness, as demonstrated for polymers like EPDM and silicon [313, 314].

6.4. Analysis of Impact of Hydrogen Aging on Material Tensile Strength

Figure 6.7 illustrates the tensile strength of NBR, Silicon, and EPDM under increasing hydrogen pressures, showing the polymers' mechanical degradation. The tensile strength of unaged NBR was recorded at approximately 75 lbf at 0 psi which was observed decreasing steadily to around 60 lbf at 7500 psi. A significant drop was observed between 0 and 1500 psi, suggesting rapid hydrogen uptake, with a more gradual reduction in tensile strength as pressure increases further. The tensile strength of Silicon was found lowest at unaged condition among the three-sealing sample. It was recorded as around 35 lbf and continued to decrease to 25 lbf by 7500 psi. The most substantial decline for Silicon took place between 0 and 3000 psi, with a slower rate of decrease beyond this pressure. Unaged EPDM possess tensile strength about 50 lbf which is in between NBR and silicon. It experiences a consistent reduction in tensile strength, reaching approximately 45 lbf at 7500 psi. EPDM’s rate of decline slows noticeably after 3000 psi, suggesting a possible saturation effect in hydrogen absorption.

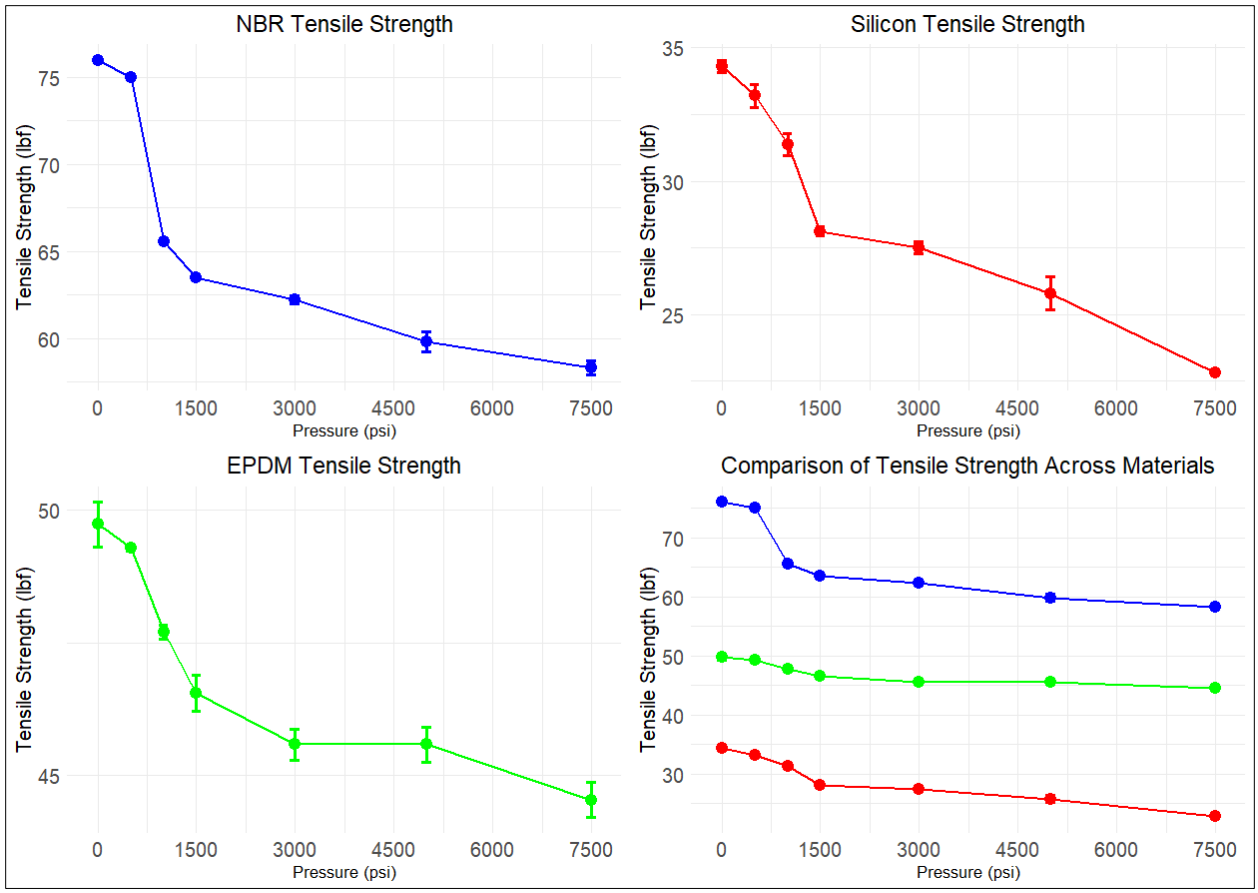

Figure 6. 7: Impact of Hydrogen aging on tensile strength of selected sealing samples

The comparative plot at Figure 6.8 shows the percentage change in tensile strength for EPDM, NBR, and Silicon materials under increasing hydrogen pressures from 0 to 7500 psi. At 0 psi, all materials consist of the inherent tensile strength. As pressure increases, each material experiences a progressive decrease in tensile strength. EPDM exhibits the lowest percentage reduction overall, with a maximum decline of around 10% by 7500 psi, and a particularly rapid drop between within 1500 psi. After 1500 psi, EPDM's reduction rate stabilizes. NBR shows a steeper decline than EPDM, reaching approximately loss of 25% tensile strength than its unaged phase by 7500 psi, with significant reductions occurring primarily between 0 and 3000 psi, after which the rate of decrease moderates. Silicon is the most affected, with tensile strength decreasing by around 35%

at 7500 psi. Silicon exhibits a substantial drop within the first 3000 psi and continues to decline steeply at higher pressures. This comparative analysis suggesting EPDM's relative stability under hydrogen exposure, with NBR and Silicon experiencing progressively larger reductions in tensile strength as pressure increases, indicating greater susceptibility to hydrogen-induced mechanical degradation.

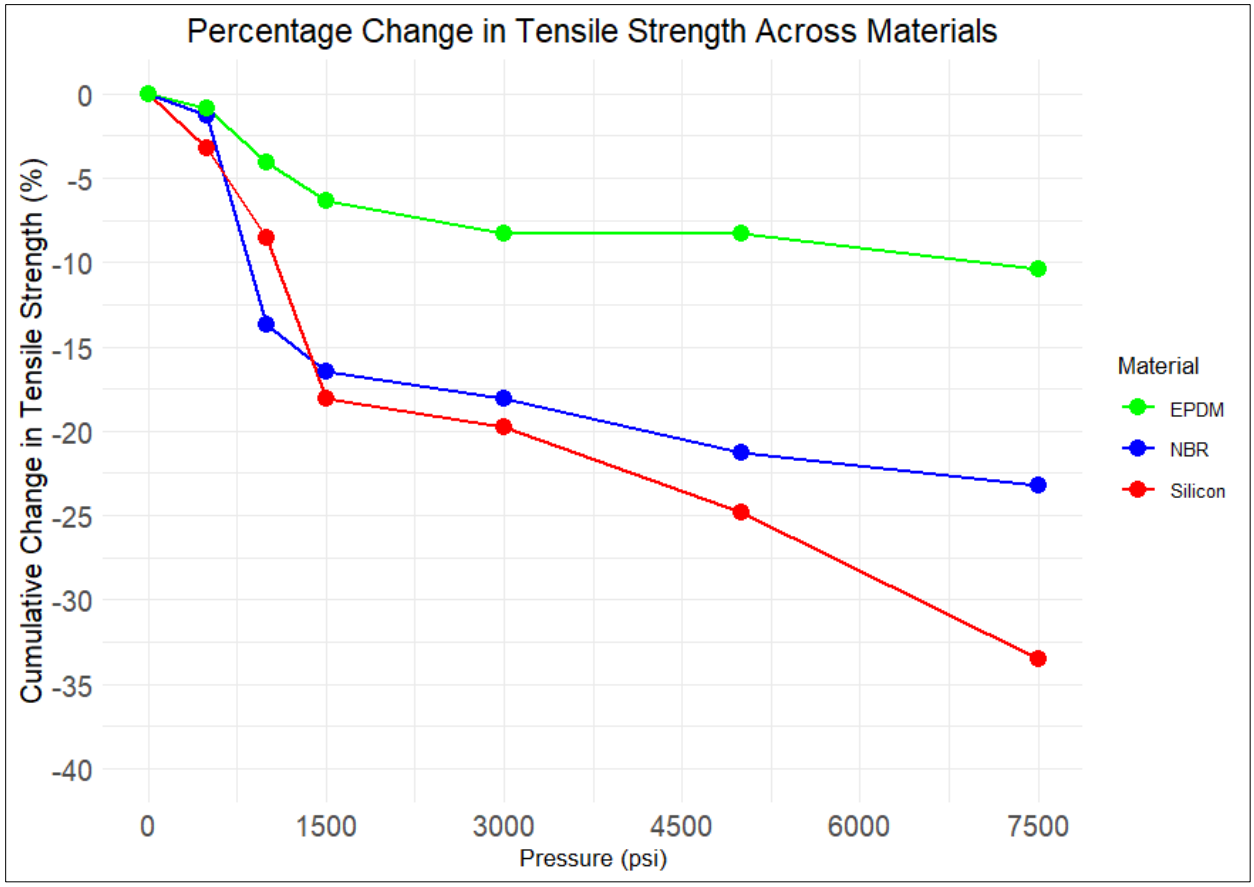

Figure 6. 8: Comparative analysis of percent change of tensile strength across sealing samples

The reduction in tensile strength with increasing hydrogen pressure may be explained by hydrogen embrittlement, swelling, and structural degradation within the polymer matrix. As hydrogen diffuses into polymers, it weaken the polymer chains and causes mechanical degradation. For NBR, the initial sharp drop in tensile strength likely indicates rapid hydrogen uptake, which

significantly weakens the polymer structure. The polar nitrile groups in NBR may interact with hydrogen, leading to internal disruptions and a substantial loss in tensile strength. This sharp reduction is prominent between 0 and 1500 psi, after which the degradation rate stabilizes. This behavior aligns with previous studies indicating that hydrogen absorption in polymers with polar groups accelerates embrittlement and degradation [315].

For Silicon, the decline in tensile strength is severe across the pressure range, showing a reduction of nearly 35% by 7500 psi. This substantial and consistent decrease can be explained by Silicon's inability to withstand hydrogen-induced microstructural changes. Being a brittle material, Silicon is less capable of accommodating the swelling and plasticization that takes place as hydrogen diffuses into its structure. Previous research indicates that hydrogen exposure can lead to micro-void formation and molecular disruptions, particularly in materials with low elasticity, which likely exacerbates the degradation in Silicon's tensile properties. This observation is supported by earlier studies demonstrating that hydrogen-induced embrittlement and swelling cause significant degradation in tensile strength, particularly in materials with inherently lower resistance to structural deformation under stress [314, 316].

EPDM, in contrast, exhibits the lowest reduction in tensile strength among the three materials, with a maximum decline of around 10% by 7500 psi. EPDM's relative stability under hydrogen exposure can be explained by its flexible, cross-linked molecular structure, which is more resistant to hydrogen-induced embrittlement. While hydrogen does permeate EPDM, leading to some swelling, its structure allows it to accommodate these changes with minimal degradation in mechanical strength. The comparatively mild reduction in tensile strength suggests that EPDM's

cross-linked network is less susceptible to hydrogen-induced weakening, maintaining structural integrity more effectively than NBR and Silicon. This aligns with findings from studies indicating that EPDM and similar elastomers exhibit lower permeability to hydrogen and maintain better mechanical stability under high-pressure conditions [314, 317].

Several studies have investigated how hydrogen exposure affects the tensile strength of polymer materials. In an in situ tensile test apparatus study for high-pressure hydrogen environments, HDPE samples were exposed to pressures as high as 35 MPa (5000 psi), revealing substantial changes in tensile behavior. The results showed that hydrogen exposure caused significant reductions in tensile strength due to the embrittlement and degradation of the polymer matrix.[315]. Pagnotta et al. (2024) explored how hydrogen permeability affects the mechanical integrity of polymers used in hydrogen storage systems. This study discussed the swelling and embrittlement of polymers when exposed to high-pressure hydrogen, leading to a weakening of tensile strength [314]. Elastomers are particularly susceptible to this effect due to hydrogen's ability to penetrate their flexible molecular structures, causing a breakdown of cross-linking and mechanical weakening [314]. San Marchi et al. provides insight into hydrogen-induced tensile strength reductions. The researchers observed that hydrogen embrittlement resulted in significant reductions in tensile strength, primarily due to hydrogen's interaction with dislocations and grain boundaries, leading to microcracks and structural degradation. While metals and polymers differ in their specific embrittlement mechanisms, the overall impact of hydrogen diffusion—weakening tensile properties—parallels what is observed in polymers under high-pressure hydrogen environment [316]. Polymers such as NBR, EPDM, and silicon, which are used in sealing applications, are particularly vulnerable due to their high permeability to hydrogen and subsequent

swelling, which weakens their mechanical strength [317]. Thus, the current investigation observed the trend of declining tensile strength across the three materials under increasing hydrogen pressure which suggest the cumulative effects of hydrogen embrittlement, swelling, and disruption of molecular structures. NBR and Silicon experience greater degradation due to their respective susceptibilities to hydrogen-induced weakening, while EPDM demonstrates more resistance, making it potentially more suitable for applications where exposure to high-pressure hydrogen is expected [316].

6.5. Analysis of Impact of Aging on Morphology

The morphology has been studied in terms of crack and cavity analysis across the different materials following the procedure mentioned at Chapter 5 (Section 5.4.5).

6.5.1. Crack Analysis of NBR

The set of images in Figure 6.9 for NBR samples illustrates the morphological changes and crack propagation under increasing hydrogen pressure using SEM (Scanning Electron Microscopy). Each row of images corresponds to a particular pressure level and contains three distinct views: (1) the original SEM image, (2) the Hough Transform edge detection, and (3) the refined crack detection. Original SEM Images represent the raw morphology of NBR samples at different hydrogen pressures, starting from 0 psi and increasing up to 7500 psi. In the initial stages (0 and 500 psi), the surface appears relatively smooth with fewer visible cracks. However, as the pressure increases the surface roughness and defects become more evident. By 7500 psi, significant crack development and surface damage is more visible, indicating significant material degradation due to the absorption of hydrogen at elevated pressures.

The original images are considered as a baseline for understanding how hydrogen pressure influences the formation of cracks and cavities on the surface. Hough Transform (Edge Detection) shows the edges and boundaries of the cracks within each SEM image using canny edge detection technique. This identifies continuous edges that likely represent cracks or surface defects. At lower pressures (0 psi), fewer edges are detected in fresh NBR seal, suggesting the inherent surface damage.

As the pressure increases, particularly beyond 1500 psi, more pronounced and elaborate edges are detected, indicating the formation of microcracks and surface discontinuities. The increase in detected edges with pressure suggest the complexity of the crack network and surface degradation in the NBR samples. Refined Crack Detection method further enhances the visibility of the cracks by focusing on regions where the cracks are more defined using image contrast enhancement and noise reduction through Gaussian smoothing. At higher pressures, especially beyond 1500 psi, the number and size of cracks become more evident. Images at 5000 and 7500 psi, we observed a complex crack network formation, suggesting that hydrogen-induced material failure is progressing for NBR with increased pressure.

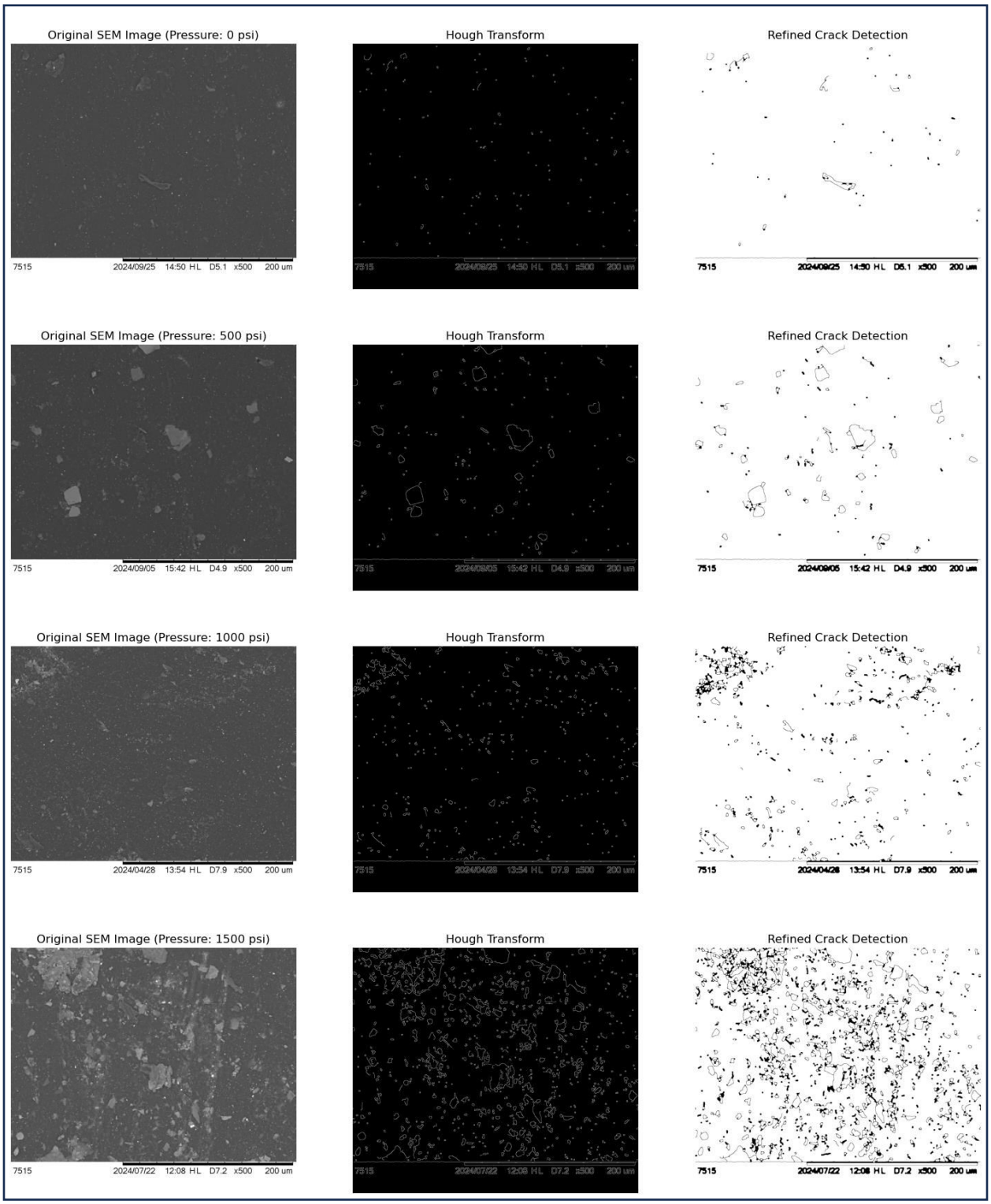
Original SEM Image (Pressure: 0 psi)
Hough Transform
Refined Crack Detection
7515 2024/09/25 14:50 HL D5.1 x500 200 um
Original SEM Image (Pressure: 500 psi)
Hough Transform
Refined Crack Detection
7515 2024/09/05 15:42 HL D4.9 x500 200 um
Original SEM Image (Pressure: 1000 psi)
Hough Transform
Refined Crack Detection
7515 2024/04/28 13:54 HL D7.9 x500 200 um
Original SEM Image (Pressure: 1500 psi)
Hough Transform
Refined Crack Detection
7515 2024/07/22 12:08 HL D7.2 x500 200 um

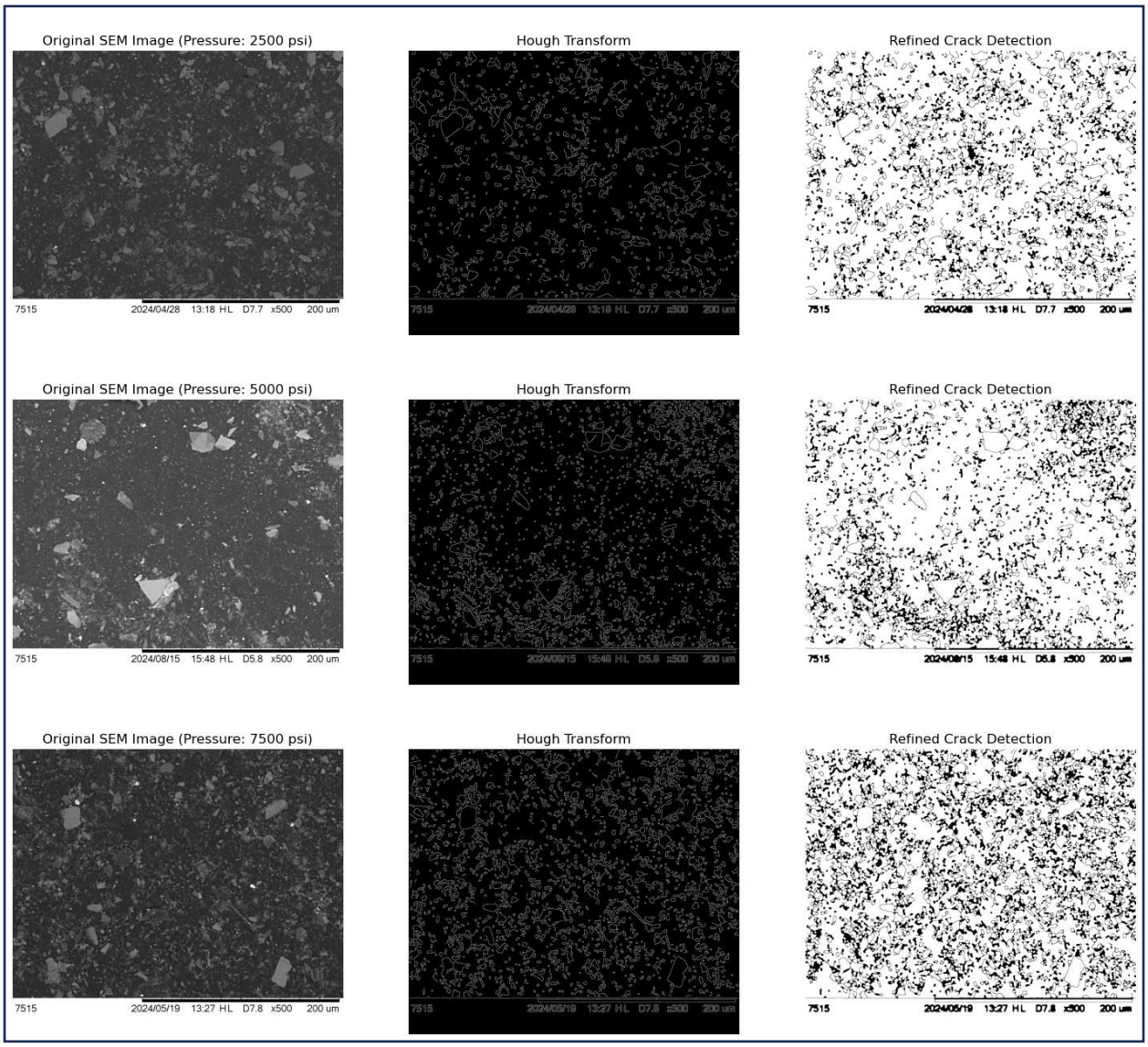

Figure 6. 9: Crack detection analysis of NBR polymer with hydrogen aging pressure

In order to have better understanding about the propagation of cracks through NBR, all the refined cracks are plotted together at Figure 6.10 where the cracks are isolated with respect to different pressure and presented in parallel.

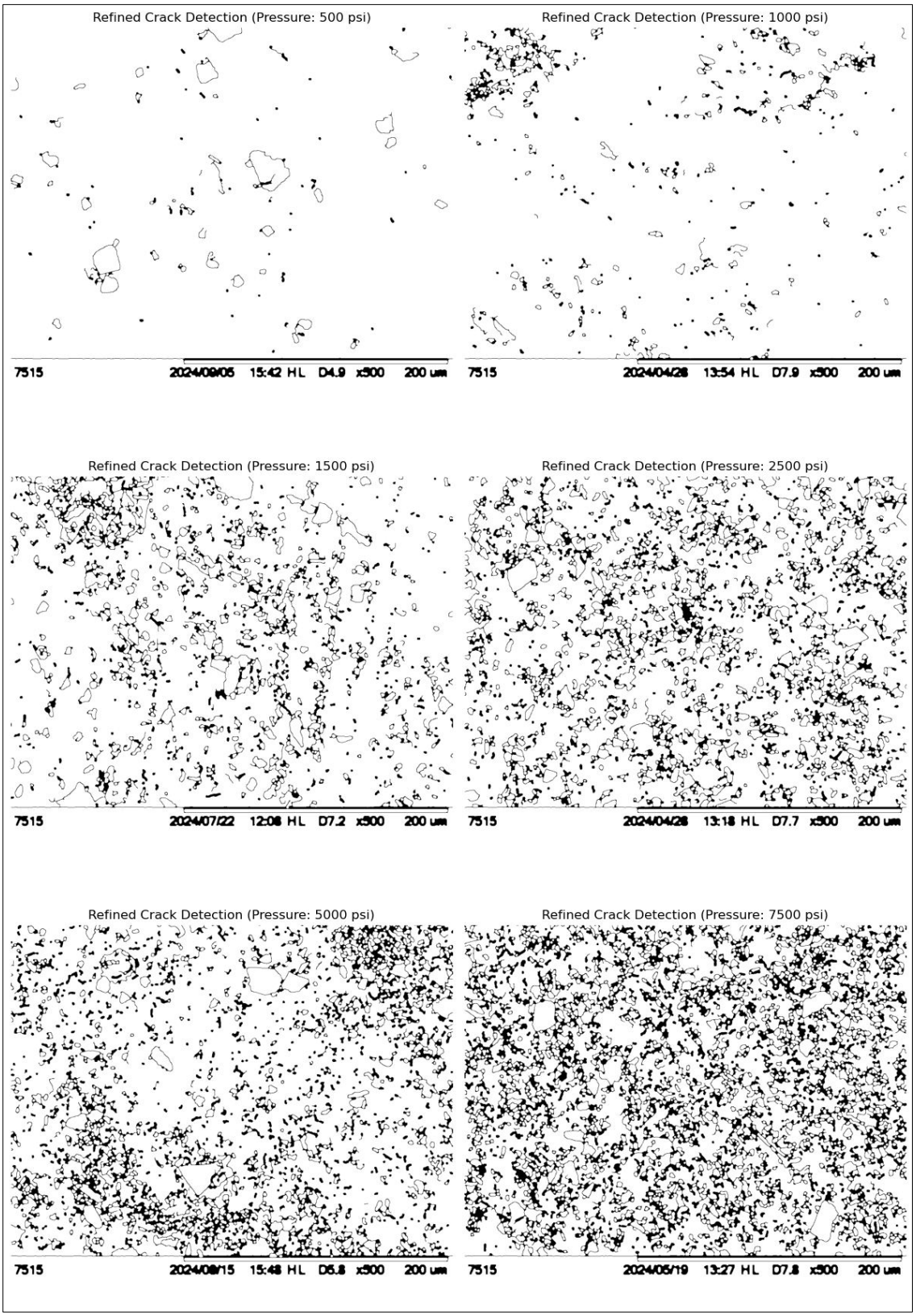

Figure 6. 10: Propagation of refined cracks with hydrogen pressure across NBR

6.5.2. Cavity Analysis of NBR

The set of images provided at Figure 6.11 illustrates the detection of cavities in NBR samples subjected to varying hydrogen pressures using cavity detection algorithms on SEM images. Each row of images showing the cavity detection result corresponds to a particular pressure level. Detected cavities are outlined in red, showing the areas where the surface shows probability of structural degradation or void formation. At low pressure (0 psi), there are very few cavities, indicating minimal surface degradation. However, at 500 psi and beyond, the cavity count start increases, and the detection becomes more extensive. The algorithm identifies a large number of small cavities as well as a few larger ones, especially at 500 psi and 1500 psi. As pressure increases to 5000 psi and 7500 psi, the surface is densely covered with detected cavities, suggesting significant surface damage due to the high pressure of hydrogen exposure. The progression from lower to higher pressures shows a correlation between increased hydrogen pressure and the formation of cavities on the NBR surface. The cavity density becomes more evident as pressure increases may lead to material degradation. The increase in cavities at higher pressures suggests that hydrogen permeation into the material results in the creation of voids or defects, impacting the material's performance as a sealing material. The detected cavities provide a quantitative measure of how the material deteriorates under increasing hydrogen pressure. As seen in the higher-pressure samples (5000 psi and 7500 psi), the surface becomes saturated with cavities, indicating that the material's inability to maintain a solid, cohesive surface integrity.

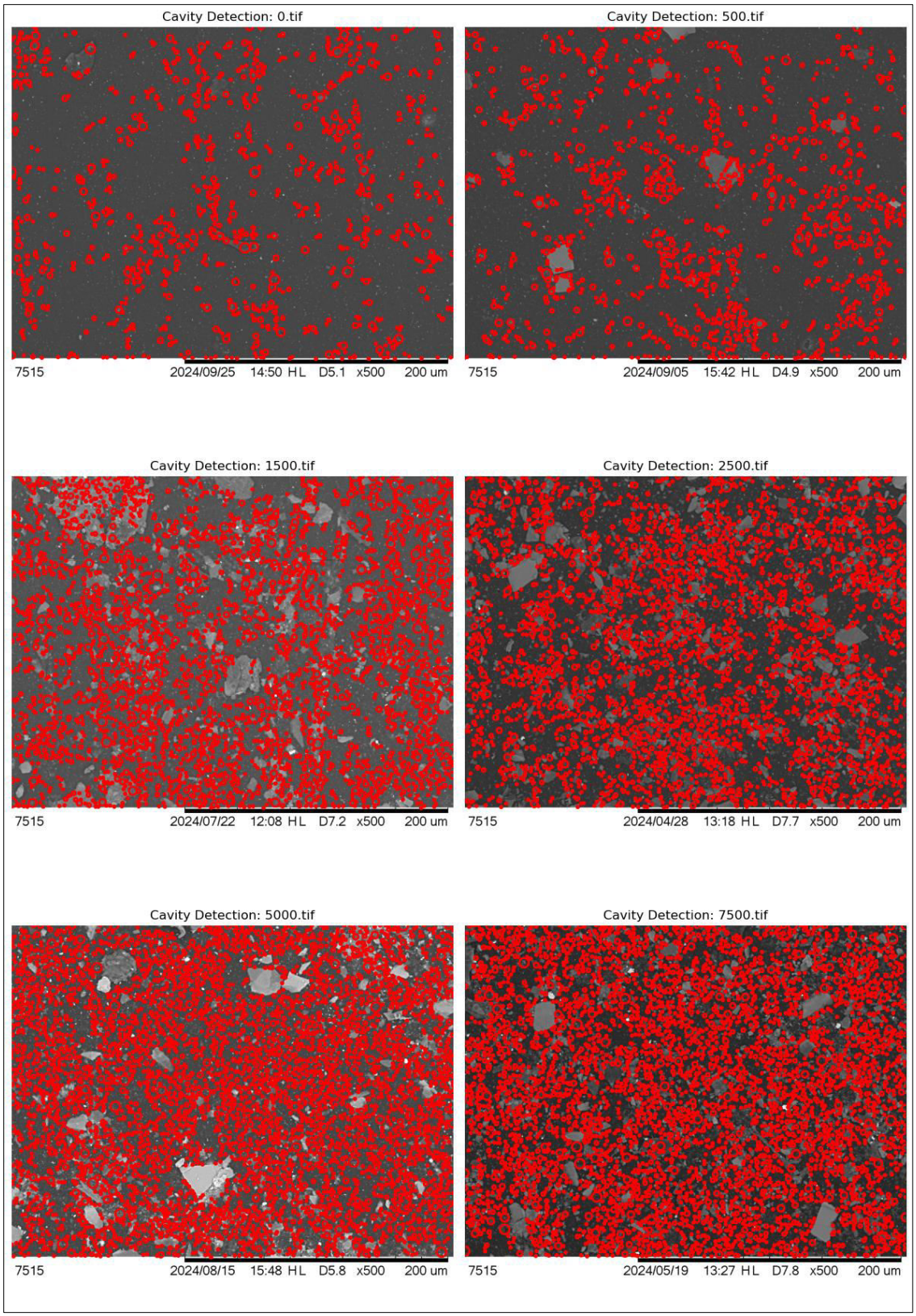

Figure 6. 11: Cavity analysis for NBR with hydrogen aging pressure

6.5.3. Crack Analysis of EPDM

The crack analysis at Figure-6.12 for EPDM under increasing hydrogen pressures from 0 psi to 7500 psi shows a clear progression of surface degradation. At 0 psi, the original image shows a relatively uniform surface with minor irregularities, and both the Hough Transform and refined crack detection methods indicate minimal surface defects, suggesting that the material is largely undamaged. As pressure increases to 500 psi, visible surface changes start to appear, with more edges and cracks detected, indicating the early stages of material degradation. By 1000 psi, the surface roughness intensifies, and the number of detected edges increases considerably, showing a higher level of crack formation and more defined surface irregularities. At 1500 psi, the surface becomes more complex, with an increasing density of cracks, suggesting more degradation as the cracks become interconnected. By 2500 psi, the surface deterioration is significant, with a denser network of cracks and extensive material breakdown visible in both the Hough Transform and refined crack detection images. The progression continues at 5000 psi, where the surface becomes highly irregular and uneven, filled with a dense network of cracks, indicating severe degradation from hydrogen exposure. Finally, at 7500 psi, the surface shows maximum roughness and damage, with an extensive network of cracks covering most of the surface, suggesting tend to material failure. Throughout this analysis, the images clearly show that as hydrogen pressure increases, the extent of surface damage and crack formation in EPDM intensifies, leading to significant structural degradation, particularly at pressures above 1500 psi.

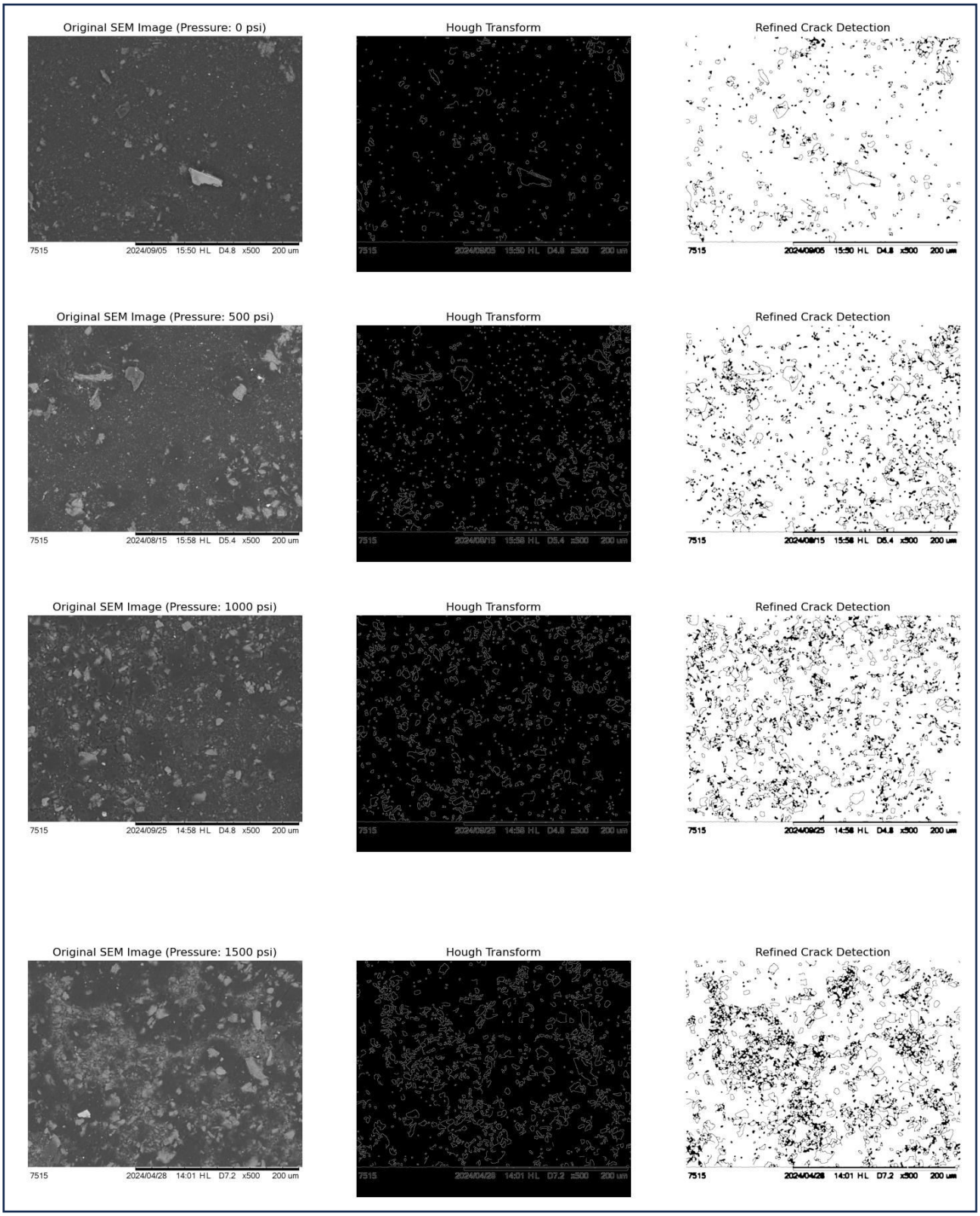
Original SEM Image (Pressure: 0 psi)
Hough Transform
Refined Crack Detection
7515 2024/09/05 15:50 HL D4.8 x500 200 um
Original SEM Image (Pressure: 500 psi)
Hough Transform
Refined Crack Detection
7515 2024/08/15 15:58 HL D5.4 x500 200 um
Original SEM Image (Pressure: 1000 psi)
Hough Transform
Refined Crack Detection
7515 2024/09/25 14:58 HL D4.8 x500 200 um
Original SEM Image (Pressure: 1500 psi)
Hough Transform
Refined Crack Detection
7515 2024/04/28 14:01 HL D7.2 x500 200 um

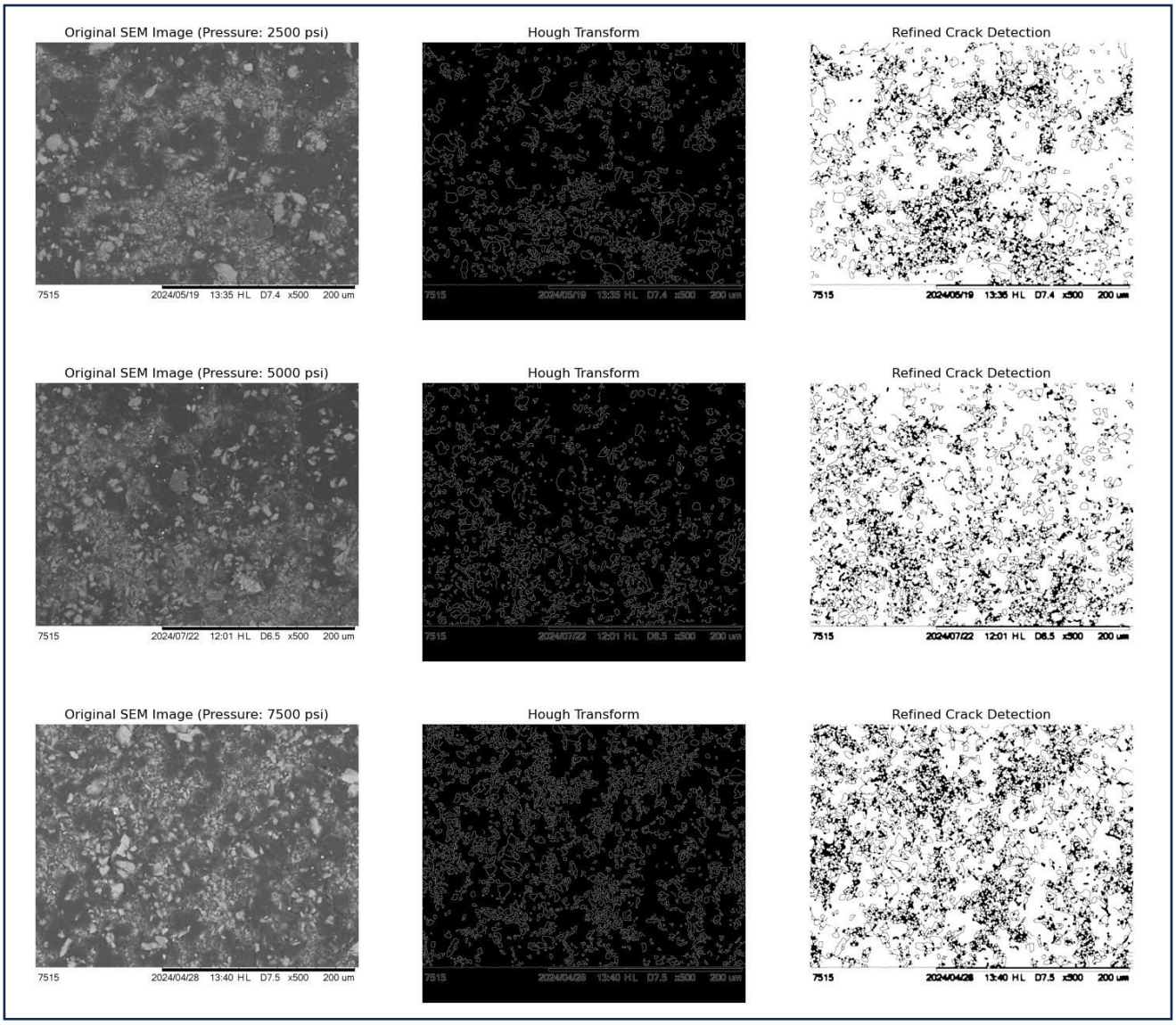

Figure 6.12: Crack detection analysis of EPDM polymer with hydrogen aging pressure

In order to have better understanding about the propagation of cracks through NBR, all the refined cracked are plotted together at Figure 6.13 where the cracks are isolated with respect to different pressure and presented in parallel.

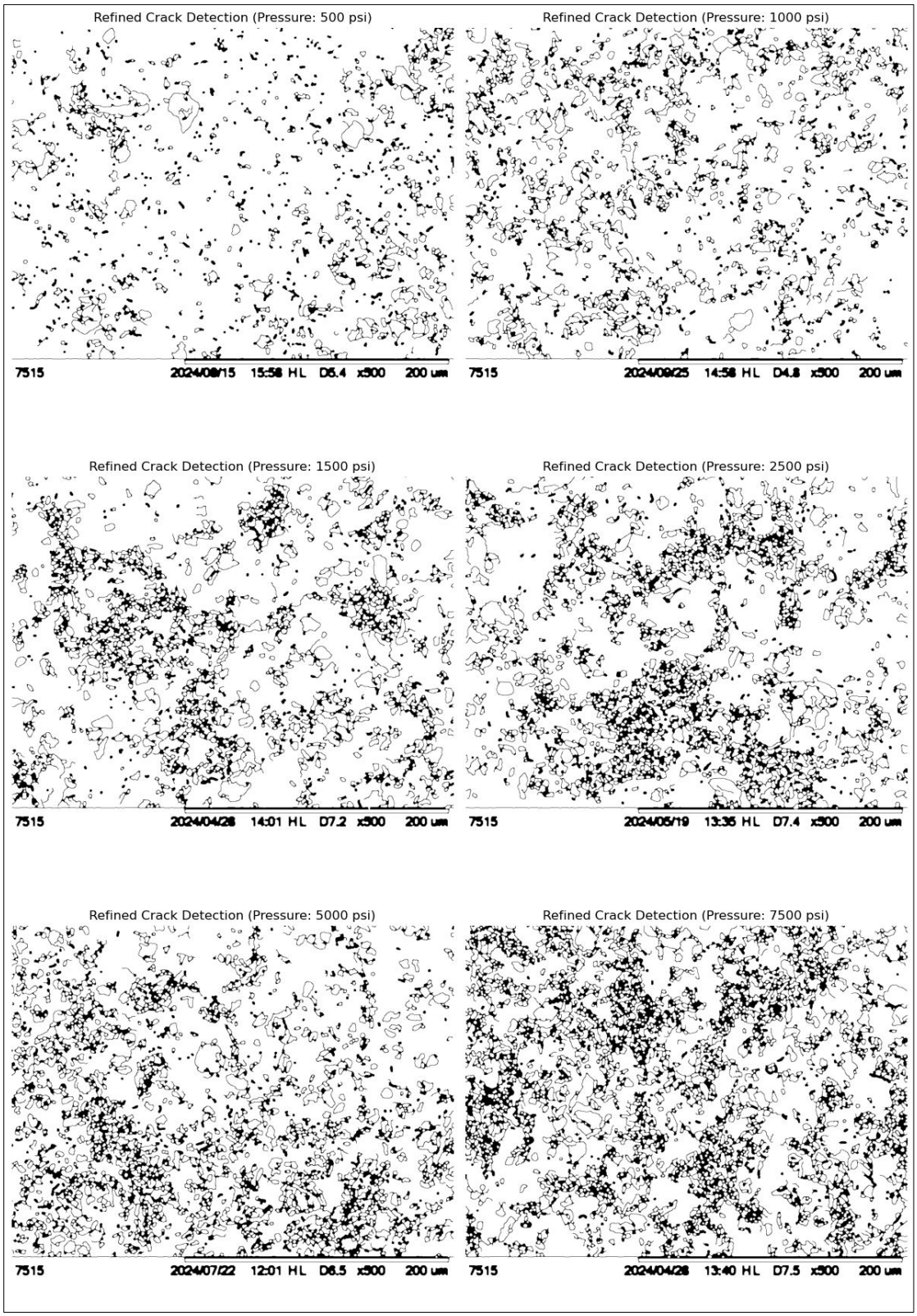

Figure 6. 13: Propagation of refined cracks with hydrogen pressure across EPDM

6.5.4. Cavity Analysis of EPDM

The cavity detection images for EPDM at Figure 6.14 show a clear progression of cavity formation as hydrogen pressure increases from 0 psi to 7500 psi. At 0 psi, the original image appears relatively smooth with minimal surface irregularities, and the cavity detection shows few cavities, indicating that the material is largely undamaged without significant voids. As the pressure increases to 500 psi, more surface irregularities become visible in the original image, and cavity detection shows a significant increase in small cavities, indicating the onset of material degradation. At 1000 psi, the surface roughness intensifies, and the cavity detection reveals a much denser network of cavities, suggesting that hydrogen exposure is beginning to cause more widespread damage.

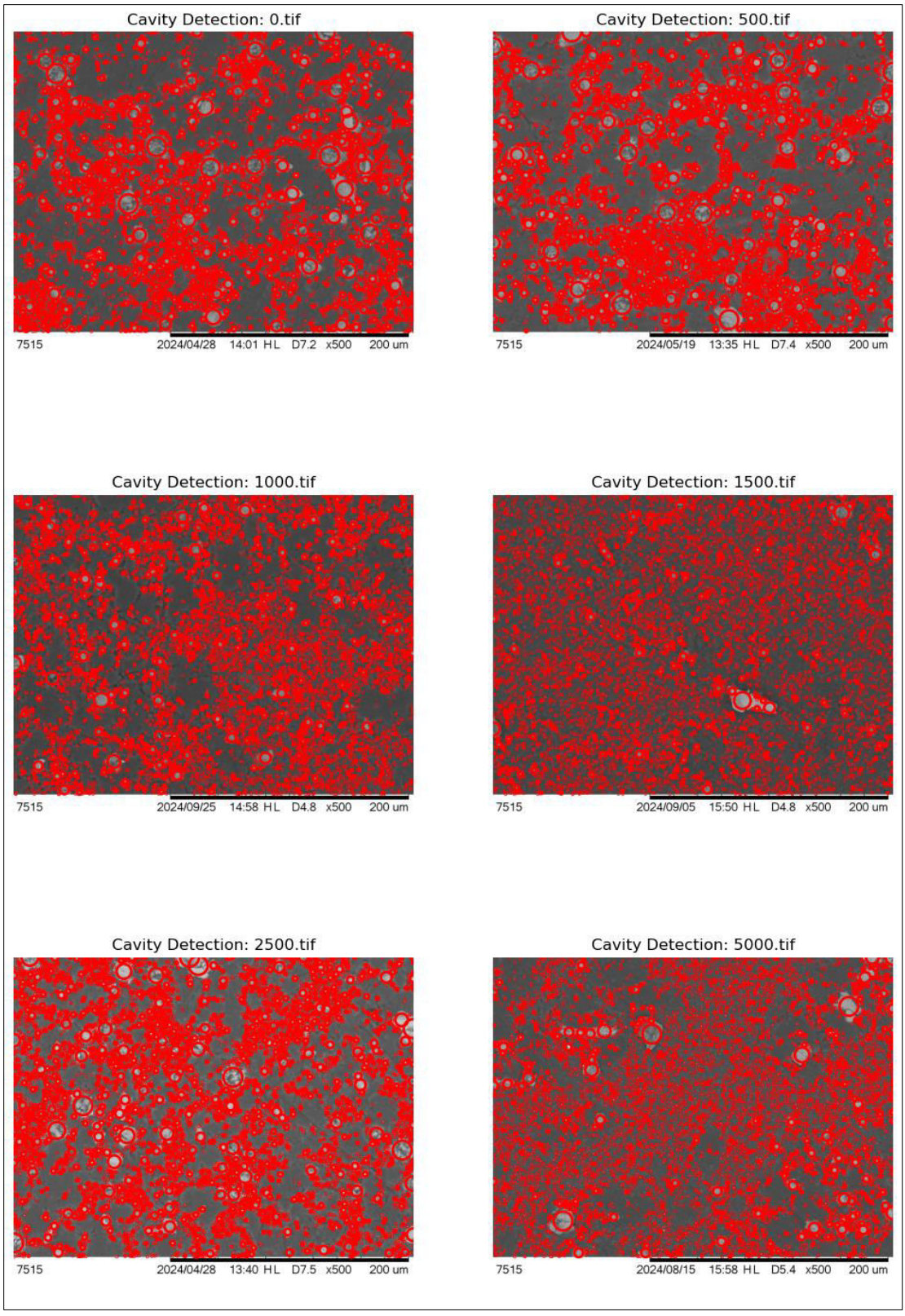

Figure 6. 14: Cavity analysis for EPDM with hydrogen aging pressure

6.5.5. Crack Analysis of Silicon

The crack analysis for silicon under various pressures (0 psi to 7000 psi) at Figure 6.15 shows a similar pattern of surface degradation with increasing hydrogen exposure. At 0 psi, the original image shows fewer surface irregularities, with a relatively smooth appearance. Though at 0 psi the refined crack detection shows the presence of noticeable cracks, which are further identified using Hough Transform. This suggests that the silicon samples may have inherent material defects or residual stresses from processing. However, as pressure increases to 500 psi, the surface features become more pronounced, with more edges detected, though the cracks are still relatively small and less interconnected. By 1000 psi, the surface becomes more complex, and there is a notable increase in the density of cracks detected, indicating that silicon begins to experience more significant surface damage at this pressure. At 1500 psi, the cracks are more numerous and interconnected, reflecting a denser network of surface degradation. This trend continues at 2500 psi, where the surface appears rougher, and the crack network becomes increasingly complex. At 7000 psi, the refined crack detection shows a saturated surface with numerous, well-defined cracks, leading to material failure. This analysis suggest that silicon begins to degrade significantly under hydrogen pressure beyond 1000 psi, and by 7000 psi, the material shows signs of severe structural degradation. The observation of crack propagation with increasing pressure is expected, given silicon's brittle nature and its limited capacity for plastic deformation. Silicon is highly susceptible to brittle fracture. Therefore, once micro-cracks are initiated, these can grow rapidly under applied stresses. This align with the trend of current research that the cracks become more interconnected and extensive as pressure escalates from 1000 psi to 7000 psi [325].

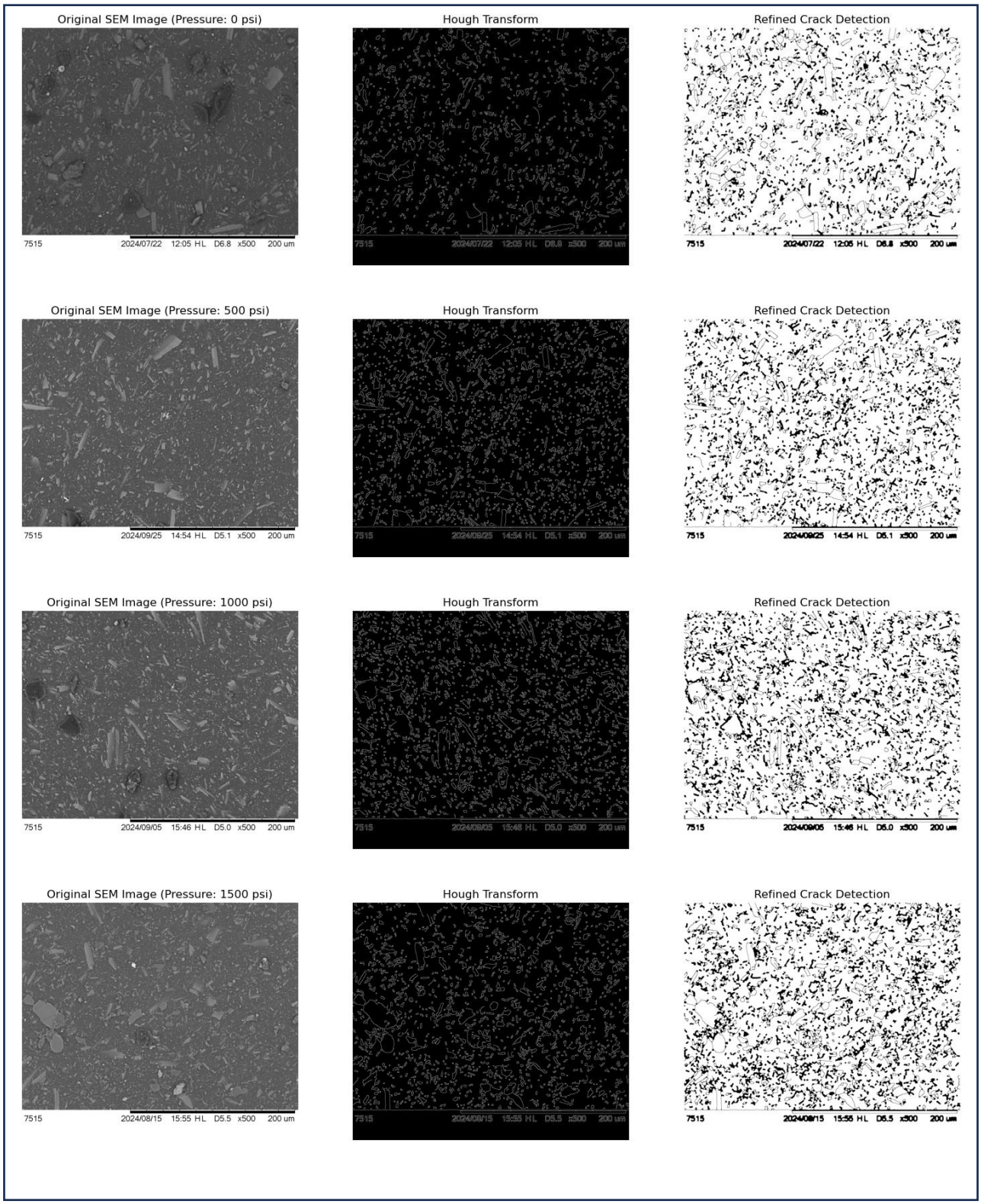
Original SEM Image (Pressure: 0 psi)
Hough Transform
Refined Crack Detection
Original SEM Image (Pressure: 500 psi)
Hough Transform
Refined Crack Detection
Original SEM Image (Pressure: 1000 psi)
Hough Transform
Refined Crack Detection
Original SEM Image (Pressure: 1500 psi)
Hough Transform
Refined Crack Detection

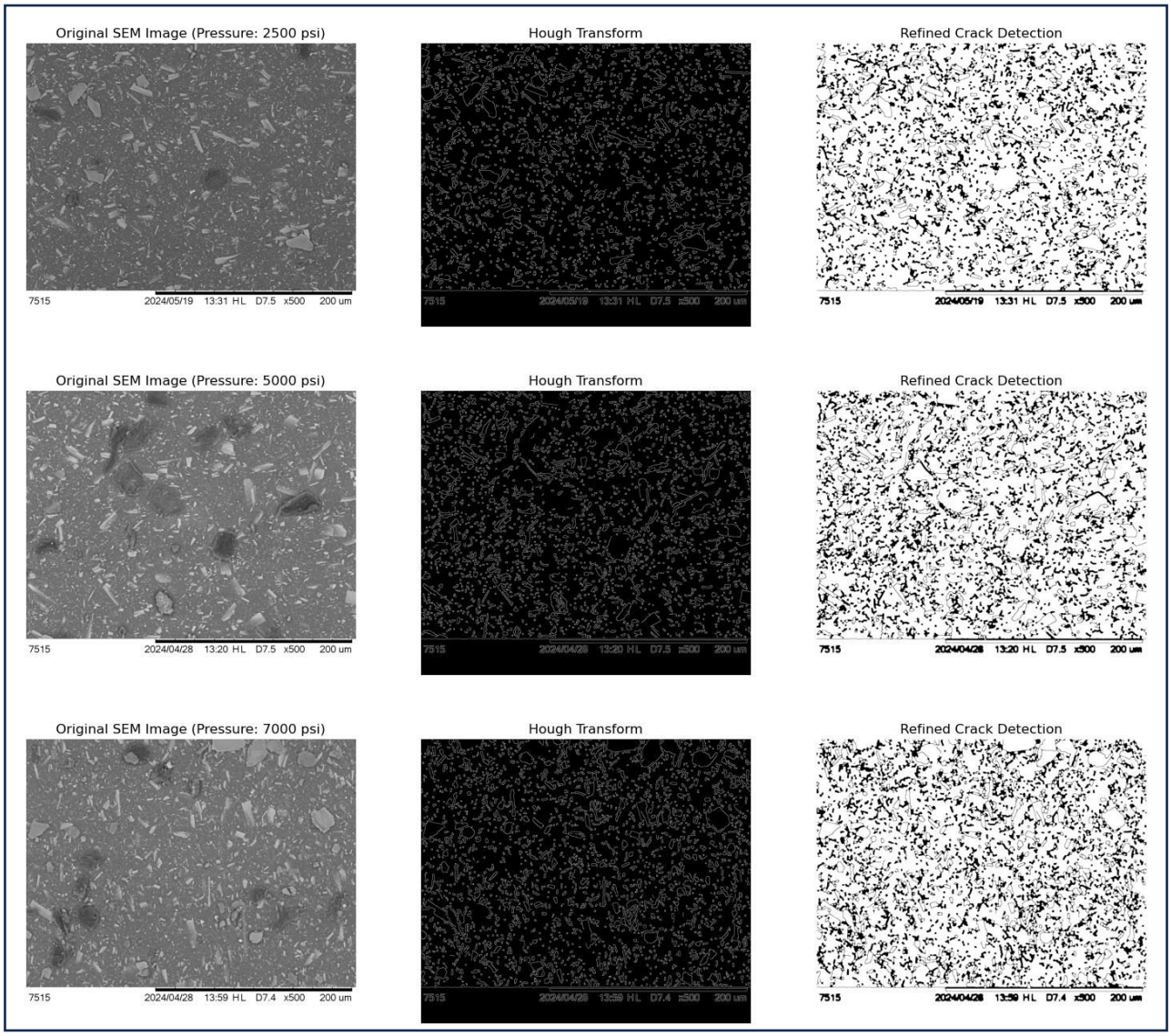

Figure 6. 15: Crack analysis for Silicon with hydrogen aging pressure

In order to have better understanding about the propagation of cracks through Silicon, all the refined cracks are plotted together at Figure 6.16 where the cracks are isolated with respect to different pressure and presented in parallel.

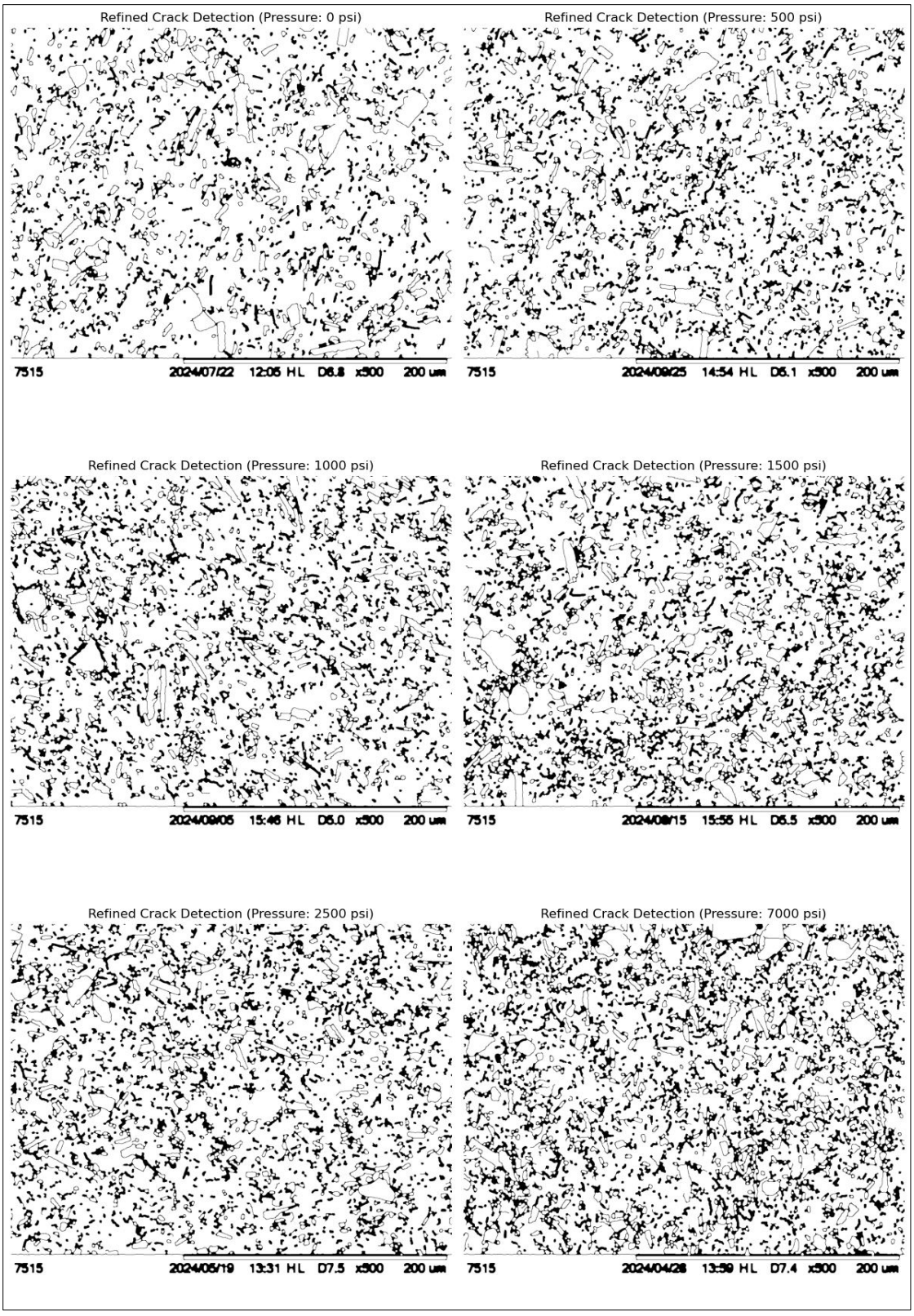

Figure 6. 16: Propagation of refined cracks with hydrogen pressure across Silicon

6.5.6. Cavity Analysis for Silicon

Figure 6.17 shows the cavity detection analysis of silicon across increasing pressures up-to 7000 psi. The images demonstrate a consistent trend of cavity formation, with a visible increase in the number of cavities as the hydrogen pressure increases. The images state that at low pressures (0 and 500 psi), cavities are fewer and more evenly distributed, while at higher pressures (2500 psi and beyond), the density of cavities becomes significantly higher, indicating a pressure-dependent degradation mechanism.

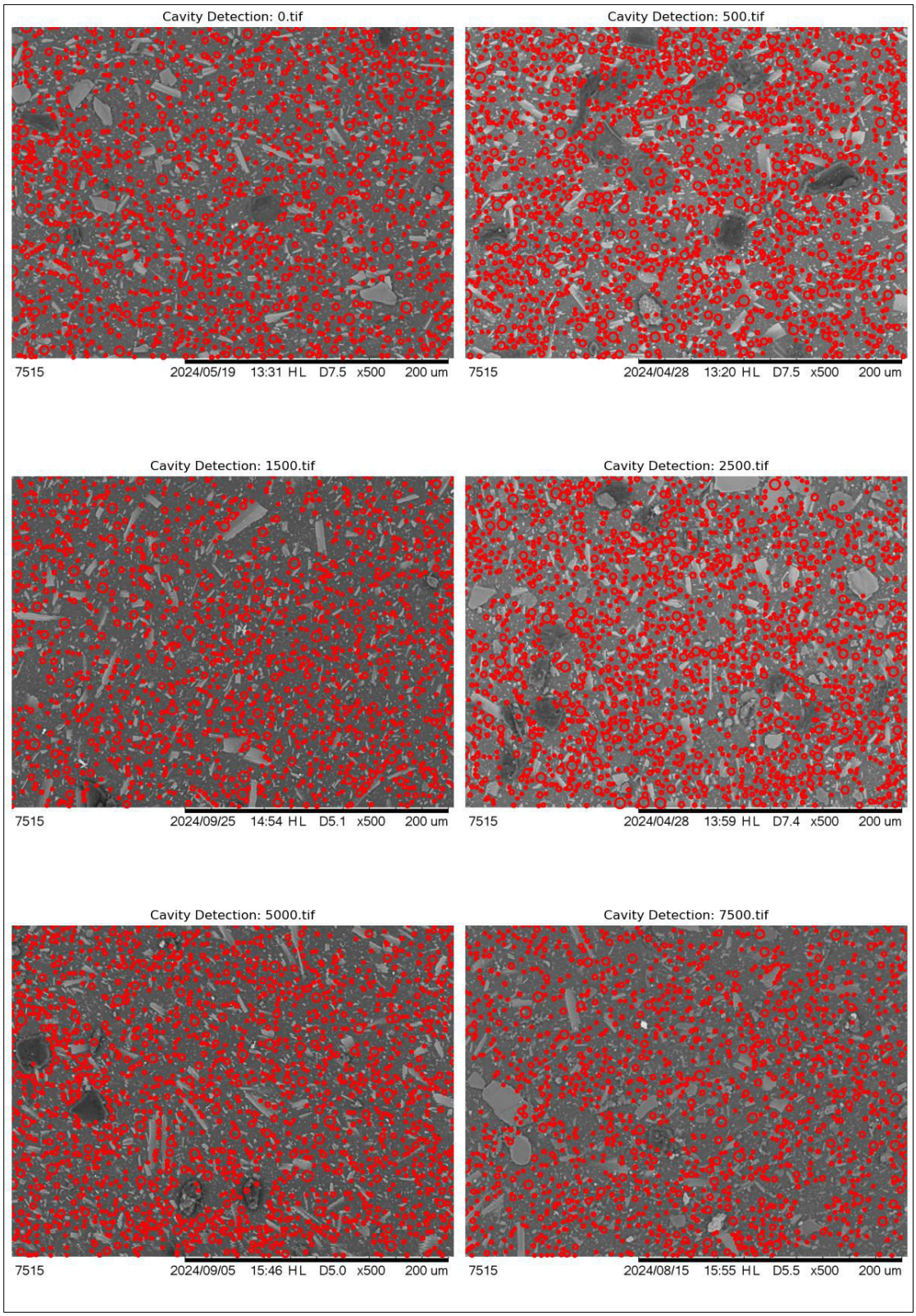

Figure 6. 17: Cavity analysis for Silicon with hydrogen aging pressure

The cavities seem uniformly circular, suggesting that hydrogen diffusion likely leads to gas-induced void formation. The relatively larger cavity size and greater density at higher pressures, particularly at 5000 and 7500 psi, indicate increased material degradation due to the buildup of internal stresses and gas diffusion effects.

6.5.7. Comparative Analysis for Crack and Cavity Across the Polymers

The crack growth across sealing materials under hydrogen pressure, as shown in Figure 6.18 and Figure 6.19, reveals distinct behaviors for each material. Silicon consistently shows the highest absolute crack count across all pressures, starting at over 400 cracks at its inherent state and increasing steadily to more than 800 cracks by 7500 psi. This high baseline and gradual rise indicate that Silicon is susceptible to significant crack formation even at lower pressures, suggesting a lack of resistance to hydrogen-induced cracking from the beginning. In contrast, NBR consist of comparatively low crack count (around 200) at 0 unaged condition but exhibits a significant increase in crack numbers as pressure rises, reaching to around 947% increase by 7500 psi. This sharp relative increase emphasizes NBR's change of morphology to hydrogen aging, where initial structural stability is rapidly degraded under higher pressures, even though its absolute crack count remains lower than that of Silicon. EPDM shows an intermediate behavior, starting with around 200 cracks at 0 psi and increasing to approximately 450 cracks at 7500 psi. EPDM's percentage increase in crack count remains relatively moderate at around 118%, reflecting a more gradual accumulation of damage compared to NBR. This suggests that while EPDM is susceptible to crack formation, its semi-rigid structure provides the resistance to accommodate rapid deterioration under hydrogen pressure, unlike NBR's sharp escalation in crack growth. The percentage increase plot in Figure 6.19 clarifies these trends: NBR experiences the

most pronounced percentage increase (947%), indicating a high sensitivity to pressure-induced damage, followed by EPDM at 118%, and Silicon with the smallest relative increase at 37% though silicon shows a significant number of cracks from its inherent phase. These differences suggest that, while silicon shows a lower rate of increase of crack formation than NBR, it has the most extensive absolute crack formation. On the contrary at lower pressure zone, NBR shows much resistance to crack formation on lower pressure zone by hydrogen. The EPDM was observed optimizing the crack formation and propagation across the lower to high pressure zone of hydrogen.

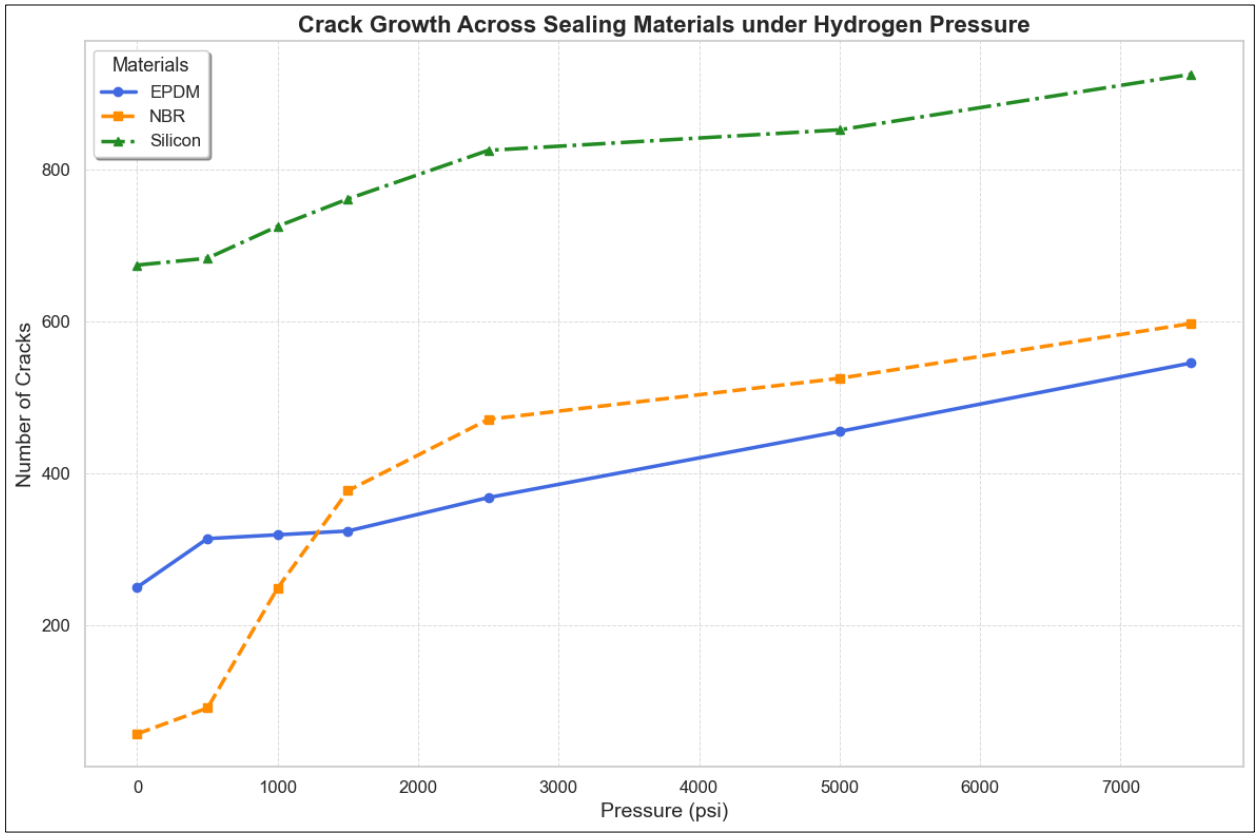

Figure 6. 18: Crack count and percent change across the material with hydrogen pressure

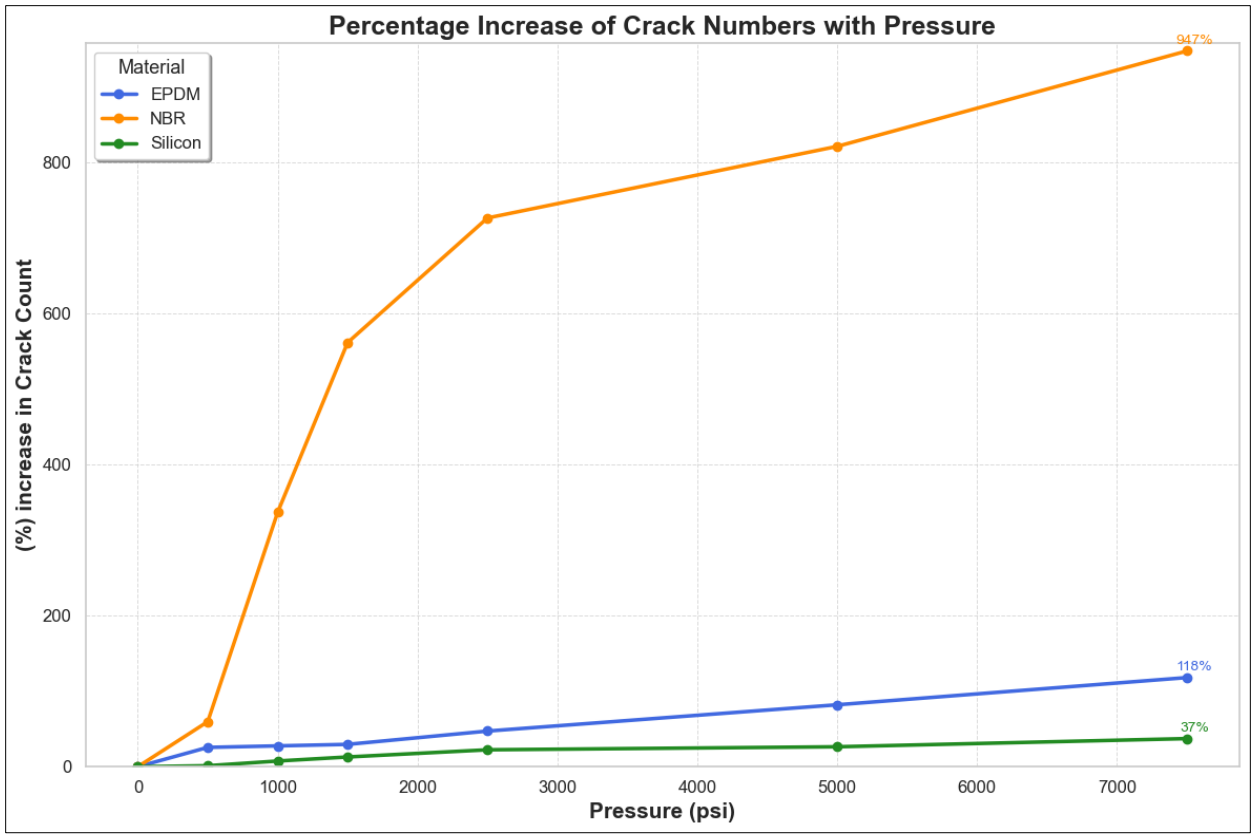

Figure 6. 19: Crack percent change across the material with hydrogen pressure

The cavity growth trends across sealing materials under hydrogen pressure, as illustrated in Figure 6.20 and Figure 6.21, show distinct behaviors for each sealing sample in terms of absolute counts and percentage increases of cavity respectively. Silicon exhibits the highest cavity count at all pressure levels, starting with over 3000 cavities at 0 psi and gradually rising to more than 4500 cavities by 7500 psi. This high baseline and moderate increase indicate that Silicon is inherently more susceptible to cavity formation but experiences relatively controlled growth with pressure, as seen by its percentage increase of closely 43%. This suggests that, while Silicon has a high tendency for initial void formation, it demonstrates stability in further cavity development under elevated pressures.

NBR shows a different pattern, beginning with the lowest absolute cavity count around 1000 at 0 psi, but experiencing a sharp rise with increasing pressure, reaching over 3000 cavities by 7500 psi. This represents a 322% increase relative to its initial count, indicating that NBR's structure is highly sensitive to pressure-induced cavity formation. Despite starting with fewer cavities, NBR undergoes rapid morphological changes, which may be explained as higher rate of degradation under prolonged high-pressure conditions.

EPDM maintains a consistent behavior, with an initial cavity count around 2500 at 0 psi, rising to approximately 3500 cavities by 7500 psi. This corresponds to a moderate percentage increase of 72%, suggesting a balanced resistance to cavity formation compared to NBR's rapid increase and Silicon's stable high count. EPDM's semi-rigid structure appears to resist rapid cavity expansion, although it does experience steady accumulation under increasing pressure. These observations suggest the optimization in material selection for hydrogen sealing applications. While silicon's incremental growth remains controlled, it has a high initial cavity count making it less potential for hydrogen exposure. NBR, despite starting with fewer cavities, shows a sharp increase under pressure, suggesting susceptibility to hydrogen-induced void formation. EPDM offers moderate resistance, balancing stability with a relatively modest cavity count increase.

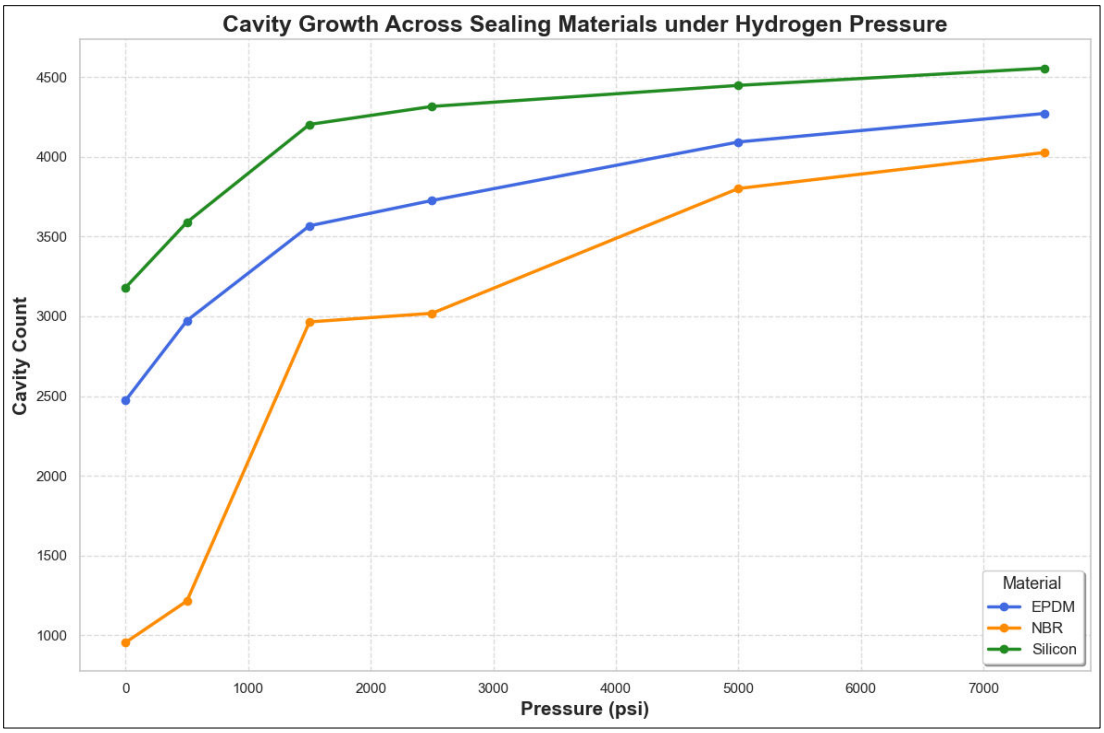

Figure 6. 20: Cavity count across the material with hydrogen pressure

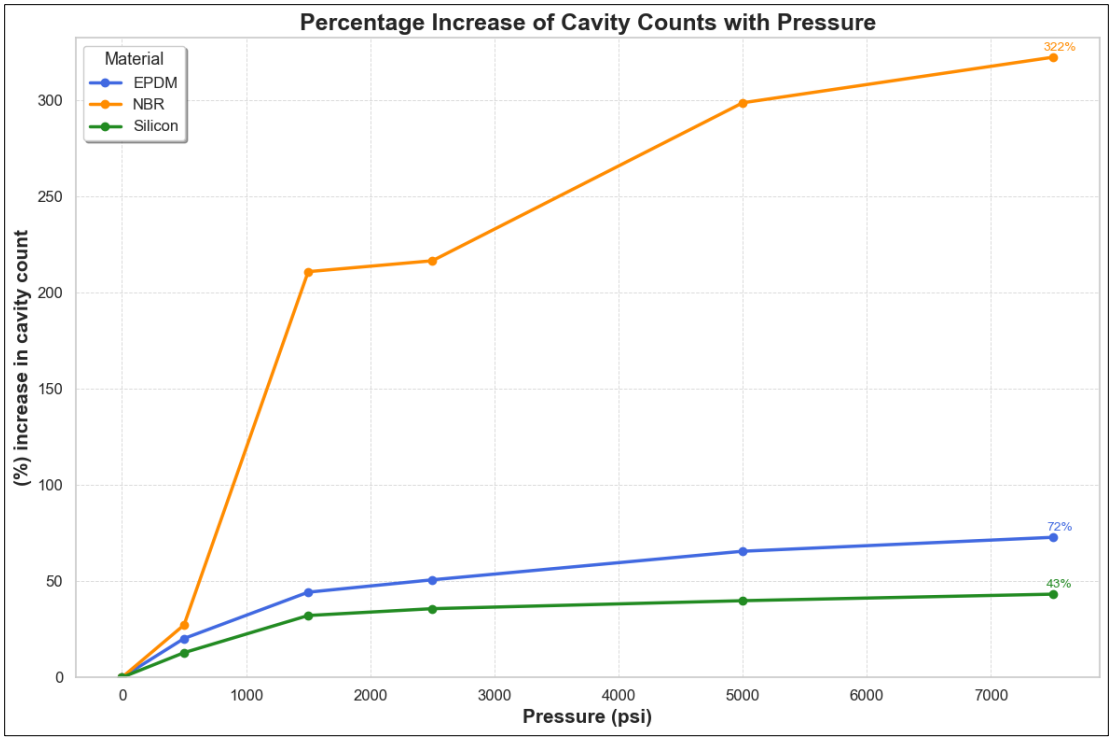

Figure 6. 21: Cavity count percent change across the material with hydrogen pressure

6.5.7.1. Comparison of crack size distribution among sealing samples

The crack size distribution for NBR, EPDM, and Silicon under varying hydrogen pressures is depicted in Figure 6.22. Silicon displays a stable median crack size across pressures, consistent with its brittleness. However, the number and size of outlier cracks increase significantly, especially at pressures above 1000 psi, with some reaching over 300 pixels by 7500 psi. This trend suggests that while Silicon's typical crack size remains steady, hydrogen exposure under high pressure promotes the formation of intermittent larger cracks, likely due to rapid crack propagation in a brittle matrix, as supported by Kulkarni et al. on polymer embrittlement in hydrogen environments [313, 325]. EPDM also maintains a stable median crack size, but larger outliers begin to appear at lower pressures at around 1000 psi, with crack sizes reaching up to 500 pixels by 7500 psi. The increased variability indicates that hydrogen permeation leads to larger crack formation, especially under prolonged exposure. This observation aligns with Junichiro et al.'s findings on hydrogen-induced bubble formation in EPDM, where microvoids coalesce into larger defects under elevated pressures [197, 324]. Research on elastomer degradation under hydrogen pressure suggests that hydrogen permeation induces internal stresses that increase susceptibility to crack formation and growthNBR shows a relatively stable median crack size as well, but outlier crack sizes increase noticeably from 500 psi, with some cracks reaching nearly 500 pixels by 7500 psi. This suggests that NBR's structure initially resists crack propagation but becomes more susceptible as pressure rises, leading to rapid crack growth in isolated instances. A study by the Pacific Northwest National Laboratory (PNNL) on high-pressure hydrogen effects in rubber seals found that high cyclic pressures exacerbated crack expansion and blistering, supporting this observation for NBR [323].

Comparatively, Silicon has the highest frequency of large crack outliers, EPDM demonstrates moderate crack variability, and NBR shows rapid outlier growth under high pressure, suggesting differences in each material's resistance to crack propagation.

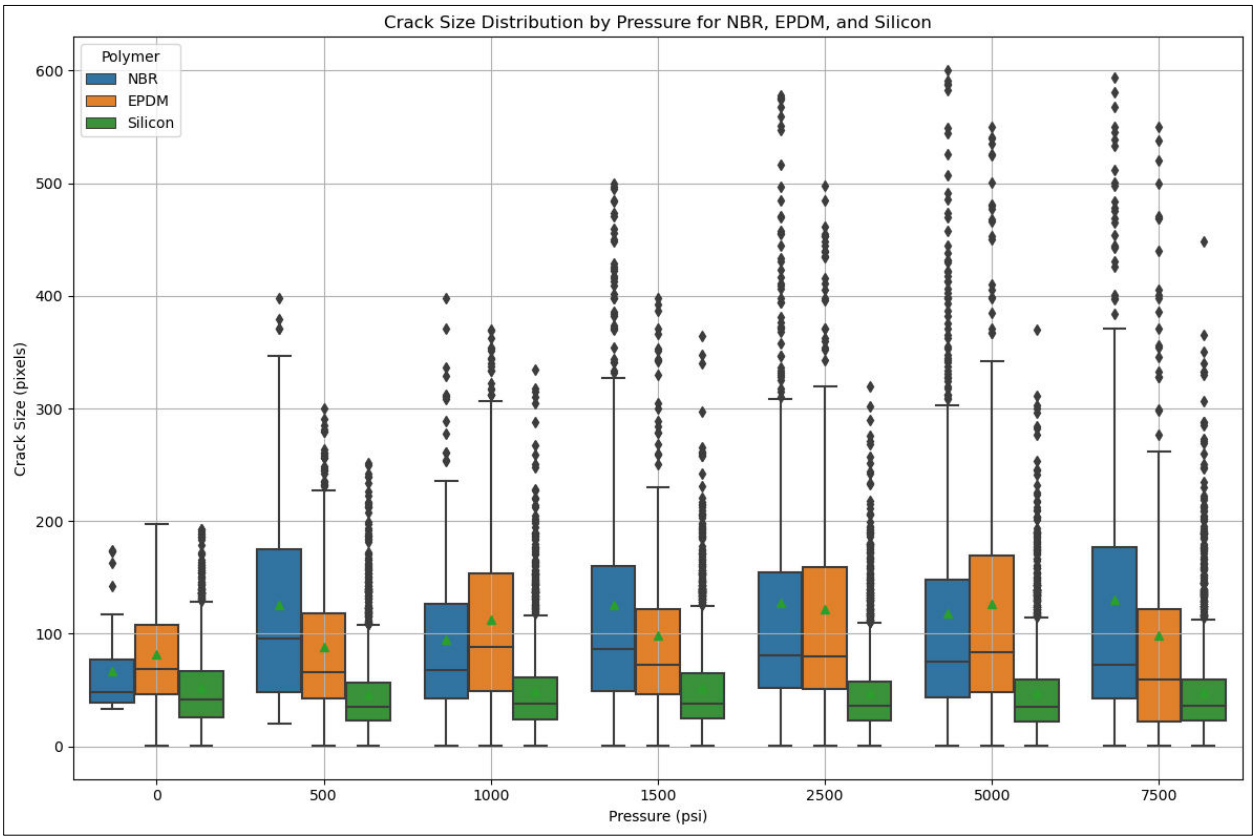

Figure 6. 22: Crack size distribution among sealing samples across the hydrogen pressure

Larger crack formation at elevated pressures across NBR, EPDM, and Silicon can be explained by possible hydrogen-induced embrittlement, stress concentration and microvoid coalescence. When polymers are exposed to high-pressure hydrogen, hydrogen molecules permeate the material, accumulating within microvoids and initiating cracks due to internal stress. At elevated pressures, this process may be intensified as hydrogen diffuses more, filling microvoids and creating higher localized stresses that promote crack growth and coalescence. For Silicon, its brittleness exacerbates crack propagation once cracks are initiated, leading to larger outliers in crack size.

EPDM, although more flexible, forms microvoids that combine under sustained pressure, allowing larger cracks to develop over time. NBR exhibits hydrogen-induced blistering and cracking due to repeated pressure cycles, where internal hydrogen pressure leads to rapid outlier growth in crack sizes under high-pressure conditions. These insights emphasizing the need for material selection based on both absolute resistance to initial cracking and stability under prolonged high-pressure hydrogen exposure, essential for hydrogen sealing applications.

6.5.7.2. Comparison of cavity size among sealing samples

Figure 6.23 and Figure 6.24 plots provide insights into the cavity size and cavity density distribution across NBR, EPDM, and Silicon under increasing hydrogen pressures. The cavity size distribution box plot at Figure 6.23 indicates that NBR exhibits the largest variation in cavity size, with a median around 4.0 and a wide interquartile range from 3.7 to 4.1, suggesting that NBR's structure is highly responsive to hydrogen-induced cavity expansion. This variability could be explained by hydrogen's tendency to induce blistering in elastomers like NBR, leading to larger and more diverse cavity sizes. In contrast, Silicon have narrower cavity size distributions, with the smallest median cavity size around 3.8. The range of cavity sizeee for EPDM falls in between NBR and silicon. EPDM cavity size range from 3.8 to 3.9 suggesting the resistance to cavity expansion under pressure. This consistency in cavity size for EPDM may result from the crosslink density that restricts cavity growth, as hydrogen diffusion is less likely to coalesce into larger voids in these materials.

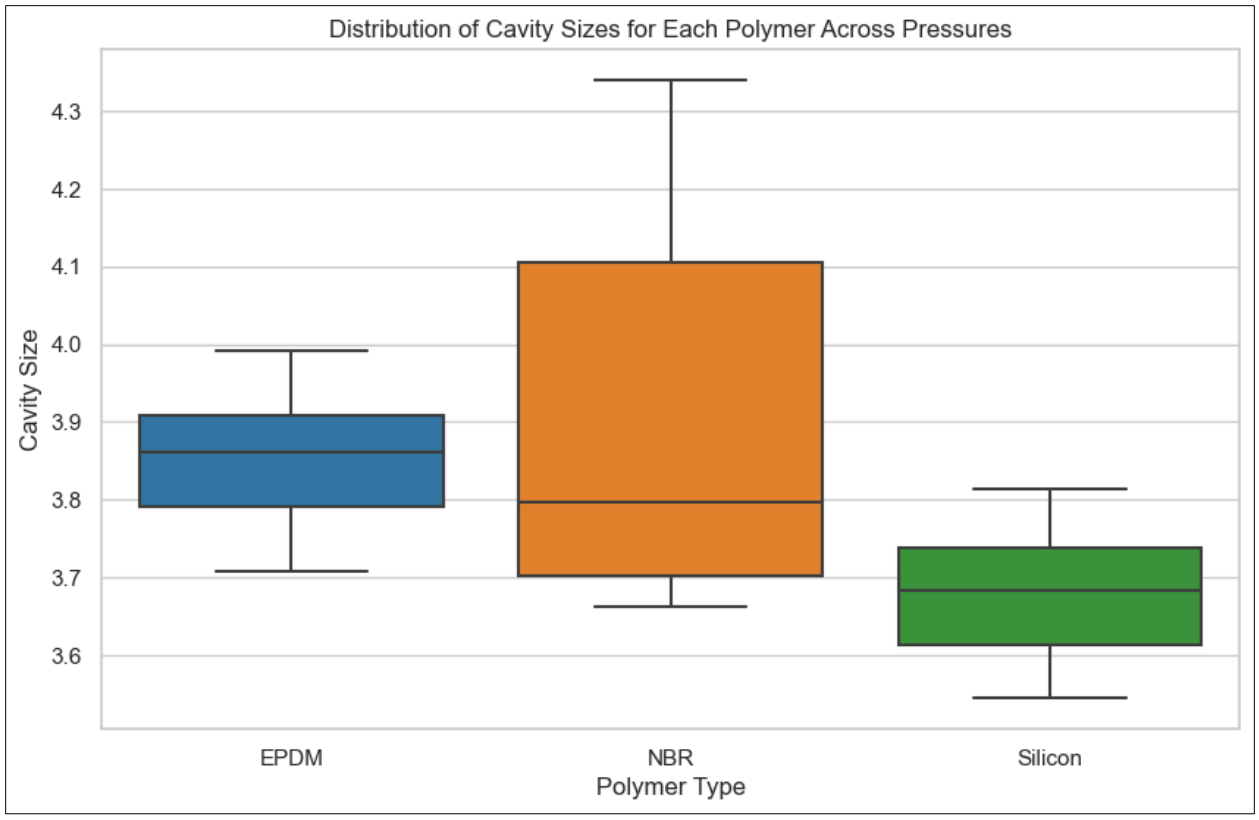

Figure 6. 23: Cavity size distribution among sealing samples across the hydrogen pressure

The cavity density heatmap at Figure 6.24 shows how cavity density changes for EPDM, NBR, and Silicon as hydrogen pressure rises from 0 to 7500 psi. NBR shows the least density of 0.000678 at low pressure zone but significant increase rate in density with increasing pressure. At 7500 psi hydrogen pressure, the cavity density of NBR was observed at 0.003003. This suggest the high responsiveness to hydrogen-induced cavity formation to NBR with increasing hydrogen exposure. Unlike NBR, EPDM exhibits comparatively denser cavities at lower pressure zone but the incremental rate of cavity formation with pressure is slower than NBR. Therefore, it is observed that the cavity density in higher pressure zone is very close for both NBR and EPDM. The initial density for EPDM was observed as 0.001898 at 0 psi and reaching 0.003319 at 7500 psi, suggests a steady and consistent buildup of micro-voids with pressure. Silicon, on contrary, shows the

denser phase across all the pressure zone. This start with a high initial density of 0.002685 reaches to 0.003023 at 7500 psi. Though silicon shows uniformly accumulated cavities, it remains more denser compared to NBR and Silicon across the range of hydrogen pressure. This pattern suggests that while EPDM and NBR experience structural compromise at elevated pressures, silicon shows lack of structural integrity across all pressure zones.

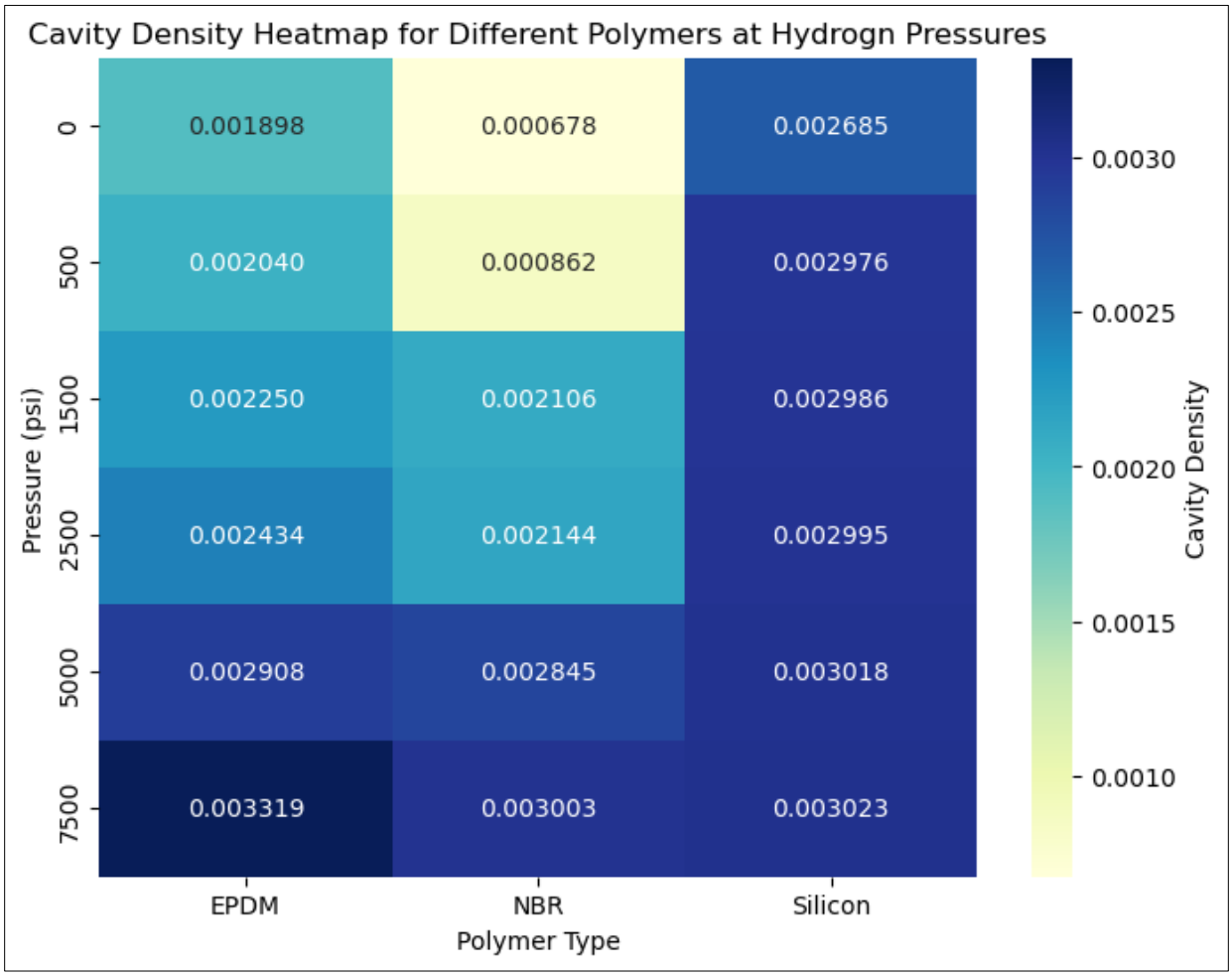

Figure 6. 24: Cavity density heatmap among sealing samples across the hydrogen pressure

In conclusion, there is a strong correlation observed between crack and cavity growth under hydrogen pressure for the selected samples. This assist in understanding the material-specific degradation patterns in sealing polymers. Silicon exhibits the highest absolute counts of both cracks and cavities, reflecting its inherent vulnerability to hydrogen-induced void formation, though with controlled incremental growth. NBR, despite starting with lower defect counts, undergoes rapid increases in both cracks and cavities, indicating high sensitivity to pressure-induced morphological changes. EPDM shows a more moderate and consistent increase in defects, suggesting a balanced resistance to structural breakdown. These trends emphasize the need to balance absolute defect resistance with stability under high pressure, guiding the selection of materials for hydrogen applications based on their tolerance to crack and cavity formation.

6.6. Comparative Sealing Resistance Assessment

NBR, EPDM and Silicon samples were aged under identical operating condition and consequently installed into the leaking chamber following the procedure mentioned at Chapter 5. All aged sealing samples were charged by around 2000 psi hydrogen pressure to record the sealing resistance exerted by all three sealing samples in term of pressure drop. The pressure profile was recorded for 48 hrs. The pressure drop across the upstream of the leak test chamber was monitored for each sealing sample. The slop was computed to compare the drop of pressure at high-pressure zone where the installed seal was exposed to inlet hydrogen pressure for this investigation. Figures 6.25 and Figure 6.26 provide an analysis of the pressure drop and percentage reduction in pressure over time for three aged sealing materials. Figure 6.25 shows the pressure drop for each material individually and comparatively. EPDM and NBR both show a steady and gradual drop of pressure

with time while Silicon exhibit a sharp pressure decline within 70,000 seconds of time range. But NBR and EPDM is observed more stable with the increasing time exposure in gaseous hydrogen environment.

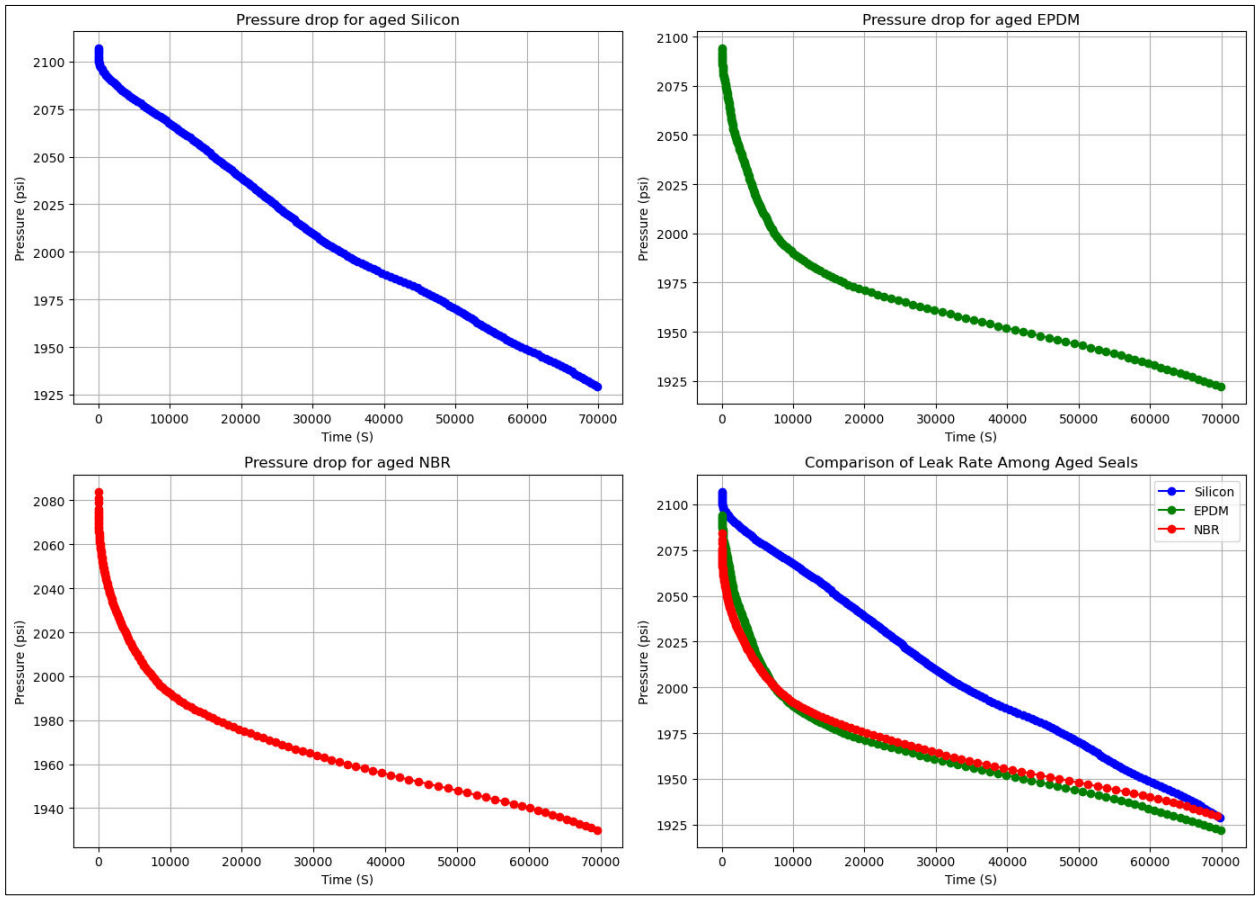

Figure 6. 25: Comparison of pressure drop among aged sealing samples

In Figure 6.26, the percentage reduction in pressure over time for each material is presented, allowing for a normalized comparison of the materials' degradation rates. Silicon shows the largest percent reduction, reaching close to 12%, indicating substantial degradation over time. EPDM shows about a 4% reduction, while NBR reaches around 6%, with a noticeable initial drop that tapers off.

The comparative plot illustrates that Silicon experiences the most significant percentage reduction from the beginning of pressure exertion, likely due to its high formation of cavity at it's unaged phase observed at section 6.5. Also, NBR showed prolonged crack and cavity formation with high swelling rate compared to EPDM that has been identified at section 6. These findings are analogous to the observation of sealing resistance comparison between NBR and EPDM. EPDM found more stable and holding the pressure for longer than NBR at exposed hydrogen pressure. These findings suggest that while Silicon may initially retain pressure better, it undergoes greater long-term degradation, whereas EPDM exhibits a more consistent performance with moderate leakage, making it potentially more suitable for applications requiring extended durability under pressure.

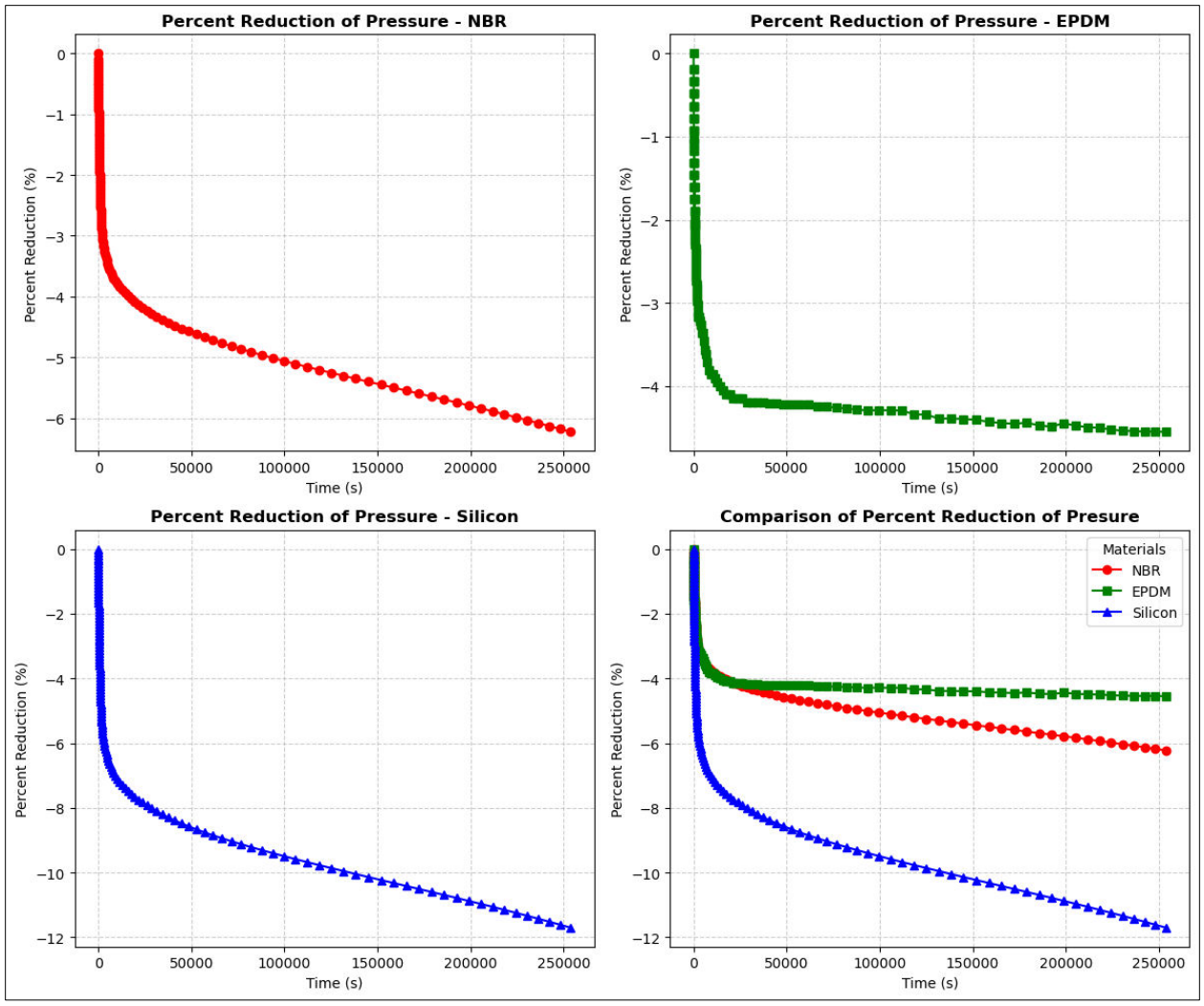

Figure 6. 26: Comparison of percent reduction of pressure drop among aged sealing samples

6.7. Analysis of Machine Learning Model Output to Predict Sealing Properties

As discussed at Chapter 5 Modeling section, we have developed three dedicated models: one for each sealing samples after the optimization and integration of multiple models based on numeric and image dataset to obtain the final combined model. The models developed for each polymer with respective output are analyzed as follows.

6.7.1. Prediction of NBR Sealing Properties

Figure 6.27 illustrate the relationships between Pressure and four key material properties for NBR: Hardness, Resistivity, Swelling, and Tensile Strength. The downward trend observed in Hardness and Tensile Strength with increasing pressure suggests that NBR undergoes a reduction in both hardness and tensile strength under higher pressure conditions, indicating a softening and weakening effect. In contrast, Resistivity shows an upward trend, implying that electrical resistivity in NBR increases as pressure rises. Swelling also increases with pressure, reflecting a potential expansion or absorption effect under high-pressure environments. These trends confirm the pressure-dependent behavior of NBR, which is essential for assessing its performance and stability in applications requiring pressure resistance.

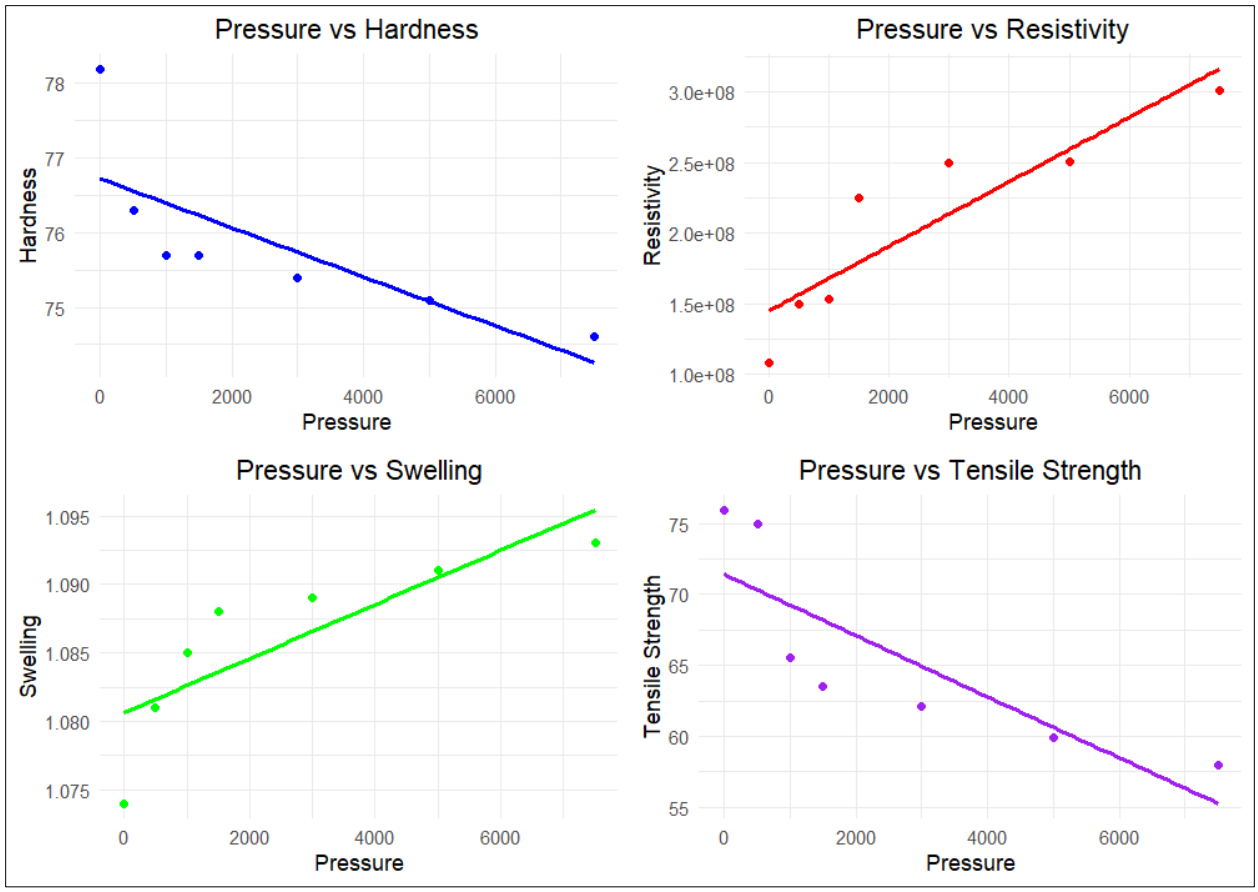

Figure 6. 27: Interaction of pressure on material properties of NBR

The Pearson correlation analysis heatmap at Figure 6.28 displays the relationships among the dependent variables Hardness, Resistivity, Swelling, and Tensile Strength for NBR. Strong positive correlations are evident between Resistivity and Swelling (0.94), Tensile Strength and Hardness (0.89), and Tensile Strength and Swelling (0.96). Negative correlations are observed between Hardness and Swelling (-0.97), Hardness and Resistivity (-0.87), and Tensile Strength and Resistivity (-0.92), indicating that as one variable increases, the other tends to decrease. These correlations suggest interdependent changes in NBR properties under varying conditions, providing information into how mechanical, electrical, and physical characteristics may interact.

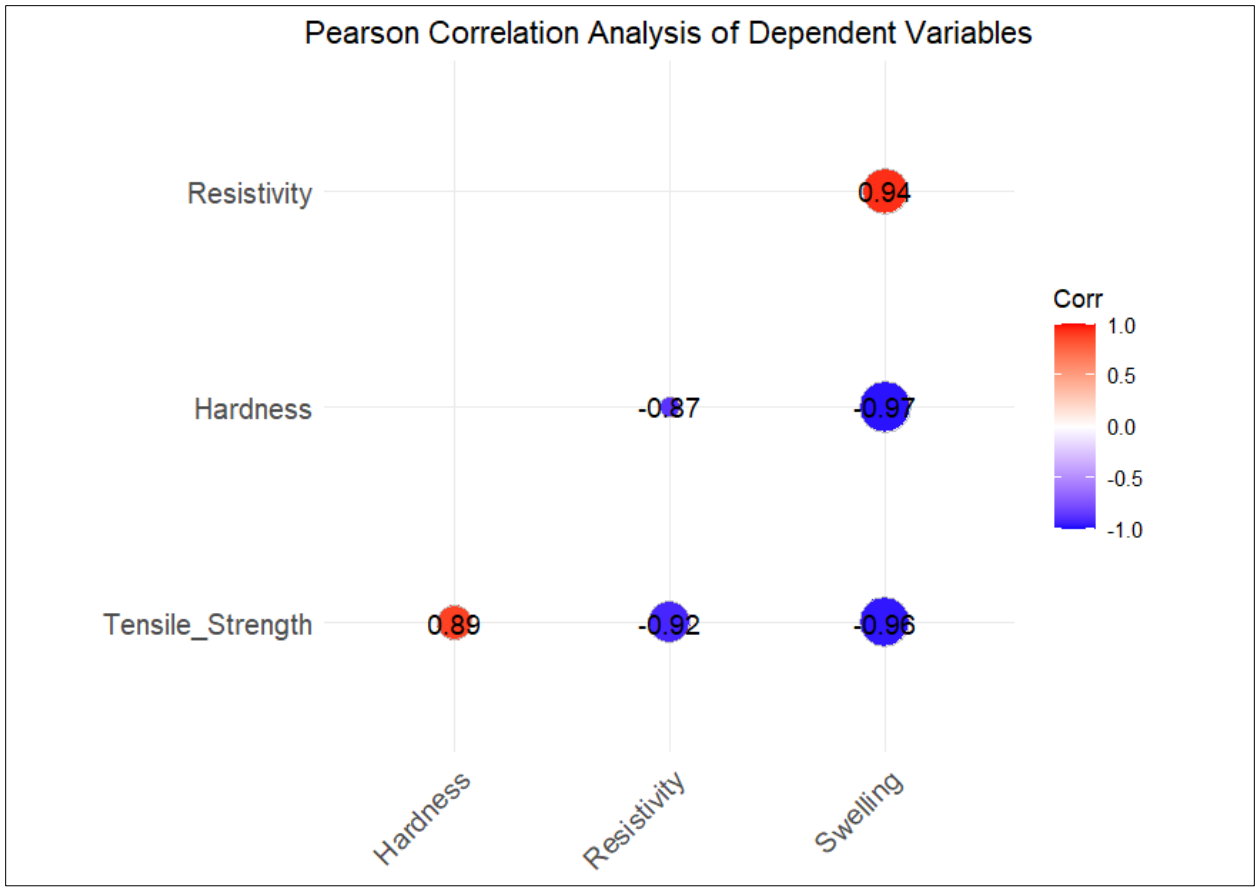

Figure 6. 28: Pearson Correlation Analysis of Dependent Variables for NBR

Table 6.1 and Table 2 shows the comparison between the accuracy metrics for the Multivariate Linear Regression (MLR) model and Generalized Additive Model (GAM) across the four target variables: Hardness, Resistivity, Swelling, and Tensile Strength. The MLR model shows larger R-squared values for all variables indicating a better overall fit compared to the GAM model. This difference suggests that the MLR model captures the linear relationships within the data more effectively, particularly for Swelling and Tensile Strength. In terms of error metrics, the MLR model generally exhibits lower Root Mean Squared Error (RMSE) and Mean Absolute Error (MAE) values for Resistivity and Tensile Strength, but the GAM model perform better in Swelling based on MAE and RMSE values, likely due to its ability to capture some degree of non-linearity.

However, the MLR model's relatively high R-squared values and competitive error metrics across variables indicate that it provides a more consistent baseline model.

Table 6. 1: Accuracy matrix obtained from Multivariate Linear Regression Model

Multivariate Linear Regression Model (MLR)				
Metric	Hardness	Resistivity	Swelling	Tensile Strength
R-squared	0.636702	0.734894	0.722924	0.775814
Mean Absolute Error	0.601939	27106933	0.002856	2.932012
Root Mean Squared Error	0.665314	29582667	0.003306	3.206838

Table 6. 2: Accuracy matrix obtained from Generalized Additive Model

Generalized Additive Model (GAM)				
Metric	Hardness	Resistivity	Swelling	Tensile Strength
R-squared	0.14563	0.203675	0.490692	0.317883
Mean Absolute Error	0.514346	58814807	0.002813	2.877965
Root Mean Squared Error	0.588688	65946181	0.002855	3.126047

A hybrid model was also carried out combining the strengths of the MLR model's linear accuracy with the GAM model's capability to address non-linear patterns in order to improve predictive accuracy. Particularly in scenarios where material properties exhibit complex dependencies on pressure. The hybrid model was developed by combining predictions from Generalized Additive Models (GAM) for Resistivity and Swelling. The prediction for Hardness and Tensile Strength were considered from Multivariate Linear Regression (MLR) model. The model accuracy were calculated and shown in Table 6.3. Also, Random Forest model was applied to assess if there is any improvement opportunities to predict the sealing properties and to be able to select the best suited model. Table 6.4 shows the accuracy matrix for Random Forest method applied to predict NBR sealing properties.

Table 6. 3: Accuracy matrix obtained from Hybrid Model

Hybrid Model (MLR + GAM)				
Metric	Hardness	Resistivity	Swelling	Tensile Strength
R-squared	0.251194	0.203675	0.490692	0.254731
Mean Absolute Error	1.025758	58814807	0.002813	6.887803
Root Mean Squared Error	1.030709	65946181	0.002855	7.128785

Table 6. 4: Accuracy matrix obtained from Random Forest Model

Random Forest Model				
Metric	Hardness	Resistivity	Swelling	Tensile Strength
R-squared	0.59168	0.663657	0.089795	0.6279
Mean Absolute Error	0.621725	34896883	0.003816	5.172504
Root Mean Squared Error	0.69389	42858343	0.003816	5.309662

The performance metrics for the Hybrid Model and the Random Forest Model at Table YY and Table 6.5 shows distinct strengths and weaknesses across the target variables. The Hybrid Model achieved moderate R-squared values for Resistivity and Swelling but showed lower accuracy for Hardness and Tensile Strength with higher Mean Absolute Error (MAE) and Root Mean Squared Error (RMSE) values, particularly for Tensile Strength. Conversely, the Random Forest Model shows higher average accuracy than hybrid and GAM method but falls behind multivariate linear regression model. Based on these metrics, Multivariate Regression Model showed the best consistency and performance, making it the preferred model to be combined with the CNN model for final prediction. The CNN model's performance metrics on the NBR dataset found the best Test Mean Absolute Error (MAE) of 1.42. Table AA shows the Mean Squared Error (MSE) of individual output variables. For Tensile Strength, the model achieved a Mean Squared Error (MSE) of 61.09, while Hardness showed a relatively low MSE of 2.25, indicating strong predictive capability for this property. However, Resistivity exhibited a significantly higher MSE of 3.11 x

10^15, suggesting challenges in accurately modeling this variable. Swelling yielded a minimal MSE of 0.0001235, reflecting the model's performance in capturing swelling behavior.

Table 6. 5: Accuracy Matrix of CNN Model

convolutional neural network	
Variables	Mean Squared Error (MSE)
Tensile Strength	61.09
Hardness	2.25
Resistivity	3.110135e+9
Swelling	0.0001235

The comparison of Mean Absolute Error (MAE) values between the CNN and Multivariate model is shown at Table 6.6. A significant difference in predictive accuracy across the NBR properties are observed between the two models. While the Multivariate model demonstrates consistently lower MAE values for Hardness, Tensile Strength and Swelling, the CNN model demonstrate higher accuracy for Resistivity. Therefore, a combined model was developed by customizing Multivariate and CNN model to pull the strengths of the Multivariate approach in handling numerical dependencies, while utilizing CNN's capability to incorporate morphological features. The combined model aims to achieve balanced, more accurate predictions across all material properties by integrating the advantages of both models. The comparison of Mean Absolute Error (MAE) values between the CNN and Multivariate and Combined Model is depicted at Table 6.6. The comparison reveals that the Combined model achieves the lowest MAE for Hardness. The combined model again shows improvement over CNN, reducing MAE for Hardness, Swelling and Tensile Strength.

Table 6. 6: MAE Comparison Among Multivariate, CNN, and Combined Models

Metric	Multivariate MAE	CNN MAE	Combined MAE
Hardness	0.6019	5.5832	0.5395
Resistivity	27100000	13100000	16100000
Swelling	0.0029	0.075	0.104
Tensile Strength	2.932	66.2275	4.1372

Figure 6.29 shows the Actual vs. Predicted plots for NBR using the Combined Model illustrate the accuracy of predictions across four properties. Each plot shows the actual values on the x-axis and the predicted values on the y-axis, with a dashed line representing the line of perfect prediction. Observing the distribution of points around this line provides insight into model performance. The Hardness and Tensile Strength plots demonstrate moderate alignment with the ideal line, indicating that the model provides a reasonable fit for these properties, though some deviation is noticeable. In the Resistivity plot, predictions show larger variation, particularly at lower values, suggesting that the model may struggle to accurately capture resistivity variations in NBR. The Swelling plot also shows some deviation from the ideal line, though the predicted values follow a generally upward trend. These results emphasizes the varying predictive capabilities of the combined model across different properties, with relatively strong performance for Hardness and Tensile Strength, while Resistivity and Swelling also shows better performance benefitted from the non-linear pattern of the model.

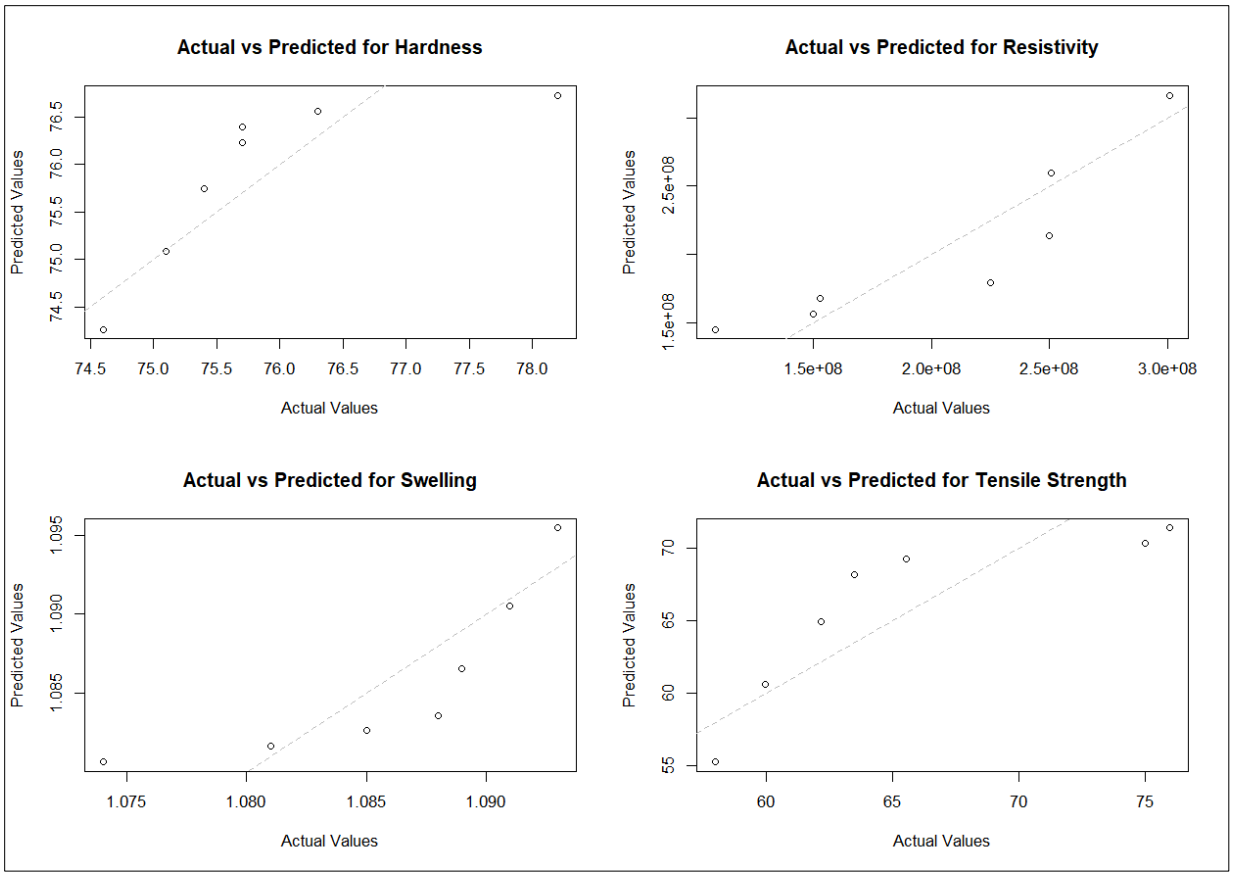

Figure 6. 29: Actual vs. Predicted plots for NBR sealing properties

Figure 6.30 shows the Residuals vs. Fitted plots for Hardness, Resistivity, Swelling, and Tensile Strength of NBR following the combined model. This provide insight into the performance of the combined model on the NBR dataset. In the Hardness plot, the residuals are generally small and scattered around the zero line, indicating a reasonable fit with minimal systematic error. The Resistivity plot, however, shows more dispersion, particularly at higher fitted values, suggesting that the model faces challenges to accurately predict resistivity at certain ranges. For Swelling, residuals remain close to zero, indicating good accuracy and minimal bias in predictions for this property. The Tensile Strength plot exhibits larger residuals, showing some variability, although the residuals do not follow a clear pattern.

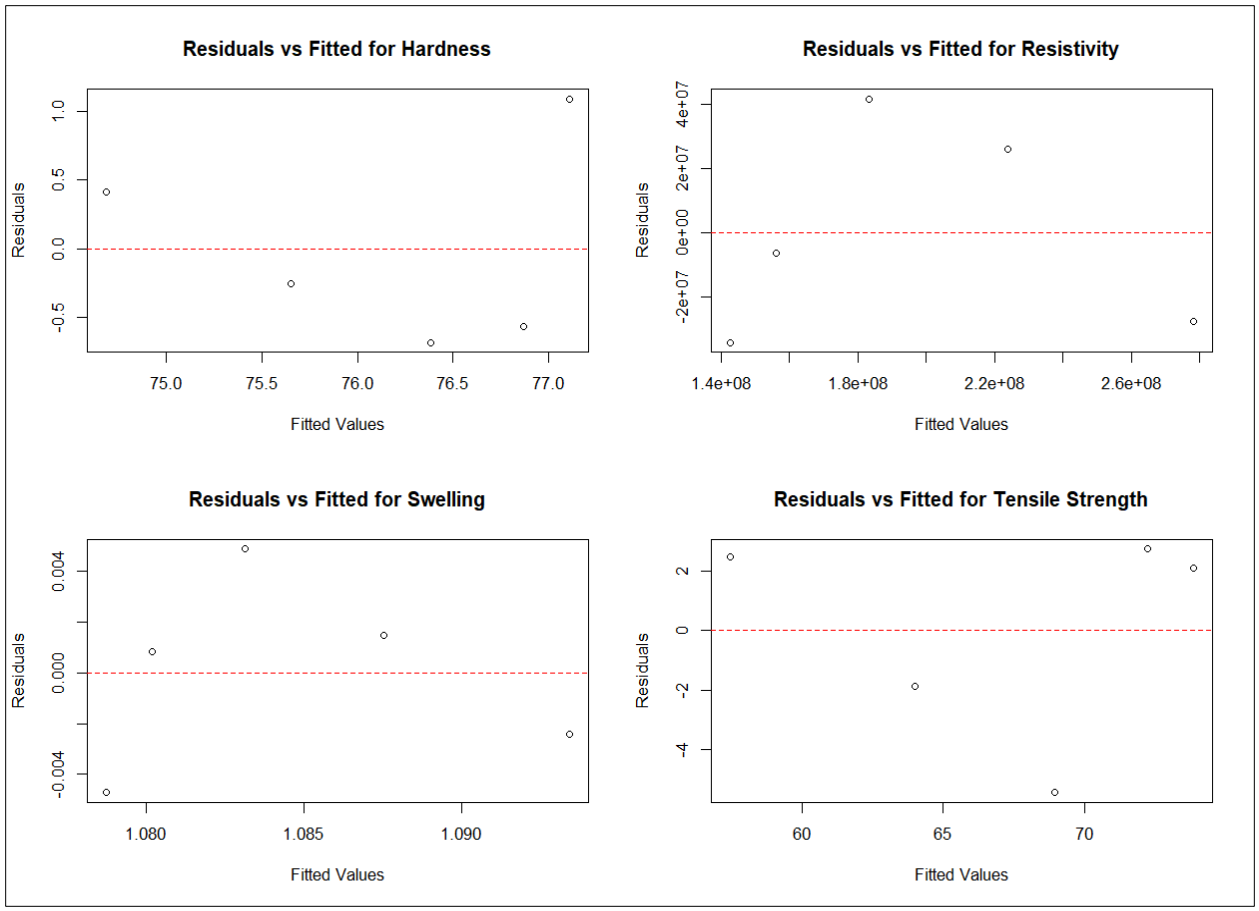

Figure 6. 30: Residual vs. Fitted plots for NBR sealing properties

Figure 6.31 shows the QQ Plot for NBR sealing properties to assess the normality of residuals for each property in the Combined Model. The sample quantiles of the residuals are plotted against the theoretical quantiles from a normal distribution. For Hardness and Swelling, the points lie relatively close to the 45-degree line, suggesting that residuals for these properties are approximately normally distributed, which supports the model's validity. However, Resistivity and Tensile Strength show more deviation from the line, indicating that the residuals for these properties may not be normally distributed. This deviation suggests that the model may have improvement opportunities to capture the variability for Resistivity.

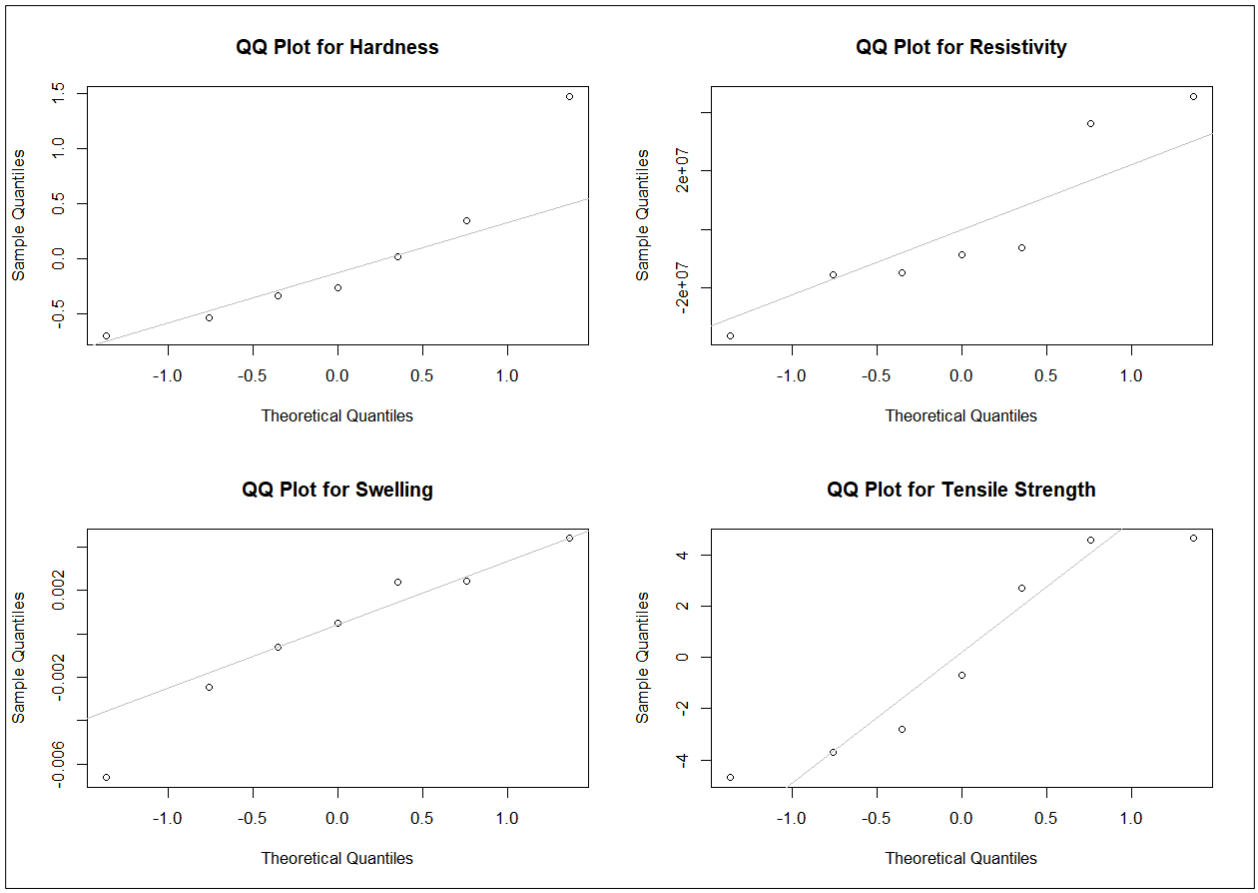

Figure 6. 31: QQ plot for NBR sealing properties

6.7.2. Prediction of EPDM Sealing Properties

Figure 6.32 illustrates the relationship between pressure and four properties of EPDM: hardness, resistivity, swelling, and tensile strength. As pressure increases, there is a clear decreasing trend in both hardness and tensile strength, indicating that higher pressure may lead to a reduction in the resistance to deformation and material strength. Conversely, resistivity and swelling show a positive correlation with pressure, suggesting that EPDM's ability to resist electrical flow increases with pressure. The swelling trend reflects volumetric expansion under high pressure, indicative of material volume expansion in response to hydrogen exposure.

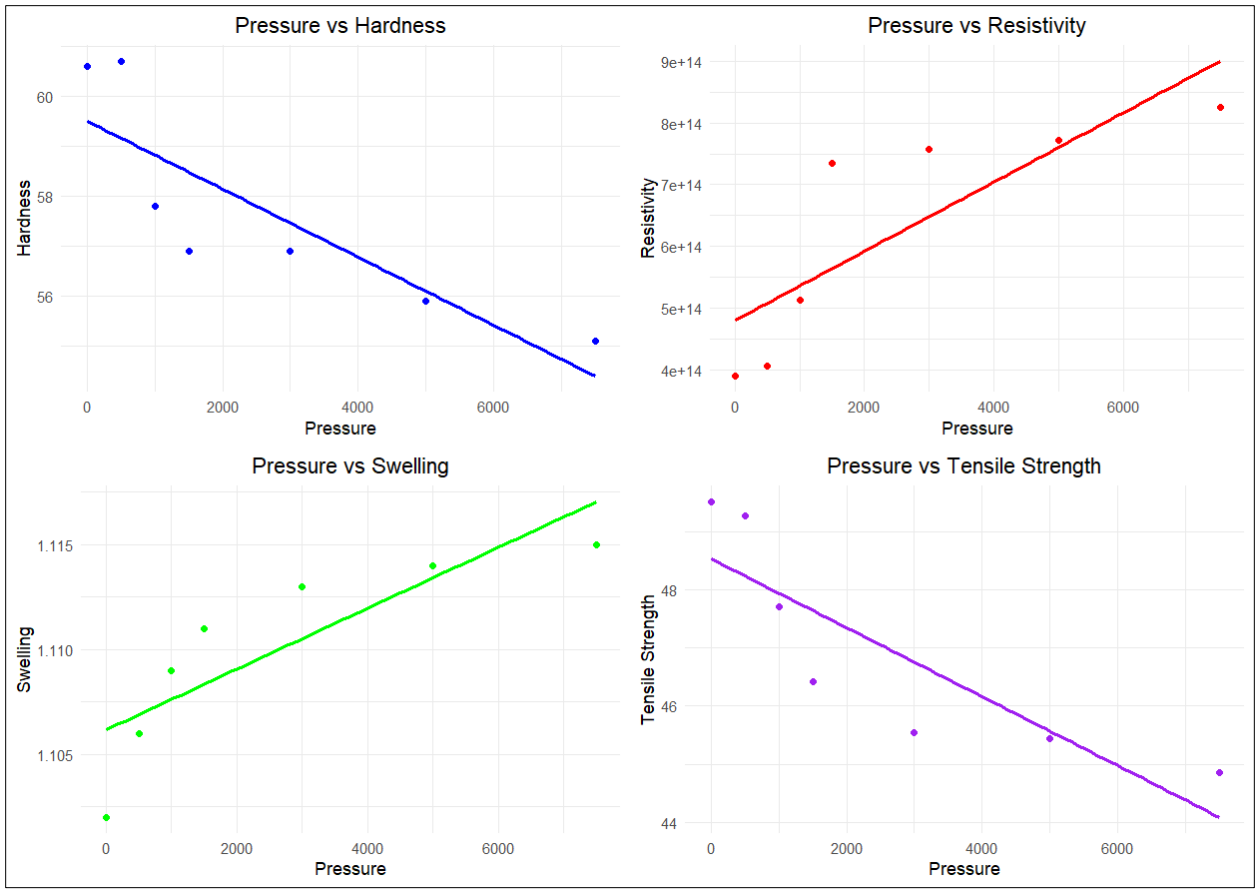

Figure 6. 32: Interaction of pressure on material properties of EPDM

The Pearson correlation analysis at Figure 6.33 shows the relationships between the dependent variables: hardness, resistivity, swelling, and tensile strength for EPDM. There is a strong negative correlation between tensile strength and hardness (-0.96), indicating that as hardness decreases, tensile strength tends to reduce as well. Resistivity and swelling show positive correlations with each other (0.95), suggesting they increase together under similar conditions. The negative correlations between tensile strength and swelling (-0.97) and between resistivity and hardness (-0.99) suggest that mechanical and electrical properties in EPDM are inversely impacted by pressure, suggesting the interdependence of these variables in the aging process.

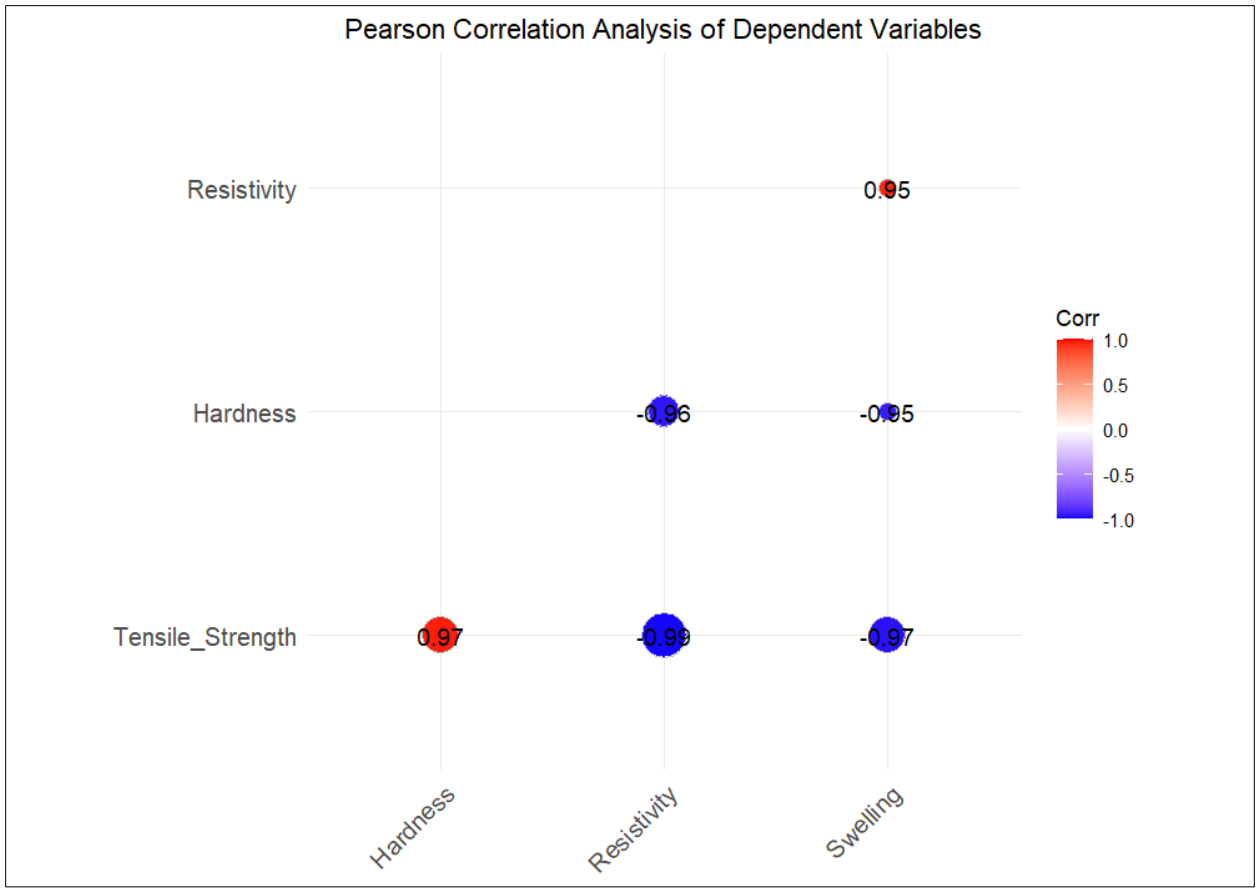

Figure 6. 33: Pearson Correlation Analysis of Dependent Variables for EPDM

Table 6.7 shows the accuracy metrics for the Multivariate Linear Regression (MLR) and Generalized Additive Model (GAM). A notable difference in predictive performance was observed. The MLR model generally has higher R-squared values, indicating better overall fit, especially for swelling ($R^2 = 0.714$) and tensile strength ($R^2 = 0.735$), with lower error rates than GAM. However, the GAM performs better in terms of Mean Absolute Error and Root Mean Squared Error for some properties like hardness. Also, for resistivity, the Generalized Additive Model (GAM) has a slightly higher R-squared value (0.695) compared to the Multivariate Linear Regression (MLR) model (0.681), and it also significantly reduces the MAE and RMSE. This suggests that the GAM is more effective at capturing the non-linear relationship in resistivity with

respect to pressure. Therefore, a hybrid approach was performed combining GAM and MLR to check if the overall accuracy of EPDM properties can be improved. Also, the other model; Random Forest was applied to the dataset to capture complex, non-linear relationships among the variables and the accuracy was checked to be able to select the best suited prediction model based on numeric data.

Table 6. 7: Accuracy matrix from Multivariate Linear Regression and Generalized Additive model

Multivariate Linear Regression Model (MLR)				
Metric	Hardness	Resistivity	Swelling	Tensile Strength
R-squared	0.723	0.681	0.714	0.735
Mean Absolute Error	0.957	8.32E+13	0.002	0.796
Root Mean Squared Error	1.066	9.73E+13	0.002	0.899
Generalized Additive Model (GAM)				
Metric	Hardness	Resistivity	Swelling	Tensile Strength
R-squared	0.573	0.695	0.569	0.679
Mean Absolute Error	0.77	8.04057E+13	0.002	0.604
Root Mean Squared Error	0.881	8.61666E+13	0.002	0.807

Table 6.8 shows the accuracy matrix of Hybrid and Random Forest model. From Table 6.8 it was observed that Random Forest model performs best for resistivity ($R^2 = 0.879$) and tensile strength ($R^2 = 0.649$), suggesting its strength in handling complex, non-linear relationships. In comparison, the Hybrid model shows relatively lower R^2 values, for hardness and tensile strength, indicating poorer fit. When comparing all the models with the Multivariate Linear Regression (MLR) model, it seems MLR performs comparatively consistent and better for most of the variables. Therefore, for the MLR was further coupled with the CNN model to incorporate the morphological changes for performing better prediction of the EPDM properties.

Table 6. 8: Accuracy matrix from Hybrid and Random Forest model

Hybrid Model (MLR + GAM)				
Metric	Hardness	Resistivity	Swelling	Tensile Strength
R-squared	0.928	0.695690175	0.569	0.421
Mean Absolute Error	1.821	8.04057E+13	0.002	1.38
Root Mean Squared Error	1.875	8.61666E+13	0.002	1.699
Random Forest Model				
Metric	Hardness	Resistivity	Swelling	Tensile Strength
R-squared	-0.448	0.87868704	0.356	0.649
Mean Absolute Error	1.617	4.66715E+13	0.002	0.833
Root Mean Squared Error	1.624	5.44045E+13	0.002	0.844

The comparison of accuracy metrics at Table 6.9 shows that the Multivariate Linear Regression (MLR) model generally perform better in terms of Mean Absolute Error (MAE) and Root Mean Squared Error (RMSE) for tensile strength and hardness while CNN model perform better for Resistivity and Swelling. However, the CNN model, which incorporates SEM images, provides predictions that account for morphological changes, is expected to capture subtle variations due to structural transformations in the material from aging pressure. Although CNN has slightly higher error rates, integrating it with MLR could improve predictive accuracy by combining the strengths of both approaches—numerical data from MLR and morphological insights from CNN. This combined approach will be carried out by customization of weights of process variables among the MLR and CNN and subsequently integrated to predict material properties under varying hydrogen pressure. The accuracy matrix of the combined model is shown in Table 6.10.

Table 6. 9: Comparison of model accuracy between MLR and CNN model

	Tensile Strength		Hardness		Resistivity		Swelling	
	MLR	CNN	MLR	CNN	MLR	CNN	MLR	CNN
MAE	0.796	1.052	0.957	1.5739	8.32e+13	6.94e+13	0.002	0.003
RMSE	0.899	1.182	1.066	1.711	9.73e+13	1.09e+12	0.002	0.003

Table 6. 10: Comparison of model accuracy of the combined model

Combined Model (MLR + CNN)				
Metric	Hardness	Resistivity	Swelling	Tensile Strength
MAE	1.059	1.196768e+13	0.003	0.930
RMSE	1.007	1.500282e+13	0.004	1.108

Figure 6.34 shows the box plot representing the residuals for the combined model across the Tensile Strength, Hardness, Resistivity, and Swelling. The residuals of Tensile Strength, Hardness, and Swelling appear very close to zero with minimal variation, indicating the combined model's predictions for these outputs are closely aligned with the actual values. The box plot for Resistivity shows a larger spread in the residuals, with some positive residuals reaching higher values, suggesting that the model's predictions for Resistivity may need further improvement. There is also a noticeable outlier below zero, indicating one prediction that deviates significantly from the actual value.

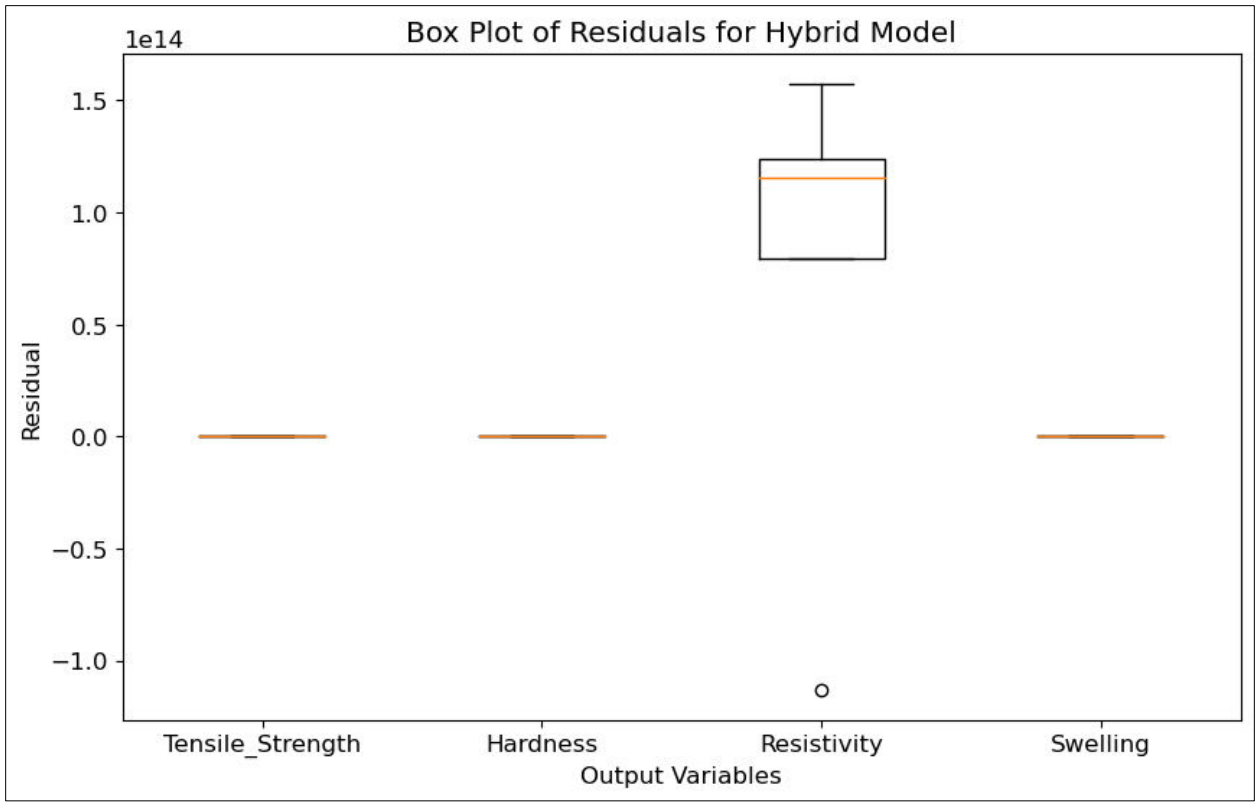

Figure 6. 34: Box Plot of Residuals for combined Model for EPDM

Figure 6.35 presents a comparison of actual versus predicted values for EPDM sealing properties using a combined model. Each subplot shows actual values on the x-axis and predicted values on the y-axis, with a dashed line indicating perfect agreement (y = x). Points close to this line suggest accurate predictions, while those farther away indicate discrepancies between the model's predictions and actual values. The plot suggest a generally good fit for Hardness and Tensile Strength, while Resistivity and Swelling exhibit larger deviations, suggesting the model performs better on some properties than others. The plot suggest that the model accuracy can be further improved for Resistivity and Swelling.

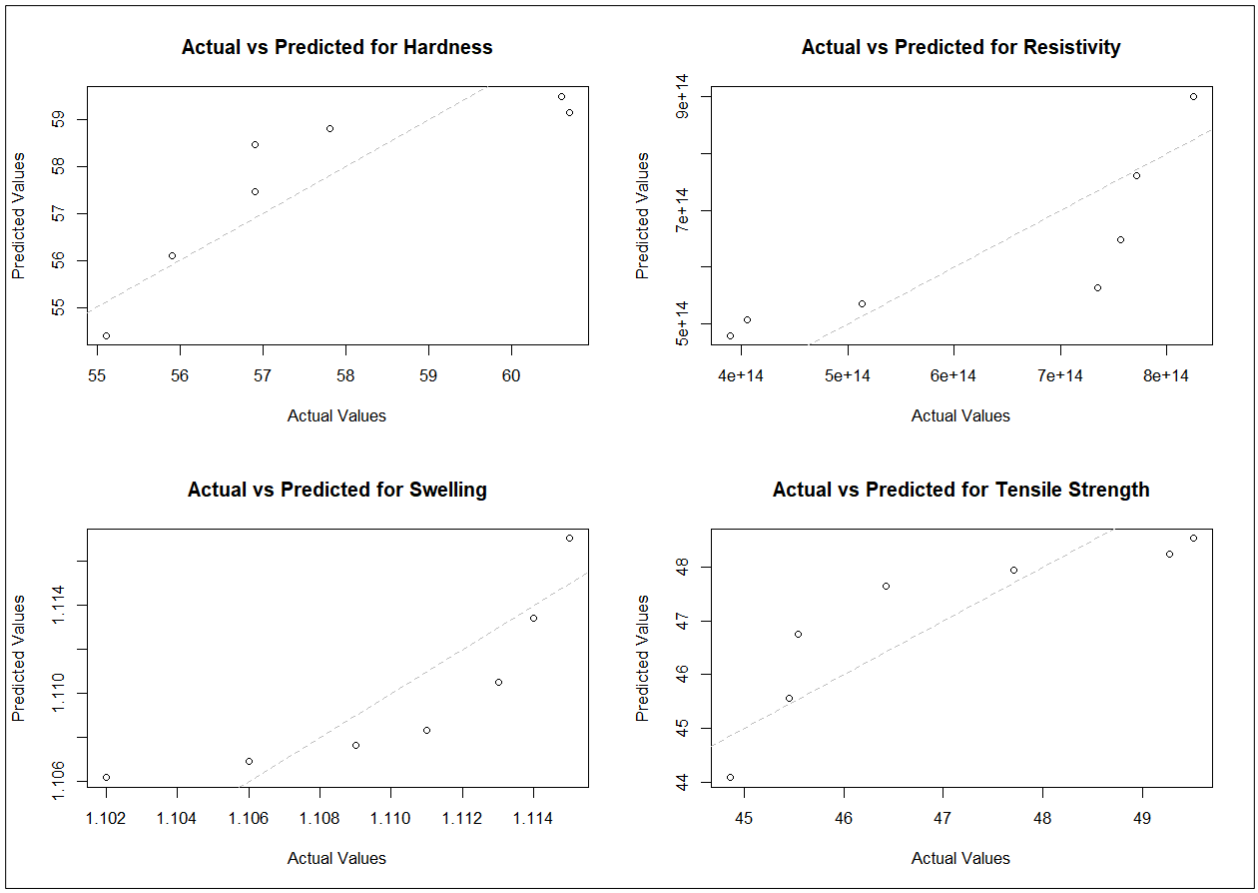

Figure 6. 35: Actual vs. Predicted plots for EPDM sealing properties

Figure 6.36 shows the residuals versus fitted values plot which reveals specific patterns in the combined model's performance for EPDM properties. For Hardness and Swelling, the residuals are evenly distributed around zero, suggesting that the model provides a stable and unbiased fit for these properties. In contrast, Resistivity exhibits a wider spread of residuals, indicating higher variability and potential underfitting, possibly due to complex relationships. Tensile Strength shows a slight trend where residuals increase with fitted values, suggesting mild heteroscedasticity and potential underprediction at higher values. Overall, these finding suggest that the model performs reliably for Hardness and Swelling but may benefit from refinement for Resistivity, possibly through additional feature engineering or model complexity adjustments, and a transformation for Tensile Strength to achieve more consistent predictions across its range.

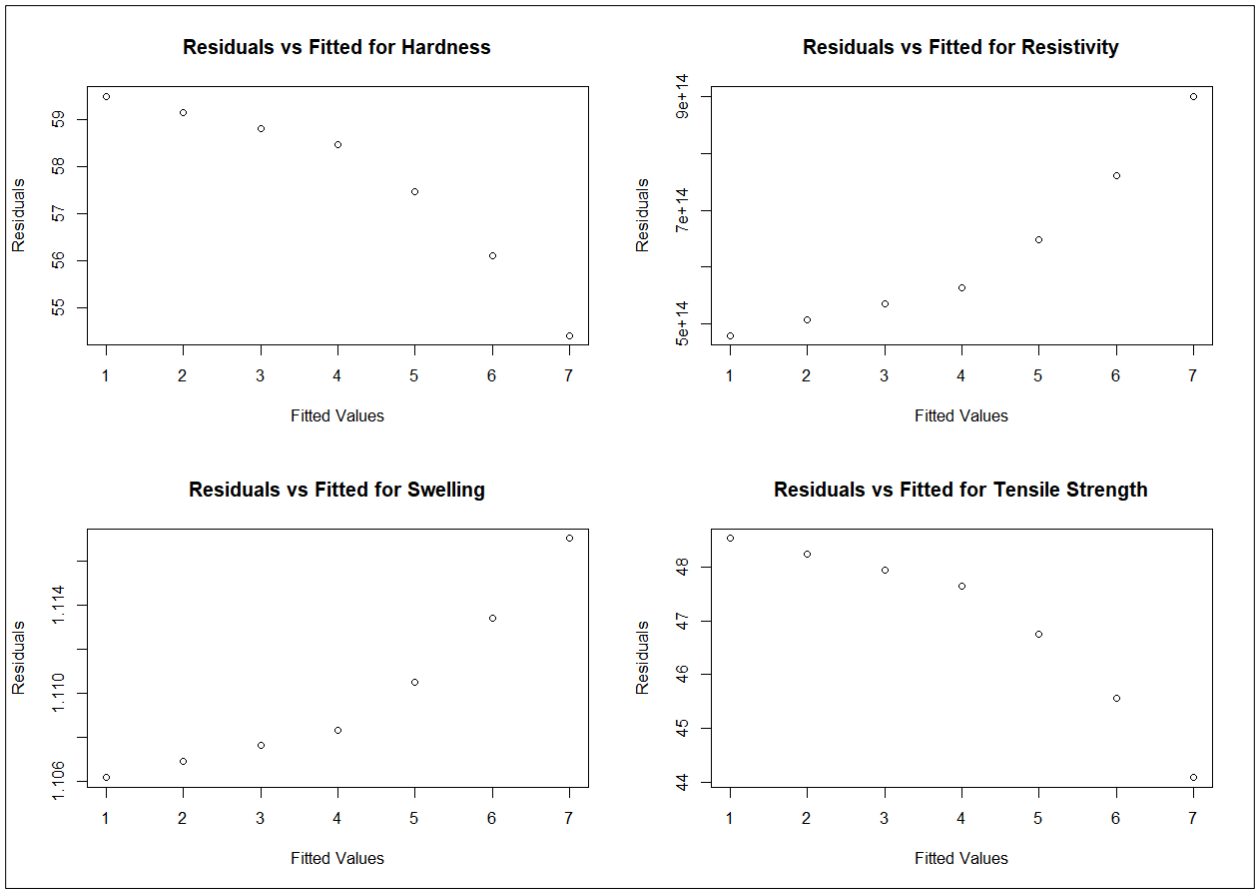

Figure 6. 36: Residual vs. Fitted plots for EPDM sealing properties

Figure 6.37 shows the QQ plots for EPDM sealing properties to assess the normality of residuals for the combined model predictions. Ideally, residuals should align closely with the theoretical quantile, indicating normally distributed errors and supporting model validity. For Hardness and Tensile Strength, the points align well with the diagonal line, suggesting a reasonable approximation to normality and implying that the model's assumptions may hold for these properties. However, the plot for Resistivity deviates substantially, especially at the upper quantiles, indicating heavy-tailed or skewed residuals and suggesting that the model may be further improved for Resistivity. The Swelling QQ plot shows a slight deviation, but residuals are generally closer to the line, indicating mild non-normality. Overall, these findings imply that the

model performs acceptably for Hardness, Swelling, and Tensile Strength but may require further adjustments for Resistivity to better capture its distribution and reduce prediction error.

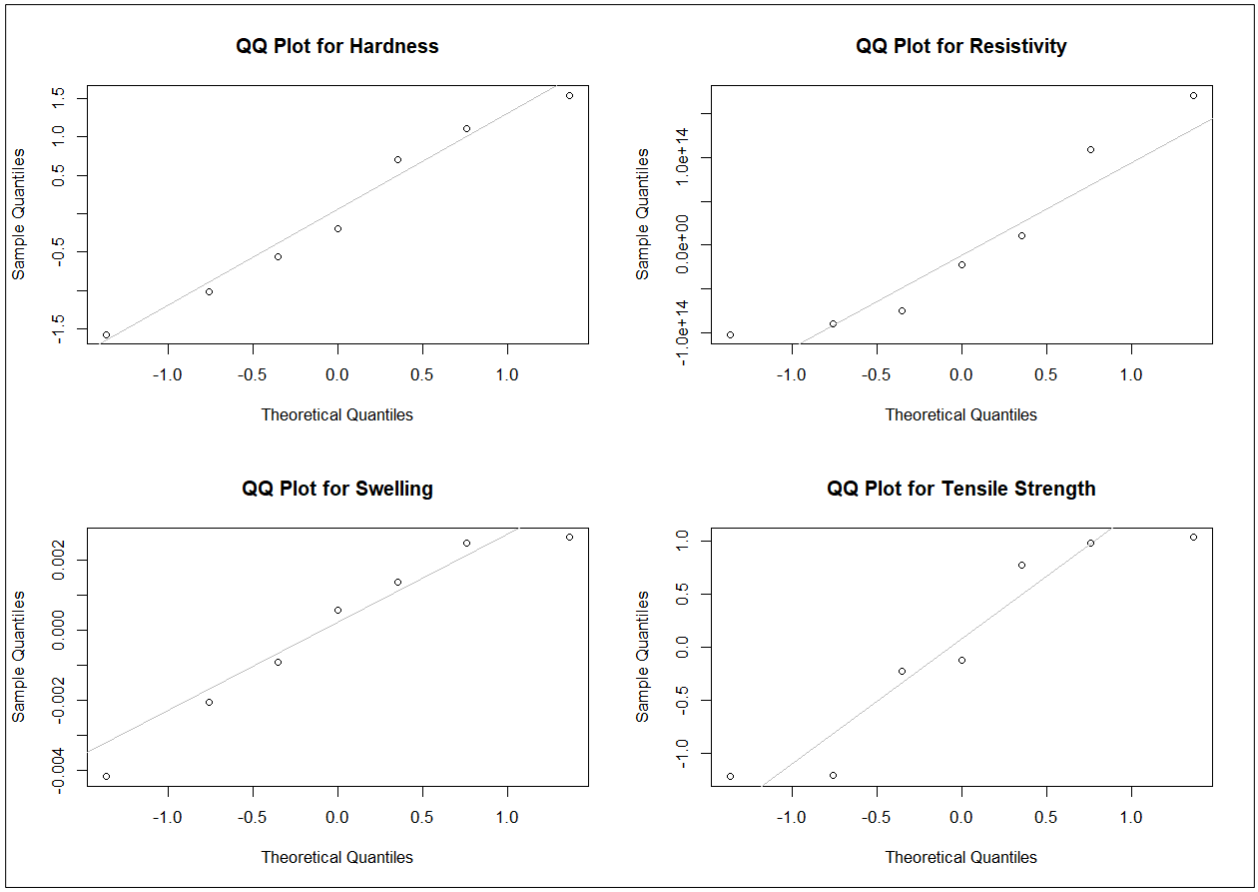

Figure 6. 37: QQ plot for EPDM sealing properties

6.7.3. Prediction of Silicon Sealing Properties

Interaction of pressure on material properties of Silicon is shown in Figure 6.38. It is observed that, for silicon, increasing pressure results in a clear decrease in hardness and tensile strength, while resistivity and swelling show a positive correlation with pressure. This pattern indicates that under higher hydrogen pressures, silicon's structural integrity diminishes as it softens and becomes more conductive, with slight swelling observed. These trends are consistent with hydrogen-induced aging effects seen in NBR and EPDM.

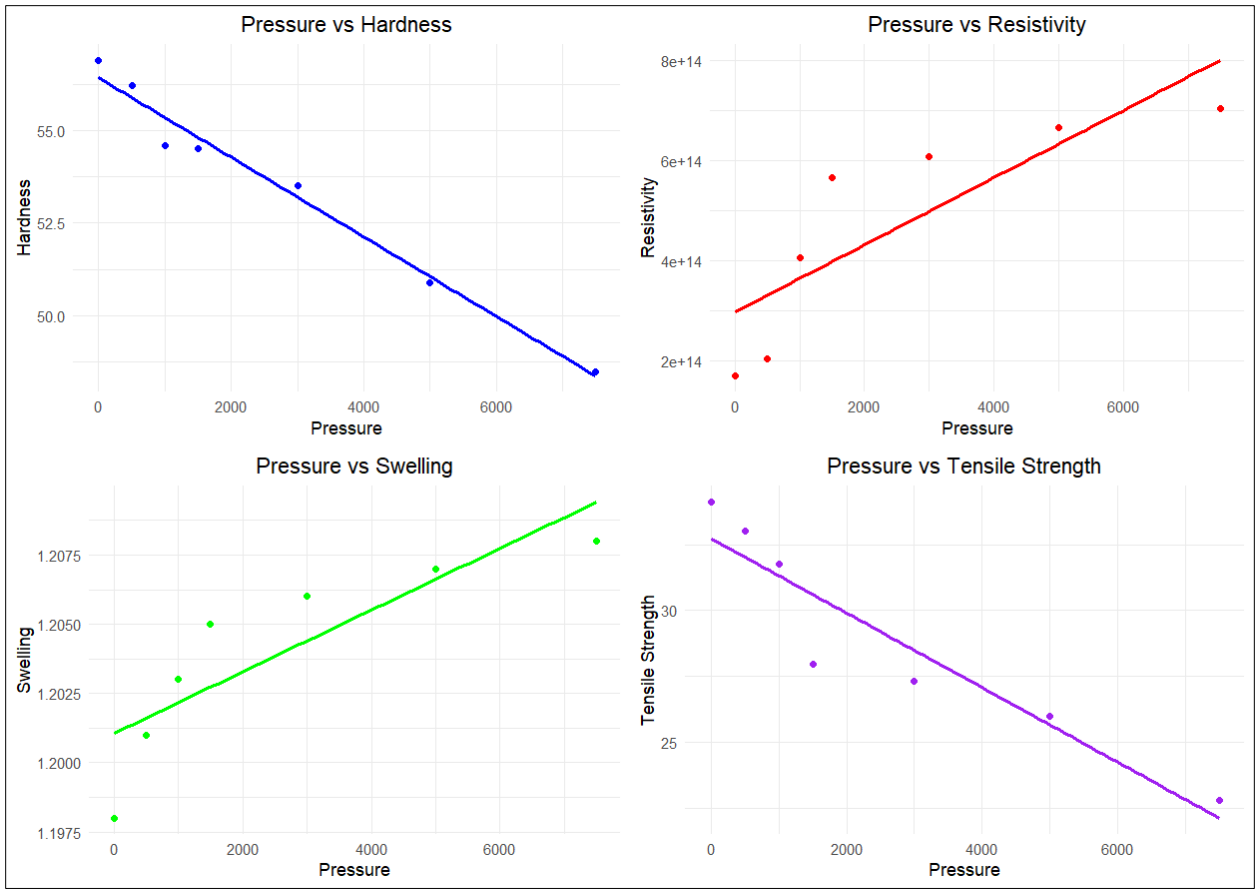

Figure 6. 38: Interaction of pressure on material properties of Silicon

The accuracy data shown at Table 6.11 compares the performance metrics of four models; Multivariate Linear Regression (MLR), Generalized Additive Model (GAM), Hybrid Model (MLR + GAM), and Random Forest Model on predicting hardness, resistivity, swelling, and tensile strength for silicon under varying hydrogen pressures. MLR demonstrates the highest R-squared values for hardness (0.985) and tensile strength (0.802), indicating strong predictive accuracy, particularly in capturing linear relationships between pressure and these properties. While the MLR model yields slightly lower R-squared values for resistivity (0.763) and swelling (0.772) compared to GAM, it maintains lower Mean Absolute Errors (MAE) and Root Mean Squared Errors (RMSE), suggesting more consistent and reliable predictions across all variables.

GAM, on the other hand, perform better in modeling resistivity with an R-squared of 0.916, which is higher than MLR's; however, GAM sacrifices some accuracy in tensile strength, showing a higher MAE and RMSE. The Hybrid Model, combining MLR and GAM, attempts to capture both linear and non-linear interactions, achieving a high R-squared for resistivity (0.916) and tensile strength (0.900), but it does not significantly improve over MLR in terms of MAE or RMSE, especially for hardness and swelling. The Random Forest model performs poorly in comparison, with notably lower R-squared values for all metrics, particularly in hardness (0.188) and swelling (0.478), and the highest error metrics among all models, representing its limitations in handling the dataset's structure and possibly overfitting. Based on the comparative performance, MLR was selected as the ultimate model for predicting silicon properties due to its balance of high accuracy and consistency in capturing linear relationships.

Table 6. 11: Comparison of accuracy matrix of multiple numeric models for silicon properties

Multivariate Linear Regression Model (MLR)				
Metric	Hardness	Resistivity	Swelling	Tensile Strength
R-squared	0.985	0.763	0.772	0.802
Mean Absolute Error	0.199	9.48852E+13	0.001	1.311
Root Mean Squared Error	0.259	1.0299E+14	0.002	1.450
Generalized Additive Model (GAM)				
Metric	Hardness	Resistivity	Swelling	Tensile Strength
R-squared	0.938	0.916	0.707	0.749
Mean Absolute Error	0.722	4.22123E+13	0.001	1.998
Root Mean Squared Error	0.760	4.33372E+13	0.001	2.255
Hybrid Model (MLR + GAM)				
Metric	Hardness	Resistivity	Swelling	Tensile Strength
R-squared	0.938	0.916	0.707	0.900
Mean Absolute Error	0.722	4.22123E+13	0.001	1.224
Root Mean Squared Error	0.760	4.33372E+13	0.001	1.424
Random Forest Model				
Metric	Hardness	Resistivity	Swelling	Tensile Strength
R-squared	0.188	0.569	0.478	0.539
Mean Absolute Error	2.408	9.80485E+13	0.002	2.174
Root Mean Squared Error	2.748	9.81641E+13	0.002	3.056

The CNN model showed the best test MAE for silicon is 1.60 which means that, on average, the model's predictions are 1.60 units off from the actual values. Therefore, CNN is supposed to predict silicon properties better from image data. The mean square error (MSE) across all the variables for the CNN model is depicted at Table 6.12.

Table 6. 12: Mean Square Error (MSE) of the CNN model

Variable	MSE
Tensile Strength	15.443
Hardness	10.135
Resistivity	2.370444e+28
Swelling	0.0000301434

The initial evaluation focused on the CNN model's performance in predicting silicon's mechanical and electrical properties, with Mean Squared Error (MSE) values indicating moderate accuracy for tensile strength (15.443), hardness (10.135), and swelling (0.0000301434), while resistivity exhibited a high MSE suggesting that the CNN alone struggles to capture different patterns in the data. To enhance predictive accuracy, especially for variables with complex linear dependencies, the CNN model's predictions were combined with those of a multivariate model. This combined approach contains the strengths of both models, with CNN capturing non-linear features from image data and the multivariate model addressing linear relationships more effectively. By combining the couple of models, it is aimed to improve overall prediction accuracy by following the principle of complementarity, where each model compensates for the other's limitations, especially in variables like resistivity where CNN's performance alone was observed lack of accuracy. The accuracy matrix of the combined model (Multivariate + CNN) was estimated and shown in Table 6.13.

Table 6. 13: Accuracy matrix of Combined model

Properties	MAE	RMSE
Hardness	2.283	2.309
Resistivity	8.80e+13	1.14e+14
Swelling	4.961	4.969
Tensile Strength	2.848	3.209

Figure 6.39 shows the plot of actual versus predicted values for silicon's sealing properties. Different degrees of alignment with the ideal prediction line (y = x) was observed, which indicates better prediction accuracy. For Hardness, the points closely follow the ideal line, showing that the model is reasonably accurate in capturing its variation with pressure. Resistivity shows a wider spread around the line, with some notable deviations at higher values, indicating that while the model captures general trends, it faces difficulties with precise predictions in this range, likely due to the complex, nonlinear nature of resistivity changes under pressure. Swelling exhibits a gradual alignment with the ideal line, but with minor discrepancies, suggesting that the model is effective in capturing overall swelling trends but could be affected by small-scale variations. For Tensile Strength, there's a moderate alignment with the line, though some predicted values deviate below the actual values, particularly at lower tensile strength levels, suggesting slight underestimation by the model in this range. Overall, the plot reveals that the model performs best for Hardness and has reasonable predictive accuracy for Swelling and Tensile Strength, while improvements can be made for Resistivity due to the higher spread of residuals, suggesting the model's limitations in capturing the complex behavior of resistivity.

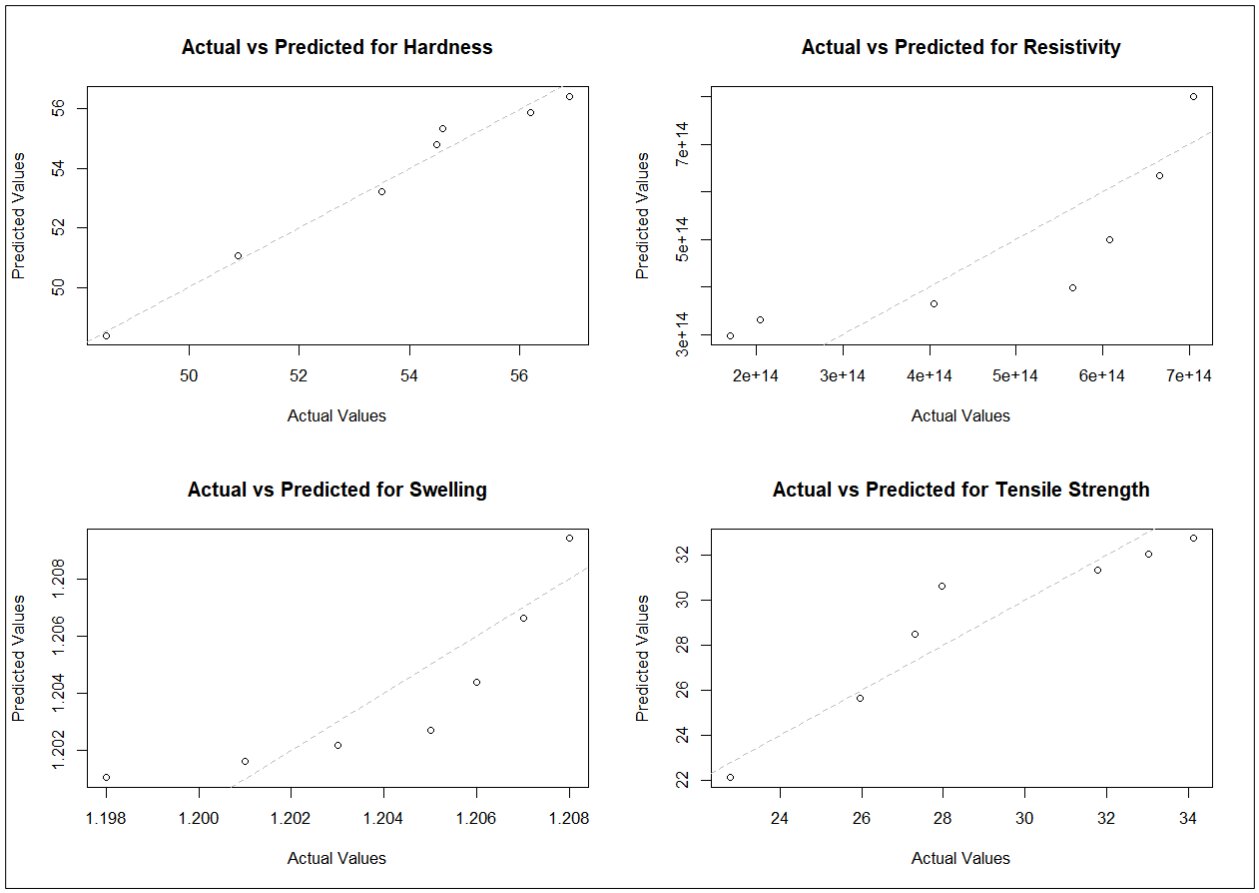

Figure 6. 39: Actual vs. Predicted plots for Silicon sealing properties

Figure 6.40 is the residuals versus fitted values plot for the model's predictions of silicon's properties; Hardness, Resistivity, Swelling, and Tensile Strength. It provide insights into the model's performance and any potential biases or patterns in prediction errors. For Hardness, the residuals show a trend, with higher fitted values corresponding to lower residuals, suggesting that the model tends to overestimate at lower hardness values and becomes more accurate as hardness increases. This trend also indicates a systematic bias in how the model interprets hardness based on its inputs. In the Resistivity plot, residuals increase with higher fitted values, indicating that as the predicted resistivity rises, the model's accuracy decreases, likely due to challenges in capturing the non-linear relationship between resistivity and pressure. This trend shows limitations in the

model's capacity to handle the complex factors influencing resistivity. For Swelling, residuals are relatively clustered but exhibit a gradual upward trend with fitted values, suggesting a consistent underestimation across different swelling levels. Finally, Tensile Strength residuals shows a similar pattern to Hardness, where higher fitted values align more closely with zero residuals, while lower fitted values show a larger discrepancy, indicating potential underestimation at lower tensile strengths.

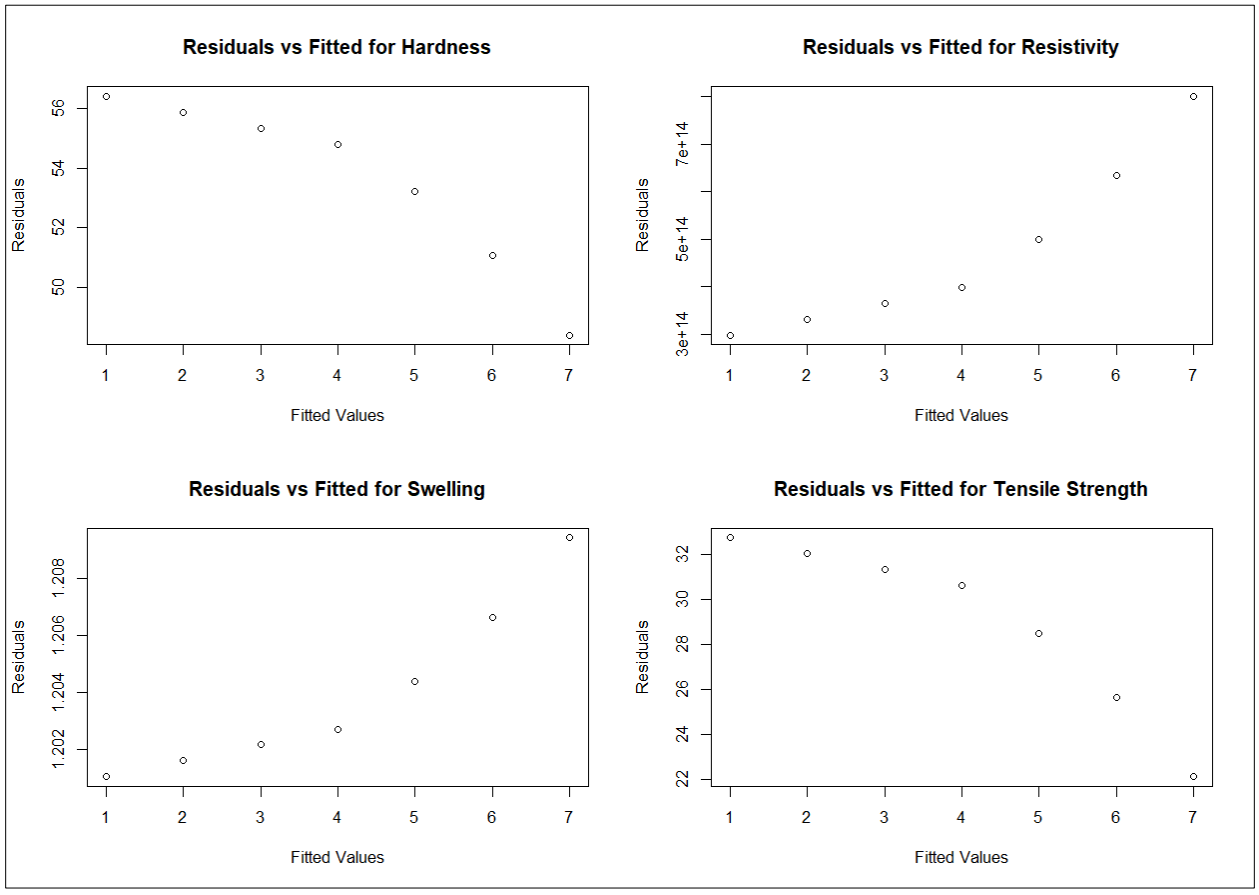

Figure 6. 40: Residual vs. Fitted plots for Silicon sealing properties

Figure 6.41 is the QQ plots for the residuals of silicon's properties. It allow to assess the normality of the residuals, which is important for validating model assumptions. For Hardness, the residuals closely align with the theoretical quantile line, suggesting that the residuals are approximately

normally distributed, which is a positive indicator for the model's predictive reliability. Resistivity shows more deviation from the line, especially at the lower and upper quantiles, indicating that the residuals for resistivity are not normally distributed and may contain outliers or systematic biases. This non-normality suggests that the model can be further improved to capture the underlying patterns affecting resistivity. In the Swelling plot, residuals are relatively close to the line, though there is a slight deviation at the lower quantiles, which may indicate minor skewness or underestimation at specific points but generally suggests an acceptable distribution. The Tensile Strength QQ plot shows some deviation from normality, particularly at the extremes, where residuals fall below the line at the lower quantiles and above it at the upper quantiles. Overall, while Hardness and Swelling residuals exhibit approximate normality, deviations in Resistivity indicates that the model might benefit from adjustments to better capture the distributional characteristics of electrical property.

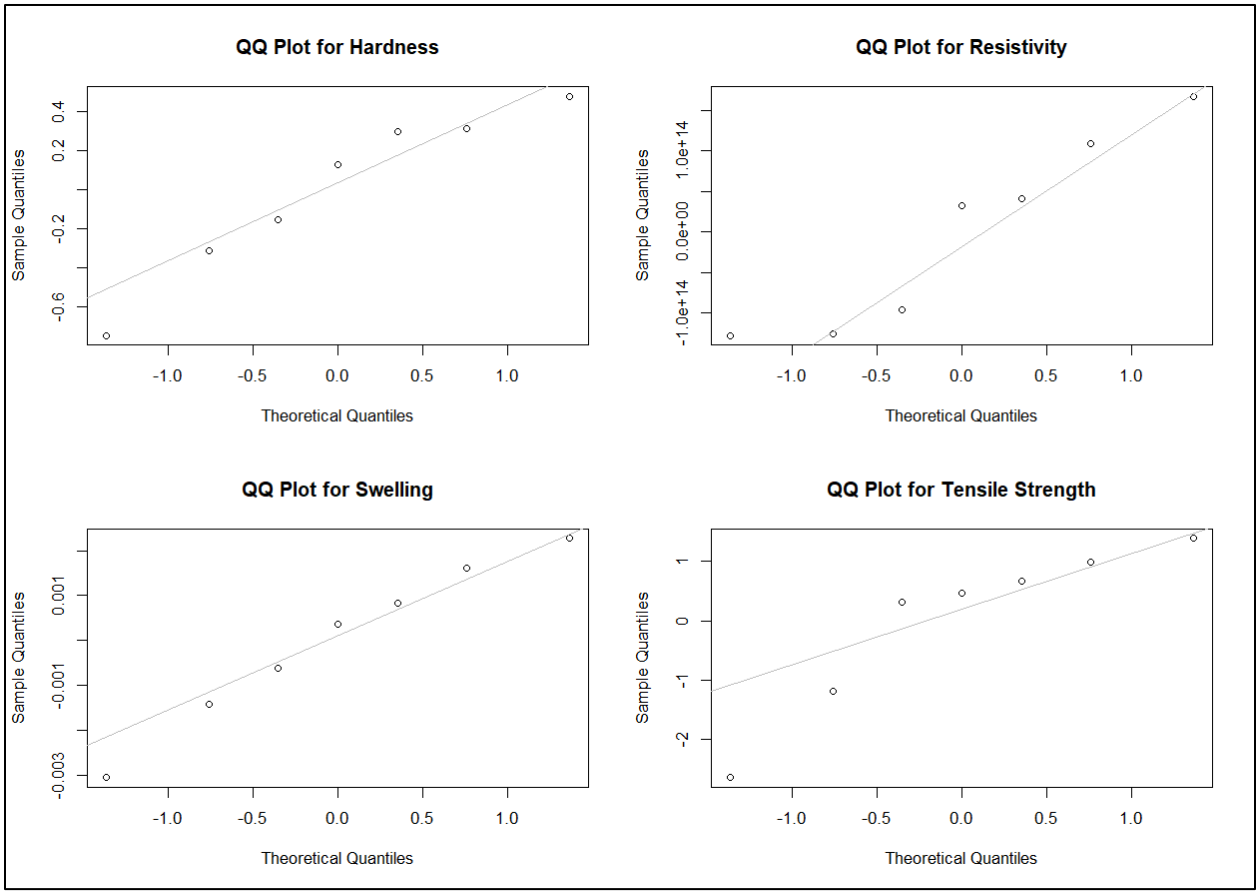

Figure 6. 41: QQ plot for Silicon sealing properties

Reference

310. Abdihamzehkolaei, A.; Ahad, M.T.; Siddique, Z. Volume Resistivity of Viton Polymer under Thermal Aging. *Polymers* **2021**, *13*, 773. https://doi.org/10.3390/polym13050773

311. Liang, Q., Nyugen, M.T., Moon, KS. *et al.* A Kinetics Study on Electrical Resistivity Transition of *In Situ* Polymer Aging Sensors Based on Carbon-Black-Filled Epoxy Conductive Polymeric Composites (CPCs). *J. Electron. Mater.* **42**, 1114–1121 (2013). https://doi.org/10.1007/s11664-013-2525-z

312. Frigione, M. Assessment of the Ageing and Durability of Polymers. *Polymers* **2022**, *14*, 1934. https://doi.org/10.3390/polym14101934

313. Kulkarni S.S., K. Choi, W. Kuang, N.C. Menon, B. Mills, A. Soulami, and K.L. Simmons. 2021.**Damage evolution in polymer due to exposure to high-pressure hydrogen gas.** *International Journal of Hydrogen Energy* 46, no. 36:19001-19022.PNNL-SA-158973. doi:10.1016/j.ijhydene.2021.03.035

314. Sgambitterra, E.; Pagnotta, L. Permeability: The Driving Force That Influences the Mechanical Behavior of Polymers Used for Hydrogen Storage and Delivery. *Energies* **2024**, *17*, 2216. https://doi.org/10.3390/en17092216

315. K. J. Alvine, T. A. Kafentzis, S. G. Pitman, K. I. Johnson, D. Skorski, J. C. Tucker, T. J. Roosendaal, M. E. Dahl; An *in situ* tensile test apparatus for polymers in high pressure hydrogen. *Rev. Sci. Instrum.* 1 October 2014; 85 (10): 105110. https://doi.org/10.1063/1.4899315

316. Astafurova, E.G., Moskvina, V.A., Maier, G.G. *et al.* Effect of hydrogenation on mechanical properties and tensile fracture mechanism of a high-nitrogen austenitic steel. *J Mater Sci* **52**, 4224–4233 (2017). https://doi.org/10.1007/s10853-016-0676-z

317. Li, Q.; Ghadiani, H.; Jalilvand, V.; Alam, T.; Farhat, Z.; Islam, M.A. Hydrogen Impact: A Review on Diffusibility, Embrittlement Mechanisms, and Characterization. *Materials* **2024**, *17*, 965. https://doi.org/10.3390/ma17040965

318. Junichiro YAMABE, Shin NISHIMURA, Tensile Properties and Swelling Behavior of Sealing Rubber Materials Exposed to High-Pressure Hydrogen Gas, Journal of Solid Mechanics and Materials Engineering, 2012, Volume 6, Issue 6, Pages 466-477, ISSN 1880-9871 https://doi.org/10.1299/jmmp.6.466

319. Jeon, S.K.; Jung, J.K.; Chung, N.K.; Baek, U.B.; Nahm, S.H. Investigation of Physical and Mechanical Characteristics of Rubber Materials Exposed to High-Pressure Hydrogen. *Polymers* **2022**, *14*, 2233. https://doi.org/10.3390/polym14112233

320. Zhou, C., Chen, G. & Liu, P. Finite Element Analysis of Sealing Performance of Rubber D-Ring Seal in High-Pressure Hydrogen Storage Vessel. *J Fail. Anal. and Preven.* **18**, 846–855 (2018). https://doi.org/10.1007/s11668-018-0472-y

321. Simmons, Kevin L., Kuang, Wenbin, Burton, Sarah D., Arey, Bruce W., Shin, Yongsoon, Menon, Nalini C., and Smith, Barton. *H-Mat Hydrogen Compatibility of Polymers and Elastomers*. United States: N. p., 2020. https://doi:10.1016/j.ijhydene.2020.06.218.

322. https://h2tools.org/sites/default/files/8100TechRef_polymers.pdf (visited on 6th October, 24)

323. Pacific Northwest National Laboratory (PNNL). (2021, September 17). Hydrogen compatibility study characterizes performance of rubber additives. Pacific Northwest National Laboratory. https://www.pnnl.gov/news-media/hydrogen-compatibility-study-characterizes-performance-rubber-additives

324. Junichiro YAMABE, Shin NISHIMURA, Crack Growth Behavior of Sealing Rubber under Static Strain in High-Pressure Hydrogen Gas, Journal of Solid Mechanics and Materials Engineering, 2011, Volume 5, Issue 12, Pages 690-70 https://doi.org/10.1299/jmmp.5.690

325. Mueller, M.G., Žagar, G. & Mortensen, A. Stable room-temperature micron-scale crack growth in single-crystalline silicon. *Journal of Materials Research* **32**, 3617–3626 (2017). https://doi.org/10.1557/jmr.2017.238

326. Zha ng, W. Technical Problem Identification for the Failures of the Liberty Ships. *Challenges* **2016**, *7*, 20. https://doi.org/10.3390/challe7020020

327. DeArmitt, Chris & Hancock, M. (2003). Particulate-Filled Polymer Composites.

328. Robb WL. Thin silicon membranes--their permeation properties and some applications. Ann N Y Acad Sci. 1968 Jan;146(1):119-37. doi: 10.1111/j.1749-6632.1968.tb20277.x. PMID: 5238627.

329. Lee, C.-L.; Chapman, H.L.; Cifuentes, M.E.; Lee, K.M.; Merrill, L.D.; Ulman, K.L.; Venkataraman, K. Effects of polymer structure on the gas permeability of silicon membranes. J. Membr. Sci. 1988, 38, 55–70, https://doi.org/10.1016/s0376-7388(00)83275-5.

330. Hirotada Fujiwara, Hiroaki Ono, Shin Nishimura, Effects of fillers on the hydrogen uptake and volume expansion of acrylonitrile butadiene rubber composites exposed to high pressure hydrogen: -Property of polymeric materials for high pressure hydrogen devices (3)-, International Journal of Hydrogen Energy, Volume 47, Issue 7, 2022, Pages 4725-4740, ISSN 0360-3199, https://doi.org/10.1016/j.ijhydene.2021.11.061.

331. Simmons, K. L., & LaFleur, C. B. (2019). Compatibility of polymeric materials used in the hydrogen infrastructure. U.S. Department of Energy, Hydrogen and Fuel Cells Program. Retrieved from https://www.hydrogen.energy.gov/docs/hydrogenprogramlibraries/pdfs/review19/scs026_simmons_2019_o.pdf

332. Simmons, K. L., & LaFleur, C. B. (2018). FY 2018 Annual Progress Report: Safety, Codes, and Standards for Hydrogen Compatibility of Polymer Materials. U.S. Department of Energy, Hydrogen and Fuel Cells Program. Retrieved from https://www.hydrogen.energy.gov/docs/hydrogenprogramlibraries/pdfs/progress18/scs_simmons_2018.pdf

CHAPTER 7: CONCLUSIVE REMRKS OF TECHNO-ECONOMICAL ASSESSMENT OF HYDROGEN AND FUTURE RECOMMENDATION

Chapter 7 provides a literature review on how the selected sealing samples behave while exposed to hydrocarbon or natural gas and then provide the summary of the key findings from the earlier chapters of this dissertation. The core objectives of this dissertation are to evaluate the possible effectiveness of hydrogen energy within the global energy transition, address the technological and material challenges in hydrogen production and storage, and explore the mechanisms and mitigation strategies for hydrogen-induced aging in sealing materials. Chapter 7 consolidates these insights to provide enhanced understanding of hydrogen's role as a sustainable energy carrier, highlighting both its potential and the barriers to its widespread adoption. The brief literature review on hydrocarbon induced sealing resistance will provide a comparative ground work for future research on blending energy. It aims to bridge the gap between current technological limitations and future innovations required for a resilient hydrogen economy, offering strategic recommendations to enhance the durability, efficiency, and economic viability of hydrogen energy systems. Through this integrated approach, Chapter 7 elaborates on the need for continued research, development, and policy support to drive the successful implementation of hydrogen as a cornerstone of sustainable energy infrastructure.

Nitrile Butadiene Rubber (NBR) is widely used in sealing applications in methane or natural gas environments. When exposed to methane, NBR can absorb the gas, leading to swelling. This swelling is influenced by the pressure and temperature of the gas. Higher pressures increase the solubility of methane in NBR, resulting in greater swelling. While there is a lack of research on NBR swelling methane exposure, but there was a study conducted on swelling of nitrile rubbers in gasoline-methanol-ethanol (GME) ternary fuel blend. The study investigated the swelling behavior of NBR when exposed to fuel blends containing alcohols and found that NBR samples exposed to gasoline doped with alcohol showed a two-fold increase in swelling compared to the original gasoline [348]. Another study investigated NBR swelling in CO_2-Enriched Water and explored how CO_2 gas affects the swelling and mechanical properties of NBR. The results indicate that CO_2 bubbles in water severely destroy the cross-linking network of rubber, leading to defects such as cracks and holes, which in turn increase the swelling increment [349]. Specific permeability coefficients for methane in NBR are less commonly studied. However, molecular simulations have shown that the permeability coefficients of gases like hydrogen, oxygen, nitrogen, carbon dioxide, and methane in hydrogenated nitrile butadiene rubber (HNBR) decrease in the order: $P(H_2) > P(CO_2) > P(O_2) > P(CH_4) > P(N_2)$.

EPDM is lacking in compatibility with natural gas environments [350]. EPDM absorb oil and gas; therefore it is not an efficient overall barrier [350]. Additionally, chemical compatibility charts suggest that EPDM is not recommended for use with methane, indicating potential compatibility issues in natural gas applications [351]. The molecular size of methane is 0.38 while for hydrogen it is 0.289. The larger molecular size and solubility behavior of methane possibly lead to structural degradation and loss of sealing integrity of EPDM.

Another sealing sample; Silicon rubber also exhibits poor resistance to hydrocarbons, including methane. Exposure to methane can lead to swelling, softening, and degradation of the silicon material, compromising its sealing effectiveness. Chemical compatibility charts indicate that silicone rubber is not recommended for use with methane, categorizing the interaction as having a severe effect [352].

There is a study that investigated the high-temperature performance of EPDM and silicon rubber O-rings under helium gas exposure using a pressure drop method. EPDM was found to be highly degradable, with significant degradation and leakage at elevated temperatures. At 316°C, EPDM exhibited mass losses ranging from 3.3% to 28.3%, with fragmentation observed, while at 450°C, over 60% mass loss occurred, and the material disintegrated into powder. Silicon rubber demonstrated better resistance, with minimal mass loss (1.9%–2.8%) at 316°C and no leakage detected during tests [353]. Another study by Brehm et al., showed the permeability coefficients of various elastomers to helium were measured at temperatures ranging from 290 K up to their decomposition points (approximately 600 to 700 K) upon application of 2 bar pressure. The results indicated that silicon rubber exhibited the highest helium permeability, followed by EPDM, with fluorocarbon rubber showing the lowest permeability among the materials tested. The activation energy of diffusion was estimated 2.3 kcal/mol for Silicon and 4.9 (kcal/mol) for EPDM upon helium application [354].

7.1. Research Objective and Outlined Findings

This section is designed to summarize the findings obtained through the literature review and experimental analysis of this study and outline these findings with the set of research objectives made at Chapter 1.

Assessing Hydrogen Energy Resilience in Global Energy Transitions: Technological, Economic and Strategic Perspectives

Chapter 2 thoroughly addresses hydrogen's resilience and possible effectiveness on the energy transition. It aligns with this objective by analyzing key properties of hydrogen, zero CO_2 emissions for reducing greenhouse gas emissions and advancing a low-carbon economy. The chapter emphasizes the role of strategic investments, supportive policies, and international collaboration in overcoming current challenges and establishing hydrogen's viability in decarbonizing transportation, industrial processes, and power generation. Additionally, the chapter reviews the significance of global cooperation and public engagement in promoting adoption and acceptance, positioning hydrogen as a resilient and adaptable solution for sustainable growth.

The key findings of Chapter 2 demonstrate the complex challenges and requirements in advancing hydrogen technology. The chapter identifies that one of the main technological obstacles is the hydrogen embrittlement of metals, which limits the durability and safety of storage tanks and pipelines. To address this, it suggest the development of specialized alloys and polymers that resist embrittlement and maintain structural integrity under high-pressure hydrogen environments. Economically, the chapter identifies that while hydrogen production costs remain high, effective financing mechanisms and government incentives are important to make clean hydrogen

competitive with fossil fuels. In terms of infrastructure, the findings show that large-scale deployment of hydrogen refueling stations, and the establishment of regional hydrogen production hubs are essential to support hydrogen adoption, particularly in the transportation and industrial sectors. These initiatives, alongside coordinated international efforts, are presented as strategic possibilities for mitigating hydrogen's logistical and economic barriers, thus promoting its role in decarbonizing energy-intensive industries.

Addressing Challenges in Hydrogen Energy: Production, Storage and Material Compatibility

Chapter 3 addressed the research objective of identifying and evaluating the primary challenges in implementing hydrogen energy technologies, particularly in production, storage, and material compatibility. Chapter 3 provided an in-depth analysis of various hydrogen production methods, including steam methane reforming, electrolysis, coal gasification, biomass conversion, and methane splitting. The findings highlighted the significant technical barriers associated with each method, such as high CO_2 emissions from steam methane reforming and coal gasification, the high cost and efficiency of electrolysis, and the material compatibility challenges in biomass and methane splitting. Furthermore, the chapter explored limitations of current hydrogen storage techniques, emphasizing the effects of hydrogen embrittlement on materials used in storage tanks, pipelines, and other infrastructure components. It discussed how hydrogen's interaction with materials like steel, composites, and polymers can lead to significant degradation and affect the structural integrity and long-term reliability.

In production, the chapter identifies the potential for carbon capture utilization and storage (CCUS) to reduce emissions from fossil-fuel-derived hydrogen, and it evaluates electrolysis efficiency improvements through membrane and catalyst advancements. For storage, it emphasizes advancements in composite materials for high-pressure storage tanks and analyzes hydrogen's permeation behavior in polymers and metals, with recommendations for enhancing durability under cycling pressures and temperatures. On material compatibility, the findings indicate that while austenitic stainless steels and certain polymers show resilience to hydrogen-induced degradation, high-strength steels remain to develop, particularly under dynamic loading. This information may assist in addressing the objective by establishing a framework for overcoming the technical challenges in hydrogen production and storage, thereby supporting the advancement of more resilient and economically viable hydrogen energy systems.

Investigating Hydrogen-Induced Aging in Storage and Sealing Materials: Mechanisms, Challenges, and Mitigation Strategies

Chapter 4 addressed the objective of investigating the mechanisms, challenges, and mitigation strategies associated with hydrogen-induced aging in storage and sealing materials. Chapter 4 discussed various aging processes, including thermal, chemical, mechanical, mechanical-chemical, and thermo-mechanical aging, providing a detailed analysis of how these mechanisms impact the structural integrity of materials. The findings identified that hydrogen exposure significantly accelerates material degradation through phenomena like cracking, embrittlement, and blistering, with each aging process contributing to different forms of damage. For instance, mechanical aging in hydrogen environments was shown to cause crack propagation and matrix

debonding in composite materials, while chemical aging led to chain scission and increased brittleness in elastomeric seals. Furthermore, the chapter explored the role of operating conditions such as pressure, temperature, and stress in exacerbating these degradation processes, emphasizing the need for innovative material solutions. Mitigation strategies were also analyzed, focusing on the development of advanced materials with enhanced resistance to hydrogen permeation and the implementation of accelerated durability tests to predict material lifetime. The analyses provided a framework for understanding and mitigating the challenges of hydrogen-induced aging, aligning with the objective of enhancing the durability and performance of storage and sealing materials in hydrogen applications.

Experimental Investigation of Hydrogen Exposure on Polymer-Based Sealing Materials: Effects on Mechanical, Electrical, and Physical Properties

Elastomers are natural or synthetic polymers that have elastic properties. The mechanical properties of elastomers can undergo a series of changes that alters their material properties over time while used in hydrogen infrastructure. This negatively affect the service life as a sealing barrier. The molecular chains that make up elastomers are held together by weak intermolecular forces. These molecular chains get degraded due to aging and this effect on sealing performance. Generally, sealing material has low Young's modulus and high yield strength. Therefore, these elastomers also have the unique property of regaining their original shape and size after being stretched or compressed. Accelerated aging tests are typically conducted to get a better understanding of how elastomers degrade over time. Two primary chemical reactions occur when rubber ages: hardening and softening. Hardening occurs when the polymer chains that make up a

rubber start to bind together. Softening occurs with age due to weakening in the molecular chain . The tensile strength of the material also decrease which results in the elastomer becoming brittle. If the material ages and becomes hardened, it will reduce friction on the system but may lose its sealing ability. Additionally, because of the strength decrease, it will also be more susceptible to damage and will likely have a shorter service life. Therefore, an experimental investigation was performed to understand the effect of hydrogen exposure on properties of sealing materials and the summary of the findings are outlined at Figure 7.1.

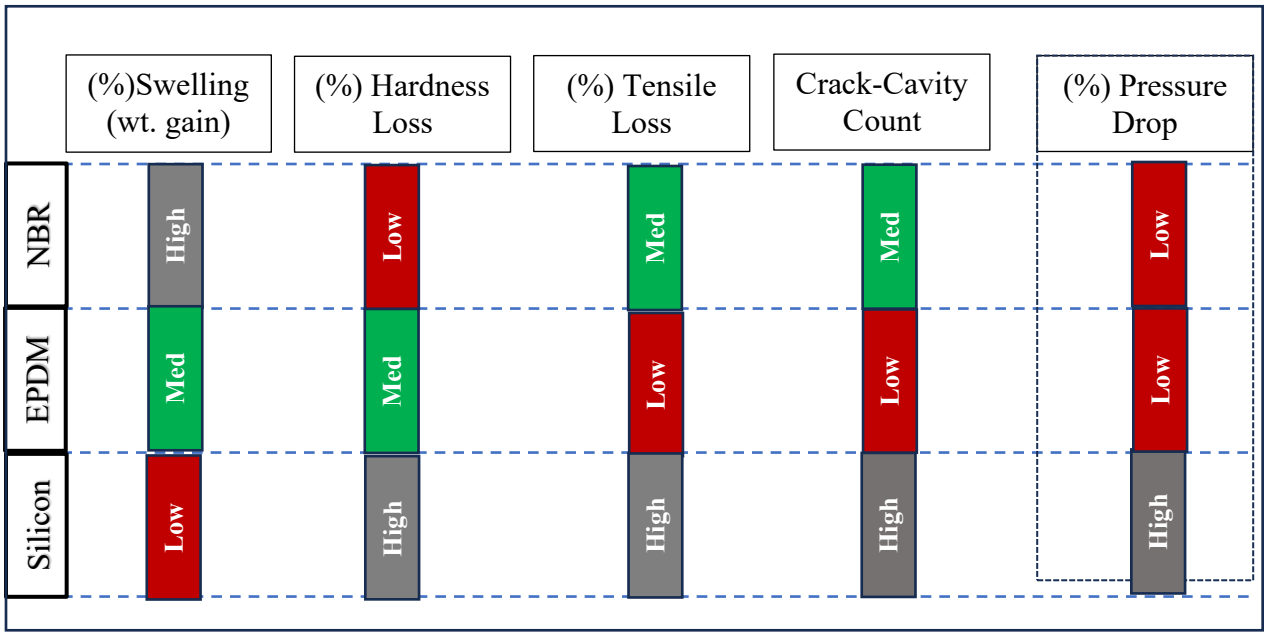

Figure 7. 1: Summary of the findings from experimental analysis of accelerated aging

- **Observation of Each Materials Under Hydrogen Aging**:

Silicon:

Silicon showed lowest swelling but high reductions in tensile strength and hardness, with large number of cracks and cavities count, leading to least sealing resistance under high pressure hydrogen.

The observed minimal swelling of silicon under hydrogen exposure may be explained by its stable siloxane backbone structure (Si-O-Si). The low hydrogen solubility and permeability of silicon limits the absorption and diffusion of hydrogen molecules within its matrix. However, when hydrogen penetrates, it interacts more with the Si-O bonds and physical disruptions takes place. This interaction leads to local stresses that promote embrittlement and microstructural degradation over time. Consequently, the tensile strength and hardness reductions occur. The reduction rate of tensile strength and hardness was observed higher in silicon, as the microstructural changes accumulate over time and increase under higher pressures. Silicon exhibits a higher presence of cracks and cavities because its lower intermolecular interactions and flexible polymer chains which may allow stress concentrations to localize more easily around hydrogen-induced voids, increasing likelihood to crack propagation and mechanical weakening.

EPDM:

EPDM displayed moderate swelling and hardness loss but strong in leak resistance, and lowest morphological degradation despite its comparatively higher reduction in hardness than NBR.

EPDM is a synthetic elastomer; made of chemicals ethylene, propylene, and diene monomers. The molecular structure of EPDM includes a saturated backbone and tight crosslinked molecular structure, which enhance its resistance to gas permeation and leak paths compared to unsaturated rubbers like NBR. The hydrogen solubility for EPDM was obtained from literature as (26.6 ± 1.1) mol/m^3 MPa following thermal desorption analysis GC method while for NBR, the hydrogen solubility was found as (31.4 ± 1.3) mol/m^3 MPa [333]. Therefore, EPDM's lower hydrogen solubility limits internal gas absorption, reducing swelling compared to more permeable elastomers like NBR. However, EPDM still undergoes surface cracking over time due to localized hydrogen interaction like accumulation of hydrogen at microstructural flaws, such as voids or grain boundaries which gradually reduce the elasticity and hardness. EPDM has also limited reduced free volume which mitigate excessive gas diffusion and associated mechanical weakening. The comparatively stable morphology of EPDM is also evidenced by its fewer voids and microstructural degradations which supports its durability and leak resistance under higher hydrogen pressure.

NBR:

NBR demonstrated the highest swelling but lowest reduction of hardness with moderate surface degradation and leaking resistance (more than silicon but less than EPDM) under hydrogen exposure.

NBR exhibits significant swelling under hydrogen exposure due to its relatively high free volume and hydrogen solubility, enabling greater gas absorption compared to EPDM and silicon. With a moderate to high crosslink density, especially when cured with carbon black, sulfur, or peroxides, NBR resists excessive mechanical weakening, helping it retain hardness and tensile strength better than silicon. Again, NBR's unsaturated structure allows increased hydrogen diffusion which causes localized stress, and higher microcracking and cavities formation under prolonged high-pressure hydrogen environments compared to what was observed in EPDM. Despite allowing greater permeation than EPDM, NBR's dense molecular structure affords strong leak resistance, making it less permeable than silicon. These characteristics make NBR an intermediate choice for hydrogen sealing applications where a balance of elasticity and durability is required.

- **Interactions Among Properties and Implications:**

Swelling and Hardness Reduction

While swelling is assumed to have correlation directly with hardness reduction, the materials' molecular structures is also a contributing factor. NBR, with the highest swelling, retains hardness better than EPDM. The interaction between hydrogen and elastomers can be explained by their crosslinking density and molecular polarity. NBR has a nitrile group (–CN) in its structure, which enhance intermolecular interactions, contributing to its chemical resistance and lower gas permeability compared to non-polar elastomers. This polarity helps NBR maintain hardness even when swelling takes place. These polar interactions limit molecular mobility and support retaining hardness. EPDM swells less in hydrogen than NBR due to its lower polarity, which limits hydrogen uptake. However, EPDM's elastic, less dense crosslinked network allows hydrogen molecules to penetrate more deeply, leading to plasticization effects that reduce hardness over NBR.

Tensile Strength Reduction and Morphological Degradation

A strong link between tensile strength reduction is observed with crack and cavity formation. Silicon experiences the highest tensile strength loss, is also found most susceptible to cracks and cavities, weakening its structural integrity and reducing its sealing capacity. In elastomers, tensile strength reduction is closely tied to morphological degradation under harsh conditions, such as hydrogen exposure. This reduction occurs as hydrogen penetrates the elastomer matrix, initiating microstructural changes like crack formation, micro-cavities, and polymer chain scission. These changes impair the elastomer's load-bearing capacity by reducing the inter-chain interactions that contribute to tensile strength. This is consistent with literature suggesting that materials with high

initial tensile strength but low resilience to tensile degradation under stress tend to form micro-cracks, which compromise long-term sealing [334,335].

Hardness Reduction and Leak Performance

There is a complex interaction between hardness and sealing resistance observed. EPDM, despite higher hardness loss, performs better in leak resistance than NBR due to its flexibility and ability to adapt to high-pressure changes without developing more micro-defects. Hardness reduction in elastomers directly impacts the sealing performance in high-pressure environments. When an elastomer becomes too soft due to exposure due to swelling or hydrogen-induced plasticization, its ability to maintain sealing pressure weakens, increasing leak rates and making the material susceptible to deformation or tearing under pressure. Conversely, if an elastomer hardens excessively, it can lose flexibility, creating poor surface conformity and higher risk of interfacial leaks due to rigid, less adaptable seals. NBR's hardness retention comes due to its elasticity, but causing it to become brittle under high pressure, which leads to micro-cracking and less sealing resistance than EPDM at high pressure zone [336].

- **Scientific Insights on the findings:**

Hydrogen Permeation vs. Cross-Link Density

The different behaviors of the sealing materials in terms of swelling and sealing performance align with their molecular and cross-link structures. EPDM's lower cross-link density allows it to absorb hydrogen more uniformly, mitigating localized stress and reducing crack formation. NBR, with higher cross-link density, localizes hydrogen permeation, causing stress points that can lead to structural failure. NBR's polar nitrile groups create strong intermolecular forces which might restrict swelling but increase stress under gas diffusion. This trend supports EPDM's high sealing resistance and lower loss of mechanical properties under hydrogen exposure, as its more flexible network can manage hydrogen-induced stresses better than the rigid NBR structure [337,338].

Resistance to Fatigue-Induced Cracking

Fatigue resistance is another essential factor. EPDM's ability to withstand repeated hydrogen cycling without significant cracking or loss in structural integrity makes it more reliable as a sealing material over time. EPDM's low polarity and flexible network assist uniform swelling well, minimizing microstructural degradation under increasing pressure. In contrast, NBR, while initially stable, develops microstructural cracks due to its inability to accommodate hydrogen expansion, leading to leaks in dynamic environments [336].

Reduced Compression Set in EPDM

EPDM's lower compression set also reinforces its sealing performance, as it retains its shape better after compression, maintaining contact in a seal and reducing potential leak paths. This property, particularly important for high-pressure environments, gives EPDM an advantage over NBR and Silicon, which tend to lose structure more easily under similar conditions due to presence of large volumes of cracks and cavities [337]. From this research and analysis, it is suggested that EPDM offers a balanced performance as a sealing material under hydrogen exposure, followed by NBR, where Silicon falls short. In lower pressure zones up to 1500 psi hydrogen pressure, both EPDM and NBR perform at an equal rate, but with increasing pressure, EPDM showed better resistance than NBR. Its unique combination of flexibility, lower cross-link density, and resilience to fatigue-induced cracking and compression set deterioration under high-pressure hydrogen makes it suitable for applications requiring consistent sealing.

7.2. Limitations and Future Research

In the perspective of the comprehensive findings presented throughout this dissertation, several critical areas have been identified for future research to advance the field of hydrogen energy and its associated technologies. While this work has extensively explored the effects of hydrogen exposure on polymer-based sealing materials and the challenges in hydrogen production, storage, and integration, further investigations are essential to address the remaining gaps and enhance the long-term viability of hydrogen systems. The following recommendations outline specific technical areas that may be taken into deeper analysis, advanced approaches, and interdisciplinary collaboration to drive improvements in material compatibility, system optimization, and sustainable integration of hydrogen into the global energy infrastructure.

Life-Cycle Assessment (LCA) of Sealing Materials in Hydrogen Technologies

The life cycle analysis (LCA) of polymer sealing materials in hydrogen applications is important to advancing sustainable hydrogen energy systems. Current research in hydrogen infrastructure primarily focuses on the material performance during operational phases, overlooking the full life cycle impacts, from material extraction to end-of-life disposal. Comprehensive analyses are necessary because polymer seals are integral to hydrogen storage and distribution systems, where they are exposed to high-pressure exposure, degradation, and mechanical wear due to hydrogen permeation. These factors directly impact their durability and overall system efficiency. Incorporating LCA into research on polymer sealing materials would enable a deeper understanding of the environmental impacts associated with their production, usage, and disposal. However, there is a lack of standardized methods and detailed data for life cycle analysis, partly

due to the relatively recent adoption of hydrogen technologies and the complexity of measuring the impacts of material degradation under varied conditions. Additionally, the absence of explicit end-of-life strategies for polymer materials, coupled with inadequate recycling processes, restrict the ability to mitigate the environmental impact effectively. Existing research lacks detailed insights into how the sealing materials behave under the cyclic pressures typical of hydrogen storage, emphasizing the need for more specific studies to address the gaps in polymer lifespan under hydrogen exposure.

Impact of Microstructure on Hydrogen Permeation

The microstructural analysis of sealing materials, including crack and cavity detection, has provided critical insights into the impact of hydrogen-induced aging. Current research primarily relies on techniques of Scanning Electron Microscopy (SEM) for surface morphology characterization to observe crack propagation and cavity formation at increasing hydrogen pressures. Although these methods have proven effective in identifying surface damage and degradation patterns, there remains a gap in quantifying these changes at molecular and nanoscale level. Future research could benefit from incorporating more advanced techniques such as Atomic Force Microscopy (AFM) and Transmission Electron Microscopy (TEM), which allow for higher resolution imaging and a more precise analysis of the microstructural features. These techniques would enable a better understanding of the molecular interactions between hydrogen and polymer matrices, particularly in terms of polymer chain orientation, crystallinity, and nanoscale defect formations. Additionally, the existing studies mostly focus on the macro-level mechanical impacts which can be coupled with a detailed exploration of nanoscale features to develop more understanding on hydrogen-induced degradation.

Material Innovations for Enhanced Durability

Developing advanced materials that can withstand the detrimental effects of hydrogen-induced aging is essential for enhancing the longevity of sealing materials in hydrogen storage systems. Future work should focus on designing polymer blends and nanocomposite materials that integrate fillers like carbon nanotubes, graphene, or boron nitride to reinforce the polymer matrix. Current study is focused on commercially available polymeric o'rings while blending of polymer based on the characterization outcome of available polymers may assist to increase the mechanical strength, reduce swelling, and improve resistance to embrittlement under hydrogen exposure. The use of functionalized nanoparticles to create barrier layers within the polymer structure can limit hydrogen diffusion and mitigate material degradation. Extending this research will involve exploring cross-linking techniques to improve the chemical stability of elastomers and conducting accelerated aging tests to validate their long-term performance in hydrogen applications.

Integration of Advanced Machine Learning Techniques in Hydrogen Systems

The integration of advanced machine learning (ML) into hydrogen systems offers the potential to optimize hydrogen production, storage, and utilization processes by predicting system behavior and identifying efficiency improvements. Convolutional Neural Networks (CNNs), Long Short-Term Memory (LSTM) networks, and hybrid deep learning architectures can be considered to enhance the prediction of sealing performance more precisely. CNNs are particularly well-suited for extracting detailed spatial features from SEM images, capturing the morphology of cracks and cavities in polymer seals more effectively than traditional models. LSTM networks can also be integrated to analyze temporal sequences of image data or pressure changes, providing insights

into the progression of material degradation over time. Incorporating these advanced techniques would benefit significantly from more detailed datasets, including high-resolution SEM images at various pressure levels, real-time data on hydrogen diffusion rates, and microstructural changes in sealing materials. Additionally, combining image-based data with comprehensive material properties like chemical composition, mechanical stress factors, and temperature variations would create a more comprehensive dataset, enabling the development of complex algorithms that can better predict the long-term sealing performance in hydrogen environments. Integrating these advanced methods with real-time sensor data and adaptive learning algorithms can update predictions, providing a more precise understanding of sealing material behavior under diverse operational conditions.

Exploring the Role of Hydrogen Blends in Existing Infrastructure

The current study primarily focuses on the effects of hydrogen exposure on polymer-based sealing materials, particularly examining their electrical, mechanical, and physical properties under controlled conditions. Current research analyzed hydrogen-induced aging by studying changes in tensile strength, swelling behavior, hardness, resistivity, and microstructural morphology of elastomers. While this research investigated these specific materials' degradation under hydrogen pressures, it did not explore the impact of hydrogen blended natural gas within existing pipeline infrastructure or the broader implications for material compatibility in those systems. Determining the impact of hydrogen blended natural gas into the pipelines could be valuable to utilize a cost-effective approach to decarbonize energy systems without entirely overhauling the infrastructure. Further investigation may involve evaluating the thermo-mechanical properties of pipeline materials and coatings under varying hydrogen concentrations, assessing their susceptibility to

hydrogen embrittlement, and determining necessary modifications for compression and transportation systems. Integrating these aspects with the existing analysis of polymer behavior in current study can significantly contribute to developing sustainable energy infrastructure.

Thermal Aging Introduction

Current study investigated the pressure aging on sealing materials by hydrogen. However, the sealing materials are also exposed to a wide range of temperatures along with different pressures for respective applications. Thermal exposure significantly impacts polymer seals by increasing crosslink density, reducing elasticity, and forming micropores in the surface, which degrade their tribological and sealing performance. Introducing thermal aging studies into the current study would be more helpful in comprehensively evaluating how high temperatures conjugated with pressure impact the sealing property of elastomers for hydrogen energy. Extending this research will include varying the thermal cycles to evaluate their impact on the physical and chemical stability of different elastomers, helping develop materials that maintain their integrity even at high operating pressure and temperatures.

In-Situ Property Characterization

The current methodology in this dissertation performs an ex-situ characterization, where samples are removed from the hydrogen aging chamber before characterization. This approach has several limitations, primarily due to the changes that can occur when the sample is exposed to air during transfer. Oxidation or other chemical interactions may alter the surface morphology and mechanical properties of the samples. This may lead to deviation from the actual results in industrial applications, the seals are exposed to hydrogen and are degraded in the properties

simultaneously. Ex-situ methods may not capture the dynamic processes and real-time reactions that occur during hydrogen exposure, making it difficult to understand the precise mechanisms of degradation. In-situ characterization techniques are recommended for future research to address these limitations. In-situ methods allow for real-time monitoring of material properties under controlled hydrogen exposure conditions, providing a more accurate representation of the material's behavior. The in-situ characterization may be obtained by conducting the aging and material testing in a hydrogen-filled glove box. Techniques like in-situ transmission electron microscopy (TEM) or X-ray diffraction (XRD) can be used to observe structural changes, crack formation, and other microstructural evolutions as they happen. This approach offers a significant advantage by preserving the native environment of the sample, enabling the direct correlation of changes in material properties with respective operating conditions.

Enhanced Aging Duration

Extending the aging duration in hydrogen exposure experiments is important to evaluate the long-term durability of sealing materials beyond standard testing times. Prolonged aging studies will help in identifying slow-developing degradation mechanisms like stress relaxation, creep, and molecular reorganization within the polymer matrix. The current study is performed on a constant duration of aging which is 192 hrs. That time cycle can be multiplied by a constant factor and applied to assess the sealing performance. Implementing extended studies with periodic characterization may provide insights into the rate of property deterioration and the lifespan prediction of sealing materials in hydrogen storage applications.

Supply Chain Routes for Hydrogen Energy

This dissertation reviews the role of hydrogen in energy systems, focusing on its use in transportation, power generation, reducing greenhouse gas emissions, and market dynamics. It elaborates on the investments and policy measures necessary for scaling up hydrogen adoption and touches upon the deployment of hydrogen infrastructure, such as fuel cell vehicles and refueling stations. However, a detailed analysis of the hydrogen supply chain, specifically regarding the logistics of hydrogen production, storage, and transportation can be further investigated. Analyzing and optimizing the supply chain routes for hydrogen energy is essential to reduce transportation costs, enhance energy efficiency, and minimize carbon emissions. A detailed assessment of the logistical challenges in hydrogen production, storage, and distribution will help identify bottlenecks and areas for improvement. Future research may focus on developing new strategies for integrating green hydrogen production with existing energy systems and evaluating the feasibility of regional hydrogen hubs for establishing hydrogen supply chain systems.

Overall findings from this dissertation is that for lower pressure hydrogen application (< 1500 psi) either EPDM or NBR can be utilized at room temperature. But for higher pressure zone (> 5000 psi) and prolonged exposure duration (> 24 hrs) EPDM can be preferred over NBR to hold the pressure at room temperature. In general, based on thermal properties of silicon, at low pressure zone silicon can be a good choice based on its thermal stability. In terms of tensile strength, NBR and EPDM showed high inherent tensile strength 75 lbf and 50 lbf respectively, while silicon showed only 32 lbf of initial tensile strength. The trends of change in tensile strength was observed to be negatively correlated to the trend of leakrate. A material of intermediate tensile strength like Viton (39 lbf) can be suggested depending on the operating condition to fill up the gap. The hardness of Viton is also close to NBR (77 lbf), hence it can be a good candidate where softening of seal is a concern. From the experimental results, it was observed that saturation appears after 1500 psi hydrogen pressure, which was followed by a slow rate of reduction of the mechanical strength. Additional experiments are needed to better understand the change of properties at post saturation phase. The developed machine learning model can be utilized to understand the complex interplay taking place at post saturation zone and to consider one from EPDM and NBR according to the application requirement. Incorporating the leak rate results into the developed model can assist to predict the pressure gradient (psi/sec) of a particular sealing material by correlating tensile strength reduction and SEM-quantified microstructural changes under any specific hydrogen pressure. This will enable material optimization in hydrogen storage and transportation systems. While this study is not explicitly intended to find one specific sealing material, it is expected to contribute to picking the application driven suitable candidate from the comparative assessment. The other potential sealing candidates with associate mechanical properties can also be checked using the machine learning model developed in this work to understand the sealing resistance.

References

333. J.K. Jung, I.G. Kim, K.T. Kim, Evaluation of hydrogen permeation characteristics in rubbery polymers, Current Applied Physics, Volume 21, 2021, Pages 43-49, ISSN 1567-1739, https://doi.org/10.1016/j.cap.2020.10.003

334. Jiang, S.; Yong, Z. Modulation of Mechanical Properties of Silica-Filled Silicon Rubber by Cross-Linked Network Structure. *Polymers* **2024**, *16*, 2304. https://doi.org/10.3390/polym16162304

335. Mazurek, P., Vudayagiri, S., & Skov, A. L. (2019). How to tailor flexible silicon elastomers with mechanical integrity: A tutorial review. *Chemical Society Reviews, 48*(5), 1448-1464. https://doi.org/10.1039/C8CS00963E

336. Simmons, K. L., Alam, M. K., & Keller, J. (2017). *Safety, Codes and Standards: Technical Area Review for the DOE Hydrogen and Fuel Cells Program*. U.S. Department of Energy. https://www.hydrogen.energy.gov/docs/hydrogenprogramlibraries/pdfs/review17/scs026_simmons_2017_o.pdf

337. Nghieu, D. (2021, February 26). *Effects of aging on elastomer seals*. Sealing & Contamination Control Tips. https://www.sealingandcontaminationtips.com/effects-of-aging-on-elastomer-seals/

338. Angst Pfister. (2023). *Sealing solutions for hydrogen applications*. Retrieved from https://www.angst-pfister.com/dam/jcr:74e5366c-5239-4ff0-9003-d53fecbcf959/20240514_Sealing%20Solut%20ions%20for%20Hydrogen_Digital.pdf

339. U.S. Department of Energy. Compatibility of Polymeric Materials Used in the Hydrogen Infrastructure. 2017, https://www.hydrogen.energy.gov/docs/hydrogenprogramlibraries/pdfs/progress17/viii_9_simmons_2017.pdf.

340. HySafe. (2021). H-Mat hydrogen compatibility of NBR elastomers. Retrieved from https://hysafe.info/uploads/papers/2021/156.pdf

341. Effect of Hydrogen Pressure on the Fretting Behavior of Rubber Materials, The Free Library. (2014). Retrieved Nov 20 2024 from https://www.thefreelibrary.com/Effect+of+Hydrogen+Pressure+on+the+Fretting+Behavior+of+Rubber...-a0803498567

342. Trelleborg Sealing Solutions. (n.d.). Hydrogen sealing solutions. Retrieved November 20, 2024, from https://www.trelleborg.com/en/seals/your-industry/hydrogen-sealing

343. ERIKS. (n.d.). Hydrogen gaskets: Ensuring sealing integrity for hydrogen applications. Retrieved November 23, 2024, from https://eriks.com/content/dam/com/know-how-hub/content/case-studies/ERIKS_H2-Gaskets-brochure-online-version.pdf

344. Infinita Lab. (n.d.). In-situ linear reciprocating high-pressure tribometry. Retrieved November 23, 2024, from https://infinitalab.com/case-study/in-situ-linear-reciprocating-high-pressure-tribometry/

345. U.S. Department of Energy. (2018). Hydrogen and Fuel Cells Program: 2018 Progress Report - Safety, Codes, and Standards Overview. Retrieved from https://www.hydrogen.energy.gov/docs/hydrogenprogramlibraries/pdfs/progress18/scs_overview_2018.pdf

346. Trelleborg Sealing Solutions. (n.d.). H2Pro: Sealing solutions for hydrogen applications. Retrieved November 23, 2024, from https://www.trelleborg.com/seals/-/media/tss-media-repository/tss_website/pdf-and-other literature/brochures/h2pro_en.pdf?openpdf=1&rev=83692c8de9714638a07b71b3deb92b42%3F

347. SilcoTek. (n.d.). How silicon coatings help fuel the hydrogen economy. Retrieved November 23, 2024, from https://www.silcotek.com/blog/silicon-coatings-help-fuel-the-hydrogen-economy

348. Aji Satria Nugraha, Bambang Purnomo, Usman, Siska Pebriani, Soraya Ulfa Muzayanha, Dwi Febriantini; The swelling of different nitrile rubbers in gasoline-methanol-ethanol (GME) ternary fuel blend. AIP Conf. Proc. 23 September 2021; 2376 (1): 020009. https://doi.org/10.1063/5.0063660

349. Xiaoren Lv, Shuyuan Song, Huiming Wang, Shijie Wang. Effect of CO2 Gas on the Swelling and Tribological Behaviors of NBR Rubber in Water[J]. J. Mater. Sci. Technol., 2015, 31(12): 1282-1288. https://www.jmst.org/EN/10.1016/j.jmst.2015.09.014

350. Apple Rubber. (n.d.). The permeability of rubber compounds. Retrieved November 23, 2024, https://www.applerubber.com/hot-topics-for-engineers/the-permeability-of-rubber-compounds/

351. Kelco Engineering Pty Ltd. (2009). EPDM chemical compatibility guide. Retrieved from https://kelco.com.au/wp-content/uploads/2009/02/epdm-chemical-compatibility-guide1.pdf

352. PermSelect. (2019). Silicone chemical compatibility chart. Retrieved from https://www.permselect.com/sites/default/files/2019-09/Silicone_Chemical_Compatibility_Chart.pdf

353. U.S. Nuclear Regulatory Commission. (n.d.). Modeling the impacts of hydrogen effects on nuclear power plant equipment. Retrieved November 23, 2024, from https://www.nrc.gov/reading-rm/doc-collections/nuregs/contract/cr7115/initial/index.html

354. International Symposium on the Packaging and Transportation of Radioactive Materials (PATRAM). (1986). Proceedings of the 9th International Symposium on the Packaging and Transportation of Radioactive Materials. Retrieved from https://resources.inmm.org/system/files/patram_proceedings/1986/359.PDF